UNIVERSITAT DE BARCELONA

Links Between Dimethylated Sulfur and Phytoplankton Photophysiology in the Surface Ocean Geographical Paterns And Short-Term Variability

Relación entre el Dimetilsulfuro y la Fotofsiología del Fitoplancton en la Superfície del Océano Patrones Geográfcos y Variabilidad a Corto Plazo

Sarah-Jeanne Royer

Links between Dimethylated Sulfur and Phytoplankton Photophysiology in the Surface Ocean

Geographic Patterns and Short-Term Variability

Sarah-Jeanne Royer

Barcelona, 2015

Universitat de Barcelona

Institute of Marine Sciences

Links Between Dimethylated Sulfur and Phytoplankton Photophysiology in the Surface Ocean Geographical Patterns and Short-Term Variability

Relación entre el Dimetilsulfuro y
la Fotofisiología del Fitoplancton en la Superficie del Océano
Patrones Geográficos y Variabilidad a Corto Plazo

Sarah-Jeanne Royer

Barcelona, 2015

Memòria presentada per Sarah-Jeanne Royer per optar al grau de doctor per la Universitat de Barcelona.

Programa de Doctorat en Ciències del Mar

La Doctoranda	El Director	El Tutor
Sarah-Jeanne Royer	Dr. Rafel Simò	Dr. Miquel Canals

À ma mère Monique,
À ma magnifique famille,
Et à Anoop, for his forever support.

"C'est pas l'homme qui prend la mer
C'est la mer qui prend l'homme, tatatin
Moi la mer elle m'a prit, J'me souviens un lundi"

Renaud

Acknowledgements

Acknowledgements

Being an ocean apart or a few blocks away, several people made this adventure possible and enjoyable. These few lines are dedicated to all of you for being there for me!

First and foremost, this journey would not have been possible without the guidance and help of several individuals who, in one way or another, contributed and extended their valuable assistance in the preparation and completion of this study.

This thesis would not be the same without my supervisor Rafel, whose encouragement, guidance and support from start to finish, enabled me to develop an understanding of the subject. Thank you, Rafel, for your patience through this complex academic endeavour. Thanks to Maurice, who helped me take the plunge into this aquatic research. Thanks to Eric, Cyril and Tom for their invaluable help during my NaNs moments and my concerns with "La máquina infernal". Thanks also to Cris for her photo-kinetic knowledge and to Pep, who assisted me several times in work and travel issues.

To all my colleagues who were there for me in their own way. A special thanks to Martí for his time and patience while sharing his knowledge, his life (Aida) and his family and friends. Ana-Maria, Fran (El niño de Isabela), Raquel, Rachele, Nuria, Isabel, David, Jean-Ba, Bea (y su ayuda preciosa de maquetación), Pedro, Daffne, Sdena, Mirella, Arancha, Clara, Juancho, Monste, Elena, Guillem, Massimo, Sara, Vanessa, Clara, and the institution that is ICM: muchas gracias!

My oceanographic campaigns would not have been the same without my valuable friends on board who kept me going with their constant support, Eva mi super compañera chilena de noche y de día en el barco, Francesca, Max, Lara, Fran, Joannie, Ana, Pau, Pablo, Daffne, Sdena, Mirella, Marina, Encarna, Carolina, Belem, Laura, Maria-Carmen, Gemma, Resi, Montse, Celia, Gonzalo, Dolors y todos los Malaspineros y Pegaseros!

People onshore in Barcelona helped me with my authentic Spanish experience, starting with Ana-Maria and Fran, who made me feel at home right from the get-go and Eva, who helped me live the true Catalan experience over the last five years.

My precious flatmates that made my life so much easier and enjoyable here: Alessa (my playa global yoga master), Mirko, Nico, Dario, Laura, Fernanda, Brian, Maria, las dos preciosas catalanas Eva(s), Silvija, Ana -- you guys rock. I'll miss living with you!

All the friends from Toledo as well and from everywhere around the world: Silvija who helped me discover Barcelona Cultura, Carlos (who helped greatly with the design of the thesis), Alejandra, Lottie, Aracelie, Ana, Mar, Juan-Carlos, Alfonso, Cris, Azhu, Diego, Justine, Arthur, Gladys y Dil Se. All the friends from India that made me discover a whole new world: Rahul, Sev, Hrishi, Louise, Varun, Bhargav, Janhavi, Neha, and Saurabh.

All my closest friends from miles away who are close to my heart no matter what: Martine, Sophie, Pat, Carole, Chrystelle, Ludo (who greatly helped graphically with the thesis), Fannie, Greg, Dan, Mélanie, Nathalie, Laura-Kim, Nelson, Bastien, Toto, Jen(s), Annie, Manon, Vic, Steph, Sophie, Suzanne et Christian.

A special thank you to my loving Indian family that is always there for me, pampering me whenever I go back home. Thank you Aunty Neeta, Uncle Sharad, Pauravi, Amit, Manu and Kuki. You make my life better!

And my adorable family who supported me through happy and difficult moments during the PhD. Merci à toi ma maman chérie Monique, et merci à toutes mes matantes et tous mes mononcles; Carolle, Francine, Claude, Serge, Robin, Roland, Jacynthe, Jean-Pierre, Mimi, Alain, Jacynthe, Jean-Pierre, Gaby et Violette (et tous les chats)!

And last but not least, my adorable fiance Anoop who started and finished this adventure with me, whose support has meant the world. For your everyday support to me, to your help and patience, I thank you. Merci!

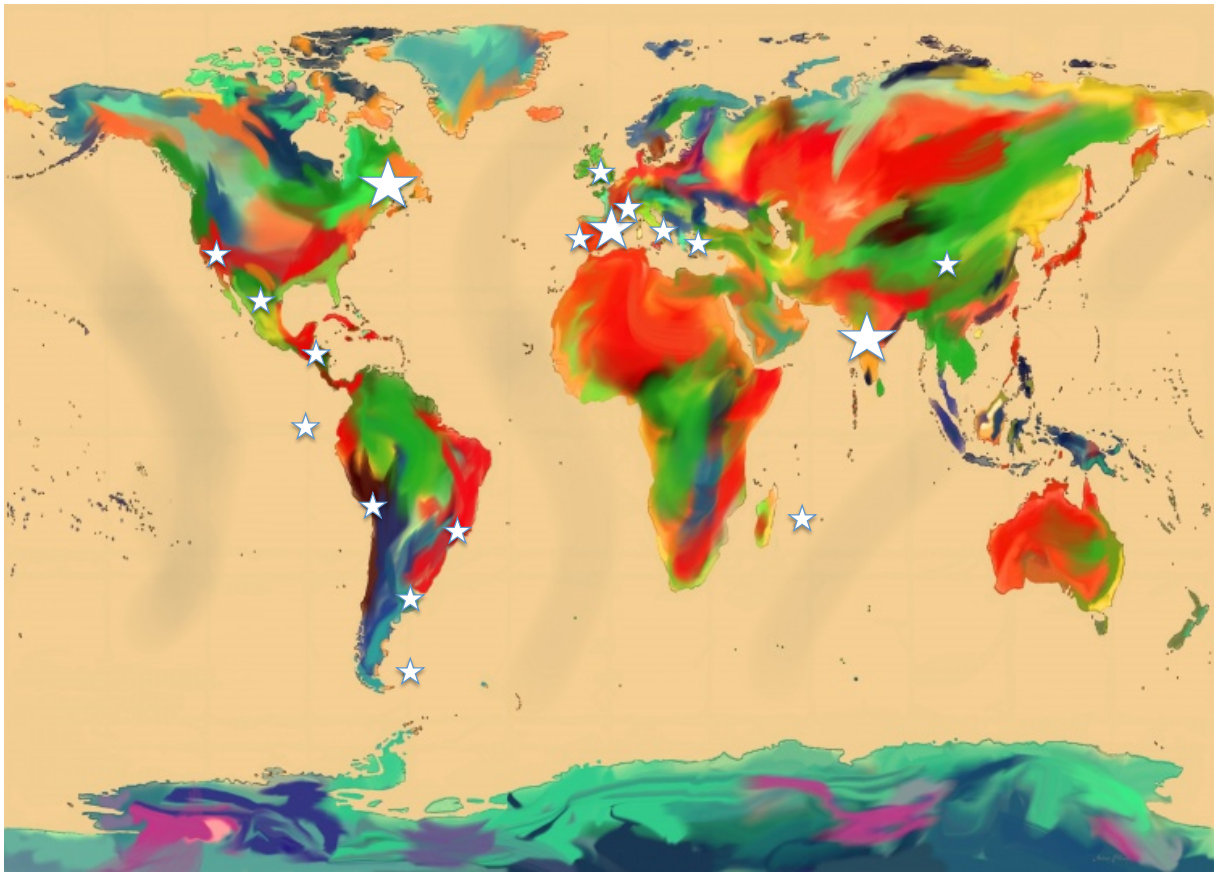

Representation of the geographic distribution of people that participated in this adventure from close or far. The size of the star represents the number of people from the particular country.

Table of Contents

List of Acronyms		2
Abstracts		4
General Introduction		11
Chapter 1	Short-term effects of solar radiation on phytoplankton photophysiology and dimethylated sulfur production in two contrasting environments (Western Mediterranean Sea and the Arctic Ocean).	49
Chapter 2	Differential response of planktonic primary, bacterial, and dimethylsulfide production rates to static vs. dynamic light exposure in upper mixed-layer summer sea waters.	91
Chapter 3	Development and validation of a shipboard system for measuring high-resolution vertical profiles of aqueous dimethylsulfide concentrations using chemical ionisation mass spectrometry.	129
Chapter 4	A high-resolution of time-depth view of dimethylsulfide cycling in the surface sea.	159
Chapter 5	Small-scale variability patterns of DMS and phytoplankton in surface waters of the tropical and subtropical Atlantic, Indian and Pacific oceans.	193
Chapter 6	Sea surface DMS distribution patterns and environmental and biological drivers across the tropical and subtropical oceans.	219
Summary of Results		259
General Discussion		267
Conclusions		285
References		291
Annex		303

List of Acronyms

List of the most common acronyms and abbreviations used in this thesis:

APCIMS	Atmospheric Pressure Chemical Ionization Mass Spectrometer
Chl*a*	Chlorophyll *a*
CDOM	Coloured/Chromophoric Dissolved Organic Matter
DIC	Dissolved Inorganic Carbon
DOC	Dissolved Organic Carbon
DMS	Dimethylsulfide
DMSO	Dimethylsulfoxyde
DMSP	Dimethylsulfoniopropionate
DMSPp	particulate Dimethylsulfoniopropionate
DMSPd	dissolved Dimethylsulfoniopropionate
FRRf	Fast Repetition Rate fluorometry
FvFm	Maximum quantum yield of photosystem II photochemistry
GC-FPD	Gas Chromatographer – Flame Photometric Detector
GP_{DMS}	Gross DMS production
MIMS	Membrane Inlet Mass Spectrometer
mLD	Mixing Layer Depth
MLD	Mixed Layer Depth
MSE	Mean Squared Error
NPP	Net Primary Production
PCA	Principal Component Analysis
PAR	Photosynthetically Active Radiation (400-700 nm)
PSII	Photosystem II
PTR-MS	Proton Transfer Reaction-Mass Spectrometry
SCM	Subsurface Chlorophyll Maxima
SIM	Single Ion Monitoring
SST	Sea Surface Temperature
SZAn	normalized Solar Zenith Angle
ULD	Upper Layer Depth
UVA	UltraViolet Radiation A (320-400 nm)
UVB	UltraViolet Radiation B (280-320 nm)
UVR	UltraViolet Radiation (280-400 nm)
VLS	Variability Length Scale

Longhurst provinces visited:

NATR	North Atlantic Tropical Gyral
WTRA	Western Tropical Atlantic
ETRA	Eastern Tropical Atlantic
SATL	South Atlantic Gyral
CNRY	Canary Coastal
GUIA	Guianas Coastal
MEDI	Mediterranean Sea
CARB	Caribbean
NASE	North Atlantic Subtropical Gyral
BRAZ	Brazil Current Coastal
BENG	Benguela Current Coastal
ISSG	Indian South Subtropical Gyre
EAFR	East Africa Coastal
AUSW	Australia-Indonesia Coastal
TASM	Tasman Sea
SPSG	South Pacific Subtropical Gyre
NPTG	North Pacific Tropical Gyre
PNEC	North Pacific Equatorial Countercurrent
PEQD	Pacific Equatorial Divergence
CAMR	Central American Coastal
AUSE	East Australian Coastal
SSTC	South Subtropical Convergence
ARCT	Arctic

Abstract

Dimethylsulfide (DMS) and its algal precursor, dimethylsulfopropionate (DMSP), are major players in the oceanic and atmospheric sulfur cycle. DMS is the most abundant volatile organic sulfur compound in the upper ocean and its global emission accounts for ca. 28 Tg S per year, thus representing the main natural source of sulfur to the troposphere and about 30% of the global (including anthropogenic) sulfur emissions. DMS cycle has been the subject of hundreds of studies over the last 28 years because of its hypothesized role in climate regulation (CLAW hypothesis), where it has been postulated to regulate the number of cloud condensation nuclei over the oceans and hence reduce the total amount of solar radiation reaching the Earth's surface. However, this simplistic view has not been proven so far as the relationship between oceanic DMS concentrations and solar radiation is complex and involves several different actors. Both DMS and DMSP (hereafter referred together as DMS(P)) concentrations are variable in the surface ocean and physics, chemistry and biology in the photic upper layer all play important roles in their cycling, from DMSP biosynthesis to DMS ventilation, with their relative importance varying amongst the diversity of biomes and pelagic ecosystem settings encountered in the world's oceans. Hence, predicting DMS at a global scale needs an intricate understanding of processes affecting its cycle at all temporal and spatial scales. The premise of the thesis is to contribute to a better understanding of the different physical, chemical and biological drivers that shape the DMS(P) cycle in polar, tropical and sub-tropical oceanic environments from very short to longer term temporal scales. This work combines an extensive database of DMS measured at low and high frequency, in different regions and across environmental gradients, and at temporal scales that span from minutes to seasons. In the short term (minutes to hours), exposure to UVR seems to play an important role in the physiological response of phytoplankton cells and DMS(P) production. Solar radiation also dictates the pace

of variability in DMS concentration over diel (day-night) cycles, where DMS seems to be surprisingly coupled to photobiological clocks. However, while gross biological DMS production generally increases with light exposure, concentration depends on the net effect of production and losses by photolysis, microbial consumption and ventilation. As a result, no single pattern for diel DMS oscillations is valid for the global oceans. Extensive data gathering across many biogeographical provinces in the tropical and subtropical oceans confirmed that DMS distribution is better explained by abiotic factors (solar radiation, vertical mixing, light absorption by organic matter) and phytoplankton physiology (efficiency of photosystem II) than by indicators of plankton abundance and general activity. Our work also shows that inferences about the causes of the variability of DMS depend on the frequency of the data collection. During a circumnavigation cruise, data collected at low frequency showed a relatively low variation factor (5.1) within a given biogeochemical provinces. In contrast, in the same province, high frequency data revealed a much higher variation factor (96) because of the capture of sub-mesoscale variability. Statistical analysis on high frequency data showed that critical variability distances for DMS average 15 and 50 km for coastal and open ocean marine provinces, respectively. DMS distribution patchiness increases with productivity and latitude, with important implications for designing fieldwork and computational mapping of DMS concentration and emissions. Overall, this thesis sheds light on the complex interplay of physical, chemical and biological variables in the DMS cycle and emphasizes the difficulty of finding simple environmental drivers of quantitative applicability at global scales.

Resum

El dimetilsulfur (DMS) i el seu su precursor algal dimetilsulfoniopropionat (DMSP) són part fonamental del cicle del sofre als oceans i l'atmosfera. El DMS és el compost volàtil de sofre més abundant a l'oceà superficial, que n'emet a l'atmosfera una quantitat aproximada de 28 Tg S l'any. Això representa la principal font natural de sofre a la troposfera, i aproximadament un terç de l'emissió global de sofre, incloent-hi l'antropogènica. El cicle del DMS ha estat objecte de centenars d'estudis en els darrers 28 anys, motivats sobretot per la hipòtesi CLAW que proposava que el DMS és la principal font de nuclis de condensació de núvols sobre els oceans i, d'aquesta manera, ajuda a regular la quantitat de radiació solar que arriba a la superfície de la Terra i, de retruc, el clima. Aquesta hipòtesi, avui vista com a simplista, no s'ha arribat a provar totalment, sobretot perquè la relació entre radiació solar i concentració i emissió de DMS és complexa i hi intervenen múltiples factors. Tant la concentració del DMS com la del DMSP (que referim conjuntament com a DMS(P)) varien força en l'oceà superficial com a resultat de processos que van de la biosíntesi del DMSP a la ventilació del DMS. Aquests processos, a la vegada, responen a factors i actors físics, químics i biològics, la importància relativa dels quals varia entre biomes i configuracions de l'ecosistema pelàgic. Com a conseqüència, predir la distribució del DMS a escala global demana un coneixement profund de tots els processos implicats, a totes les escales temporals i espacials. L'objectiu general de la tesi és contribuir a conèixer millor els factors físics, químics i biològics que governen el cicle dels DMS(P) en aigües polars, subtropicals i tropicals a escales temporals molt diverses. El treball combina una base de dades extensa de mesures de DMS obtingudes a baixa i alta freqüència, en regions diverses, a través de gradients ambientals, i d'escales de temps que van des dels minuts fins a les estacions de l'any. A més curt termini (minuts a hores), l'exposició a la llum UV sembla jugar un paper important en la resposta fisiològica del fitoplàncton i la subseqüent producció de

DMS(P). La radiació solar també dicta el ritme de variació de la concentració de DMS en cicles dia-nit, en què el DMS es mostra sorprenentment acoblat amb els rellotges fotobiològics. Tanmateix, malgrat que la producció biològica bruta de DMS generalment augmenta amb l'exposició a la llum, la concentració depèn de l'efecte net d'aquesta producció amb les pèrdues per fotòlisi, consum microbià i ventilació. Al capdavall, no sembla que hom pugui definir un patró d'oscil·lació dia-nit únic per al DMS a l'oceà global. L'obtenció de dades en moltes províncies oceàniques tropicals i subtropicals va confirmar que la distribució del DMS s'explica millor amb factors abiòtics tals com la radiació solar, la barreja vertical, l'absorció de la llum per la matèria orgànica, i també per factors de fisiologia de fitoplàncton, com l'eficiència del fotosistema II, més que amb els indicadors d'abundància i activitat general del plàncton. El treball mostra també que les inferències que hom pugui fer sobre les causes de variabilitat de la concentració del DMS depenen força de la freqüència d'observació. En una campanya de circumnavegació, les mesures fetes a baixa freqüència mostraven, per a una província donada, una amplitud de variació d'un factor de 5. En la mateixa província, les mesures d'alta freqüència mostraven una amplitud d'un factor de 96, perquè capturaven la variabilitat de mesoescala i submesoescala. L'anàlisi estadístic de les dades d'alta freqüència va mostrar que les distàncies de variabilitat crítiques per al DMS eren de 15 i 50 km per aigües més costaneres i més oceàniques, respectivament. Les distàncies d'heterogeneïtat en la distribució del DMS es fan més curtes amb la latitud i com més productives són les aigües. Això té implicacions importants en el disseny de treball de camp i en els esforços de 'mapejat' computacional. En conjunt, la tesi aporta llum a la complexitat de les interaccions que intervenen en el cicle del DMS, i ressalta la dificultat de trobar una relació simple que permeti predir la concentració i emissió del DMS en qualsevol punt de l'oceà global a partir de variables ambientals conegudes.

Resumen

El dimetilsulfuro (DMS) y su precursor algal dimetilsulfoniopropionato (DMSP) son parte fundamental del ciclo del azufre en los océans y la atmósfera. El DMS es el compuesto volátil de azufre más abundante en el océano superficial, que emite a la atmósfera una cantidad aproximada de 28 Tg S al año. Ello representa la principal fuente natural de azufre a la troposfera, y aproximadamente un tercio de la emisión global de azufre, incluida la antropogénica. El ciclo del DMS ha sido objeto de centenares de estudios en los últimos 28 años, motivados sobre todo por la hipótesis CLAW, que proponía que el DMS es la fuente principal de núcleos de condensación de nubes sobre los océanos y, de esta manera, ayuda a regular la cantidad de radiación solar que llega a la superficie de la Tierra y, en consecuencia, el clima. Esta hipótesis, hoy vista como simplista, no se ha llegado a probar totalmente, sobre todo porque la relación entre radiación solar y concentración y emisión de DMS es compleja y en ella intervienen múltiples factores. Tanto la concentración del DMS como la del DMSP (que referimos conjuntamente como DMS(P)) varían en el océano superficial como resultado de procesos que van de la biosíntesis del DMSP a la ventilación del DMS. Dichos procesos, a su vez, responden a factores y actores físicos, químicos y biológicos, cuya importancia relativa varía entre biomas y configuraciones del ecosistema pelágico. En consecuencia, predecir la distribución del DMS a escala global requiere un conocimiento profundo de todos los procesos implicados, a todas las escalas temporales y espaciales. El objetivo general de la tesis es contribuir a conocer mejor los factores físicos, químicos y biológicos que gobiernan el ciclo de los DMS(P) en aguas polares, subtropicales y tropicales a escalas temporales muy diversas. El trabajo combina una base de datos extensa de medidas de DMS obtenidas a baja y alta frecuencia, en regiones diversas, a través de gradientes ambientales, y de escalas de tiempo que van des de los minutos hasta las estaciones del año. A corto plazo (minutos a horas), la exposición a la luz UV parece jugar un papel importante en la respuesta fisiológica del fitoplánctón y la subsiguiente

producción de DMS(P). La radiación solar també dicta el ritmo de variación de la concentración de DMS en ciclos día-noche, donde el DMS se muestra sorprendentemente acoplado a los relojes fotobiológicos. Sin embargo, a pesar de que la producción biológical bruta de DMS generalmente aumenta con la exposición a la luz, la concentración depende del efecto net de dicha producción con las pérdidas por fotólisis, consumo microbiano y ventilación. En definitiva, no parece que se pueda definir un patrón único de oscilación día-noche para el DMS en el océano global. La obtención de datos en muchas provincias oceánicas tropicales y subtropicales confirmó que la distribución del DMS se explica mejor con factores abióticos tales como la radiación solar, la mezcla vertical, la absorción de luz por la materia orgánica, y también con factores de fisiología del fitoplancton, como la eficiencia del fotosistema II, que con los indicadores de abundancia y actividad general del plancton. El trabajo también muestra que las inferencias que se puedan hacer sobre las causas de variabilidad de la concentración del DMS dependen bastante de la frecuencia de observación. En una campaña de circunnavegación, las medidas hechas a baja frecuencia mostraban, para una provincia dada, una amplitud de variación por un factor de 5. En la misma provincia, les medidas de alta frecuencia mostraban una amplitud por un factor de 96, porque capturaban la variabilidad de mesoescala y submesosescala. El análisis estadístico de los datos de alta frecuencia mostró que las distancias de variabilidad críticas para el DMS eran en promedio 15 y 50 km para aguas más costeras y más oceánicas, respectivamente. Las distancias de heterogeneidad en la distribución del DMS se acortan con la latitud y la productividad. Este resultado tiene implicaciones importantes a la hora de diseñar futuras campañas de campo y en los esfuerzos de 'mapeo' computacional con análisis objetivo. En conjunto, la tesis arroja luz a la complejidad de las interacciones que intervienen en el ciclo del DMS, y resalta la dificultad de encontrar una relación simple que permita predecir la concentración y emisión del DMS en cualquier punto del océano global a partir de variables ambientales conocidas.

Introduction

Life on Earth

About 13.8 billion years ago, an enormous explosion likely marked the beginning of the universe. With this explosion began the process of the formation of the Earth that eventually led to the origin, diversification and evolution of life on Earth, which is believed to be formed about 4.5 Gyr ago, with the first ocean condensing about 4.4 Gyr ago (Wilde et al. 2001). The oceans are the largest habitat for living things in our solar system and cover more than 70% of the Earth's surface. Life in the oceans developed from complex chemistry and today it is home to the greatest diversity of major plants, animals, and microbial groups. In this complex oceanic system, abiotic and biotic factors are the major actors controlling the balance and diversity of life in the oceans. A combination of random and accidental abiotic conditions favored the emergence of life, and is thought to have taken place in the vicinity of hydrothermal vents of the ocean floor (Martin and Russell 2003).

The first prokaryotic cells appeared about 3.6 billion years ago and soon after (about 3.4 billion years ago) cyanobacteria performing photosynthesis made its appearance (Walter 1993; Nisbet and Sleep 2001). Photosynthetic mechanisms slowly built-up atmospheric oxygen, becoming responsible for the supply of most of the energy necessary for life on Earth and giving rise to the complex ecosystems encountered today. Marine phytoplankton play a vital role in maintaining the present oxygen levels on Earth and in contributing to the carbon cycle; they are now responsible for more than 50% of the primary productivity on Earth (Field 1998).

Dynamics in the Ocean: a Balance of Many Factors

The ocean plays a fundamental role in the stability of the Earth because it acts as a heat and carbon reservoir, where the transfer of energy takes place through exchanges with the atmosphere. However, for the oceans to be able to adjust to the several natural and anthropogenic processes they are exposed to, they themselves need to be in equilibrium. To achieve this equilibrium, several biotic and abiotic factors work in consortium. Amongst the abiotic factors, physics plays a major role as it governs the motion of the ocean and its properties. At a larger scale, the dynamics between temperature and salinity creates the thermohaline circulation, commonly known as the conveyor belt (Figure 1A). On a smaller scale, the combinations of a wide range of physical properties give rise to the panoply of oceanic currents and water masses present in the world's oceans (Figure 1B). Individual water masses represent a body of water characterized by a common formation history with physical properties different from the neighboring water masses. On a vertical plane, ocean stratification occurs because of the formation of different layers composed of distinct physical properties (temperature, salinity and density) in the water column.

Amongst the different vertical layers, the mixed-layer depth (MLD) represents the homogenous seawater layer in contact with the atmosphere and is derived from the temperature, salinity and density gradient. This strong gradient in stratification generally strengthens and shallows from spring into late summer, before mixing events deepen the MLD in fall and winter, with the deepest mixing occurring in late winter. The MLD is mostly influenced by the direct frictional forcing of the wind, which only penetrates to depth of ca. 10 to 100 m (Kara et al. 2003; de Boyer Montégut 2004; Sarmiento and Gruber 2006). The MLD varies with seasons and depending on the latitude can reach several hundred meters (high latitudes), where surface cooling impacts on the stability of the water column (Figure 2). Different features in surface layer profiles may

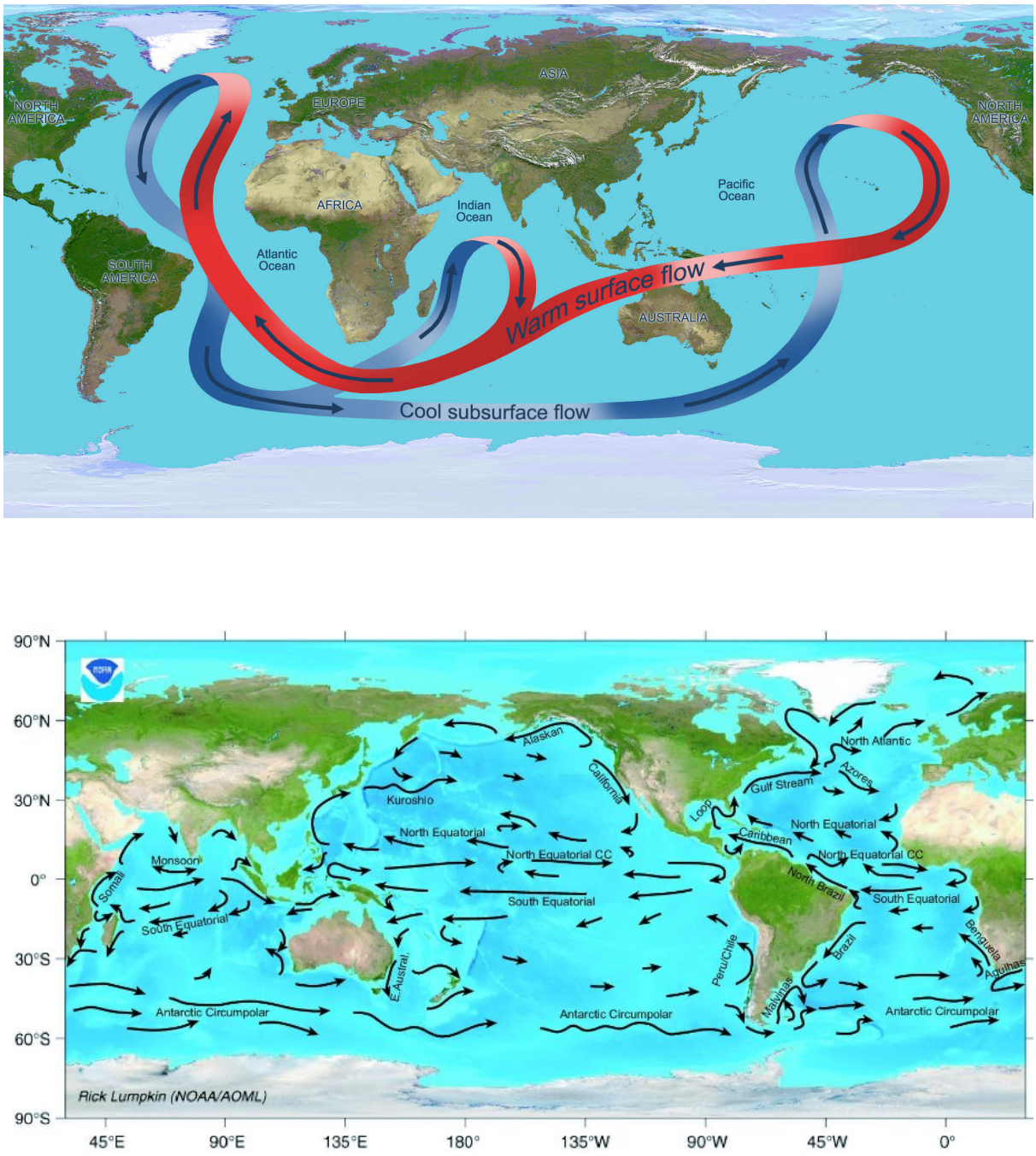

Figure 1: Oceanic physical drivers in the world ocean. A. Thermohaline circulation, commonly known as the global ocean conveyor system. The red belts represent warmer and fresher water masses (less dense) and the blue belts represent colder saline water masses that are denser and sink. Warmer water masses are found near equatorial regions and colder water masses are found near polar regions; from Climate Science Investigation, NASA. B. Major ocean surface currents in the world ocean; from NOAA.

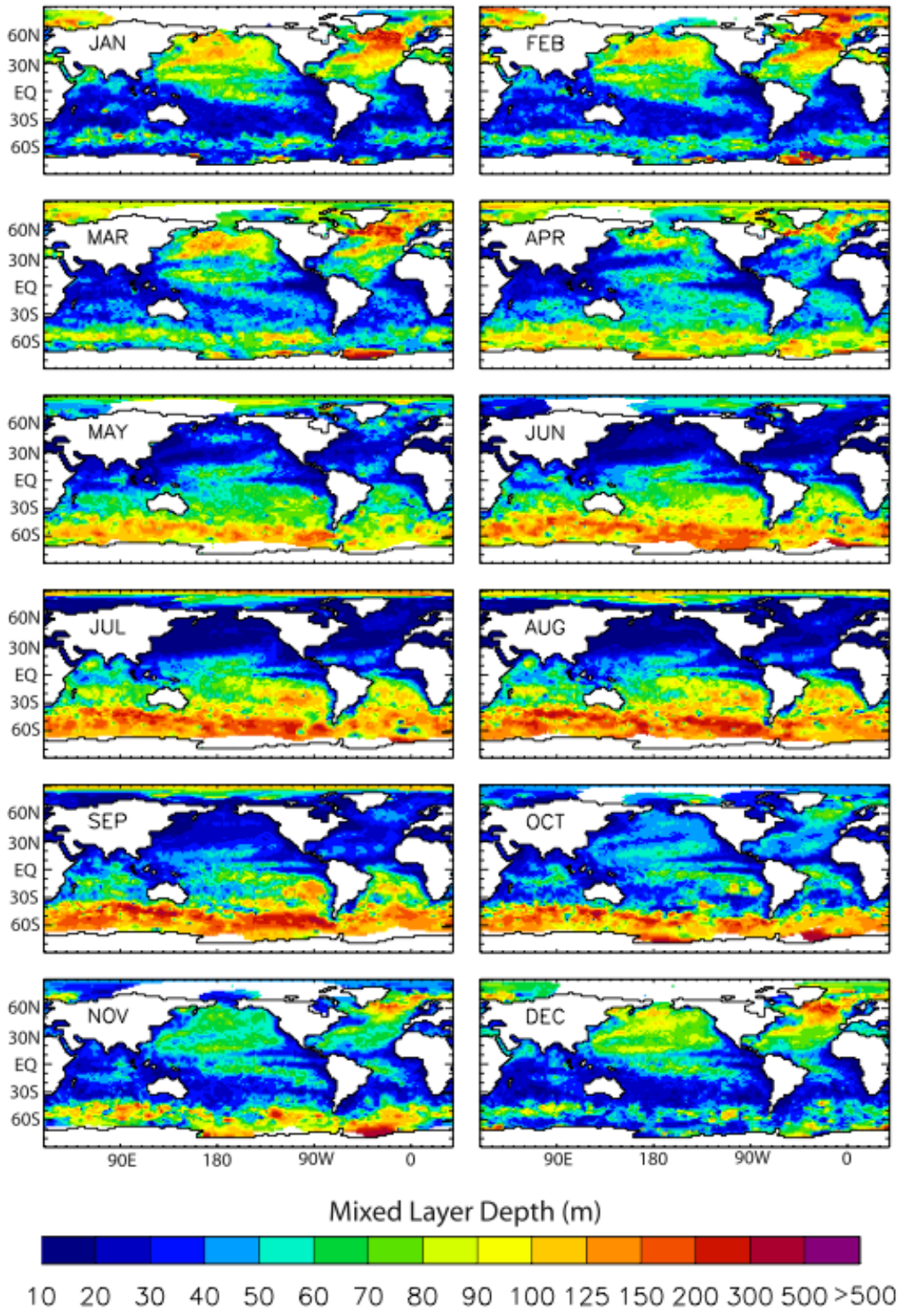

Figure 2: Variability in the mixed layer depth (MLD) across latitudes. The climatology is estimated from individual profiles, with an optimal temperature difference criterion of 0.2°C from temperature at 10 m depth; from de Boyer Montégut et al., 2004.

occur in the ocean (Sprintall and Tomczak 1992). Temporal variability of the MLD is linked to several physical processes occurring in the mixed layer (surface forcing, lateral advection, internal waves, etc.). It ranges from diurnal variability (Brainerd and Gregg 1995), which consists of an ephemeral shallower stratification occurring on top of the seasonal mixing due to increased heat fluxes during the day (or stagnation of the upper mixed layer (UML) because of reduced wind), to inter-annual variability, including seasonal and intra-seasonal variability (e.g., McCreary and Kohler 2001; Kara et al. 2003). The daily stratification is named mixing layer depth (mLD) and depending on the water properties might equal the MLD at dawn since this shallow mixing occurs during the day and breaks during the night. Water stratification does not only isolate physical properties but is also responsible for creating barriers to marine chemicals that will in turn affect the primary productivity in the photic zone.

The chemical composition of the ocean results from a balance between the input to the ocean from external sources (e.g. river inflow, dust deposition, Earth crust) and its removal, with an important fraction being dictated by biological activity. For biological activity to occur, essential micro (e.g., iron) and macro-nutrients (nitrates, phosphates and silicates) need to be present in high enough concentrations in the photic zone. Nitrogen is most typically the limiting macro-nutrients for phytoplankton growth control since it generally becomes depleted before phosphorus. Different forms of nitrogen are found in the ocean: reduced nitrogen (mainly NH_4^+), which is one of them, will be preferred over oxidized nitrogen (NO_3^-) by phytoplankton because of its reduced form resulting in low metabolic cost, which helps optimize the growth rates (Wheeler and Kokkinakis 1990). Phosphate is also an essential macro-nutrient and is taken up by phytoplankton cells during photosynthesis process and used for the synthesis of essential molecules such as adenosine triphosphate (ATP), nucleotide coenzymes and signaling pathways. In some of the world's oceans, nitrate concentrations are high, but mean chlorophyll *a* (Chl*a*) is low. This is because the bioavailable iron, a micro-nutrient necessary for the

photosynthesis machinery, is not available and limits the assimilation of bioavailable nitrogen and even restricts atmospheric nitrogen fixation (Falkowski 1997). This occurs in broad oceanic regions (Martin and Fitzwater 1988; Coale et al. 1996; Boyd et al. 2000; Tsuda et al. 2003; Behrenfeld et al. 2006), which account for about 30% of the world's oceans, mainly in the North Pacific, the Equatorial Pacific and the Southern Oceans. The distribution of nutrients in the world ocean depends strongly on the hydrography but also on their biological remineralisation rates governed by their circulation through the food web. Indeed, if it were not for the biological pump (Figure 3), most chemicals in the ocean would have a more uniform distribution like that of salinity.

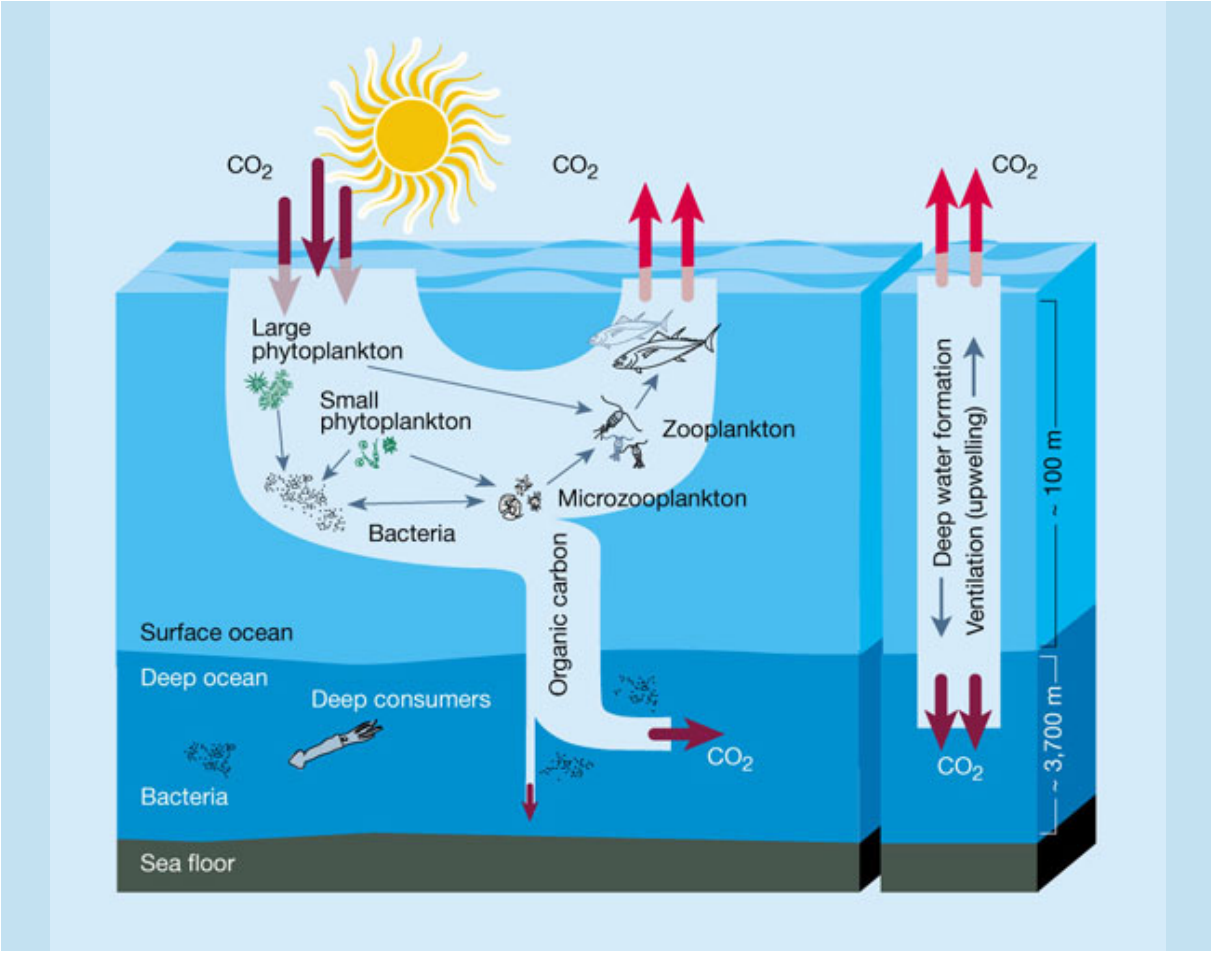

Figure 3: Phytoplankton and the biological pump, which play an important role in taking up CO_2 from the atmosphere and recycling it through the oceanic water column; from Antarctic Climate and Ecosystems Cooperative Research Centre.

The biological pump, in essence, is responsible for removing the carbon dioxide at the surface ocean and distributing it in the different layers of the ocean (Figure 3). At the surface of the ocean, it is also responsible for reducing the nutrient content, while the physics is responsible for circulating and mixing the components in the water column, which results in reinjections of nutrients into surface waters. Conversely, in the deep oceans, the biological pump is responsible for the increase in nutrients through remineralisation of the organic matter that sinks because of the gravitational force and the physical processes are responsible for reducing the nutrient content by bringing it to the surface (Figure 3).

The efficiency of the biological pump is defined as high when the phytoplankton successfully maintains low nutrient concentrations. If vertical mixing were not playing a role in this complex dynamic, there would be no return path for nutrients from deep waters and the biological pump would eventually deplete the surface waters and thermocline of nutrients; surface biological productivity would plummet (Sarmiento et al. 2004). Overall, the distribution of phytoplankton biomass and net primary production (NPP) is defined by the bio-availability of light and nutrients, and these growth limiting factors are in turn regulated by physical processes. The complex dynamics combining the different forces shaping the bottom levels of the food web are responsible for the high level of ecosystem diversity and the rise of new adapted species.

Phytoplankton Diversity and Physiology

The ocean is responsible for generating more than half the planetary primary production (Field 1998). In the open ocean, most of the organic biomass occurs in the smallest size fractions categories (cyanobacteria, pico- and nano-phytoplankton), while in highly productive coastal ecosystems, the micro, meso, and macro phytoplankton dominate most of the biomass (Sarmiento and Gruber 2006). The reason for such discrepancy is

due to the nutrient levels that vary widely in time and space for both environments and are found to be more limiting in open ocean compared to the coastal regions. In such cases, low nutrient environment favors species with high surface-to-volume ratios for efficient nutrient absorption resulting in the dominance of small phytoplankton cells under oligotrophic conditions and creating an evolutionary motive for adopting non-spherical shapes and internal vacuoles (Behrenfeld et al. 2008b). On top of evolving different strategies adapted to nutrient conditions, phytoplankton cells also need to optimize their growth under distinct environmental physical conditions. After nutrients, light, temperature and salinity are considered to be the major elements dictating the shape of the phytoplankton community and individual species within the community will respond differently to the environmental variations.

Phytoplankton photosynthesis links global ocean productivity and climate-driven fluctuations in the physical and chemical environment. In other words, the effect of the interactions between the diverse physico-chemical combinations is expressed through the changes in phytoplankton physiology and productivity. These interactions require an accurate understanding of environmental factors, which in turn regulate phytoplankton growth (Behrenfeld et al. 2008a). Phytoplankton physiologists have made an effort over the past few decades to elucidate the controlling factors, conditions, mechanisms and strategies that control phytoplankton cell growth. Characterizing the phytoplankton physiological status on a global level still remains challenging (Behrenfeld et al. 2009; Cullen 2009). For this reason, most of the hypotheses assessing the importance and impacts of these fluctuating variables are tested in the laboratory using single cell species exposed under very tightly controlled conditions. Amongst the controlling factors, nutrients, light, temperature, salinity and pH are the ones playing a major role in the growth success of the cells.

Although conditions in laboratory cultures are simplistic and cannot hope to duplicate the complex conditions encountered in the field, they can be used effectively

to identify potentially important parameters. Laboratory experiments in a controlled environment permits to examine the effects of singular variable on phytoplankton physiology. The cyanobacteria *Prochloroccoccus* and *Synechococcus* are the two most abundant and widespread taxa throughout the world's oceans. For this reason, and because they are relatively easy to grow, they have been used extensively in laboratory experiments. These two cyanobacteria are known for their small size and their physiological characteristics that allow them to maintain the growth of their population or even dominate in a changing climate (Glover et al. 1988; Carey et al. 2012). Several experimental studies using these two laboratory models helped the scientific community to understand how the physiological machinery of phytoplankton cells reacts to an artificial induced stress. Amongst the past studies, Moore et al. (1995) tested the physiological effect of light on *Prochloroccoccus* and *Synechococcus* growth by exposing the cells to different light regimes and found differences in terms of absorption and light utilization for both species. At that time, the tolerance of *Synechococcus* to cope with higher irradiance compared to *Prochlorococcus* was the factor explaining most of its ubiquity in shallower waters compared to deeper waters. Some years later, Moore et al. (2002) showed that not only low light and high light adapted ecotypes are responsible for partitioning the distribution of *Synechococcus* and *Prochlorococcus* in the water column but also their nitrogen (N) utilization capabilities. In this case, *Synechococcus* is limited to surface waters because they cannot balance the high cellular N required for their N-rich phycobilisomes, since the low light levels in the deep euphotic zone may not provide enough energy to reduce NO_2^- to NH_4^+(Carr and Mann 1994). This type of finding not only added a level of complexity due to new factors modeling phytoplankton community but also opened a new door to co-limitation phenomena, which is an omnipresent condition in the global ocean. This highlights the importance of considering the inter-play between the different stressor when transposing the theory behind laboratory experiments to natural environmental conditions.

DMSP as an Intra-Cellular Osmolyte

Quantifying the effect of physico-chemical stressors on phytoplankton physiology can be done through phytoplankton growth measurement, chlorophyll content, fluorescence level and intracellular molecular compounds synthesized by the phytoplankton cells. Among the most common natural products in marine organisms, dimethylsulfoniopropionate ($(CH_3)_2S^+ CH_2CH_2COO^-$; DMSP) is found to be an important one and stands out as a major carrier in organic sulfur transference and cycling through the trophic levels.

DMSP is synthesized by various groups of phytoplankton species and its intracellular concentrations vary across five orders of magnitude among phylogenetic groups (Stefels et al. 2007). The high DMSP producers are mostly small eukaryotes and found in high concentrations in the cytosol of prymnesiophytes, dinoflagellates, chrysophytes, prasinophytes, and pelagophytes and at lower concentrations in typically bigger size cells such as diatoms (Keller 1989; Stefels et al. 2007).

The physiological role of intracellular DMSP is still not clear and can serve as a primary or a secondary metabolite (Stefels 2000; Steinke et al. 2002; Yoch 2002). DMSP can be resumed as a multifunctional compound and an anti-stress molecule because of the several physiological roles it plays in the cytosol of the cell. Besides its primary function as osmolyte, DMSP hypothetically participates in cells homeostasis by serving as an overflow mechanism for excess reduced sulfur when the cells are under unbalanced growth (Stefels 2000), a methyl-donor in metabolic reaction (Kiene et al. 1999), as a part of an anti-oxidant cascade to help cells regulate themselves under light and nutrient stress (radical scavenger; Sunda et al. 2002) and as a cryoprotectant under extreme conditions (Karsten et al. 1996; Malin and Kirst 1997).

The Fate of DMSP in the Water Column

Pathways through which intracellular/particulate DMSP (DMSPp) is released into the dissolved phase (DMSPd) are algal exudation, cell lysis due to auto-lysis or senescence (cell death) or to viral lysis and micro-zooplankton grazing (Stefels et al. 2007; Figure 4). Once released in the water column, DMSPd becomes one of the most abundant reduced sulfur compounds bio-available in the surface seawaters (Malin et al. 1993; Kwint and Kramer 1996) and its fate is dictated through different mechanisms. Since sulfur is an essential compound to all organisms because of its ubiquity in proteins and other important biomolecules, DMSPd is highly used by the microbial community and undergoes active microbial cycling in the seawater (Kiene et al. 2000; Moran et al. 2012). DMSPd also serves an ecological role related to its photosymbiotic interactions, like those in corals (Broadbent and Jones 2004; Van Alstyne et al. 2006), flatworms (van Bergeijk et al. 2002) and the planktonic protists Acantharia (Decelle et al. 2012), which might be related to its antioxidant function. On top of that, recently it has been discovered that DMSP acts as a strong chemoattractant for heterotrophic organisms (Seymour et al. 2010).

DMSPd can be taken up by phytoplankton cells (Vila-Costa et al. 2006) but is mostly used by bacteria for fulfilling up to 100% of their sulfur needs and 13% of their carbon needs (Kiene et al. 1999, 2000, Simó et al. 2002). A substantial fraction of the natural DMSP turnover results in incorporation of sulfur into bacterioplankton (Kiene et al. 1999). Indeed (the most common scenario), when limited in sulfur (high sulfur demand), marine bacteria will primarily use the DMSP demethylation/demethiolation pathway to generate MeSH, which can be incorporated directly into methionine or oxidized to sulfates (Kiene et al. 1999). Conversely, when demand is high in carbon (carbon limited), the bacterial community will use the enzymatic lyase pathway (DMSP-lyase) that cleaves DMSP into dimethylsulfide (DMS) and acrylate with the generation of a proton. Some phytoplankton cells also possess the DMSP-lyase intra or extracellularly

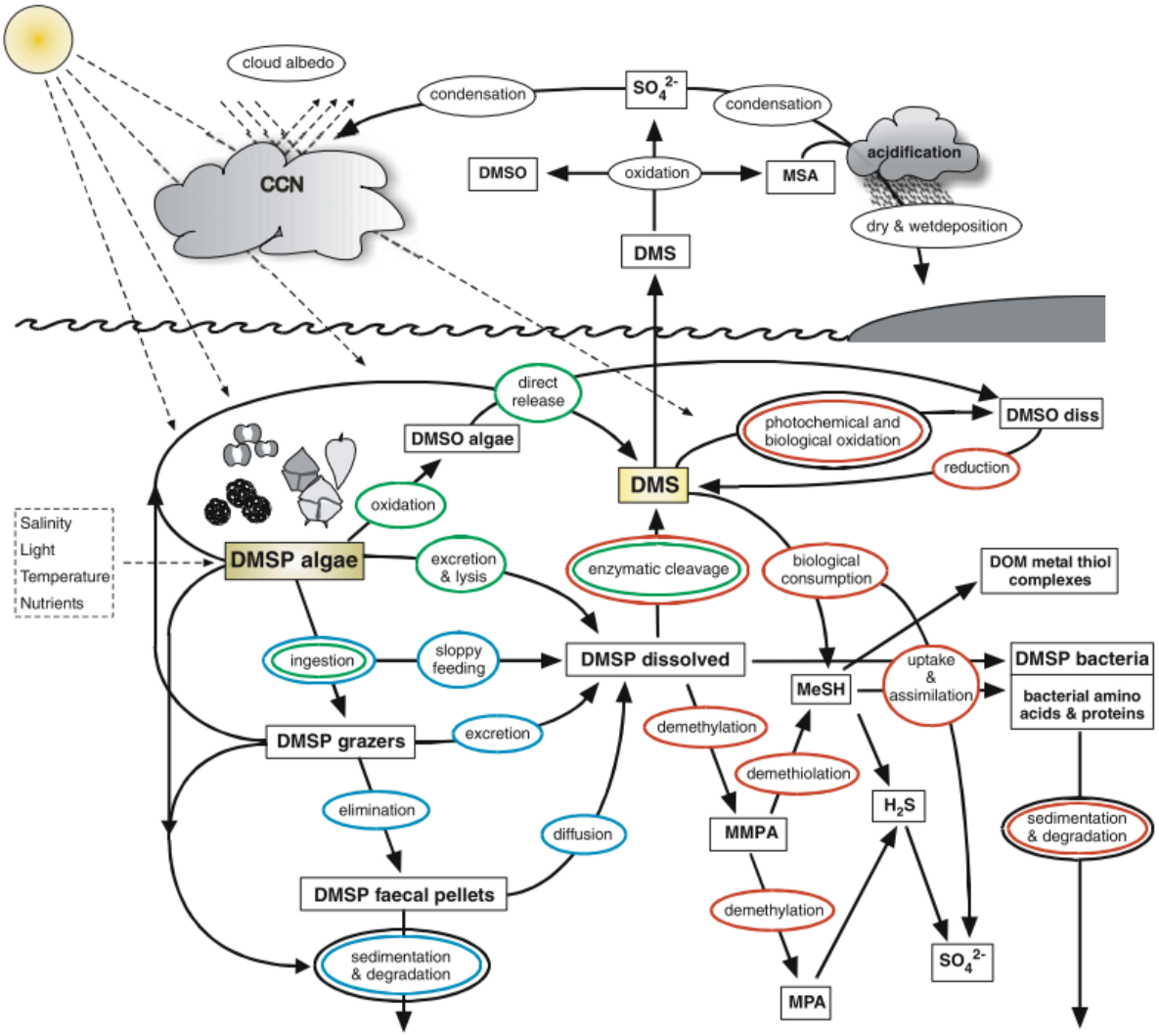

Figure 4: Current view of DMS(P,O) cycling processes - Dominant role of functional groups is indicated by colored ellipses: green, phytoplankton; blue, zooplankton; red, bacteria; black, abiotic factors. CCN, cloud condensation nuclei; DOM, dissolved organic matter; MeSH, methanethiol; MPA, mercaptopropionate; MMPA, methylmercaptopropionate; MSA, methanesulfonic acid; see text for other abbreviations; from Stefels et al. (2007).

which also permits them to generate DMS (Stefels and Dijkhuizen 1996; Figure 4). However, only a small fraction of the DMSP synthesized will result in DMS, but this fraction is very important since DMS is the major sulfur compound emitted from the oceans to the atmosphere and is known for its hypothesized role in climate regulation of the Earth (Charlson et al. 1987). DMS has also been commonly attributed for being responsible for the "odor of the sea" (White 1982).

DMS: the Odor of the Sea

The knowledge gained on DMS and its precursor DMSP over the last 40 years is of such extent that they make some of the best-studied organic substances in the world's oceans. Although controversial for its role in the plankton-climate feedback loop (Charlson et al. 1987; Quinn and Bates 2011; Iizuka et al. 2012), DMS plays a crucial role for the recycling of sulfur from oceans to continents through the atmosphere (Lovelock 1972; Simó 2001). Lana et al. (2011) estimated that ca. 28.1 Tg of sulfur are transferred from oceans into the atmosphere annually in the form of DMS. In the atmosphere, DMS participates in aerosol formation and growth through homogeneous and heterogeneous nucleation (Andreae and Barnard 1984; Hegg et al. 1991). This has important implications for cloud microphysics in remote marine regions (Vallina et al. 2006; Andreae and Rosenfeld 2008). Although only a minor fraction of dissolved DMS is vented to the atmosphere (10%; Kiene and Linn 2000), its role in the food web is still being expanded because once in the gas phase, DMS is used as an olfactory signal sensed by marine mammals (Kowalewsky et al. 2006), marine turtles (Endres and Lohmann 2012), reef fishes (DeBose et al. 2008) and birds (Nevitt 2008; Wright et al. 2011) before being oxidized and causing accretion of sulfate aerosols.

Fate of Oceanic DMS

The fate of most seawater DMS is not dominated by photolysis and neither is dominated by ventilation. In most cases, DMS is lost much faster by microbial utilization (Simó 2004). Although generally not a major sink, photolysis is still an important DMS removal process in the upper ocean (e.g., Brimblecombe and Shooter 1986; Kieber et al. 1996; Brugger et al. 1998; Hatton 2002). Because DMS does not absorb light at wavelengths >260 nm, photolysis occurs through a secondary photosensitized pathway, mainly mediated by colored dissolved organic matter (CDOM; Brimblecombe and

Shooter 1986). CDOM and nitrates absorb UVR and act as a photosensitizer for the photochemical destruction of DMS (Brimblecombe and Shooter 1986). DMS photolysis depends highly on CDOM distribution with a small contribution in the open ocean and larger one in coastal waters. Interestingly, Kieber et al. 1996 looked at the impact of UV photo-oxidation on DMS and concluded that it could be almost as fast as bacterial utilization and significantly faster than ventilation at the surface waters in low latitudes of the Pacific which is contrary to the general understanding with microbial consumption being a major factor in DMS removal. The authors gave an explanation related to UV attenuation within the water where the relative strength of the photochemical sink would decrease as the water column (MLD) becomes thicker. Soon after, Simó and Pedrós-Alió (1999) estimated DMS photolysis rates in the mLD of the subpolar North Atlantic and compared them with microbial consumption and ventilation rates. The results obtained showed that photo-oxidation dominated DMS sinks under conditions of high irradiance and shallow mLD, whereas bacterial consumption dominated under deep mLD and high irradiance. Even ventilation, generally considered a minor sink, became comparable with bacterial consumption during a windstorm event (Simó and Pedrós-Alió 1999), showing that environmental forcing can change the balance between the different DMS loss processes. If we consider the most common scenario where bacterioplankton act as a major sink in DMS and DMSP (hereafter referred to as DMS(P)) utilization, the natural fluctuations in factors controlling bacterial activity such as UV-B radiation, temperature, nutrients and dissolved organic matter (Kirchman 2000) ultimately need to be considered because of their indirect role in controlling DMS concentrations. This shows that depending on environmental conditions affecting all inter-connected factors, the proportionality between different DMS sinks may vary.

What can a bottle tell us about DMS and DMSP driving factors?

Apart from the loss processes of ventilation, photolysis and microbial consumption responsible of removing DMS at the surface water, other physico-chemical forcing of different kinds play an important role in controlling the dynamics of DMS(P). As a starting point in the cascade of bio-physiological effects on DMS(P) cycling, several factors controlling the phytoplankton production of DMSP have to be considered. Amongst them, nitrogen and iron availability, water transparency, solar irradiance fluctuations, temperature and salinity are found to play a role in controlling DMSP levels. Here are only few examples of the many studies touching the effect of controlled factors on DMS(P) cycling. In 2001, Simó summarized that nitrogen availability affect DMSP biosynthesis and accumulation in phytoplankton and implied that the probability of finding higher levels of DMSP is greater under conditions of N depletion. This is mostly because of phytoplankton succession where diatoms (low DMSP producers) have evolved to be more adapted to conditions of N repletion compared to smaller size species (composing most of the high DMSP producers) and one should not expect strong shifts in DMSP levels in response to very short pulses of N supply. Bucciarelli et al. (2003) conducted laboratory experiments comparing the effect of growth limitation by different environmentally relevant macro-nutrients (nitrate, phosphate and silicate) and examining the interrelationships among nutrient limitation, Chl*a*, and intracellular DMSP concentrations. They observed that the intracellular DMSP concentrations increased exponentially with decreasing growth rate and cellular Chl*a*, in response to the type and degree of nutrient limitation. They also opened a new door to the possible importance of diatom blooms in global sulfur cycle, generally known as poor DMSP contributors. The effect of light intensity and the bio-availability of iron, a micro-nutrient known to be essential for cell growth, metabolism and physiological functions

of phytoplankton cells have also been recognized for their role in dampening DMSPp production under different light regimes (Bucciarelli et al. 2013). Such co-limitations between different controlling factors added a level of complexity in the design of laboratory studies. However, the assessment of several inter-related driving forces is primordial for a better understanding of the physiological response at an ecosystem level. Of course, the ideal scenario represents a closed and controlled environment where biological, chemical and physical external forces can be combined and tuned independently of each other and this being tested from mono-clonal cultures (single cell specie) up to ecological populations (natural communities). This is what modelers tend to achieve using hypothesis and conclusions drawn from short-term laboratory experiments. However, for the models to be accurate a better understanding of mechanisms driving DMS(P) needs to be achieved.

Proposed Mechanisms linking Phytoplankton Physiology to DMS production

Laboratory experiments have lead the research forward in proposing new hypothesis and describing mechanisms that are still being tested and revisited today. Amongst them, the overflow mechanism suggests a production and release of DMSP to respond to a need for dissipating excess energy and excess reduced sulfur because of unbalanced growth by scarcity of nutrients (Stefels 2000). DMSP synthesis in this case plays a role in the maintenance of photosynthetic efficiency. Similarly, the controversial (Stefel et al., personal communications) antioxidant hypothesis (Sunda et al. 2002) showing that DMS, DMSP and dimethylsulfoxyde (DMSO) are effective scavengers of reactive oxygen species (ROS) and participate in cascade reaction system against oxidative stress, has been proposed over 12 years ago and is still used regularly as a physiological explanation for DMS build up under stress conditions. According to this

hypothesis, sulfur compounds play an important intracellular role that could potentially prevent cell damage. Finally, damage and repair mechanisms to counter act harmful physiological effects following short or long-term stress conditions play a major role in the acclimation, adaptation and evolution processes of the cells (Galí et al. 2013a). In order to integrate the different mechanisms involved in DMS(P) cycling, Gali et al., (2013a) proposed that overflow and antioxidant mechanisms could be integrated in an overflow-antioxidant-damage continuum, focusing on the pivotal role of phytoplankton DMS(P) release. The authors suggest that for a given exposure to irradiance, individual phytoplankton population will contribute preferentially to DMS production through overflow, antioxidant, or damage mechanisms, depending on its sunlight sensitivity, its constitutive photo-protection strategies, and its DMSP-cleaving capacity (Galí et al. 2013a). This is a very good example of the complexity of DMS dynamic and how the integration of DMS processes can help answer questions related to physiological response of the phytoplankton population in relation to DMS cycle at the food web level. Furthermore, it emphasizes the presence of several regulating factors connected to the proposed mechanisms and hypothesis, which makes DMS cycling a multifaceted problem and that requires tackling from different sides.

Factors driving DMS Distribution and Variability in the Ocean

Over the years, the interest in DMS dynamics has not only increased but has also diversified, resulting in an even more complex subject to study (Figure 4). The path linking phytoplankton to DMS through DMSP is far from being straightforward and even today predicting DMS at the global level is a grand challenge. The most common index of phytoplankton abundance and primary productivity is the distribution of Chl*a* but attempts to correlate DMS to Chl*a* on a global scale have failed (Figure

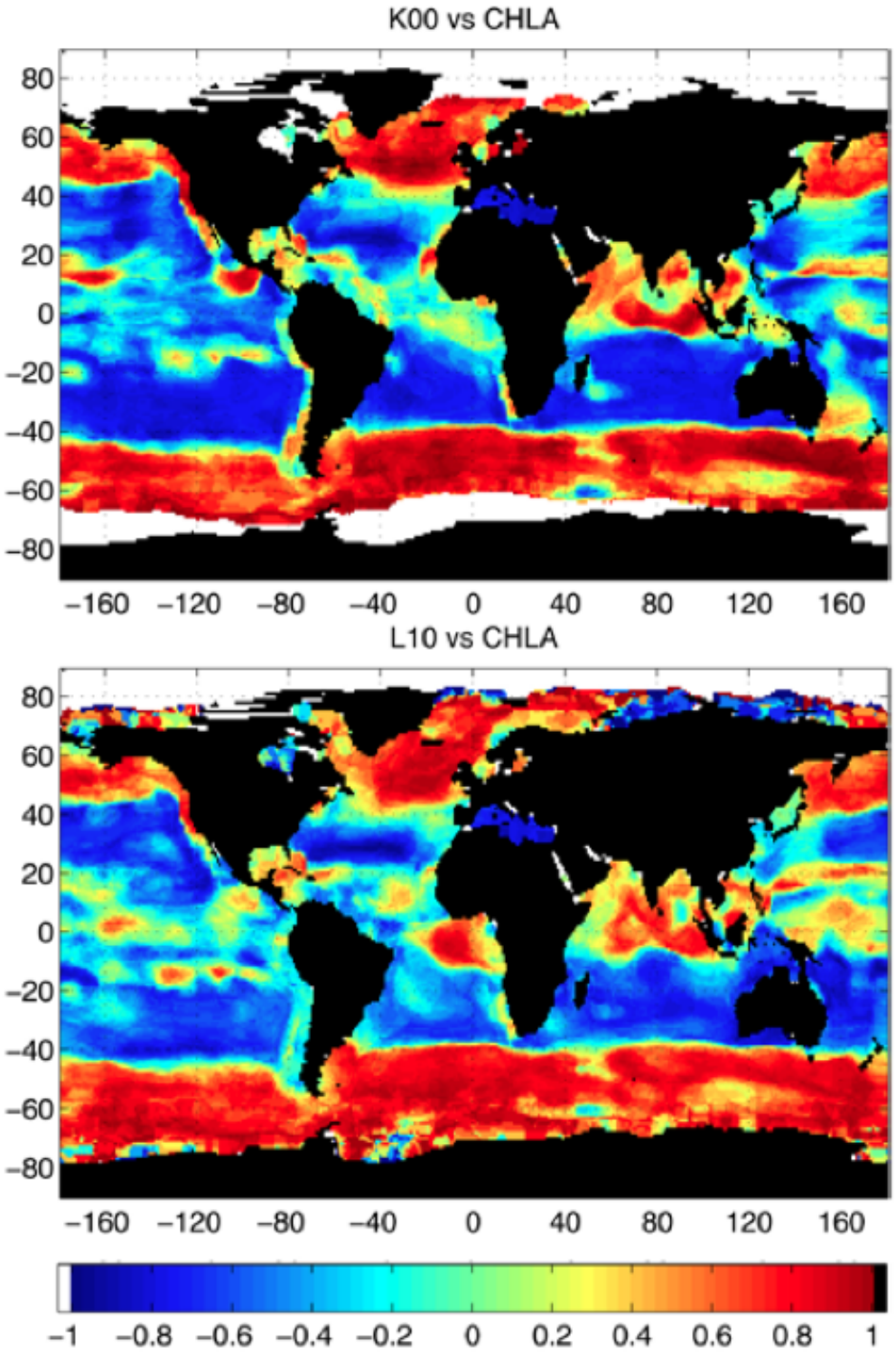

Figure 5: Global distribution of Spearman's rank coefficients of correlation between monthly series of Chl*a* concentrations (SeaWiFS climatology of the years 1997–2009) and A. K00: DMS climatology by Kettle et al., (2000), and B. L10: Updated DMS climatology by Lana et al., (2011).

5; Kettle et al. 2000; Lana et al. 2011). One could think than the obvious reason for this unintuitive result is related to the cell specificity of DMSP producer, but still the taxonomy dependence of DMSP production in algae does not explain accurately DMS global distribution. Bell et al. (2010) reported that no correlations were observed with typical biomarker pigments for DMSP-producing species using compiled data from the Atlantic Meridional Transect. However a strong correlation was found between DMSP and primary production by cells >2 um in diameter. A potential reason for any proportionality of DMSP to phytoplankton not being transferred to DMS is that DMSP breakdown into DMS involves several different metabolic steps (Figure 4) that are tuned according to the combination of environmental conditions. For DMS to be produced, it first requires DMSP being released extracellularly for which the rate will depend on the physiological state of the algae that depends on the physico-chemical conditions (nutrient availability, salinity, temperature and solar irradiance) of the water mass. Once in the water column, the fate of DMSPd will depend on the microbial community composition and its consumption rate which varies according to bacterial limitations (sulfur and carbon) and how solar irradiance affects their cycling (i.e. UVR reduces DMSP microbial consumption (Toole et al. 2006; Ruiz-González et al. 2012)). In the case of a microbial enzymatic cleavage of DMSP leading to DMS release, different loss mechanisms come into play and might restrict DMS from building up in the water column. Eventually the fraction of DMS escaped to the atmosphere is very small compared to algal DMSP production and rarely proportional (Kettle et al. 2000).

The recent advances reinforce the fact that DMS net production is related to food-web dynamics and not just to phytoplankton taxonomy, physiology and activity. Already several actors are involved between DMSP synthesis and DMS production, which is not a direct action of phytoplankton, but results from a complex set of food-web interactions where physico-chemical forcing factors potentially operate at all stages of the DMS(P) cycle and may sometimes act in opposite ways which makes the global picture even more complex.

For this reason, researchers have tried exploring the relative importance of selected environmental forcing factors on to DMS(P) dynamics.

Environmental forcing factors refer to the measurable or predictable physico-chemical variables that drive the action of the actors at any time frame, by initiating, enhancing, limiting, or suppressing it (Simó, *in preparation*). To give a few examples of possible drivers, in 1999 an empirical hypothesis by Simó and Pedrós-Alió suggested that the DMS production yield varies non-linearly with the oceanic MLD, probably because of differential photo-inhibitory effects of UV on phytoplankton and bacteria. In 2001, Anderson et al. identified high DMS production regions matching with high light, not severe nutrient limitation, and enough decoupling between primary production and grazing. Accordingly, the authors related DMS to a proxy of the algal growth rate to produce monthly global maps of surface DMS concentration, where regions of high DMS concentration were better represented than regions of low DMS concentration. Aumont et al. (2002) and Belviso et al. (2004) proposed a nonlinear parameterization that uses Chl*a* and a community structure–trophic state index for DMS prediction. They observed that DMSP occurs mostly in nano- and picophytoplankton and that DMSP is converted more efficiently into DMS when the fraction of phytoplankton contributed by the smaller algae is either very high or very low. A critical evaluation of these parameterizations was written soon after (Vézina 2004), where the author suggested that ecosystem-based dynamical approaches should be explored alongside empirical approaches for modeling global scales. Simó and Dachs (2002) were able to predict surface DMS distribution under biophysical conditions, where they suggested that the MLD can be used as the variable that integrates most of the environmental effects, either on its own, or in combination with Chl*a* concentrations. As the last example, very recently Kameyama et al. (2013) found a significant correlation with the net community production, a parameter that integrates biological activity over time in the western subarctic North Pacific Ocean.

Solar radiation intensity has been observed to exert a strong influence on DMS dynamics as a result of its multiple photochemical and photobiological effects (Simó 2004). Studies in both temperate (Kwint and Kramer 1996) and subtropical (Dacey et al. 1998) waters have found that the seasonal trends in DMS concentrations can be decoupled from the temporal changes in DMSP concentrations. A more thorough study in the Sargasso Sea helped explain this temporal decoupling where the maximum DMS accumulation occurs in summer, coupled with the minimum of Chl*a* and two months after DMSP peak. As mentioned above, this phenomenon is referred to as the *summer DMS paradox* where the authors suggest that the main agent triggering this pattern is increasing irradiance leading to light stress-induced DMS release from phytoplankton cells (Simó and Pedrós-Alió 1999).

Recently Polimene et al. (2011) revisited the hypothesis and refuted the biology light driven scenario previously proposed. The authors suggested a two-way approach to explain the phenomenon: (1) a succession of phytoplankton types in the surface water and (2) the bacterially mediated DMSPd to DMS conversion, seasonally varying as a function of nutrient limitation, further underlining the major role that bacteria potentially play in DMS production and fate. In the past, Toole and Siegel (2004) found that daily UVR could explain more than 77% of the DMS variability in the MLD in the Bermuda Atlantic Time-series Study (BATS) and might be a key factor for understanding the seasonal variations in the ratio of DMS to DMSP. The authors also suggested the presence of two regimes in the world's oceans: a stress regime and a bloom regime. The stress regime describes conditions when DMS and Chl*a* are decoupled, and DMS production occurs in response to oxidative stress, as proposed by Sunda et al. (2002). According to the authors, such a regime will occur mostly in oligotrophic gyres where nutrient concentrations are low and solar radiation high. On the other hand, the bloom regime will involve DMS concentrations being in consortium with levels of Chl*a*, such as productive regions including upwelling and coastal waters.

In 2007, Vallina and Simó proposed an increase in DMS with increasing solar radiation dose in the UML (SRD) of the open ocean, irrespective of latitude, plankton biomass, or temperature. This hypothesis has been challenged by Belviso and Caniaux 2009 and by Belviso et al. 2011. These authors believe than first the relation between SRD and DMS is very sensitive to the irradiance attenuation selected in the MLD and that relative DMS concentrations in five of the most oligotrophic regions of the world's oceans were better accounted for by their nutrient dynamics (specifically phosphorus limitation) than by physical factors such as SRD. Miles et al. (2009) also reviewed the relation between DMS and SRD and questioned the method because of the estimated surface insolation (I_0) that does not realistically account for cloud cover, especially at the temporal resolution Vallina used. The authors suggests to pay attention to the MLD component and review the light calculations by utilizing a cloud adjusted, surface irradiance product at a wavelength (UVA) with an implicated role in DMS(P) dynamics. Soon after, a study by Archer et al. (2009) concluded that PAR dose could explain 68% of the variability in DMSP/Chl*a* but only 25% of the variation in DMS concentrations. A following study showed that DMS production by phytoplankton can increase by up to one order of magnitude due to UV stress (Sunda et al. 2002; Archer et al. 2010). Finally, Miles et al. (2012) proposed that both underwater irradiance and primary production can act as controls for explaining DMS(P) concentrations where a multivariate regression analysis explains 55% of the variance for euphotic zone and 66% for surface waters. This further suggests an important role for solar irradiance in mediating the relationship between the productivity of the ecosystem, DMS(P) production and ambient seawater DMS concentrations.

Emergent relationships at more local scales have however been found and explored for their driving roles and their potential to be used in DMS prediction over large scales. Although predicting DMS levels using Chl*a* is a challenge at global level, more localized

studies succeeded. For example, in areas where coccolithophores accounted for 50% or more of the total carbon biomass, statistically significant positive correlations between DMSPp and Chl*a* were found (Malin et al. 1993). Additional studies in the Arctic also showed DMS concentrations being positively correlated with DMSPp ($r = 0.89$) and Chl*a* ($r = 0.74$; Luce et al. 2011). This gives importance to localized studies that act as natural laboratories with well defined and relatively homogenous environmental conditions. Local studies also help unrevealing factors regulating production of DMS that are still today poorly understood in most of the world's oceans.

An additional aspect to the complexity of the system is the distinct dynamic operating seasonally and across latitudes, which makes DMS prediction across the scales (day/night, seasons, years) even more difficult to define. For example at local scales, underwater irradiances can be highly variable in space and time, inducing a range of physiological states from photoinhibition to light limitation as a result of mixing (depth variations), self shading, and insolation changes due to cloud cover variation or diurnal variation (MacIntyre et al. 2000). More of these localized studies highlighting different processes for different regions during different times of the year will help the modelers at better predicting DMS distribution at different scales in the world ocean.

How fast does DMS fluctuate? All a matter of time/space scale

Over the global oceans, DMS concentration in surface ocean water is known to vary geographically and seasonally over a wide range between about 0.1 nM (oligotrophic gyres) and 350 nM (Southern Ocean). A way to understand the links between DMSP and DMS dynamics within the food-web structure is by introducing the temporal and/or spatial variability component integrated within the DMS cycling processes. Because of the usual limited time at sea, most field studies have provided only snapshots of the

DMS cycle, which is usually representative of one season in one oceanic region. This is of course useful for revealing potential couplings and decouplings, however, it can be misleading if extrapolated to longer timescales. Extrapolations are however unavoidable considering the gaps in data collection in some unvisited regions of the world ocean (Lana et al., 2011). Spatial and temporal variability of the ocean is a fundamental property when assessing oceanic dynamic and the climate system, and therefore the ocean circulation can never be regarded as being in a true steady state. To expand the knowledge and help unravel the dynamics of the sulfur cycle in relation to a dynamic environment, a collection of DMS data measured through different seasons, through short-term (e.g. storms, tides, day/night fluctuations) and long-term (e.g. El Niño) overturning events, through the vertical column, through biogeochemical provinces or mesoscale hydrodynamic structures and ideally through Lagrangian studies should be used.

There are numerous ways of looking at the data and it highly depends on the scale under consideration. The emerging patterns and features have to be studied and understood individually but in the end they need to be integrated and regarded as a whole to be propagated to the Earth system (Figure 6). Primarily, temporal and spatial variability should be distinguished to allow the data to be comparable between them.

Temporal variability

Temporal variability refers to the variability of time in space and can be interpreted according to different scales. The question is: what is the correct way of determining the scales to be used? Geo-meteorological forcing factors can be used as markers for limiting the borders between different scales. Amongst the forcing factors, solar irradiance reaching the Earth's surface at a given geographical position can be a temporal scale divider by dictating the length of the day (day/night fluctuation) as well as the changes in season, which can be identified as short- and long-term effects, respectively. On the other hand meteorological conditions also play an important temporal role scaling from

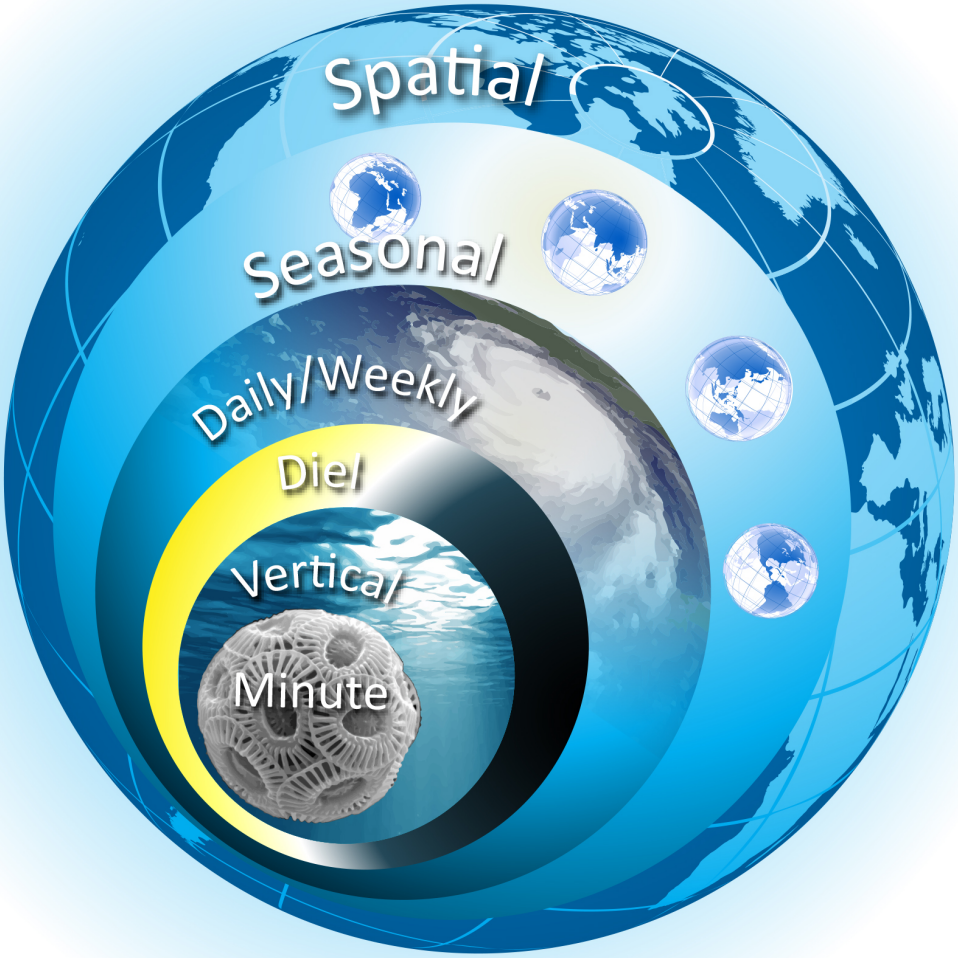

Figure 6: Scheme representing temporal and spatial dynamic that any oceanic ecosystems is exposed too. Variability occurs over different scale frames where short-term temporal variability (minute-diel) affects long-term one (seasonal-yearly) and vice-versa.

sporadic short-term events (i.e. tides, storms) in some cases and in long-term overturning events (i.e. El Niño, yearly – inter-annually) in some other cases. An additional finer scale could also be named the minute (nano) temporal scale, which could be looked at for physiological response of microbial community following a sudden change such as solar irradiance variability caused by the passage of a cloud.

Few studies have addressed in detail the evolution and the short-term variability of DMS cycling that occurs over timescales of hours to weeks (e.g. Turner et al. 1995; van Duyl et al. 1998; Le Clainche et al. 2004). In 2008, Gabric et al. looked at the diel cycle dynamic and concluded that DMS tended to be buffered because of the opposing effects of sunlight-related biological production, sunlight-inhibited biological consumption, and sunlight-mediated photo-destruction. In 2013, Galí et al. demonstrated that in the Sargasso and Mediterranean Sea waters over the four seasons, DMS budgets showed marked day versus night variability translated into highly variable but nearly balanced surface ocean DMS budgets. The authors proposed light as the main driver of DMS variability and suggest that an interplay mechanism between cumulative and instantaneous light exposure drive DMS gross production in summer. In this case, the cumulative component would be related to UV-induced irreversible damage, and the instantaneous component, to photosynthesis-related physiology. The largest amplitude in DMS concentrations occurs at the seasonal (semi-annual) scale, which are usually much larger than short-term temporal variability and much wider than the inter-annual variability at a given season, which do not exceed a factor of two (Dacey et al. 1998; Ayers and Gillett 2000; Sciare et al. 2000). These studies indicate that the variability rates increase when driven by the dynamics of the oceanic ecosystem on daily, weekly and seasonally time scales as revealed by lagrangian observations, which do not include the spatial component (Simó and Pedrós-Alió 1999; Levasseur et al. 2006; Gabric et al. 2008).

Spatial variability

Spatial variability occurs when a variable measured at different spatial locations exhibits values that differ across the geographical position. It is well known than surface seawater DMS varies geographically and has a peak-to-peak amplitude of c.a. 350 nM with a lowest of 0.1 nM in oligotrophic gyres (http://saga.pmel.noaa.gov/dms/) and a highest with values as large as ca. 350 nM in the Southern Ocean (Tortell et al. 2012).

Spatial variability does not only include the geographical component but also includes the vertical gradient present in the water column, which also varies from region to region and from season to season. One example is the DMS subsurface maxima present in some regions of the world ocean after the winter season (Toole et al. 2006; Bailey et al. 2008). These are specific to a geographical position (spatial scale) and to the time of the year (temporal scale). The "vertical" spatial variability of DMS in the water column will also depend on the light attenuation coefficient and the MLD, which indirectly include the temporal variability. To further segregate the geographical spatial variability we divided it in the following key scales.

Longhurst provinces

Discussing spatial variability at the global level is complex and masks some specific patterns occurring in selected oceanic regions. To group regions and water masses with similar biogeochemical characteristics, classified regions in biogeographic domains (including trades, westerlies, coastal and polar domains) that are further subdivided into 56 biogeographical provinces are used (Longhurst 1998). According to the classification, the vast subtropical oligotrophic gyre regions with low nutrients and low biological productivity cover the largest surface and are the main focus in the thesis. These important ecological regions originate more than 50% of the DMS ventilated from the ocean to the atmosphere (Kettle and Andreae 2000).

Mesoscale variability

Because the ocean is not in a steady state, temporal and spatial variability must be taken into account while discussing emergent patterns. The merging of these two different scales leads to local phenomena. Mesoscale phenomena represents one of them and is one of the most dominant oceanic contributor in the spectrum of chlorophyll variability (phytoplankton productivity). This oceanic feature is due to ocean eddies created in unstable flows that act as a mixing agent or isolated vortices, meandering currents or

fronts, squirts and filaments. The mesoscale variability generally refers to ocean signals with spatial variability of tens to a few hundred km and temporal variability of few days to weeks, which comprises most of the oceanic phenomena (Doney et al. 2003). Its presence in the ocean has a strong impact on the ecosystem since it isolates geophysical properties of a water mass that leads to the evolution of a unique ecological population (Sarmiento and Gruber 2006).

Given the complexity of the oceanic DMS cycle, the spatial heterogeneity of surface concentrations is difficult to resolve using conventional analytical methods and ship-based surveys of discrete sampling stations. Indeed, low-resolution data prevents us to assess the real variability scale and this is why the use of high frequency instrument for measuring fast moving processes is necessary. Yet there are very few studies looking at DMS variability using high frequency data. To our knowledge only Nemcek et al. (2008) and Asher et al. (2011) reported an estimate of the length of variability for DMS off British Columbia coast. They attributed a variability length of ca. 7 km for DMS, which is considered to be representative of the sub-mesoscale variability and much lower contrary to what was previously thought. These studies give insight on how DMS is variable in the ocean and can be seen as a new way to compare the dynamic of oceanic biological and physical features (measured at the same frequency) with the one of DMS.

Towards New Technologies

To better understand the system and explain DMS dynamic between the numerous inter-related variables, the frequency of the data collection plays a major role. To date, most of the oceanographic DMS measurements have been obtained using standard purge and trap gas chromatography (GC) methods, a time-consuming gas extraction method with a sampling frequency typically on the order of two to six measurements per hour (Bell et al. 2012). Although many questions have been answered with the use of this technique,

details related to the description of DMS spatial distribution is still poorly reported compared to the number of field campaigns studying DMS. The recent DMS updated climatology (Lana et al. 2011) has clearly demonstrated large-scale spatial and temporal variability in surface water DMS concentrations but still significant uncertainty remains concerning the fine-scale dynamics of this gas (Belviso et al. 2004a; Tortell et al. 2011).

To help resolve this issue, instruments collecting data at high frequency are necessary. Tortell et al., (2005) was one of the pioneers in the field and made high-frequency real-time gas measurements using a membrane inlet mass spectrometer (MIMS) to reveal significant small-scale heterogeneity in the distribution of DMS and other gases. The authors suggested that previous field studies might have under-estimated the true spatial variability of DMS in surface waters, which would be even more dynamic than previously believed for dynamic marine systems. Marandino et al. (2005, 2007, 2008, 2009) also made high-frequency underway measurements of DMS in surface seawater for eddy correlation air/sea flux measurements using an atmospheric pressure chemical ionization mass spectrometry system coupled with a continuous-flow membrane equilibrator (Eq-APCIMS) designed by Saltzman et al., (2009). Kameyama et al. (2009) used a proton transfer reaction-mass spectrometry (PTR-MS) for highly time-resolved measurements of DMS in the open ocean in the western subarctic North Pacific Ocean. To date very few groups are using such instrumentations and studies with DMS high-frequency data are scattered. Even though it has been suggested that small-scale variability is pervasive in the oceans (Doney et al., 2003), the processes driving sub-mesoscale variability in the open ocean regions still remain poorly documented. For this reason an effort from the scientific community should be directed towards the common goal of increasing DMS database, especially in regions not previously covered.

Aims and Outline of the Thesis

The central focus of this thesis is to understand the processes that control the oceanic DMS(P) concentrations and the links associated to phytoplankton photophysiology on a variable spatial and temporal scales.

The broad aims of the thesis can be divided in six chapters that are structured around the following key points (Figure 7):

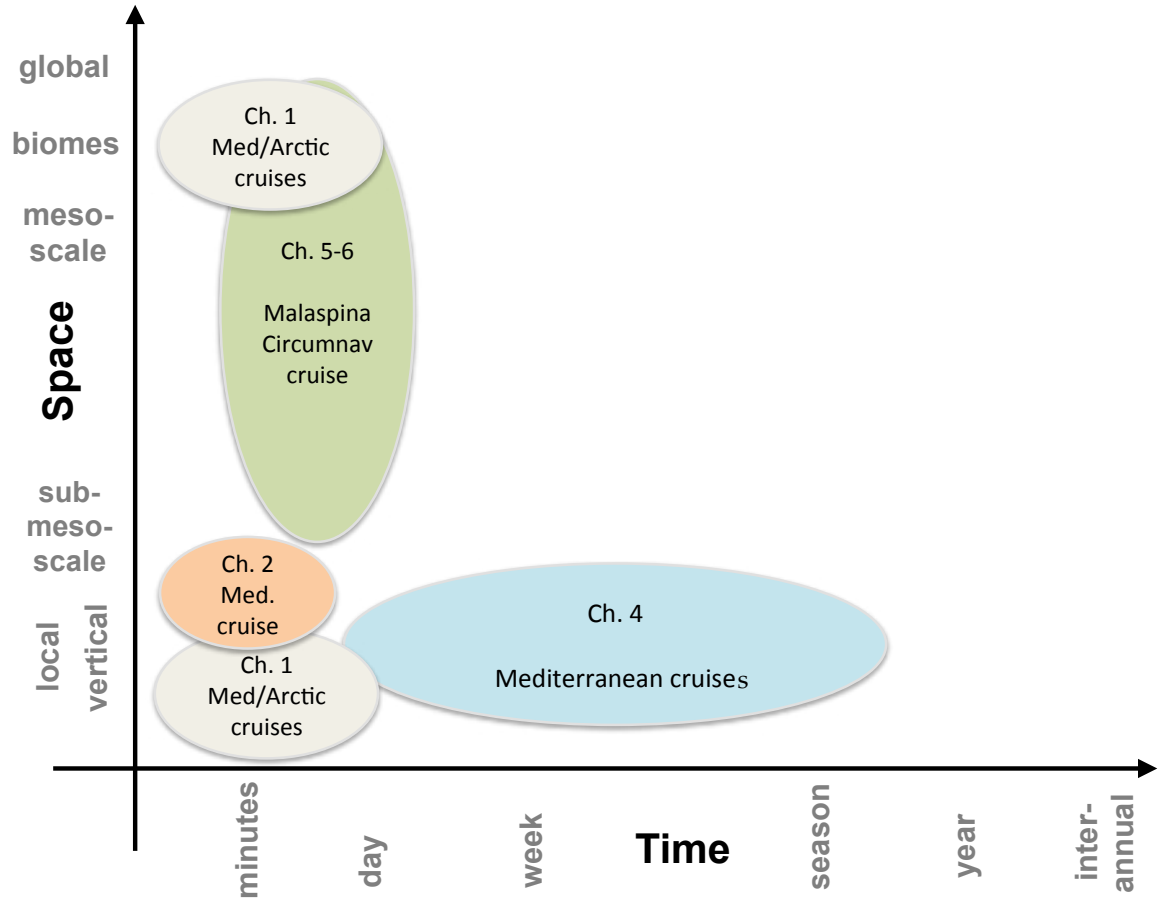

Figure 7: Scheme of the different thesis chapters across the temporal and spatial scales previously described. Although not presented here, chapter 3 consists in the development of a sampling technique, which is somehow linked to most of the data collection described in chapters 4 to 6.

Ch.1: Community level response to light in the short-term (minutes):

Detailing the minute response at the local community level through in situ experiments conducted in polar and sub-tropical environments.

Scale:	- Temporal: Short-term (minute) - Spatial: Vertical (surface/Chl max)
Variables:	- DMS(P) - FvFm - fluorescence
Where:	- Mediterranean Sea - Arctic Ocean

Ch.2: Community level cumulative response to short-term varying light conditions:

Assessing the impact of vertical mixing and changing solar irradiance on DMS(P) variability in the MLD.

Scale:	- Temporal: Short-term (hours) - Spatial: Vertical (mixing layer)
Variables:	- DMS(P) - FvFm - fluorescence - Chl*a* - bacteria - nutrients - light conditions - process rates
Where:	- Mediterranean Sea

Ch.3: Development of a system for measuring high-resolution vertical profiles:

Description of the methodology designed for measuring DMS at very high frequency in the water column. Data comparison also took place for the validation of the instrumentations using dataset for several different cruises from different biogeographical regions of the world ocean.

Scale:	- Temporal: Short-term (- hours - minutes - weeks - seasons) - Spatial: Vertical and Geographical
Variables:	- DMS
Where:	- Mediterraneen Sea - Atlantic - Pacific - Indian Oceans

Ch.4: Ecosystem level dynamics over diel, weekly and seasonal time scales:

Understanding DMS dynamic at the ecosystem level behind several temporal scales using high frequency DMS data collected from the Western Mediterranean Sea.

Scale:	- Temporal: Short-term (- hours - minutes - weeks - seasons) - Spatial: Vertical
Variables:	- DMS(P) - FvFm - fluorescence - Chl*a* - salinity - temperature - density - wind speed - process rates
Where:	- Mediterranean Sea

Ch.5: Meso and sub-mesoscale distribution across large spatial scales:

Associate the variability length scale of DMS to physical and biological drivers within specific Longhurst regions.

Scale:	- Temporal: Short-term (hours) - Spatial: - Mesoscale - Sub-mesoscale
Variables:	- DMS - FvFm - fluorescence - salinity - temperature - density
Where:	- Atlantic - Pacific - Indian Oceans

Ch.6: Ecosystem level distribution and its drivers across biogeographical provinces:

Describe sea surface DMS and identify environmental drivers across the tropical and subtropical oceans.

Scale:	- Temporal: Short-term (hours) - Spatial: - Biogeographical provinces
Variables:	- DMS(P) - FvFm - fluorescence - Chl*a* - salinity - temperature - density - MLD - SRD - zooplankton - phytoplankton - satellite data (- CDOM - calcite - POC)
Where:	- Atlantic - Pacific - Indian Oceans

These chapters are structured as scientific papers, which can result in some reiteration but allows them being read as independent pieces. A brief introduction of each chapter and the hypotheses that were tested is presented below.

Chapter 1: *Short-term effects of solar radiation on phytoplankton photophysiology and dimethylated sulfur production in two contrasting environments (Western Mediterranean Sea and the Arctic Ocean). Submitted.*

UVR is a natural fraction of the solar spectrum which exerts a major influence on biological and chemical processes in the marine environment. Here we assess the impact of PAR and UVR radiation on marine algae following plankton community incubations under different light regimes in two distinct environments, the Western Mediterranean Sea in September 2011 and the Canadian Arctic in August-September 2013.

Chapter 2: *Differential response of planktonic primary, bacterial, and dimethylsulfide production rates to static vs. dynamic light exposure in upper mixed-layer summer sea waters. Published.*

Microbial plankton experience fluctuations in total solar irradiance due to diel cycle but also because of the vertical mixing that creates intermittent light exposure due to the vertical movement of the cells in the water column. Here we assessed the response of the phyto- and bacterioplankton community with physiological indicators using vertical moving bottles in the water column. The effect of dynamic light exposure on the photoinhibition and photoacclimation processes associated to ultraviolet radiation (UVR) was studied along with its effects on gross DMS production.

Chapter 3: *Development and validation of a shipboard system for measuring high-resolution vertical profiles of aqueous dimethylsulfide concentrations using chemical ionisation mass spectrometry. Published.*

Knowledge of what governs DMS production in the surface ocean depends on our ability to measure concentration changes over time and depth. Yet limited DMS data measured at high frequency at the surface ocean are available and quasi inexistent along the vertical gradient of the water column. Here we propose the development of a sampling and analytical system for shipboard measurements of high-resolution DMS vertical profiles with the objective of combining the continuous flow DMS analysis with high-frequency hydrographic, optical, biological and meteorological measurements to help improving the spatial–temporal resolution of seagoing measurements and improve our understanding of DMS cycling.

Chapter 4: *A high-resolution time-depth view of dimethylsulfide cycling in the surface sea. To be submitted.*

Even today there is an important lack in high-frequency DMS data that prevent us from explaining important drivers at a short temporal and spatial scale. Here we present 200 continuous vertical profiles of DMS data at high frequency (30 sec) measured over two seasons in the Mediterranean Sea. We take into consideration the different scales (daily, weekly and seasonal temporal scales and vertical spatial scale) and assess the importance of solar radiation for DMS production.

Chapter 5: *Small-scale variability patterns of DMS and phytoplankton in surface waters of the tropical and subtropical Atlantic, Indian and Pacific Oceans. Published.*

Recent analysis of remotely sensed global ocean color has demonstrated that small spatial-scale variance dominates over most of the oligotrophic regimes, and contributes up to a third of the total variability of high productivity regions. In this study, we visited more than 10 biogeographical regions and try to estimate the variability length scale of DMS and compare it to the variability length of physical and biological drivers in oligotrophic and more productive waters. We also look at the diel pattern of DMS and biological variables using the normalized solar zenith angle for the total length of the cruise (60,000 km), which represents one of the longest data series for a single cruise.

Chapter 6: *Sea surface DMS distribution patterns and environmental and biological drivers across the tropical and subtropical oceans. To be submitted.*

The vast subtropical oligotrophic gyre regions with low nutrients and low biological productivity cover the largest surface ocean and more than 50% of the DMS ventilated from the ocean to the atmosphere originates from these ecological regions. Here we try explaining DMS(P) patterns across oceans using physical, chemical and biological drivers. Besides visiting important under-sampled regions and reporting new DMS(P) values to the database, we unravel some important questions regarding environmental forcing on DMS(P) cycling.

Chapter 1

Short-term effects of solar radiation on phytoplankton photophysiology and dimethylated sulfur production in two contrasting environments (Western Mediterranean Sea and the Arctic Ocean)

Sarah-Jeanne Royer, Martí Galí, Cristina Sobrino García, Antonio Fuentes-Lema, Marjolaine Blais, Michel Gosselin, Jonathan Gagnon, Jean-Éric Tremblay, Maurice Levasseur and Rafel Simó

Abstract

To test the short-term effects of solar radiation on phytoplankton photophysiology and DMSP and DMS production, we conducted 2-4 hours kinetic experiments where seawater samples were exposed to full (PAR+UVR) or UVR-removed (PAR) sunlight. Samples were collected from near the surface and ca. 35 m depth in two contrasting environments: the warm, oligotrophic and stratified Western Mediterranean Sea and the cold, productive and stratified Canadian Arctic, both in late summer. The kinetics of the fluorescence quantum yield of PSII (ΦPSII), measured using a Fast Repetition Rate fluorometer, differed according to the radiation regimes, the sampling depth and the region. Overall, exposure to near-surface irradiance resulted in photoinhibition ranging from 79% to 91% by UVR in all experiments, regardless of the phytoplankton assemblage composition and the irradiance levels. After ca. 30 minutes in the Mediterranean and approximately 100 minutes in the Arctic, steady state or slight increase in ΦPSII were observed for both light treatments. In the Arctic, ΦPSII only showed a slight photoinhibiton by full light, which in some cases recovered totally towards the end of the incubation period. On the contrary, Mediterranean assemblages showed similar photosynthetic response in PAR and full light treatments, potentially linked to high near-surface irradiance and nutrient limitation increasing sensitivity for both treatments. Deeper samples were always more sensitive than surface samples. DMSP variations were sample-dependent rather than spectrum- or photoresistance-dependent. Mediterranean samples generally showed tightly balanced DMSP synthesis and consumption, whereas Arctic samples displayed either net DMSP production (most surface samples) or net DMSP consumption (some photosensitive deeper samples). Differential UVR sensitivity was not related to variations in net DMSP synthesis. Rather, UVR-enhanced DMSP production was found in both a strongly photoinhibited and a photoresistant sample. DMSP to DMS conversion was generally favoured by UVR, which may imply faster DMSP synthesis and turnover under full spectrum sunlight.

Introduction

Ultraviolet radiation (UVR: 280-400 nm) penetrates in marine surface waters where it acts as an important environmental factor with significant effects on many chemical and biological processes, biogeochemical fluxes (e.g., nutrient cycles), species composition and organism survival (Häder et al., 2006; Sommaruga, 2003; Vincent et al., 1984; Zepp et al., 2006). At the cellular level, exposure to UVR produces molecular damage and physiological responses that entail changes in phytoplankton productivity, division rates and mortality (Holm-Hansen et al., 1993; Llabrés and Agustí, 2006; Neale, 2001).

Among the cellular targets, the photosynthetic system is one of the principal sites of UVR photodamage on phytoplankton. UVR causes inhibition of photosynthesis via direct damage of the light-harvesting complexes and reaction centers (Melis et al., 1992) and indirectly through the production of excess reactive oxygen species (ROS; Lesser, 2006) that can eventually cause the inactivation of photosystem II (PSII; Falkowsky and Laroche, 1991; Macintyre et al., 2002; Vassiliev et al., 1994; Vincent and Neale, 2000). For counter-acting the UVR negative effects phytoplankton have evolved protection mechanisms such as photoprotective pigment synthesis to channel excess energy out of reaction centers; sunscreen compounds (i.e. mycosporine-like amino acids; Garcia-Pichel, 1994; Neale et al., 1998; Sinha et al., 1998), ROS-scavenging enzymes (enzymes superoxide dismutase and ascorbate peroxidase; Martínez, 2007) and several antioxidant compounds, putatively including dimethylsulfopropionate (DMSP; Sunda et al., 2002).

DMSP is a multifunctional compound synthesized by a vast panoply of phytoplankton species and found in high concentrations in the cytosol of prymnesiophytes, dinoflagellates, chrysophytes, prasinophytes, and pelagophytes (Stefels et al., 2007). In the water column a small fraction of DMSP results in

dimethylsulfide (DMS), a volatile compound known for its hypothesized role in climate regulation of the Earth (Charlson et al., 1987) and as a key compound that transfers sulfur from oceans to land through the atmosphere (Simó, 2001). Besides its primary function as an osmolyte (Gebser and Pohnert, 2013; Spielmeyer et al., 2011; Stefels et al., 2007), DMSP is postulated to participate in cell homeostasis by serving as an overflow mechanism for excess reduced sulfur when cells are under unbalanced growth (Stefels, 2000), act as a cryoprotectant under cold conditions (Karsten et al., 1996) and be part of an anti-oxidant cascade that may help cells scavenge ROS under light and nutrient stress (Sunda et al., 2002). However, clear understanding and direct physiological evidence for either the putative antioxidant role or for the proposed metabolic overflow mechanism are lacking.

Studies in phytoplankton cultures have shown that acclimation to strong UVR exposure on a timescale of several days generally causes up-regulation of intracellular DMSP content (Slezak and Herndl, 2003; Stefels and van Leeuwe, 1998; Sunda et al., 2002) while few others showed contrasting results (Archer et al., 2010), no clear trends (van Rijssel and Buma, 2002) or a negative effect (Hefu and Kirst, 1997). Even though crucial for our understanding, studies with natural communities are scarcer (DiTullio et al., 2001; Harada et al., 2009; del Valle et al., 2012; Vance et al., 2013), and also show ambivalent results (Harada et al., 2009).

Phytoplankton DMS production has also been shown to be enhanced by UVR exposure (after correction by DMS photolysis by UVR; Galí et al., 2011, 2013c; Toole and Siegel, 2004; Toole et al., 2006). One of the potential causes is an increase in DMS yield from dissolved DMSP (DMSPd) consumption as demonstrated by Slezak et al., (2007) and del Valle et al. (2012). The stimulation has also been attributed to the synergistic effects of UVR damage on microbial community DMS production, by enhancing phytoplankton DMSP and DMS release (hereafter named as DMS(P)) and simultaneously inhibiting bacterial DMS consumption.

This translates into DMS(P) cycling processes showing large regular variation at hourly timescales over diel cycles (Galí et al., 2013a). A global analysis even suggests that solar radiation dose (SRD) is one of the main environmental drivers of DMS dynamics (Vallina and Simó, 2007) but still today this is under debate (Belviso and Caniaux, 2009; Larsen, 2008). The lack of a clear understanding can be explained because variations in DMSP and DMS concentrations upon solar exposure result from different underlying processes and for this reason both compounds can hardly be looked at as a whole. Moreover, while DMSP production is mainly physiologically controlled by the phytoplankton community, the response of community DMS production to sunlight depends on a higher number of factors such as phytoplankton DMSP production, intracellular conversion of DMSP to DMS followed by DMS permeation outside the algal cell, algal DMSP release, and DMSP transformations by the microbial food web (Galí et al., 2013c).

Even though the impact of UVR on phytoplankton has been extensively reported, the photobiological effects at the community level along with the subsequent DMSP and DMS production is still required to understand the effects of present day UVR irradiances on sulfur compound dynamics and to make predictions in different ozone depletion scenarios. Based on previous studies, we compared the kinetics of PSII photoinhibition with the concomitant changes in DMSP and DMS production under two solar radiation treatments that included (FULL, i.e., PAR+UVR) or excluded (PAR) the effect of UVR. The photosynthetic efficiency of PSII measured from changes in the fluorescence emission of Chl*a* was measured with a Fast Repetition Rate fluorometer (FRRf). This was carried out in two contrasting environments, the Western Mediterranean Sea and the Canadian Arctic, using natural seawater samples from the surface and from the oxygen or subsurface chlorophyll maxima (SCM).

Material and methods

Study site and sample collection

The experiments were performed in two distinct environments. In September 2011, a Lagrangian study was carried out in the Western Mediterranean (SUMMER) aboard *R/V* García del Cid, while in August and September 2013, a transect study was conducted in the Baffin Bay and Resolute Passage, in the Canadian Arctic (ArcticNet), aboard the CCGS Amundsen (Figure 1). Surface (2 m) and subsurface waters were sampled at pre-dawn using 30 L Niskin bottles. Subsurface samples were taken from the oxygen maximum (30 m depth) in the Mediterranean Sea, and from the SCM (ca. 35 m) in the Arctic region. Polycarbonate carboys of 20 L were darkened with a black plastic and filled using a dark silicone tube with a 200 microns mesh attached to the distal end of the tube. The samples were kept in the dark at in situ temperature until the start of the experiment, usually around noon.

Experimental design

The same experimental design was used in both cruises. UVR-transparent Whirl-Pack bags of 90 mL were filled in a dark temperature-controlled room and kept within ±1ºC of the sea surface temperature. The bags were then placed in the incubator at the front of the deck to avoid shadow from the ship, with running seawater from the ship's underway intake. Incubations, which most lasted between 115 and 240 minutes, consisted of an acclimation period (ca. 15 minutes, T15), where PAR irradiance was increased gradually by removing neutral density screens at different steps. This was followed by a full sunlight exposure period including UVR (FULL light treatment) or excluding UVR (PAR) until the end of the incubation period. For the first 15-min acclimation period, one layer of Lee 226 foil (92% of transmittance (T) at 700 nm and 50% T at 400 nm) plus three, two and one neutral density screens (24%, 38% and 62 % transmission, respectively) at T0-T5, T5-T10 and T10-T15 respectively, were used. Bags under the FULL treatment

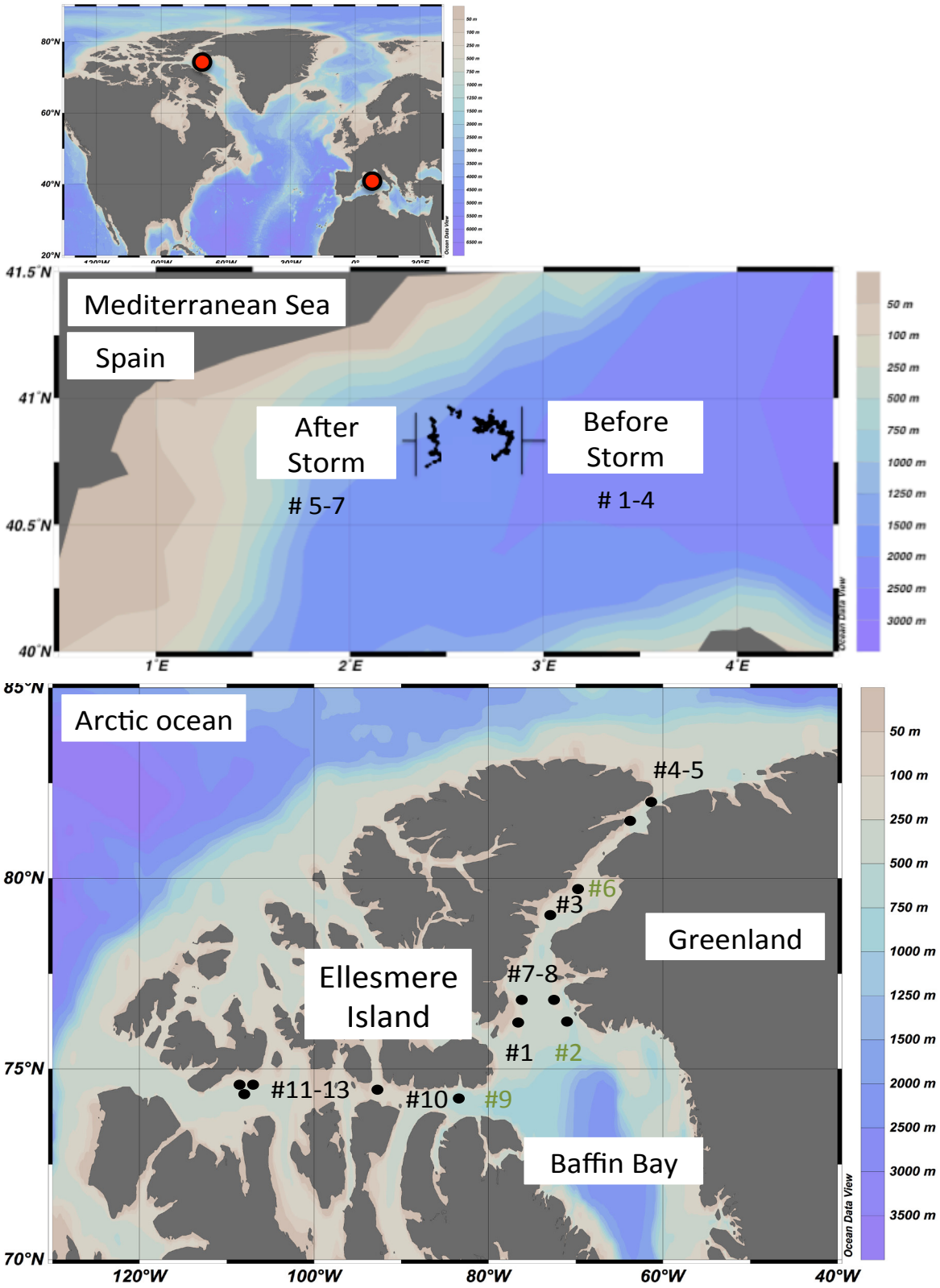

Figure 1: Sampling site for the Lagrangian Mediterranean Cruise in September 2011 and the Arctic Ocean cruise in August-September 2013. The numbers correspond to the experiment identification. The numbers in green represent incubation experiments with subsurface chlorophyll maxima (SCM) in the Arctic Ocean.

were also covered with an Ultraphan 295 foil (93% T at 700 nm and 50% T at 295 nm). At T15, the Lee 226 foil was removed from half of the bags for the FULL light spectrum treatment while it was kept for the other half corresponding to the PAR treatment. During the Mediterranean cruise, three incubations were conducted with streptomycin (250 μg $\cdot mL^{-1}$; Stein et al. 1973), an inhibitor of photosystem (PSII) photorepair (Neale et al. 1998). This inhibitor limits repair capacity to the extent that damaged proteins cannot be restored to function through turnover processes (Samuelsson et al., 1985).

The photosynthetic efficiency of PSII was monitored at the beginning of the incubation in dark-adapted samples to measure the maximum photosynthetic efficiency, throughout the acclimation (PAR only) and during the two-treatment experimental periods (PAR vs. FULL spectrum). One Whirl-Pack bag per treatment was sacrificed every 5 to 10 minutes and immediately analyzed. DMS and DMSP (hereafter named as DMS(P)) samples were measured at T0 and every 10 minutes following the acclimation period, in the same bags used for FRRf measurements.

Measurements

During the Mediterranean cruise, a gas chromatograph (Shimadzu GC14A) coupled to a flame photometric detector was used for discrete samples of DMS(P). Detection limit was ca. 3 pmol (Royer et al., 2014). The samples were analysed following the methodology described by Galí et al. (2013a). Parallel measurements with a FRRf (FASTracka, Chelsea Technologies, Surrey, UK) helped us understand the concomitant effect of UVR on phytoplankton physiology. The FRRf is a very sensitive fluorometer often used to assess the photosynthetic fitness of open water communities with relatively low chlorophyll content. It allows fast and non-intrusive measurements providing a large set of data in a short time scale (minutes to hours). Fluorescence emission responds quickly to changes in irradiance, and can be used to determine inhibition and repair kinetics under experimentally controlled conditions (Kolber et al., 1998; Sobrino et al. 2005a; Neale et al. 2012).

The excitation protocol used by the FRRf reduced the state of the primary electron acceptor in PSII by inducing a series of subsaturating flashlets (100) resulting in the capture of a single turnover fluorescence induction curve in PSII (Kolber et al., 1998). Different physiological parameters were derived from the curve of fluorescence induction in the photosystem II (PSII) according to Kolber et al. (1998). Two types of measurements were collected depending on the initial state of the cells. For samples measured at the beginning of the experiment, maximum photosynthetic efficiency was obtained from dark-adapted samples being initial fluorescence F0, maximum fluorescence Fm, variable fluorescence Fv = Fm- F0, and the ratio of variable to maximum fluorescence FvFm = Fv / Fm = (Fm-F0) / Fm. For the following samples exposed to light until the end of the experiment, the data were collected as the relative efficiency of excitation energy captured by PSII (ΦPSII) calculated as (F´m-Fs) / F´m, which has been correlated with variations in the quantum yield of photosynthesis. Fs is the steady state in vivo chlorophyll fluorescence of phytoplankton and F´m is the maximum yield of fluorescence during the illumination. Baseline and filtered seawater blank calibrations were performed at all gain levels before and after instrument deployment. The data were processed using the Chelsea FRS Software (v.1.8), with reference and baseline corrections.

In the Arctic, DMS(P) samples were similarly processed using a purge and trap system coupled to a Varian 3800 gas chromatograph equipped with a pulsed flame photometric detector. The analytical detection limit was 10 pmol for all sulfur compounds. Due to some instrumentation issues, only the first 3 experiments included DMS measurements. The other experiments only included dissolved DMSP (DMSPd) or particulate DMSP (DMSPp) samples and were analyzed on land within one month.

Subsamples for Chl*a* determination were filtered onto Whatman GF/F glass-fiber filters (0.7 μm nominal pore size). Chl*a* concentrations were measured using a Turner Designs 10-AU fluorometer, following a 24 h extraction in 90% acetone at 4°C in the dark (acidification method: Parsons et al. 1984). Subsamples for identification

and enumeration of protists were preserved with acidic Lugol's solution (Parsons et al., 1984) and stored in the dark at 4°C until analysis. Cells ≥ 2 µm in size were identified to the lowest possible taxonomic rank using an inverted microscope (Zeiss Axiovert 10) equipped with phase contrast optics (Lund et al., 1958). At least 400 cells were enumerated over a minimum of three transects. Samples for nutrients were collected directly from the Niskin type bottles after filtration through GF/F filters (Whatman). Inorganic nutrients, NO_3- and PO_4^{3-}, were analyzed using routine colorimetric methods adapted from Koroleff and Hansen (1999) with an Autoanalyzer3 (Bran and Luebbe). The analytical detection limit was 0.03 µmol L^{-1} for NO_3- and 0.05 µmol L^{-1} for PO_4^{3-}.

Spectral irradiance calculations

Irradiance received by the incubated samples

In the Mediterranean, spectral UV irradiance (µW cm^{-2} nm^{-1}), integrated PAR irradiance (µmol photons cm^{-2} s^{-1}), and temperature measurements were acquired at 6 s^{-1} frequency using a PUV-2500 radiometer (Biospherical) placed inside the incubator, with the sensor window covered by the same water depth as the samples. The measurements were low-pass filtered and decimated to a 1 min^{-1} frequency using the Matlab function "decimate", and matched to the total shortwave irradiance (W m^{-2}) acquired by the ship's meteorological station pyranometer. The spectral irradiance measured by the PUV-2500 at 6 discrete bands (centered at 305, 313, 320, 340, 380 and 395 nm) was time-integrated over each sampling interval, and multiplied by a normalized spectrum covering the 300-400 nm range at 1 nm resolution (as described by Galí et al. 2013a) to produce a 1 nm-resolution spectrum for each sampling interval. This spectrum was integrated between 300-320 nm and 320-400 nm to calculate UVB and UVA irradiance (W m^{-2}), respectively.

For the Arctic experiments irradiance in the UVB, UVA and PAR regions, together with total shortwave irradiance (all in W m^{-2} units), was recorded by broadband sensors located on the deck above the bridge at the top of the ship. PAR irradiance was converted

to quantum units using a 2.77·1018 quanta s^{-1} W^{-1} factor (Kirk, 2011; Morel and Smith, 1974). Light transmission at the air-water interface was calculated assuming 50% diffuse and 50% direct light, with a constant 0.066 reflectance for diffuse component and a variable reflectance (following Fresnel's equation) for the direct component.

In situ irradiance

The coefficients of attenuation for downward irradiance (K_d) were calculated at different wavelengths from spectral irradiance profiles (Biospherical instruments) as in Galí et al. (2013b). For surface samples, mean daily exposure was assumed to correspond to the mean irradiance within the upper mixed layer, following the "SRD" approach of Vallina and Simó (2007). SRD was calculated from daily irradiance at the water subsurface (UVB, UVA and PAR), the corresponding spectral K_d, and the mixed layer depth. For samples taken from below the mixed layer, we assumed that they were acclimated to the average daily irradiance received at the corresponding fixed (sampling) depth.

DMS photolysis correction

DMS photooxidation is photosensitized by seawater dissolved compounds that absorb in the UVR range, such as CDOM or nitrate, and follows pseudo first-order kinetics (Bouillon and Miller, 2005; Kieber et al., 1996). Nitrate-induced photolysis is thought to be relevant only at high nitrate concentrations (Bouillon and Miller, 2004; Toole and Siegel, 2004). The spectral dependence of DMS photolysis quantum yields has been shown to decrease exponentially with wavelength in different oceanic environments (Taalba et al., 2013; Toole et al., 2003).

The 1 nm-resolution time-integrated spectra in each sampling interval of the experiment were multiplied by (1) the spectral transmittance of the cut off filters (i.e. Ultraphan or Lee), (2) the CDOM absorption spectra (300-400 nm range) and (3) by an adimensional weighting function of DMS photolysis with an exponential slope of 0.0436 nm^{-1} (Galí et al., 2013a). The resulting photolysis-weighted irradiance was

multiplied by the temperature-corrected (Toole et al., 2003) photolysis rate constant obtained in parallel deck incubations using filtered seawater (see Figure 3 in Galí et al. 2013b) and by the mean DMS concentration during the sampling interval, yielding the DMS photolysis rate and thus the amount of DMS photolyzed. This is with the assumption that photolysis follows the same kinetics in whole waters as in the filtered waters.

Photolysis rate constants could not be measured during the Arctic cruise. Therefore, we used literature data to constrain DMS photolysis rates for those experiments. The rate constants reported by Galí and Simó (2010) in the Greenland Sea and Taalba et al. (2013) in the Baffin Bay were normalized to surface irradiance, and assumed to represent upper and lower bounds, respectively (Table 1). Since the average rate constants of each study differed by five fold, an important uncertainty remains regarding the photolysis-corrected DMS production rates, and the estimates should be rather viewed as a sensitivity analysis. Since almost no difference was observed between observed and photolysis-corrected DMS concentrations using the Taalba et al., (2013) data, we show only the results obtained with the photolysis k measured by Galí and Simó (2010; Table 1).

Data analysis

The amplitude of UVR-induced PSII inhibition was calculated as the difference between maximal values (FvFm) measured in the dark and the minimal ΦPSII during the subsequent experimental exposure. The amplitude of the recovery by acclimation to high light was calculated as the difference between the minimal and the highest ΦPSII in posterior data points.

The Mediterranean Sea and the Artic results for ΦPSII, DMS and DMSP under PAR and FULL solar spectra treatments were both analyzed by applying a weighted fitting procedure offered by Kaleidagraph (Synergy software). The ratios between the estimated trends for FULL solar spectra divided by those obtained for the PAR treatment allowed to show the UVR effect, independently of PAR kinetics (Sobrino et al. 2005).

Table 1: Irradiance-normalized DMS photolysis rate constants used to correct observed DMS for photochemical loss. DMS photolysis was measured in the Mediterranean experiments, but literature values had to be used in the Arctic due to the lack of simultaneous photolysis measurements. Absorption coefficients of colored dissolved organic matter (CDOM) and nitrate concentrations are shown because they are the main photosensitizers for DMS photolysis together with the corresponding irradiance- and temperature-normalized photolysis k. $a_{CDOM,330}$ is the absorption coefficient of CDOM at 330 nm; $k_{photo,0-}$ is the pseudo-first-order DMS photolysis rate constant just below the water surface, reported at in situ temperature for each study (@ in situ T), normalized to 20°C, and further normalized to broadband irradiance received in situ.

Reference	n	Latitude range (degrees N)	aCDOM,330 mean (min-max) (m-1)	NO3 mean (min-max) (µmol L-1)	kphoto,0- @in situ T (d-1)	kphoto,0- @20C (d-1)	kphoto,0-/Ed,TOT @20C (m2 MJ-1)
Mediterranean Sea							
This study (see Galí et al. 2013)	3	41	0.15 (0.10 - 0.20)	<DL	0.63 (0.58 - 0.73)	0.53 (0.48 - 0.60)	0.024 (0.022 - 0.028)
*Arctic Ocean **							
Galí and Simó 2010	4	80 - 81	0.37 (0.19 - 0.69)	0.8 (0.7 - 0.9)	0.8 (0.5 - 1.1)	1.3 (0.9- 2.1)	0.3 (0.1 - 0.5)
Taalba et al. 2013	8	70 - 77	0.66 (0.28 - 1.32)	0.1 (0.01 - 0.3)	0.2 (0.06 - 0.6)	0.36 (0.1 - 1)	0.05 (0.006 - 0.1)

* Since no DMS photolysis measurements were conducted during the Arctic experiments, the two studies above mentioned were used as lower (Taalba et al. 2013) and upper bounds (Galí and Simó 2010).

Results

Photosynthetic response to sunlight

Figure 2 shows the photosynthetic response to FULL light and PAR treatments during the Mediterranean cruise. Seawater at 30 m depth, corresponding to the oxygen maximum, was sampled for 3 out of the 4 experiments shown (panels A, B and C).

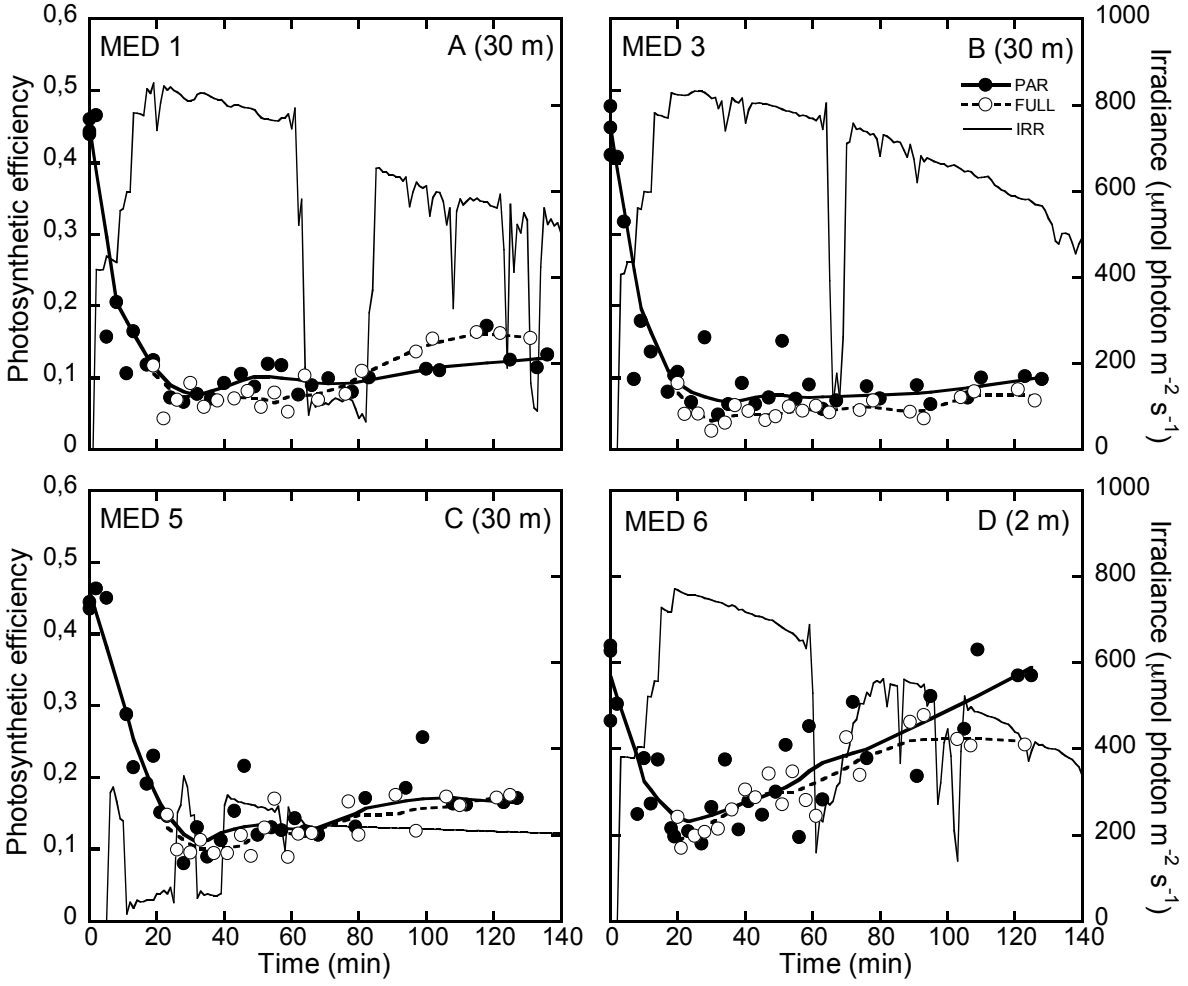

Figure 2: Changes in photosynthetic efficiency with time of exposure (FvFm at time zero and ΦPSII at subsequent sampling times) measured with the FRRf under two spectral treatments during the Lagrangian Mediterranean (MED) cruise in September 2011. A (MED 1), B (MED 3) and C (MED 5) correspond to 30 m sampling depth (O_2 maxima) and D (MED 6) corresponds to 2 m depth. Open and filled circles are observations under FULL solar radiation and PAR, respectively. Lines depict weighted fitting trends of the observations. The line in the background represents the PAR irradiance received by the samples during the incubations.

Table 2: Summarized light conditions and maximum inhibition and recovery amplitude patterns for the Mediterranean and Arctic Ocean experiments under PAR and FULL light treatments. The SRD PAR, SRD UVA and SRD UVB mean the mixed-layer irradiance, for surface samples, and irradiance at fixed depth for SCM or 30 m samples.

Exp. ID	Depth	SRD-PAR	SRD-UVA	SRD-UVB	Max PAR W m-2	Mean PAR W m-2	Mean UVR W m-2	T0	Max inhib FULL (T0 - min)	Recovery FULL (max - min)	Max inhib PAR (T0 - min)	Recovery PAR (max - min)
Mediterranean Sea												
MED 1	30 m	112	1,4	0,0013	827	504	11,4	0,46	-0,42	0,12	-0,40	0,11
MED 2*	30 m	112	1,4	0,0013	99	25	0,5	0,42	-0,33	0,18	-0,29	0,15
MED 3	30 m	104	1,3	0,0012	811	615	14,1	0,41	-0,38	0,06	-0,36	0,05
MED 4*	30 m	104	1,3	0,0012	299	75	1,5	0,43	-0,39	0,10	-0,37	0,12
MED 5	30 m	100	1,2	0,0012	557	150	5,0	0,46	-0,37	0,09	-0,38	0,18
MED 6	surface	488	8,0	0,1768	758	491	10,6	0,35	-0,17	0,25	-0,16	0,22
MED 7*	30 m	100	1,2	0,0011	805	565	12,9	0,49	-0,44	0,11	-0,41	0,10
Arctic Ocean												
ARC 1	surface	nd	nd	nd	1885	900	33,7	0,46	-0,25	0,21	-0,11	0,09
ARC 2	chl max 38m	12	0,0	0	1943	1083	50,0	0,39	-0,39	0,00	-0,39	0,00
ARC 3	surface	550	2,5	nd	204	127	7,6	0,35	-0,11	0,04	-0,09	0,00
ARC 4	surface	nd	nd	nd	nd	nd	nd	0,51	-0,02	0,02	0,00	0,01
ARC 5	surface	nd	nd	nd	nd	nd	nd	0,47	-0,33	0,00	-0,06	0,00
ARC 6	chl max 30m	nd	nd	0	1161	876	41,2	0,41	-0,36	0,15	-0,15	0,06
ARC 7	surface	330	1,8	nd	1016	590	37,8	0,41	-0,14	0,03	-0,07	0,00
ARC 8	surface	271	1,5	nd	260	86	3,9	0,43	-0,01	0,04	0,01	0,03
ARC 9	chl max 35m	13	0,0	0	1334	771	44,6	0,48	-0,45	0,04	-0,43	0,13
ARC 10	surface	nd	nd	nd	nd	nd	nd	0,33	-0,09	0,03	-0,03	0,02

* Experiments with streptomycin addition.
nd, not determined.

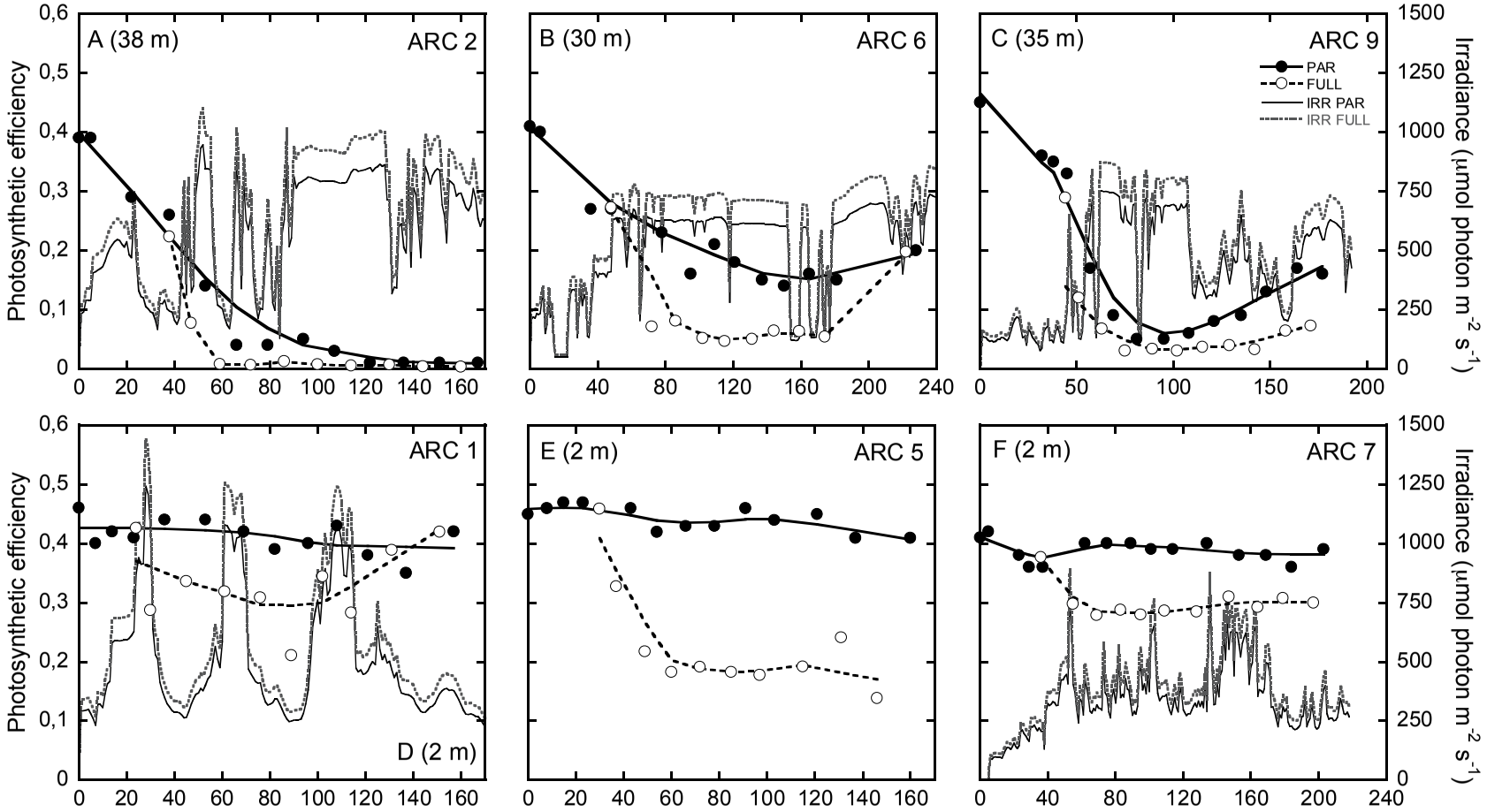

Figure 3: Changes in photosynthetic efficiency with time of exposure (FvFm at time zero and ΦPSII at subsequent sampling times) measured with the FRRf under two spectral treatments during the Arctic (ARC) cruise in August and September 2013. A (ARC 2), B (ARC 6) and C (ARC 9) correspond to 38 m, 30 m and 35 m sampling depth (SCM), respectively. ARC 1, ARC 5 and ARC 7 correspond to seawater sampled from 2 m depth. Open and filled circles are observations under FULL solar radiation and PAR, respectively. Lines depict weighted fitting trends of the observations. The solid line in the background represents the PAR irradiance received during the incubations, and the dotted line represents FULL solar radiation. Note the differences in time scale. The lack of irradiance for ARC 5 is due to technical problems with the radiometer during this experiment.

Results from three additional experiments where an inhibitor of repair (streptomycin) was added are shown in Table 2. In general, maximum photosynthetic efficiency (which corresponded to T0) was similar among samples from 30 m, with values close to 0.45 (±0.03, n=6), and slightly smaller in the surface sample (0.33±0.09; Table 2). After the start of the exposure, the photosynthetic efficiency for the FULL and PAR treatments decreased to reach its minimum value during the first 20 to 30 minutes of the experiment. This was followed by a steady state period (Figure 2A and 2B) or by an increase in the photosynthetic efficiency (Figure 2C and 2D) in both light treatments, similarly to what had been previously observed with cultures (Sobrino et al., 2005). Altogether, the maximum inhibition ranged between 80% and 91% (corresponding to ΔΦPSII between -0.37 and -0.42) for the FULL treatment and 85% and 88% (ΔΦPSII between -0.36 and -0.40) for the PAR treatment (Table 2). Similar decreases were also observed in the streptomycin-amended experiments (MED 2, MED 4 and MED 7; Table 2), which exhibited inhibition ranging 79-90% (ΔΦPSII between -0.33 to -0.44) under FULL and 66-84% (ΔΦPSII between -0.29 to -0.41) under PAR (Table 2). The final increase in photosynthetic efficiency reached the initial values in MED 6 (Figure 2D), the only experiment conducted with surface waters in the Mediterranean. For the ensemble of the 30 m depth experiments, the cells never returned to their initial state. Rather, recovery ranged 25-38% (ΔΦPSII between +0.06 and +0.12) under FULL, and 31-50% (+0.05 to +0.18) under PAR (Table 2).

Figure 3 shows the photosynthetic response to light treatments during the Arctic cruise. Three out of the 10 experiments (ARC 2, ARC 6 and ARC 9) were conducted with seawater sampled at ca. 34 m depth (Figure 3A, 3B and 3C). In those cases the photoinhibitory rates were slower than in the Mediterranean, reaching the steady state around minutes 60 to 100. This translated in very low recovery values ranging from 0% to 25% (ΔΦPSII between 0 and 0.15) under FULL and 0% and 30% (ΔΦPSII between 0 to 0.13) under PAR (Table 2). In the case of ARC 6 and ARC 9, the phytoplankton

cells showed more effective photoacclimation than in ARC 2 (Figure 3A), which exhibited the strongest photoinhibition of all the experiments. In contrast, the surface experiments ARC 1, ARC 5 and ARC 7 (Figure 3C, 3D and 3E) and additional ones also presented in Table 2 showed low inhibition values compared to SCM experiments (Table 2). Values for the PAR treatment were almost constant during the whole incubation, whereas the FULL treatment exhibited a decrease in photosynthetic activity with no complete recovery in most of the experiments (see Figure 3D, 3E, and 3F and Table 2).

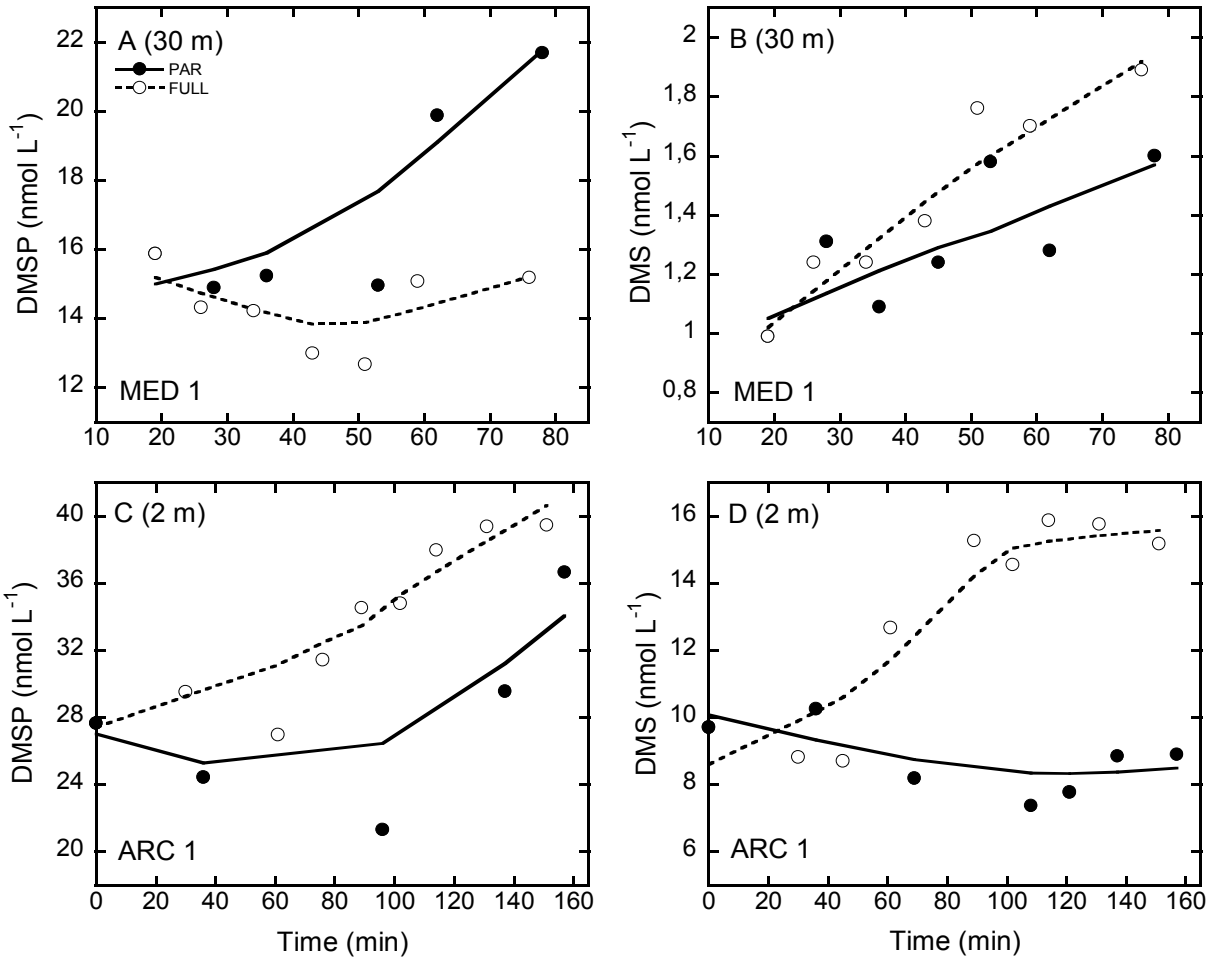

Figure 4: DMSP and DMS concentrations (nmol L^{-1}) under two different spectral treatments in two different environments. A and B correspond to the O_2 maximum in the Mediterranean Sea (MED 1), and C and D correspond to surface waters in the Arctic (ARC 1). Open and filled circles are observations under FULL solar radiation and PAR, respectively. Lines depict weighted fitting trends of the observations. Note the difference in time scale.

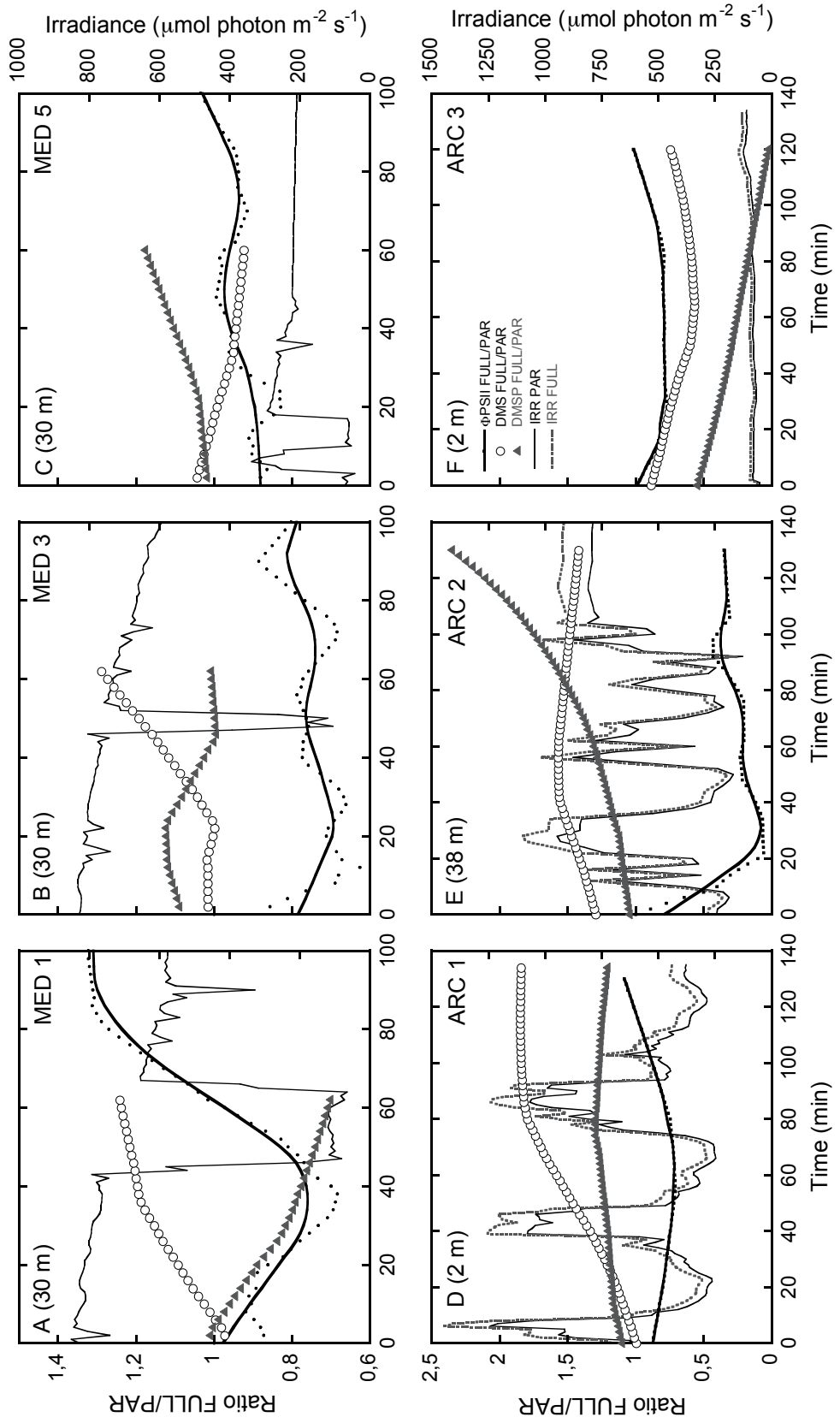

Figure 5: FULL/PAR ratio for ΦPSII, and DMS and DMSP concentrations. A (MED 1), B (MED 3) and C (MED 5) experiments correspond to 30 m samples in the Mediterranean Sea, while D (ARC 1), E (ARC 2) and F (ARC 3) experiments correspond to surface (2 m) or SCM (38 m) samples in the Arctic. Weighting functions (60-90%) were applied to produce semi-continuous data from discrete observations. The solid line in the background represents the PAR irradiance received during the incubations, and the dotted line represents FULL solar radiation. Note the differences in time scale.

Table 3: Summary of characteristics of the initial water samples for the Mediterranean and Arctic Ocean experiments.

Exp. ID	Date	Latitude (oN)	Longitude (oE)	Depth	MLD (m)	Salinity	Temp (oC)	Mean irr (W m-2)	Chl (µg L-1)	Dominant phytoplankton	NO3 (µM)	SiO4 (µM)	PO4 (µM)	DMS (nM)	DMSPt (nM)	DMSPp (nM)
Mediterranean Sea																
MED 1	15/09/2011	40,89	2,84	30 m	9,7	38,1	25,29	504	0,25	Dino>Oth>Cocco	0,00	1,08	0,04	1,0	15,9	nd
MED 2*	15/09/2011	40,92	2,75	30 m	9,6	38,1	25,89	25	0,43	Dino>>Cocco>Oth	1,77	2,06	0,09	nd	nd	nd
MED 3	17/09/2011	40,87	1,72	30 m	8,7	38,1	25,77	615	0,27	nd	0,12	1,09	0,06	1,1	12,1	nd
MED 4*	17/09/2011	40,88	1,77	30 m	9,1	38,2	26,65	75	0,20	nd	0,12	1,09	0,06	1,1	22,1	nd
MED 5	19/09/2011	40,93	3,54	30 m	13,4	38,1	24,19	150	0,22	nd	-	-	-	0,7	28,7	nd
MED 6	20/09/2011	40,88	4,84	surface	17,3	38,1	24,15	491	0,08	Dino>>Oth>Diat	0,79	1,26	0,05	2,1	20,7	nd
MED 7*	22/09/2011	40,78	1,67	30 m	14,2	38,1	24,20	565	0,16	Dino>>Cocco>Oth	nd	nd	nd	nd	nd	nd
Arctic Ocean																
ARC 1	15/08/2013	76,38	77,37	surface	3	31,5	4,2	900	0,52	Chrys>>Flag>Pras	0,11	0,63	0,45	9,7	27,6	nd
ARC 2	16/08/2013	76,32	75,75	chl max 38m	38	32,4	2,5	1083	4,27	Diat>>Flag>Prymn	5,46	5,82	1,15	2,7	17,1	nd
ARC 3	20/08/2013	78,98	72,10	surface	5	30,4	-0,7	127	2,01	Diat>>Flag>Dino	0,26	0,76	0,53	1,9	10,9	nd
ARC 4	22/08/2013	81,28	62,49	surface	5	30,4	-1,2	nd	5,27	Diat>>Flag>Choa	0,11	0,16	0,54	nd	12,0	nd
ARC 5	23/08/2013	81,91	61,20	glacier water	10	31,0	-1,1	nd	8,05	Diat>>Flag>Dino	0,80	3,02	0,59	nd	20,7	nd
ARC 6	25/08/2013	79,29	71,31	chl max 30m	30	31,4	-1,0	876	0,85	Diat>>Flag>Pras	1,24	3,59	0,79	nd	3,7	nd
ARC 7	27/08/2013	77,34	73,43	surface	9	31,9	2,2	590	0,45	Chrys>Flag>Pras	0,14	0,97	0,21	nd	35,8	11,4
ARC 8	28/08/2013	77,32	77,01	surface	5	31,0	-0,2	86	1,32	Chrys>Diat>Flag	0,16	1,84	0,62	nd	nd	23,4
ARC 9	30/08/2013	74,11	83,37	chl max 35m	35	31,9	-0,3	771	1,61	Diat>>Flag>Dino	3,97	9,03	1,04	nd	nd	3,6
ARC 10	31/08/2013	74,26	91,48	surface	2	29,8	-1,1	nd	0,43	Diat>Flag>Pras	0,00	0,69	0,46	nd	nd	10,5

* Experiments with streptomycin addition. Abbreviated phytoplankton group names are: Choa (Choanoflagellidea); Chrys (Chrysophyceae); Cocco (Coccolithophors) Diat (Diatoms); Dino (Dinophyceae); Flag (Flagellates); Pras (Prasinophyceae); Oth (Others). >> more than 50% of the counts belong to this group. nd, not determined.

Dimethylated sulfur compounds vs. light treatments

DMSP

The evolution of DMSP and DMS concentrations is presented in Figure 4 for selected experiments, and the initial concentrations are presented in Table 3 for all experiments. Overall, in the oligotrophic Mediterranean Sea, in situ concentrations of total DMSP (DMSPt = DMSPp + DMSPd) ranged between 12.1 and 28.7 nM (mean 19.9 nM ± 6.3 nM), while in the Arctic Ocean, concentrations ranged between 3.7 and 35.8 nM (mean 18.3 nM ± 10.9 nM; Table 3). DMSPt concentrations at 30 m (Figure 4A) show a 1.5-fold increase from the initial to the final value under the PAR treatment, and no net change under the FULL treatment. In contrast, the results from the surface sample in the Arctic (Figure 4C) showed a higher increase under FULL light (1.5-fold increase) compared to the PAR treatment (1.3-fold increase). In order to assess the weight of UVR on the photosynthetic rates and the production of the dimethylated sulfur compounds, the ratios FULL/PAR (rather than the absolute values) were used and presented in Figure 5. The response of DMSPt was variable amongst the experiments: four of them evolved towards a ratio FULL/PAR above 1 (Figure 5B, 5C, 5D and 5E). The two remaining experiments (Figure 5A and 5F) were completely different from the rest and showed a constant UVR-induced decrease with a ratio FULL/PAR below 1.

DMS

In the oligotrophic Mediterranean Sea, in situ concentrations of DMS ranged between 0.7 and 2.1 nM (mean 1,2 nM ± 0.5 nM) and in the Arctic Ocean they ranged between 1.9 and 9.7 nM (mean 4.8 nM ± 4.3 nM; Table 3). The DMS concentrations presented here have been corrected for photochemical DMS loss (see Material and Methods), which was negligible under PAR but significant under the FULL treatment. Therefore, the DMS change over time corresponds to net biological DMS production. DMS concentrations at 30 m (Figure 4B) showed a 2-fold and 1.6-fold increase under the FULL and PAR treatments, respectively. The results from the surface sample in the Arctic (Figure 4D) showed a

similar increase under the FULL light (1.8 fold increase) and a decrease under PAR (1.1-fold decrease). FULL/PAR ratios of DMS presented in Figure 5 are above 1 for MED 1 and MED 3 (Figure 5A and 5B) and below 1 for MED 5 (Figure 5C). In the Arctic, FULL/PAR DMS ratios for ARC 1 and ARC 2 were both above 1 with a general increase at the start of the experiment, reaching a plateau during ARC 1 (Figure 5D) and exhibiting a slight DMS decrease during ARC 2 (Figure 5E). Interestingly, ARC 3 was opposite, with a net negative effect of UVR on DMS (ratio below 1) and showed an initial decrease in the FULL/PAR DMS ratio followed by a plateau (Figure 5F).

Discussion

UVR has a significant effect on the physiological response of the phytoplankton cells and their photosynthesis efficiency in the upper ocean (Roy 2000). UVR damage occurring in the photoactive surface layer can extend due to mixing processes over much of the upper mixed layer, decreasing water column productivity (Neale et al., 2012). The sensitivity of phytoplankton cells to light fluctuations depends on their capacity to counteract UVR negative effects. Their vulnerability to changes in environmental conditions would result in an increase in damage and a decrease in repair efficiency unless photoacclimation promotes repair and protection mechanisms (Litchman et al., 2002; Neale, 2001). Here we assessed the effect of solar UVR and PAR on the efficiency of the photosystem II and compared it with concomitant changes in DMSP and DMS, two compounds potentially involved in, or indicators of, antioxidant responses (Sunda et al., 2002). Results show responses from two contrasting environments.

Phytoplankton photophysiological response to PAR and UVR

High solar exposure, temperature and nutrient limitation are expected to play a role in phytoplankton photosynthesis performance and photoinhibition (Agusti and Llabrés, 2007; Litchman et al., 2002; Roy, 2000). Indeed, the results show lower initial

ΦPSII values in the stratified surface waters (MED 6; 0.33±0.09 data not shown) compared to the 30 m samples (mean initial value of 0.45±0.03; data not shown). This difference highlights, in the first place, the persistent photodamage of PSII induced by high near-surface irradiance that limits photosynthesis efficiency (Alderkamp et al., 2011; Alderkamp et al., 2010). It also reflects the difference in nutrient availability (Litchman et al., 2002), since surface waters are nutrient depleted with respect to 30 m depth (Table 3).

The ubiquitous sharp and rapid decrease in photosynthetic rate observed at the beginning of every experiment with 30 m depth water, followed by stabilization of photosynthesis at a depressed but steady-state level, implies that damage is partially counteracted by ongoing repair of the target site within the photosynthetic apparatus (Cullen and Lesser, 1991; Lesser et al., 1994; Neale, 2000; Sobrino et al 2005a). In some of the stations (MED 5 and ARC 9) a significant steady increase was even seen indicating fast building of resistance or repair over the time course of the experiment. This increase is related to photoacclimation to UVR or high light, since the increase was observed during exposure to both, PAR and FULL irradiance, depending on the station (Sobrino et al. 2005a). Similarly to the 30 m samples, surface samples also showed a decrease in photosynthetic efficiency but for a comparatively shorter period and with a smaller degree of photoinhibition. This short photoinhibition period was followed by a fast increase in ΦPSII, especially in the Mediterranean, up to almost the initial values within 2-3 hours in some of the cases (MED 6, ARC 1). This may reflect either differences in phytoplankton assemblages between surface and 30 m (Table 3), more efficient repair mechanisms, or the capacity to deploy the repair mechanisms faster. The latter two result in better and faster photoacclimation at surface (Falkowsky and Laroche, 1991). The opposite scenario was observed in one of the deep samples from the Arctic (ARC 2), where the photosynthetic rates hardly recovered and reached values close to zero (Figure 3A, Table 2). Similar to what was suggested by Six et al. (2007), this upward fluctuation in irradiance would have resulted in the photoinactivation of PSII exceeding repair rates and thereby leading to net

photoinhibition and potentially cell death (Agusti and Llabrés, 2007). Indeed the ARC 2 data showed unusual high irradiance (90 times their acclimation PAR in the SCM; 1083 W m^{-2}; Table 3) and was one of the richest in Chl*a* and nutrient concentration (Chl*a* =4.27 ug L^{-1}; Table 3). It was also the deepest sample and the station with deeper mixed layer, so it is very likely that self-shading reduced light penetration and photoacclimation compared to the other SCM samples. Our results point out that despite using similar experimental settings, the thin line differentiating the extent of reversible and irreversible damages depends on several external factors, such as the light history of the phytoplankton cells, the assemblage composition and the physico-chemical setting, which altogether make phytoplankton physiological response hard to predict.

Although the results show that photoacclimation and repair mechanisms result in the recovery of the signal, in many cases there are no clear differences between the FULL and the PAR treatments. This applies mainly to the Mediterranean samples where only MED 1 shows a more severe effect of the UVR-inclusive (FULL) exposure for the total length of the experiment (t-test p=0.0327). Significant (though subtle) differences between FULL and PAR were only found for certain experiments and periods, e.g., T20—T60 in MED 1 and MED 3 (p = 0.01 and p = 0.005, respectively, t-test for difference between samples). This is because decreases in photosynthetic rates are due to photoinhibition but also to non-photochemical quenching (NPQ), which is mainly driven by PAR. NPQ is a mechanism employed by the phytoplankton cells to protect themselves from high-irradiance. It uses processes that dissipate heat away from the antenna or reaction center hence reducing Fm and F0. This makes it difficult to separate photoinhibition from quenching in our experimental design and to assess real percentages of UVR-photoinhibition to the observed responses.

Phytoplankton sampled at 30 m depth exposed to the full light irradiance of the upper mixing layer showed photoinhibition in all cases. To some extent this can be mimicking a strong mixing event occurring during a storm where phytoplankton

cells from deeper layers get sporadically exposed to higher solar radiation near the surface (Galí et al., 2013b). The lower ΦPSII we observed in near-surface waters adds to mounting evidence that residence times of mixing-drifted phytoplankton at surface are sufficiently long to induce quenching effects (Neale et al., 2012). The depression of electron transport in surface waters is good evidence that photosynthetic efficiencies in the uppermost photoactive zone are consistently lower compared to deeper values in the water column. Indeed, low-light acclimated cells maintain constitutively high efficiency of light harvesting, and have a limited photoprotective response despite the risk of photodamage when exposed to near-surface irradiance. In other words, they optimize light harvesting at the expenses of higher sensitivity to photoinhibition in the event of an injection into the upper mixing layer. Subsequent induction of photoprotective mechanisms, although limited and slow, results in the increase in the fraction of cells with efficient light harvesting capacities in circulation through the mixing layer (Arrigo et al., 2010; Kropuenske et al., 2009, 2010).

Geographical location effects: comparison between distinct environments

When comparing the observations from summer time experiments in the Mediterranean Sea and the Arctic Ocean, we identify some commonalities. These are especially remarkable for the deeper samples (30 m in the Mediterranean and ca. 35 m in the Arctic), where early photoinhibition was followed by a steady or slightly increasing trend towards the end of the experiments. However, on top of the similarities, there were two significant differences between the Mediterranean and the Arctic: 1) stronger effect of PAR irradiance in the Mediterranean, and 2) slower kinetics of photoinhibition in the Arctic.

As explained above, significant differences between PAR and FULL treatments were hardly observed in the Mediterranean samples. This occurred both in surface and 30 m samples despite photoacclimation of surface samples enabled recovery to values close to the beginning, while deep samples showed slight or no recovery at all. The strong

effects of PAR in the Mediterranean occurred despite the lower average irradiances, which is indicative of the relative roles of the irradiance and the spectral characteristics of the light. In the Arctic, deeper samples under PAR still showed decreases in photosynthetic efficiency but, unlike in the Mediterranean, significantly different than those including UVR (Figure 3). In contrast, Arctic surface samples did not show significant inhibition throughout the ca. 3 h of the experiment. Similar flat responses have been observed in the laboratory with cultures from temperate areas under controlled and nutrient replete conditions (Sobrino et al., 2005, Sobrino and Neale 2007).

Decreases in photosynthetic efficiency reached steady state 60 to 100 minutes after the start of the exposure in the Arctic, and after 20-30 minutes in the Mediterranean. Slower decreases of ΦPSII in the Arctic are consistent with lower rates of damage. Reduction of damage rates (min^{-1}) can be assimilated to reduction of the adverse effects of UVR on the phytoplankton assemblage due to either lower UVR doses or higher photoprotection mechanisms (e.g., higher MAA content or more active xantophyll cycle). Temperature and nutrient concentration could also act as important drivers of the differences in phytoplankton photophysiology between the two studies. Low temperature should decrease both, the rate of damage and the rate of repair, since repair is mainly related to temperature-dependent enzymatic activities. However, a previous study with a temperate diatom showed that there was an inverse relationship between temperature and the rates of damage and repair (i.e., higher temperatures had lower rates; Sobrino and Neale 2007). Nutrient limitation in the Mediterranean could be causing the increased sensitivity to UVR (Litchman et al. 2002).

Light stress-induced DMS(P) production and release by phytoplankton cells

Phytoplankton evolve different metabolic ways to counter act the damaging effect of stress triggered by high irradiance and/or nutrient depletion conditions, amongst them the production of chemical compounds such as DMSP and DMS (Stefels, 2000; Sunda

et al., 2002). Two mechanisms dealing with high irradiance and nutrient starvation have been put forward: the overflow hypothesis (Stefels, 2000) by which DMSP and DMS serve as an overflow mechanism when phytoplankton undergo unbalanced growth; and the antioxidant hypothesis (Sunda et al., 2002), which states that the downstream products of DMSP cleavage (including DMS) could act as intracellular radical scavengers. Although the experiments were not designed to infirm or confirm the veracity of the hypothesis they can still provide insights on the role of the algal metabolite DMSP as its production depends ultimately on the photosynthetic capacity of the cells (even though its production can also occur under dark conditions; Galí et al. (2013a)). Indeed, physiological responses of the cells to irradiance, including inhibition, damage, recovery and acclimation, eventually affect the capacity of the cells to allocate photosynthetically fixed carbon to DMSP. Depending on the environmental conditions, several scenarios can take place (see Results section and Tables 2 and 3).

This part of the discussion will address the general patterns rather than the differences among individual experiments. Contrasting responses were observed during both cruises, but for most of the experiments the ratio FULL/PAR for ΦPSII was below 1 indicating a stronger response to UVR than PAR concomitant to the decrease of PSII efficiency extensively described above. Under a simplistic view where DMSP would solely serve its antioxidant and overflow functions, one could expect its production to be driven by the photoefficiency of the cells. However, DMSP production or biosynthesis rates could not be measured, and concentration is not as straightforward to interpret and it depends on the balance between its de novo production and its consumption processes within the phytoplankton cell. The latter results from intracellular DMSP reaction with OH leading to dimethylsulfoxide (DMSO) production (Sunda et al., 2002) and intracellular DMSP cleavage by lyase-enzymes leading to DMS production. If DMSP concentration is measured in total seawater samples, it includes the dissolved (extracellular) pool, thought to be minor, and the concentration depends on further consumption processes such as the

extracellular DMSP cleavage by periplasmic, bacterial and free lyases (Stefels, 2000).

For DMSP, the FULL/PAR ratio showed all of the 3 possible responses: decrease (MED 1, ARC 3), no change (MED 3, ARC 1) and increase (MED 5, ARC 2). Interestingly, experiment MED 5 was conducted under considerably lower irradiance and ARC 2 had one of the highest irradiances and photoinhibition (Figure 5). Sunda et al. (2002) reported that intracellular accumulation of DMSP occurred in cultures of *E. huxleyi* exposed to moderate levels of UVR, and pointed out to UVA as the potential driver for DMSP upregulation. Severe exposure to UVR could uncouple DMSP to DMS conversion and finally lead to relative loss of intracellular DMSP. In these cases, upregulation of DMSP concentration is consistent with the hypothesized antioxidant and overflow functions of DMSP (Stefels, 2000; Sunda et al., 2002). On the contrary, in the low irradiance experiment ARC 3, DMSP seemed to have turned over faster under PAR.

Net DMS production depends on the balance between DMSP-derived production and consumption processes, the bacterial DMS consumption and the photochemical DMS oxidation (ventilation is prevented in bottle experiments). The latter was accounted for through the photolysis correction and the observed data essentially represent the balance between gross DMS production and bacterial consumption. Bacterial DMS consumption is susceptible to inhibition by UVR and PAR (Toole et al., 2006), hence accumulation of DMS production in UVR may result from higher gross DMS production, lower bacterial DMS consumption, or both. In any case, it is interesting to note that DMS showed higher production or lower consumption under FULL light in 4 of the 6 experiments. This is consistent with several studies reporting enhancement of gross DMS production under UVR (Galí et al., 2011, 2013abc). All these previous studies point out to phytoplankton as the most likely actors in UVR-enhanced DMS production.

Independently of the trends, the FULL/PAR ratios for DMSP and DMS showed opposite patterns in most of the experiments (Figure 5), except in ARC 3 and MED 4 (not shown) that had the lowest irradiances of all the experiments. Samples from

MED 4 were incubated with the antibiotic streptomycin, an inhibitor of repair (Stein, 1973), indicating that DMSP and DMS production are directly related to the active repair of UVR damage because of the low irradiance or because of the antibiotic effect. Clear trends in the FULL/PAR ratios showing net DMS production resulting from DMSP consumption were observed for stations with active damage and repair (MED 1, MED 3, ARC 1). Opposite trends showing increases in the ratios of DMSP production with decreases in DMS (MED 5, ARC 2) occurred in experiments where the photoinhibitory effect of UVR over PAR was not significant (MED 5) or extremely significant (ARC 2).

Altogether, the diversity in terms of UV response points out to the several ways in which DMSP synthesis and transformation are regulated in different phytoplankton communities, which are possibly associated to different bacterial DMSP users. The responses also differ according to physico-chemical settings, with a resulting overall physiological state impacting on dimethylated sulfur concentrations.

Conclusions

Photoinhibition and productivity responses of mixed natural phytoplankton to UVR and PAR irradiance can be hard to interpret at the community level but are critical for the understanding of the community changes in response to UVR exposure. This is important because in vitro experiments with cultured strains in the laboratory, although useful for isolating processes, have limited relevance and focus only on single species, neglecting important interactions within the community and failing to reproduce the natural variability of underwater light penetration. Also, solar radiation simulated in laboratory is often spectrally unrealistic.

This study under quasi-natural conditions indicated a negative effect of near-surface irradiance on cells by photodamage and photoinhibition of PSII during the first ca. 30 minutes for both deep and surface waters. The study also showed for the majority of the experiments a dynamic balance between damage and repair after the early photoinhibition. This was especially so under the PAR treatment where the cells in some cases recovered totally towards the end of the incubation period. In general, Mediterranean experiments showed similar photosynthetic response under PAR and FULL light treatments and lower photoacclimation compared to the Arctic experiments, where the PAR treatment had less effect on the cells. Our work highlights the involvement of UVR-induced photophysiology in DMSP and DMS production in natural communities, and its importance to deciphering the processes driving DMSP-to-DMS conversion and the fate of DMS in the water column.

Acknowledgements

We thank the marine technicians (UTM) and the crew aboard the Garcia del Cid for their assistance and cooperation. We also thank the Canadian Coast Guard officers, and the crew of the CCGS Amundsen for assistance during the cruise ArcticNet 2013. We thank Sylvie Lessard for the enumeration and identification of protists. The cell counts for ArcticNet 2013 were paid from a grant from the Canadian Museum of Nature to Michel Poulin. This work was supported by the corresponding Spanish Ministries funding science through projects SUMMER (CTM2008-03309/MAR) and PEGASO (CTM2012-37615), and through a PhD scholarship to S.J.R.

References

Agusti, S. and Llabrés, M.: Solar Radiation-induced Mortality of Marine Pico-phytoplankton in the Oligotrophic Ocean, Photochem. Photobiol., 83(4), 793–801, doi:10.1111/j.1751-1097.2007.00144.x, 2007.

Alderkamp, A., Garcon, V., Baar, H. J. W. De and Arrigo, K. R.: Short-term photoacclimation effects on photoinhibition of phytoplankton in the Drake Passage (Southern Ocean), Deep Sea Res. Part I Oceanogr. Res. Pap., 58, 943–955, doi:10.1016/j.dsr.2011.07.001, 2011.

Alderkamp, A.-C., de Baar, H. J. W., Visser, R. J. W. and Arrigo, K. R.: Can photoinhibition control phytoplankton abundance in deeply mixed water columns of the Southern Ocean?, Limnol. Oceanogr., 55(3), 1248–1264, doi:10.4319/lo.2010.55.3.1248, 2010.

Archer, S. D., Ragni, M., Webster, R., Airs, R. L. and Geider, R. J.: Dimethylsulfoniopropionate and dimethylsulfide production in response to photoinhibition in Emiliania huxleyi, Limnol. Oceanogr., 55(4), 1579–1589, doi:10.4319/lo.2010.55.4.1579, 2010.

Arrigo, K. R., Mills, M. M., Kropuenske, L. R., van Dijken, G. L., Alderkamp, A.-C. and Robinson, D. H.: Photophysiology in two major southern ocean phytoplankton taxa: photosynthesis and growth of Phaeocystis antarctica and Fragilariopsis cylindrus under different irradiance levels., Integr. Comp. Biol., 50(6), 950–66, doi:10.1093/icb/icq021, 2010.

Belviso, S. and Caniaux, G.: A new assessment in North Atlantic waters of the relationship between DMS concentration and the upper mixed layer solar radiation dose, Global Biogeochem. Cycles, 23(1), 1–12, doi:10.1029/2008GB003382, 2009.

Bouchard, J. N., Roy, S. and Campbell, D. a: UVB effects on the photosystem II-D1 protein of phytoplankton and natural phytoplankton communities., Photochem. Photobiol., 82(4), 936–51, doi:10.1562/2005-08-31-IR-666, 2006.

Bouillon, R.-C. and Miller, W. L.: Determination of apparent quantum yield spectra of DMS photo-degradation in an in situ iron-induced Northeast Pacific Ocean bloom, Geophys. Res. Lett., 31(6), L06310, doi:10.1029/2004GL019536, 2004.

Bouillon, R.-C. and Miller, W. L.: Photodegradation of dimethyl sulfide (DMS) in natural waters: laboratory assessment of the nitrate-photolysis-induced DMS oxidation., Environ. Sci. Technol., 39(24), 9471–7, 2005.

Buma, A. G. J., Helbling, E. W., de Boer, M. K., Villafañe, V. E., Walter Helbling, E. and VillafaÒe, V. E.: Patterns of DNA damage and photoinhibition in temperate South-Atlantic picophytoplankton exposed to solar ultraviolet radiation., J. Photochem. Photobiol., 62(1-2), 9–18, 2001.

Charlson, J. R., Lovelock, J. E., Andreae, M. O. and Warren, S. G.: Oceanic phytoplankton, atmospheric sulphur, cloud albedo and climate., Nature, 326, 655–661, 1987.

Cullen, J. J., Ciotti, Á. M. and Davis, R. F.: The relationship between near-surface chlorophyll and solar-stimulated fluorescence: biological effects, SPIE, 2963, 272–277, 1997.

Cullen, J. J. and Lesser, M. P.: Inhibition of photosynthesis by ultraviolet radiation as a function of dose and dosage rate: Results for a marine diatom, Mar. Biol., 111(2), 183–190, doi:10.1007/BF01319699, 1991.

Cullen, J. J. and Macintyre, J. G.: Behavior, physiology and the niche of depth-regulating phytoplankton, Physiol. Ecol. Harmful Algal Bloom., (1978), 1998.

DiTullio, G. R., Sedwick, P. N., Jones, D. R., Boyd, P. W., Crossley, a. C. and Hutchins, D. a.: Effects of iron, silicate, and light on dimethylsulfoniopropionate production in the Australian Subantarctic Zone, J. Geophys. Res., 106(C12), 31585, doi:10.1029/2000JC000446, 2001.

Falkowski, P. G. and Laroche, J.: Acclimation to spectral irradiance in algae., J. Phycol., 27, 8–14, 1991.

Fritz, J., Neale, P., Davis, R. and Peloquin, J.: Response of Antarctic phytoplankton to solar UVR exposure: inhibition and recovery of photosynthesis in coastal and pelagic assemblages, Mar. Ecol. Prog. Ser., 365, 1–16, doi:10.3354/meps07610, 2008.

Galí, M., Ruiz-González, C., Lefort, T., Gasol, J. M., Cardelús, C., Romera-Castillo, C. and Simó, R.: Spectral irradiance dependence of sunlight effects on plankton dimethylsulfide production, Limnol. Oceanogr., 58(2), 489–504, doi:10.4319/lo.2013.58.2.0489, 2013a.

Galí, M., Saló, V., Almeda, R., Calbet, A. and Simó, R.: Stimulation of gross dimethylsulfide (DMS) production by solar radiation, Geophys. Res. Lett., 38(15), 1–5, doi:10.1029/2011GL048051, 2011.

Galí, M. and Simó, R.: Occurrence and cycling of dimethylated sulfur compounds in the Arctic during summer receding of the ice edge, Mar. Chem., 122(1-4), 105–117, doi:10.1016/j.marchem.2010.07.003, 2010.

Galí, M., Simó, R., Pérez, G. L., Ruiz-González, C., Sarmento, H., Royer, S.-J., Fuentes-Lema, A. and Gasol, J. M.: Differential response of planktonic primary, bacterial, and dimethylsulfide production rates to static vs. dynamic light exposure in upper mixed-layer summer sea waters, Biogeosciences, 10(12), 7983–7998, doi:10.5194/bgd-10-8851-2013, 2013b.

Galí, M., Simó, R., Vila-Costa, M., Ruiz-González, C., Gasol, J. M. and Matrai, P.: Diel patterns of oceanic dimethylsulfide (DMS) cycling: Microbial and physical drivers, Global Biogeochem. Cycles, 27, 1–17, doi:10.1002/gbc.20047, 2013c.

Garcia-Pichel, F.: A model for internal self-shading in planktonic organisms and its implications for the usefulness of ultraviolet sunscreens, Limnol. Oceanogr., 39(7), 1704–1717, doi:10.4319/lo.1994.39.7.1704, 1994.

Garcia-Pichel, F., Wingard, C. E. and Castenholz, R. W.: Evidence Regarding the UV Sunscreen Role of a Mycosporine-Like Compound in the Cyanobacterium Gloeocapsa sp, Appl. Environ. Microbiol., 59(1), 170–176, 1993.

Gebser, B. and Pohnert, G.: Synchronized regulation of different zwitterionic metabolites in the osmoadaption of phytoplankton., Mar. Drugs, 11(6), 2168–82, doi:10.3390/md11062168, 2013.

Geider, R., Graziano, L. and McKay, R. M.: Responses of the photosynthetic apparatus of Dunaliella tertiolecta (Chlorophyceae) to nitrogen and phosphorus limitation, Eur. J. Phycol., 33(4), 315–332, doi:10.1080/09670269810001736813, 1998.

Häder, D., Kumar, H. D., Smith, C. and Worrest, R. C.: Effects of solar UV radiation on aquatic ecosystems and interactions with climate change, in Environmental effects of ozone depletion and its interactions with climate change: 2006 assessment., pp. 95–134., 2006.

Harada, H., Vila-Costa, M., Cebrian, J. and Kiene, R. P.: Effects of UV radiation and nitrate limitation on the production of biogenic sulfur compounds by marine phytoplankton, Aquat. Bot., 90(1), 37–42, doi:DOI: 10.1016/j.aquabot.2008.05.004, 2009.

He, Y. and Häder, D.-P.: Reactive oxygen species and UV-B : effect on cyanobacteria, Photochem. Photobiol. Sci., 1(1), 729–736, doi:10.1039/b110365m, 2002.

Hefu, Y. and Kirst, G. O.: Effect of UV-radiation on DMSP content and DMS formation of Phaeocystis antarctica, Polar Biol., 402–409, 1997.

Henley, W. J. and Ramus, J.: Optimization of pigment content and the limits of photoacclimation for Ulva rotundata (Chlorophyta), Mar. Biol., 274, 267–274, 1989.

Holm-Hansen, O., Lubin, D. and Helbling, E. W.: Ultraviolet radiation and its effects on organisms in aquatic environments., in Environmental UV Photobiology., pp. 379–425, New York., 1993.

Kana, B. Y. T. M., Geider, R. J. and Christacritchley, D.: Regulation of photosynthetic pigments in micro-algae by multiple environmental factors : a dynamic balance hypothesis, New Phytol., 629–638, 1997.

Karsten, U., Kück, K., Vogt, C. and Kirst, G. O.: Dimethylsulfoniopropionate production in phototrophic organisms and its physiological function as a cryoprotectant., in Biological and environmental chemistry of DMSP and related sulfonium compounds., edited by R. P. Kiene, P. Visscher, M. D. Keller, and G. O. Kirst, pp. 143–153, New York., 1996.

Keller, M. D. and Korjeff-Bellows, W.: Physiological aspects of the production of DMSP by marine phytoplankton., in Biological and Environmental Chemistry of DMSP and Related Sulfonium Compounds., edited by G. O. Kiene, R.P., Visscher, P.T., Keller, M.D., Kirst, pp. 131–142, New York., 1996.

Kieber, D. J., Jiao, J., Kiene, P. and Bates, T. S.: Impact of dimethylsulfide photochemistry on methyl sulfur cycling in the Equatorial Pacific Ocean., J. Geophys. Res., 101, 3715–3722, 1996.

Kirk, J. T. O.: Light and photosynthesis in aquatic ecosystems, Cambridge., New York, NY., 2011.

Kolber, Z., Prasil, O. and Falkowski, P. P. G.: Measurements of variable chlorophyll fluorescence using fast repetition rate techniques: defining methodology and experimental protocols, Biochim. Biophys. Acta, 1367(1-3), 88–106, doi:10.1016/S0005-2728(98)00135-2., 1998.

Kolber, Z., Zehr, J. and Falkowski, P.: Effects of Growth Irradiance and Nitrogen Limitation on Photosynthetic Energy Conversion in Photosystem II, Plant Physiol., 923–929, 1988.

Koroleff, F. and Hansen, H. P.: Determination of nutrients, in Methods of Seawater Analysis, edited by K. Grasshoff, K. Kremling, and M. Ehrhardt, pp. 159–228, Wiley, Weinheim, New York., 1999.

Krause, H. G. and Weis, E.: Chlrophyll fluorescence and photosynthesis : The Basics, Annu. Rev. Plant Physiol. Plant Mol. Biol., 42, 313–319, 1991.

Kropuenske, L. R., Mills, M. M., van Dijken, G. L., Alderkamp, A.-C., Mine Berg, G., Robinson, D. H., Welschmeyer, N. a. and Arrigo, K. R.: Strategies and Rates of Photoacclimation in Two Major Southern Ocean Phytoplankton Taxa: Phaeocystis Antarctica (Haptophyta) and Fragilariopsis Cylindrus (Bacillariophyceae)1, J. Phycol., 46(6), 1138–1151, doi:10.1111/j.1529-8817.2010.00922.x, 2010.

Kropuenske, L. R., Mills, M. M., van Dijken, G. L., Bailey, S., Robinson, D. H., Welschmeyer, N. a. and Arrigo, K. R.: Photophysiology in two major Southern Ocean phytoplankton taxa: Photoprotection in Phaeocystis antarctica and Fragilariopsis cylindrus, Limnol. Oceanogr., 54(4), 1176–1196, 2009.

Larsen, S. H.: Comment on "Analysis of a potential 'solar radiation dose-dimethylsulfide-cloud condensation nuclei' link from globally mapped seasonal correlations" by S. M. Vallina et al., Global Biogeochem. Cycles, 22(3), 2008.

Van Leeuwe, M. a. and Stefels, J.: Photosynthetic responses in Phaeocystis antarctica towards varying light and iron conditions, Biogeochemistry, 83(1-3), 61–70, doi:10.1007/s10533-007-9083-5, 2007.

Lesser, M. P.: Oxidative stress in marine environment : Biochemistry and Physiological Ecology, Annu. Rev. Physiol., (68), 253–278, doi:10.1146/annurev.physiol.68.040104.110001, 2006.

Lesser, M. P., Cullen, J. J. and Neale, P. J.: Carbon uptake in a matine diatom during acute exposure to ultraviolet B radiaton: relative importance of damage and repair, J. Phycol., 30(2), 183–192, 1994.

Litchman, E., Neale, P. J. and Banaszak, A. T.: Increased sensitivity to ultraviolet radiation in nitrogen-limited dinoflagellates: Photoprotection and repair, Limnol. Oceanogr., 47(1), 86–94, 2002.

Llabrés, M. and Agustí, S.: Picophytoplankton Cell Death Induced by UV Radiation: Evidence for Oceanic Atlantic Communities, Limnol. Oceanogr., 51(1), 21–29, 2006.

Lopez-Rosado, R.: Photosynthetic Efficiency of Phototrophic Plankton and Bio-Optical Variability as Influenced by Mesoscale Processes In the Eastern Caribbean Basin., 2008.

Lund, J. W. G., Kipling, C. and Le Cren, E. D.: The Inverted Microscope Method of Estimating Algal Numbers and the Statistical Basis of Estimations by Counting, Hydrobiologia, 11, 143–170, 1958.

Macintyre, H. L., Kana, T. M. and Geider, R. J.: Photoacclimation of photosynthesis irradiance response curves and photosynthetic pigments in microalgae and cyanobacteria, J. Phycol., 38(July 2000), 17–38, 2002.

Martinez, G., Retamal, L., Hannach, G., Montecino, V. and Molina, X.: Ecophysiological strategies in response to UV-B radiation stress in cultures of temperate microalgae isolated from the Pacific coast of South America, Rev. Chil. Hist. Nat., 74, 293–311, 2001.

Marwood, C. a, Smith, R. E., Furgal, J. a, Charlton, M. N., Solomon, K. R. and Greenberg, B. M.: Photoinhibition of natural phytoplankton assemblages in Lake Erie exposed to solar ultraviolet radiation, Can. J. Fish. Aquat. Sci., 57(2), 371–379, doi:10.1139/f99-258, 2000.

Matrai, P. A., Vernet, M., Hood, R., Jennings, A., Brody, E. and Saemundsdóttir, S.: Light-dependence of carbon and sulfur production by polar clones of the genus Phaeocystis, Mar. Biol., 124, 157–167, 1995.

Melis, A., Nemson, J. A. and Harrison, M. A.: Damage to functional components and partial degradation of Photosystem II reaction center proteins upon chloroplast exposure to ultravic let-B radiation, Biochim. Biophys. Acta, (1100), 312–320, 1992.

Melling, H., Gratton, Y. and Ingram, G.: Ocean circulation within the North Water polynya of Baffin Bay, Atmosphere-Ocean, 39(3), 301–325, doi:10.1080/07055900.2001.9649683, 2001.

Morel, A. and Smith, R. C.: Relation between total quanta and total energy for aquatic photosynthesis, Limnol. Oceanogr., 19(July), 1974.

Neale, P. J.: Spectral weighting functions for quantifying the effects of ultraviolet radiation in marine ecosystems., in The Effects of UV Radiation on Marine Ecosystems, edited by S. de Mora, S. Demers, and M. Vernet, pp. 73–100, Cambridge University Press, Cambridge, United Kingdom., 2000.

Neale, P. J.: Modeling the effects of ultraviolet radiation on estuarine phytoplankton production: impact of variations in exposure and sensitivity to inhibition, J. Photochem. Photobiol. B Biol., 62(1-2), 1–8, 2001.

Neale, P. J., Banaszak, A. T. and Jarriel, C. R.: Ultraviolet sunscreens in gymnodinium sanguineum (dinophyceae): mycosporine-like amino acids protect against inhibition of photosynthesis, J. Phycol., 938, 928–938, 1998a.

Neale, P. J., Davis, R. F. and Cullen, J. J.: Interactive effects of ozone depletion and vertical mixing on photosynthesis of Antarctic phytoplankton, Nature, 392(6676), 585–589, 1998b.

Neale, P. J., Sobrino, C. and Gargett, A. E.: Vertical mixing and the effects of solar radiation on photosystem II electron transport by phytoplankton in the Ross Sea Polynya, DSR Part I., 63, 118–132, 2012.

Parsons, T. R., Maita, Y. and Lalli, C. M.: A Manual of Chemical & Biological Methods for Seawater Analysis, Pergamon., Elsevier, Toronto., 1984.

Petrou, K., Doblin, M. a., Smith, R. a., Ralph, P. J., Shelly, K. and Beardall, J.: State Transitions and Nonphotochemical Quenching During a Nutrient-Induced Fluorescence Transient in Phosphorus-Starved Dunaliella Tertiolecta 1, J. Phycol., 44(5), 1204–1211, doi:10.1111/j.1529-8817.2008.00585.x, 2008.

Richardson, K., Beardall, J. and Raven, J. a.: Adaptation of unicellular algae to irradiance: an analysis of strategies, New Phytol., 93(2), 157–191, doi:10.1111/j.1469-8137.1983.tb03422.x, 1983.

Van Rijssel, M. and Buma, A. G. J.: UV radiation induced stress does not affect DMSP synthesis in the marine prymnesiophyte Emiliania huxleyi, Aquat. Microb. Ecol., 28(2), 167–174, 2002.

Roy, S.: Strategies for the Minimisation of UV-induced Damage, in The Effects of UV Radiation in the Marine Environment., 2000.

Royer, S.-J., Galí, M., Saltzman, E. S., McCormick, C. A., Bell, T. G. and Simó, R.: Development and validation of a shipboard system for measuring high-resolution vertical profiles of aqueous dimethylsulfide concentrations using chemical ionisation mass spectrometry, Environ. Chem., 11, 309–317, 2014.

Samuelsson, G., Lönneborg, a, Rosenqvist, E., Gustafsson, P. and Oquist, G.: Photoinhibition and Reactivation of Photosynthesis in the Cyanobacterium Anacystis nidulans., Plant Physiol., 79(4), 992–5, 1985.

Simó, R.: Production of atmospheric sulfur by oceanic plankton: biogeochemical, ecological and evolutionary links., Trends Ecol. Evol., 16(6), 287–294, 2001.

Simó, R., Hatton, A. D., Malin, G. and Liss, P. S.: Particulate dimethyl sulphoxide in seawater: production by microplankton, Mar. Ecol. Prog. Ser., 167, 291–296, 1998.

Sinha, V., Williams, J. and Meyerh, M.: Air-sea fluxes of methanol, acetone, acetaldehyde, isoprene and DMS from a Norwegian fjord following a phytoplankton bloom in a mesocosm experiment, Atmos. Chem. Phys., 739–755, 2007.

Six, C., Finkel, Z. V, Irwin, A. J. and Campbell, D. a: Light variability illuminates niche-partitioning among marine Picocyanobacteria., PLoS One, 2(12), e1341, doi:10.1371/journal.pone.0001341, 2007.

Slezak, D. and Herndl, G. J.: Effects of ultraviolet and visible radiation on the cellular concentrations of dimethylsulfoniopropionate (DMSP) in Emiliania huxleyi (strain L), Mar. Ecol. Prog. Ser., 246, 61–71, 2003.

Slezak, D., Kiene, R., Toole, D., Simó, R. and Kieber, D.: Effects of solar radiation on the fate of dissolved DMSP and conversion to DMS in seawater, Aquat. Sci., 69(3), 377–393, 2007.

Smith, R. C. and Baker, K. S.: Stratospheric ozone, middle ultraviolet radiation and phytoplankton productivity, Oceanography, 1989.

Sobrino, C. and Neale, P. J.: Short-term and long-term effects of temperature on photosynthesis in the diatom Thalassiosira pseudonana under UVR exposures, J. Phycol., 43, 426–436, doi:10.1111/j.1529-8817.2007.00344.x, 2007.

Sobrino, C., Neale, P. J., Lubián, L. M. and Lubia, L. M.: Interaction of UV Radiation and Inorganic Carbon Supply in the Inhibition of Photosynthesis : Spectral and Temporal Responses of Two Marine Picoplankters, Photochem. Photobiol., 81(2), 384–393, doi:10.1562/2004-08-27-RA-295, 2005a.

Sobrino, C., Neale, P. J., Montero, O. and Lubia, L. M.: Biological weighting function for xanthophyll de-epoxidation induced by ultraviolet radiation, Physiol. Plant., 125, 41–51, 2005b.

Sommaruga, R.: UVR and its effects on species interactions, in UV effects in aquatic organisms and ecosystems. Comprehensive Series in Photosciences., pp. 485–508, London., 2003.

Spielmeyer, A., Gebser, B. and Pohnert, G.: Dimethylsulfide sources from microalgae : Improvement and application of a derivatization-based method for the determination of dimethylsulfoniopropionate and other zwitterionic osmolytes in phytoplankton, Mar. Chem., 124(1-4), 48–56, 2011.

Stefels, J.: Physiological aspects of the production and conversion of DMSP in marine algae and higher plants., J. Sea Res., 43, 183–197, 2000.

Stefels, J. and van Leeuwe, M. A.: Effects of iron and light stress on the biochemical composition of antarctic phaeocystis sp . (prymnesiophyceae). i . intracellular dmsp, J. Phycol., 495, 486–495, 1998.

Stefels, J., Steinke, M., Turner, S., Malin, G. and Belviso, S.: Review: Environmental constraints on the production and removal of the climatically active gas dimethylsulphide (DMS) and implications for ecosystem modelling., Biogeochemistry, 83(1-3), 245–275, 2007.

Strid, Å., Chow, W. S. and Anderson, J. M.: Effects of supplementary ultraviolet-B radiation on photosynthesis in Pisum sativum, Biochim. Biophys. Acta - Bioenerg., 1020(3), 260–268, 1990.

Sunda, W., Kieber, D. J., Kiene, R. P. and Huntsman, S.: An antioxidant function for DMSP and DMS in marine algae., Nature, 418(6895), 317–20, 2002.

Taalba, a., Xie, H., Scarratt, M. G., Bélanger, S. and Levasseur, M.: Photooxidation of dimethylsulfide (DMS) in the Canadian Arctic, Biogeosciences, 10(11), 6793–6806, doi:10.5194/bg-10-6793-2013, 2013.

Toole, D. A., Kieber, D. J., Kiene, R. P., Siegel, D. A., Norman, B. and Nelson, N. B.: Photolysis and the dimethylsulfide (DMS) summer paradox in the Sargasso Sea, Limnol. Oceanogr., 48(3), 1088–1100, 2003.

Toole, D. a. and Siegel, D. A.: Light-driven cycling of dimethylsulfide (DMS) in the Sargasso Sea: Closing the loop, Geophys. Res. Lett., 31(9), 5–8, doi:10.1029/2004GL019581, 2004.

Toole, D. a., Slezak, D., Kiene, R. P., Kieber, D. J. and Siegel, D. a.: Effects of solar radiation on dimethylsulfide cycling in the western Atlantic Ocean, Deep Sea Res. Part I Oceanogr. Res. Pap., 53(1), 136–153, 2006.

Del Valle, D. a., Kiene, R. P. and Karl, D. M.: Effect of visible light on DMSP assimilation and conversion to DMS in the North Pacific Subtropical Gyre, Aquat. Microb. Ecol., 66(1), 47–62, 2012.

Vallina, S. M. and Simó, R.: Strong relationship between DMS and the solar radiation dose over the global surface ocean., Science (80-.)., 315(5811), 506–8, 2007.

Vance, T., Davidson, A., Thomson, P., Levasseur, M., Lizotte, M., Curran, M. and Jones, G.: Rapid DMSP production by an Antarctic phytoplankton community exposed to natural surface irradiances in late spring, Aquat. Microb. Ecol., 71(2), 117–129, 2013.

Velders, G. J. M., Andersen, S. O., Daniel, J. S., Fahey, D. W. and McFarland, M.: The importance of the Montreal Protocol in protecting climate., Proc. Natl. Acad. Sci. U. S. A., 104(12), 4814–9, 2007.

Vincent, W. F. and Neale, P. J.: Mechanisms of UV damage to aquatic organisms., in The Effects of UV Radiation on Marine Ecosystems., edited by M. (Eds. . de Mora, S.J., Demers, S., Vernet, pp. 149–176, Cambridge., 2000.

Vincent, W. F., Neale, P. J. and Richerson, P. J.: Photoinhibition: algal responses to bright light during diel stratification and mixing in a tropical alpine lake, J. Phycol., 20, 201–211, 1984.

Vincent, W. F. and Roy, S.: Solar ultraviolet-B radiation and aquatic primary production: damage, protection, and recovery, Environ. Rev., 1(1), 1–12, doi:10.1139/a93-001, 1993.

Wilhelm, C., Bida, J., Domin, A., Hilse, C., Kaiser, B., Kesselmeier, J. and Lohr, M.: Interaction between global climate change and the physiological responses of algae., Photosynthetica, 33, 491–503, 1997.

Zeeshan, M. and Prasad, S. M.: Differential response of growth, photosynthesis, antioxidant enzymes and lipid peroxidation to UV-B radiation in three cyanobacteria, South African J. Bot., 75(3), 466–474, 2009.

Zepp, R. G., Erickson, D. J. 3rd, Paul, N. D. and Sulzberger, B.: Interactive effects of solar UV radiation and climate change on biogeochemical cycling., Environ. Eff. ozone Deplet. its Interact. with Clim. Chang. 2006 assessment., 6(3), 286–300, doi:10.1039/b700021a, 2006.

Zhu, S.-H. and Green, B. R.: Photoprotection in the diatom Thalassiosira pseudonana: role of LI818-like proteins in response to high light stress., Biochim. Biophys. Acta, 1797(8), 1449–57, doi:10.1016/j.bbabio.2010.04.003, 2010.

Chapter 2

Differential response of planktonic primary, bacterial, and dimethylsulfide production rates to static vs. dynamic light exposure in upper mixed-layer summer sea waters

---

Biogeosciences, V10, p. 7983-7998, 2013

Martí Galí, Rafel Simó, Gustavo Pérez, Clara Ruiz-González, Hugo Sarmento, Sarah-Jeanne Royer, Antonio Fuentes-Lema and Josep M. Gasol

Abstract

Microbial plankton experience short-term fluctuations in total solar irradiance and in its spectral composition as they are vertically moved by turbulence in the oceanic upper mixed layer (UML). The fact that the light exposure is not static but dynamic may have important consequences for biogeochemical processes and ocean–atmosphere fluxes. However, most biogeochemical processes other than primary production, like bacterial production or dimethylsulfide (DMS) production, are seldom measured in sunlight and even less often in dynamic light fields. We conducted four experiments in oligotrophic summer stratified Mediterranean waters, where a sample from the UML was incubated in ultraviolet (UV)-transparent bottles at three fixed depths within the UML and on a vertically moving basket across the same depth range. We assessed the response of the phyto- and bacterioplankton community with physiological indicators based on flow cytometry singe-cell measurements, fast repetition rate fluorometry (FRRf), phytoplankton pigment concentrations and particulate light absorption. Dynamic light exposure caused a subtle disruption of the photoinhibition and photoacclimation processes associated with ultraviolet radiation (UVR), which slightly alleviated bacterial photoinhibition but did not favor primary production. Gross DMS production (GP_{DMS}) decreased sharply with depth in parallel to shortwave UVR, and displayed a dose-dependent response that mixing did not significantly disrupt. To our knowledge, we provide the first measurements of GP_{DMS} under in situ UV-inclusive optical conditions.

Introduction

The characteristic response times of microbial plankton match the natural variability of light exposure, which changes at different temporal scales with solar elevation, the passage of clouds, vertical mixing and even wave focusing (Gallegos and Platt, 1985). In transparent oceanic waters, exposure to high irradiance (photosynthetically available radiation, PAR) is accompanied by exposure to detrimental ultraviolet radiation (UVR) in the upper portion of the water column (Vincent and Neale, 2000). Short-term irradiance fluctuations elicit fast and reversible responses (Roy, 2000), whereas continued exposure to high PAR and UVR may elicit photoacclimation (MacIntyre et al., 2002) or permanent physiological changes, i.e., irreversible damage (Buma et al., 2001).

Vertical mixing can have a positive, neutral or negative effect on water-column-integrated processes depending on the interplay between mixing rates, damage and repair kinetics, and underwater attenuation of PAR and UVR (Neale et al., 2003). In the absence of repair mechanisms, damage will be proportional to cumulative exposure (i.e., it will be dose-dependent). If moderate repair exists, mixing will allow the cells to recover in the UVR shaded portion of the upper mixed layer (UML; Figure 1A). In this situation the photodamage will no longer be dose-dependent and a steady state will be achieved provided that the cells spend sufficient time under constant exposure conditions. In the idealized situation where damage is completely counteracted by repair on a timescale much shorter than the mixing time, or in the absence of repair, vertical mixing will have neutral effects. These responses can change with exposure time. The effects of dynamic light exposure have concerned the aquatic photosynthesis research community for almost 40 yr (see Gallegos and Platt, 1985, and references therein), and apparently contradictory findings have often been reached using either experimental or modeling approaches (Ross et al., 2011a, b). It appears that the ability to take advantage of dynamic light exposure may depend on the taxonomic composition

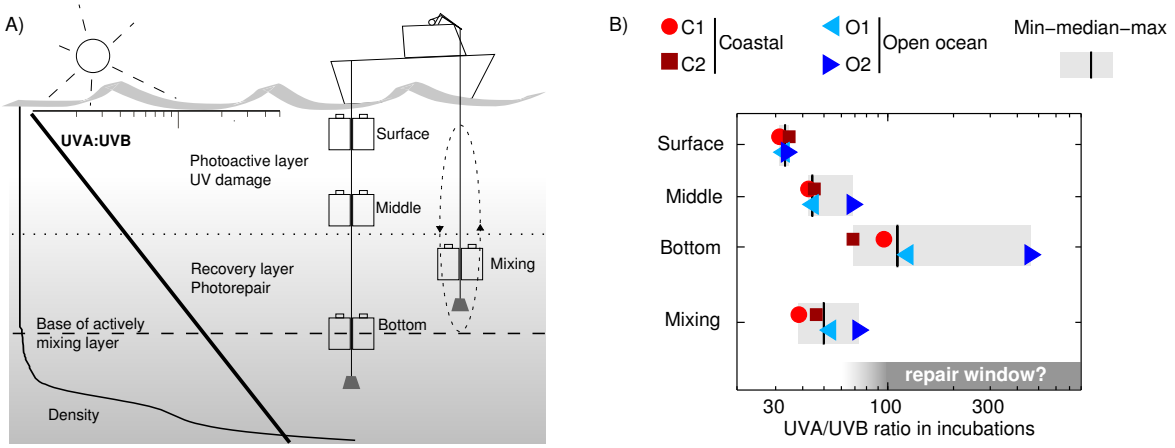

Figure 1. (A) Illustration of the experimental design. Vertically moving and fixed-depth bottles were incubated in a spectral irradiance gradient, depicted by the UVA/UVB ratio. The dotted and the dashed lines represent the depth of the hypothetical photoactive layer and actively mixing layer, respectively; (B) UVA/UVB in the different treatments in each experiment. The horizontal bar indicates the UVA/UVB window where photolyase repair of bacterioplankton is more efficient, calculated from underwater UVR profiles according to Kaiser and Herndl (1997).

and size structure of the phytoplankton community, their light history, and their nutritional status (Barbieri et al., 2002; Brunet and Lavaud, 2010; Helbling et al., 2013). Knowledge on the photoresponse of (bacterial) heterotrophic activity is much more limited, but a number of studies suggest that significant PAR-driven stimulation frequently occurs (Morán et al., 2001; Church et al., 2004), as does inhibition due to UVR (Aas et al., 1996; Kaiser and Herndl, 1997). There is mounting evidence that UVR resistance and photostimulation responses vary among bacterial phylogenetic groups (Agogué et al., 2005; Alonso-Sáez et al., 2006; Ruiz-González et al., 2012), which might be related to the occurrence of photoheterotrophic metabolisms in the ocean (Kolber et al., 2000; Béjà et al., 2000; Kirchman and Hanson, 2012) or to their interaction with other light-driven processes (see references in Ruiz-González et al., 2013).

Besides carbon and nutrient cycling, solar radiation modulates the biogeochemical cycles of other elements such as sulphur or halogens (Carpenter et al., 2012). The volatile dimethylsulfide (DMS) is produced mainly by the enzymatic cleavage of the phytoplankton osmolyte dimethylsulfoniopropionate (DMSP) as a result of

microbial food web interactions (Simó, 2004). Marine DMS emission represents the main natural source of sulphur to the atmosphere (Lana et al., 2011) and has potential implications for climate regulation, which in turn depends on its response to solar radiation (Vallina and Simó, 2007). Yet, the climatic effects of DMS and the underlying atmospheric processes remain highly controversial (Quinn and Bates, 2011; Woodhouse et al., 2013). The response of community DMS production to sunlight depends on a number of interdependent effects: phytoplankton DMSP production, its intracellular conversion to DMS followed by DMS permeation outside the algal cell, algal DMSP release (due to grazing, cell lysis or active exudation), and DMSP transformations by the microbial food web (Galí et al., 2013a). Phytoplankton culture studies have shown that acclimation to strong UV exposure (and also strong PAR) on a timescale of several days generally causes up-regulation of intracellular DMSP content (Sunda et al., 2002; Slezak and Herndl, 2003), although this view has been challenged (van Rijssel and Buma, 2002). Nutrient limitation (particularly nitrogen) also causes up-regulation of intracellular DMSP (Bucciarelli and Sunda, 2003; Yang et al., 2011), and may interact in complex ways with UVR (Harada et al., 2009). Evidence obtained from culture studies is supported by field observations of higher DMS and DMSP concentrations per unit phytoplankton biomass (and often in absolute terms) during summer stratification (Simó and Pedrós-Alió, 1999; Vila-Costa et al., 2008; Archer et al., 2009). Phytoplankton DMS production is also enhanced by UV exposure (Hefu and Kirst, 1997; Sunda et al., 2002; Archer et al., 2010) and nitrogen limitation (Sunda et al., 2007). Yet, most phytoplankton culture studies have failed to account for photochemical DMS loss, which has precluded a neat assessment of UV effects on phytoplankton DMS production. The ensemble of these observations tends to support the view that DMSP and its metabolites play an antioxidant role in phytoplankton cells (Sunda et al., 2002). In this regard, it is important to note that long- and short-term responses may differ. I.e., a long-term up-regulation response caused by acclimation to oxidative stress is compatible with a short-

term decrease in the intracellular DMSP pool due to enhanced DMSP destruction, as observed by Hefu and Kirst (1997) and van Rijssel and Buma (2002). It has recently been shown that sunlight stimulates community gross DMS production (GP_{DMS}; Galí et al., 2011) in an irradiance- and spectrum-dependent manner (Galí et al., 2013a). Moreover, community gross DMS production rates followed the diurnal irradiance cycle in summer stratified waters (Galí et al., 2013b). Phytoplankton radiative stress was the primary explanation invoked by the authors, but food web interactions might also play a role, as thoroughly discussed in those articles.

We designed an experiment where a single surface seawater sample was incubated in UVR-transparent bottles at three fixed optical depths, approximately corresponding to the water subsurface, the optical middle, and the bottom of the UML. An additional set of bottles was regularly moved up and down across the same depth range and radiation gradient (Figure 1; Table 1). Simulating turbulent mixing experimentally is extremely difficult, and the mixing rates applied to the dynamic incubations were probably not realistic due to being too fast, being constant and having a fixed oscillation period (see Section. 3.1). Yet, dynamic light exposure might still be more realistic than fixed-depth incubations and provide relevant insights into the photoinhibition and photoacclimation processes occurring in upper mixing waters. The experimental design was aimed at answering two questions regarding the short-term response of planktonic activity to dynamic light exposure. (1) Photobiological: should the mixing bottles display the same response as the ones incubated at the middle optical depth considering that both treatments received a similar cumulative dose? If the response was the same this would imply that the measured processes were dose-dependent. (2) Biogeochemical and methodological: in UVR-transparent and shallow mixing layers, are the rates obtained from vertical integration of static bottle incubations equivalent to those obtained in vertically moving bottles?

Methods

Experimental setting and irradiance calculations

Surface (0.2 to 3 m deep) seawater samples were taken predawn in 20–30 L polycarbonate carboys dimmed with a black plastic bag. In the coastal experiments (C1 and C2) the samples were taken from a boat at the Blanes Bay Microbial Observatory coastal site (BBMO; 0.5 miles offshore over a water column depth of 20 m), brought to the lab, maintained within ±1 °C of the sea surface temperature, and incubated at the pier of the Barcelona Olympic Harbor during 4 h centered on the solar noon. The oceanic experiments (O1 and O2) were done in the open Mediterranean Sea during a Lagrangian cruise over a water column depth of ca. 2000 m (*R/V* García del Cid). In these experiments the samples were maintained in a thermostated bath at the sea surface temperature until they were incubated in situ (Figure 1A), beginning 4 h before solar noon and ending 2 h after solar noon (with an intermediate sample taken after the first 2 h). In C1 and C2 mixing was applied by moving the bottle basket (Figure 1A) manually every 15 min, completing a mixing cycle every 60 min. In the ship-based experiments the mixing bottles were continuously moved using the winch of the ship at the smallest possible vertical speed (3–4 cm s^{-1}), completing a cycle in 10–18 min. Since the waters were less transparent in the harbor than at the BBMO, in C1 and C2 the bottles were incubated at shallower depths to approximate the equivalent in situ optical depths (Table 1). Mixing layer depths (MLD) were estimated from temperature profiles obtained with a conductivity-temperature-depth (CTD) probe, and defined by a > 0.1 °C deviation with respect to 1 m depth. The buoyancy or Brunt–Väisälä frequency was calculated in 1 m bins (Figure 2), and used as an additional criterion to distinguish the weakly stratified UML from the more stratified waters below. The irradiance just below the water surface (subsurface irradiance) during the incubations was recorded with a PUV-2500 (Biospherical) multichannel filter radiometer, which was also used to measure

Table 1. Summary of initial sample characteristics, ecosystem settings and experimental conditions. Phytoplankton group dominance is indicated in a qualitative manner, with biomass calculations made following Simó et al. (2009). All biogeochemical process rates refer to the experimental incubation except for LIR t0, which correspond to the initial sample. GP_{DMS} and NPbio, DMS stand for gross and net biological DMS production, respectively. Pro: Prochlorococcus; Syn: Synechococcus; PPeuk: photosynthetic picoeukaryotes; Diat: diatoms; Dino: dinoflagellates; Hapto: haptophytes; na: not available. See text for other abbreviations.

Experiment code	Coastal 1 (C1)	Coastal 2 (C2)	Oceanic 1 (O1)	Oceanic 2 (O2)
Date	27 Jul 2010	29 Jul 2010	16 Sep 2011	20 Sep 2011
Sampling position	41.67 N 2.81 E		40.9 N 2.67 E	40.9 N 2.44 E
Physicochemical characteristics of the upper mixed layer				
SST (°C)	23.0	22.7	25.2	23.6
Nitrate + nitrite (μmol L^{-1})	0.53	0.67	0.03	0.04
Phosphate (μmol L^{-1})	0.08	0.15	0.06	0.06
Silicate (μmol L^{-1})	0.77	1.05	0.53	0.59
MLD (m)	4	3	7	16
Z 10 % 320 nm (m)	7	7	12	11
Z 10 % 380 nm (m)	20	20	38	32
Buoyancy frequency (h^{-1})	6.2 ± 1.7	8.8 ± 2.7	8.1 ± 2.8	4.9 ± 0.9
Wind speed (m s^{-1})	2.4–6.7	1.4 –7.1	0.3–4.8	1.0–9.5
UVB range (W m^{-2})	0.4–1.4	0.4–1.1	0.3–1.1	0.04–1.1
UVA range (W m^{-2})	22–37	21–31	19–30	9–30
PAR range (μmol phontons m^2 s^{-1})	1100–1580	1010–1330	830–1360	410–1340
Experimental conditions				
Incubation depth (m)	0.3, 1, 3	0.5, 1.5, 3.5	0.5, 3, 11	0.5, 5.5, 18
Equivalent depth UVB (m)	1.3, 4, 10	1.3, 3.5, 6	2.5, 5, 13	2.5, 7, 20
Mixing time (min)	60	60	18	10
UVB range (W m^{-2})	0.04–0.9	0.13–0.7	0.09–0.7	0.01–0.65
UVA range (W m^{-2})	4–28	9–24	11–23	5–22
PAR range (μE)	460–1930	600–1210	610–1360	320–1290
Initial sample characteristics				
DMS (nmol L^{-1})	7.5	8.5	2.1	2.1
DMSPt (nmol L^{-1})	23.0	18.5	18.2	19.6
Chl *a* (μg L^{-1})	0.24	0.25	0.08	0.08
Dominant phytoplankton (biomass)	PPeuk > Diat > Pro		Syn > Dino > PPeuk (Hapto)	
Bacteria (10^5 cells mL^{-1})	9.0	7.3	9.4	7.3
Intact-membrane bacteria (%)	54	52	56	56
Biogeochemical process rates (min–max)				
PPp (nmol C L^{-1} h^{-1})	80–150	160–200	20–26	21–25
LIR t_0 (pmol leu L^{-1} h^{-1})	32	21	36	18
LIR (pmol leu L^{-1} h^{-1})	33–37	16–21	37–44	17–27
GP_{DMS} (nmol DMS L^{-1} h^{-1})	0.05–0.40	0.24–0.49	na	0.07–0.17
$NP_{bio,DMS}$ (nmol DMS L^{-1} h^{-1})	0.03–0.32	0.18–0.44	0.02–0.10	0.04–0.16

underwater irradiance profiles in C1 and C2. In O1 and O2, the vertical profiles were measured with a PRR-800 (Biospherical). Diffuse attenuation coefficients of downward irradiance (Kd) were calculated as the linear regression between ln-transformed spectral irradiance and depth (z) in the optically homogeneous surface layer where the incubations were done. The time series of subsurface irradiance were converted to the irradiance seen by each water sample by applying the attenuation due to seawater ($e^{-Kd \cdot z}$) and the attenuation due to the incubation bottles. We used polytetrafluoroethylene (Teflon, Nalgene) bottles, which according to our measurements transmit 65 %, 77% and

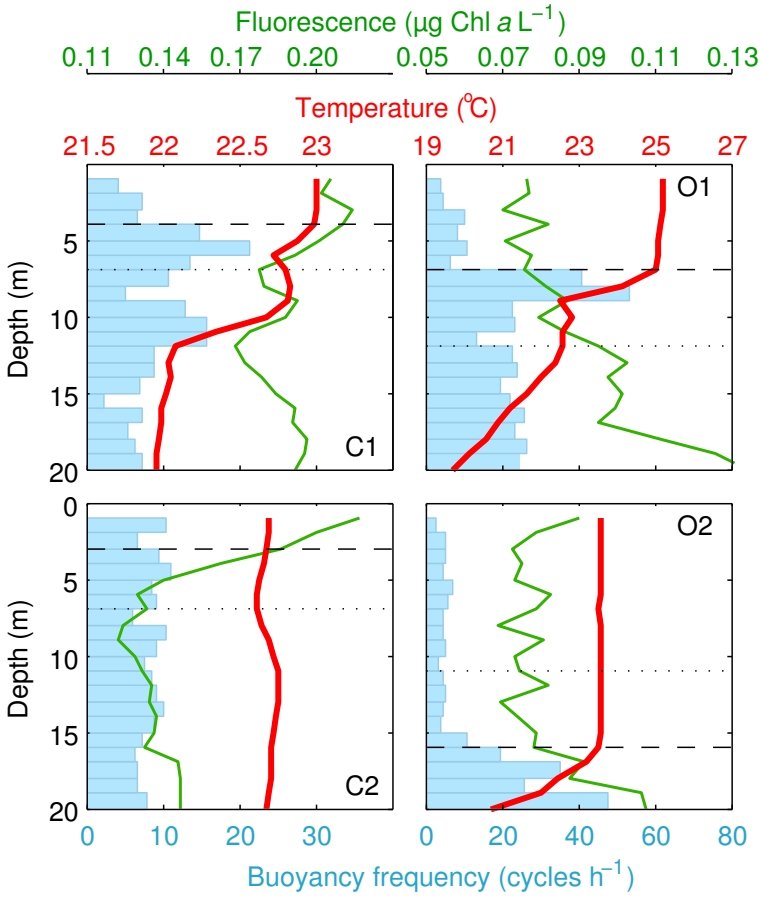

Figure 2. Vertical profiles of temperature, Chl*a* fluorescence and buoyancy (Brunt–Väisälä) frequency at the time of sampling in the four experiments. The horizontal dashed line indicates the depth of the mixing layer and the dotted line the 10%penetration of 320 nm radiation (see also Table 1).

100% of spectral irradiance in the UVB, UVA and PAR bands, respectively (Galí et al., 2013a). The bottles were placed in a metallic basket, which caused a minimal alteration of the tridimensional light field. For the mixing bottles, the irradiance calculation was made using a time-varying depth that corresponded to the vertical displacement of the basket. In each incubation, the mean UVB (300–320 nm) and UVA (320–400 nm) irradiance was calculated by integrating over the spectrum the mean spectral irradiance in the 6 bands measured by the PUV-2500 (centered at 305, 313, 320, 340, 380 and 395 nm) as described by Galí et al. (2013a). PAR was measured in a single integrated band (400–700 nm) so that no spectral integration was required. The irradiance dose was calculated by multiplying the mean irradiance by the total incubation time.

Process measurements and analysis techniques

Primary production was measured as the ^{14}C incorporated into particles in duplicate 40mL Teflon bottles inoculated with $NaH^{14}CO_3$ (Morán et al., 1999) and incubated in situ (including dark controls). Bacterial heterotrophic production rates were measured as ^{3}H-leucine incorporation rates (LIRs; Kirchman et al., 1985; Smith and Azam, 1992) in the initial samples and on subsamples taken from the larger (2.3 L) Teflon incubation bottles after in situ light exposure. Triplicate subsamples plus one killed control from each Teflon bottle were further incubated for 2 h in the dark at in situ temperature in 1.5 mL Eppendorf vials. In C1 and C2, LIRs were measured only in initial and final (4 h) samples. In O1 and O2, incubation-averaged LIRs were calculated as the time-weighted average of intermediate (2 h) and final time (6 h) incubations. We assumed the intermediate LIR measurement to represent the initial 2 h exposure, and the final LIR measurement the subsequent 4 h period. In C1 and C2 leucine incorporation was also measured during "in situ" sunlit incubations in 40 mL Teflon bottles to which ^{3}H-leucine had been added. Samples for pigment analysis were obtained by filtering 1–2 L seawater onto GF/F filters at the beginning and the end of the incubations (O1 and O2 only) and the filters were immediately stored in liquid

nitrogen. Pigments were extracted and analyzed by HPLC following Zapata et al. (2000) on a Spectra SYSTEM (Thermo) using a Waters Symmetry C8 column (150 X 4.6 mm, 3.5 μ particle size, 10 nm pore size). Calibration was made using commercial external pigment standards (DHI, Denmark), and the pigments were identified according to their elution time. The absorption spectra of total particulate matter ap were determined by the quantitative filter technique, using the simple transmittance method in a Lambda 800 (Perkin-Elmer) spectrophotometer. Water samples (2 L) were filtered onboard using 25 mm-diameter GF/F filters. Immediately after filtration absorbance scans were measured from 350 to 750 nm at 1 nm intervals. The quantitative filter technique was applied according to NASA's optics protocols for absorption coefficient measurements (Mitchell et al., 2000). In order to minimize light scattering, the wet filters were placed as close to the spectrophotometer detector as possible and measured against a blank clean filter wetted with filtered (0.2 μm) seawater. Absorption coefficients were estimated according to the relationship:

$$a_{\mathrm{p}}(\lambda) = \frac{2.303\, A_{\mathrm{filter}}(\lambda)\, s}{V_{\mathrm{filt}}\, \beta(\lambda)}$$

where $A_{filter}(\lambda)$ is the measured absorbance, s is the clearance area of the filter, V_{filt} is the volume of filtered water, and $\beta(\lambda)$ is the amplification factor vector (Mitchell and Kiefer, 1984). The maximum quantum yield of photosystem II photochemistry (FvFm), an indicator of phytoplankton photosynthetic performance and photoinhibition, was measured by fast repetition rate fluorometry (FastTracka I, Chelsea), as detailed by Galí et al. (2013a). A FACSCalibur (Becton & Dickinson) flow cytometer equipped with a 15 mW Argon-ion laser (488 nm emission) was used to enumerate picophyto- and bacterioplankton populations and to measure their performance at the single-cell level. The cell-specific fluorescence of each different picophytoplankton population (normalized to their side scatter – SSC, a proxy for cell size) was measured following Marie and Partensky (2006). At least 30 000 events were acquired for each subsample. Fluorescent

beads (1 μm, Fluoresbrite carboxylate microspheres, Polysciences Inc., Warrington, PA, USA) were added at a known density as internal standards. Two subpopulations of heterotrophic bacterioplankton were distinguished based on the nucleic acid double-staining (NADS) viability protocol: intact membrane (or "live") bacteria and membrane-compromised (or "dead") bacteria (Grégori et al., 2001). This protocol uses a combination of the cell-permeant nucleic acid stain SybrGreen I (SGI, Molecular Probes, Eugene, OR, USA) and the cell-impermeant propidium iodine (PI, Sigma Chemical Co.) fluorescent probe. We used a 1 : 10 SGI and 10 $\mu g mL^{-1}$ PI concentrations that were added to live samples less than 2 h after sampling. After simultaneous addition of each stain, the samples were incubated for 20 min in the dark at room temperature and then analyzed.

DMS and total DMSP (DMSPt) were measured by purge and trap gas chromatography (Shimadzu GC14A) coupled to flame photometric detection. Net biological DMS production (NPbio,DMS) was obtained by incubating whole water samples in 2.3 L Teflon bottles and correcting afterward for photochemical DMS loss, as described by Galí et al. (2013a). Gross DMS production was measured in the same way in additional bottles amended with 200 $\mu mol\ L^{-1}$ dimethyldisulfide (Galí et al., 2011), an effective inhibitor of bacterial DMS consumption (Wolfe and Kiene, 1993; Simó et al., 2000). DMS photolysis was measured in 0.2 μm filtered-water incubations in 40mL Teflon bottles or 50 mL quartz flasks. As expected, DMS photolysis was linearly related to the photochemically weighted irradiance dose (Figure 3). Since we observed distinct DMS photolysis yields in coastal (C1–C2) versus oceanic (O1–O2) experiments, a distinct photolysis rate constant (k^*_{photo}) for each type of experimental location (i.e., coastal or oceanic) was used to correct the biological rates for photochemical DMS loss. The process rates and indicator variables were measured in duplicate with the exceptions of DMS production rates, pigment concentrations and particulate absorption coefficients due to water volume constraints. The measurement of DMS production rates requires large incubation volumes to properly account for food web processes like microzooplankton grazing (Saló et al., 2010).

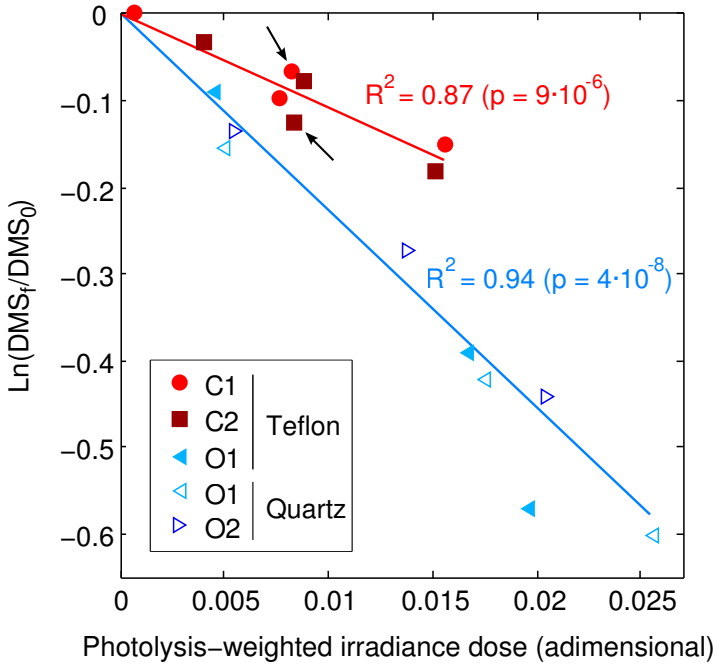

Figure 3. DMS photolysis in fixed and vertically moving incubations. The two types of incubation showed consistent dose-response behavior. Filled symbols: Teflon bottles incubated in C1 and C2 at three fixed depths and in a vertically moving basket (marked by arrows). Empty symbols: Teflon or quartz flasks incubated on board and withdrawn at different times (samples taken on three different days during the SUMMER-I cruise). The slope of the regression lines is k*photo: the apparent quantum yield of DMS photolysis with respect to weighted spectral UV irradiance normalized to 300 nm (as defined by Galí et al., 2013a). k*photo was 10.8 and 23.9 at the coastal station and at the oceanic station, respectively.

Statistical analyses

Each variable was normalized within each experiment to the vertical integral of the fixed incubations. The integration was calculated as the area under the trapezoids formed by depth vs. rate data points. After pooling the four experiments together we checked for significant differences among treatments (df = 3). If the Bartlett's equal variance test was successfully passed ($p > 0.05$) a parametric one-way analysis of variance (ANOVA) was used. Otherwise, a non-parametric Kruskal–Wallis ANOVA was performed. After a significant ANOVA ($p < 0.05$) multiple comparisons were done with the Tukey–Kramer test.

Results and Discussion

Oceanographic settings

The sampled UML was in all cases exposed to high proportions of UVR, i.e., > 10% of the subsurface UVA and UVB levels. Only in C2 the deeper portion of the UML was exposed to < 10% of subsurface UVB (Figure 2; Table 1). The phytoplankton community was typical of oligotrophic conditions, with low biomass and large contributions of the pico-sized fraction (Prochlorococcus, Synechococcus and picoeukaryotes) though in different proportions (Table 1). The picoeukaryote fraction was likely dominated by haptophytes (prymnesiophytes) and pelagophytes in O1 and O2 according to HPLC pigment data (Pérez et al., unpublished). Diatoms in C1 and C2 and small dinoflagellates (< 10 μm) in O1 and O2 also made significant contributions to total phytoplankton biomass.

The mixing layer was very shallow at the coastal site (MLD of 3–4 m). In the oceanic setting, the UML deepened from 7 m (O1) to 16 m (O2) due to the passage of a storm (Figure 2). The fact that all experiments took place in soft wind conditions, and the relatively high values of the buoyancy (Brunt–Väisälä) frequency within the UML suggest that it was not mixing actively at the time of the CTD casts (Table 1). If we assume that vertical diffusivity (K_z) in the UML interior was in the range 10^{-2}–10^{-4} m^2 s^{-1} (Denman and Gargett, 1983; Ross et al., 2011b), it would take ca. 0.25 to 100 h for a population of particles released at a single depth to diffuse across one optical depth in the UML depending on the wavelengths and MLD considered (Gallegos and Platt, 1985). A similar range is obtained by calculating the mixing timescale as MLD^2 / K_z as suggested by Ross et al. (2011a, b). The highest K_z might be representative of nighttime convective overturning, while the lowest K_z might be more representative of the daytime, when mixing was likely inhibited by solar heating (Brainerd and Gregg, 1995). From these calculations we conclude that the simulated mixing times were considerably faster than the actual mixing times. Although we tried to simulate the optical gradient experienced by the organisms and solutes within the UML, in practice

the incubations spanned a larger optical gradient once the attenuation due to seawater and the incubation bottles was taken into account (Table 1). Indeed, some of the differences between experiments and particularly between O1 and O2 may arise from slight differences in experimental exposure and prior light history of the plankton. Yet, our discussion will focus on the general trends rather than the differences among individual experiments.

Phytoplankton photosynthetic performance and photoacclimation

Particulate primary production (PPp) was moderately inhibited at the surface, optimal at the middle depth, and slightly lower at the bottom, with the exception of C1 (Figure 4A). PPp in mixing bottles resembled that in surface bottles and was 18% lower than in middle bottles except in C1 ($p < 0.01$). As a result, vertically integrated PPp from fixed bottles generally exceeded that in mixing bottles by 10–17% (except in C1). This result contrasts with that obtained by Bertoni et al. (2011), who observed a neutral to positive effect of dynamic light exposure in coastal Mediterranean waters in late spring. The response of primary production may be explained by different photoacclimation, photoprotection and damage and repair processes that will be explored in the paragraphs below.

At the end of the incubations, the average fluorescence of Synechococcus and picoeukaryote cell populations was generally lowest at the surface and increased with depth (Figure 4B, 4C). Fluorescence was generally lower than average in mixing bottles (although different patterns were observed for picoeukaryotes in O2). Similar responses were observed for nanoeukaryotes in C2 and for Prochlorococcus in O1 (data not shown). In addition, we observed a ca. 30% decrease in Prochlorococcus cell counts likely due to UV-caused mortality in surface bottles, as previously shown by Sommaruga et al. (2005). In concordance with the response of populations analyzed with single-cell techniques, bulk phytoplankton FvFm tended to increase with incubation depth (Figure 4D). FvFm in mixing bottles was (again) lower than the vertical integral of fixed bottles in C1 and O1, but not in O2, potentially due to the high fluorescence yields of the picoeukaryote

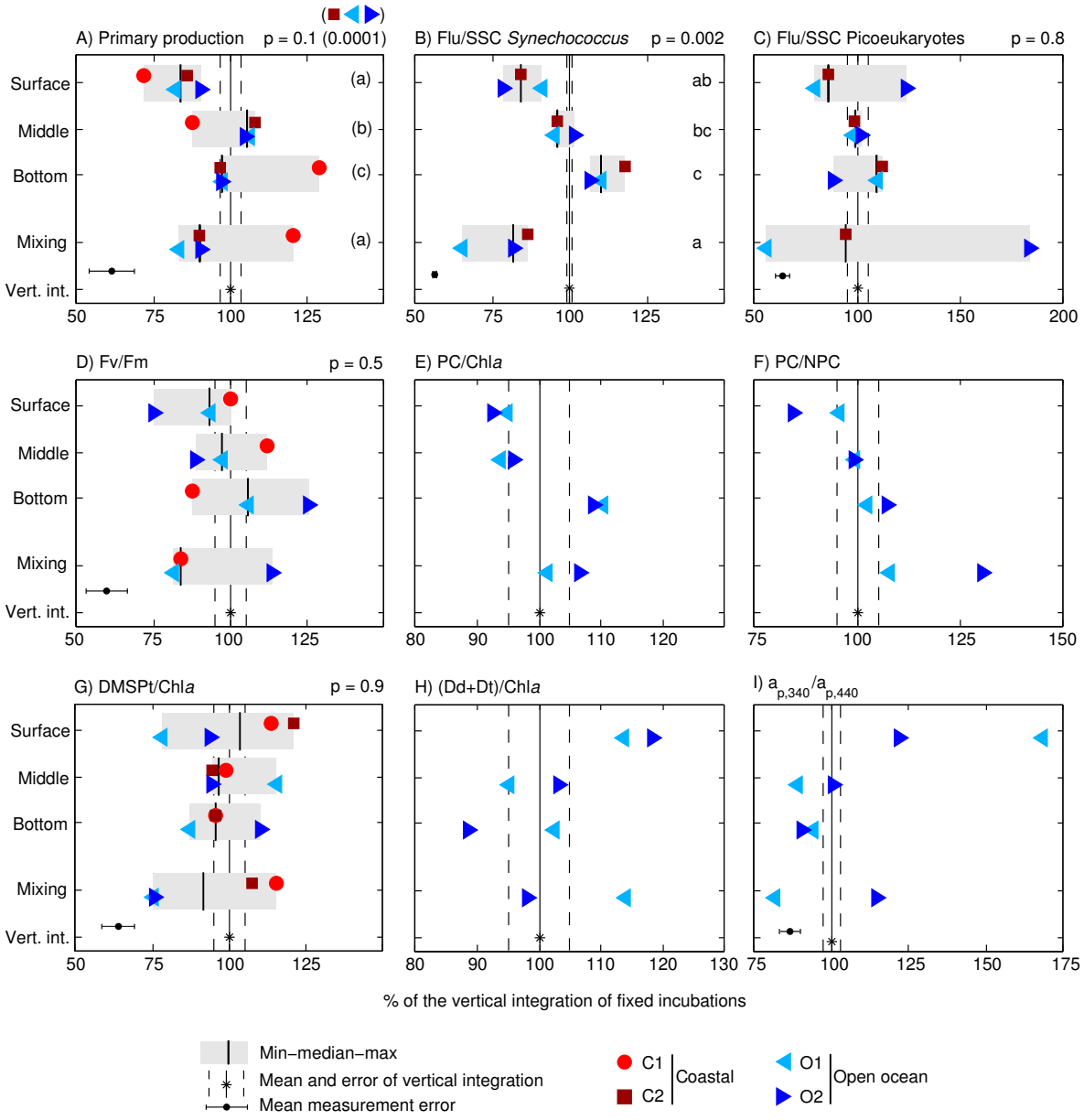

Figure 4. Response of phytoplankton to irradiance gradients in static and vertically moving incubations. Primary production rates (A) and indicators of phytoplankton photoresponse (B-I) have been normalized, within each experiment, to the vertical integral of fixed incubations. Flu/SSC: side-scatter-normalized cell-specific fluorescence. FvFm: maximum quantum yield of photosystem II photochemistry. PC: photosynthetic carotenoids. NPC: non-photosynthetic carotenoids. Dd: diadinoxanthin. Dt: diatoxanthin. $a_{p,340}$ / $a_{p,440}$:ratio of particulate light absorption coefficient at 340 nm and 440 nm. Differences between treatments are represented by p values of ANOVA tests followed by multiple comparisons (see text for details). In (A), a test was performed on a subset of experiments (C2, O1 and O2) that exhibited a more coherent response, and the resulting p value and multiple comparisons are shown in parentheses.

population (Figure 4C). The decrease in fluorescence yields may simultaneously result from a decrease in chlorophyll *a* (Chl*a*) content per cell (MacIntyre et al., 2002), an increase in excess energy dissipation as heat by photoprotective carotenoids (non-photochemical quenching), photodamage of photosystem II, and pigment bleaching (Vincent and Neale, 2000). Chl*a* concentrations generally increased (by 10–30 %) during the experiments except in O1, where a ca. 20% decrease was found. In O1 and O2, the ratio of photosynthetic carotenoids to Chl*a* (PC / Chl*a*) increased with depth, from ca. 0.48 at the surface to ca. 0.56 in bottom bottles. PC / Chl*a* in mixing bottles was close to the vertical integral of fixed bottles (Figure 4E). This suggests that phytoplankton photoacclimated during the time frame of the experiment (6 h) by adjusting PC / Chl*a* to the average spectral irradiance they were exposed to, likely seeking to optimize photosynthesis. Another physiological indicator that is worth analyzing is the ratio of photosynthetic carotenoids to non-photosynthetic carotenoids (PC / NPC; Figure 4F), as defined by Bricaud et al. (1995). In the fixed bottles, this ratio increased from about 0.66 to 0.90 from surface to bottom. At the surface, the low PC / NPC values were due to the net synthesis of NPC (with a 20–40% increase during the incubation). These results indicate an increasing investment in photoprotection through non-photochemical quenching at higher spectral irradiance. This is consistent with the decrease in photosystem II fluorescence yields (Figure 4D), since NPC compete for excitation energy with the other energy dissipation pathways: photochemistry and fluorescence emission. Surprisingly, mixing bottles displayed the highest values of PC / NPC due to higher-than-average PC concentrations, a response that remains difficult to interpret.

The xanthophyll cycle pigments diadinoxanthin (Dd) and diatoxanthin (Dt) were up-regulated by about 35% (up to 75 %) during the exposure relative to their initial concentration. Likewise, (Dd+Dt) concentrations relative to Chl*a* increased by 50% in the ensemble of all treatments in O1 and O2. (Dd+Dt) / Chl*a* generally increased towards the surface, and showed intermediate values in mixing bottles (Figure 4H).

These xanthophylls constitute a photoprotective mechanism in haptophytes, dinoflagellates and diatoms (van de Poll and Buma, 2009) by which the epoxidated form (Dd) is enzymatically de-epoxidated to Dt, and vice versa, depending on the cells' need for photoprotection. No clear trends were observed in the de-epoxidation state index, defined as Dt/(Dd+Dt), perhaps because the Dt vs. Dd interconversion responds on a timescale of few minutes (van de Poll and Buma, 2009), which is shorter than the filtration time of the samples after the exposure.

UV-absorbing (sunscreen) compounds, possibly mycosporine-like amino acids (Shick and Dunlap, 2002), were observed in particulate absorption spectra in O1 and O2 (Figure 4I). The ratio of particulate light absorption at 340 nm relative to that at the blue peak of Chl*a* at 440 nm, $a_{p,340} / a_{p,440}$, was highest (1–1.5) in surface bottles and lower (0.7–0.8) in middle and bottom bottles. Mixing bottles showed an ambiguous response, with low $a_{p,340} / a_{p,440}$ in O1 and slightly higher $a_{p,340} / a_{p,440}$ in O2.

The several photoresponse indicators we have explored indicate that, although phytoplankton deployed different photoprotection mechanisms, these were not enough to counteract high PAR- and UV-driven photoinhibition in surface bottles. Seen another way, the investment in photoprotection might have decreased the allocation of resources to carbon fixation. In middle bottles, conversely, the combination of high PAR and longwave UVA, which can also be used for photosynthesis, (Helbling et al., 2003) and a lower investment in photoprotection due to lower proportions of UVR resulted in optimal PPp. It is also important to bear in mind that different phytoplankton groups likely preferred different photoprotection mechanisms within those cited.

The response of mixing bottles is more difficult to interpret. The reduced photosynthetic performance in C2, O1 and O2 might indicate that the short surface exposure received by mixing bottles was enough to cause some irreversible inhibition, and that phytoplankton repair capacity was limited. However, this is not clearly supported by the radiative stress indicators measured. In addition, repair is thought to be more

efficient at elevated temperatures like those encountered in our study (Campbell et al., 1998; van de Poll and Buma, 2009). The fact that surface inhibition was only moderate and that highest PPp occurred in the middle bottle suggests that the photosynthetic machinery of phytoplankton was well adapted to a stratified system and thus not geared to take advantage of fast changes in spectral irradiance. This contrasts with what has been found for coastal tropical phytoplankton thriving in turbid waters (Helbling et al., 2003) or even for coastal Mediterranean assemblages in late spring (Bertoni et al., 2011).

Response of bacterial heterotrophic production

In fixed bottle incubations, LIRs were significantly inhibited at the surface by 14–28% with respect to the vertical integral (except in C1), and increased with depth to find their optimum at the bottom of the mixed layer (Figure 5A). LIRs in mixing bottles resembled those of bottom bottles in 3 out of 4 experiments, and were higher (though

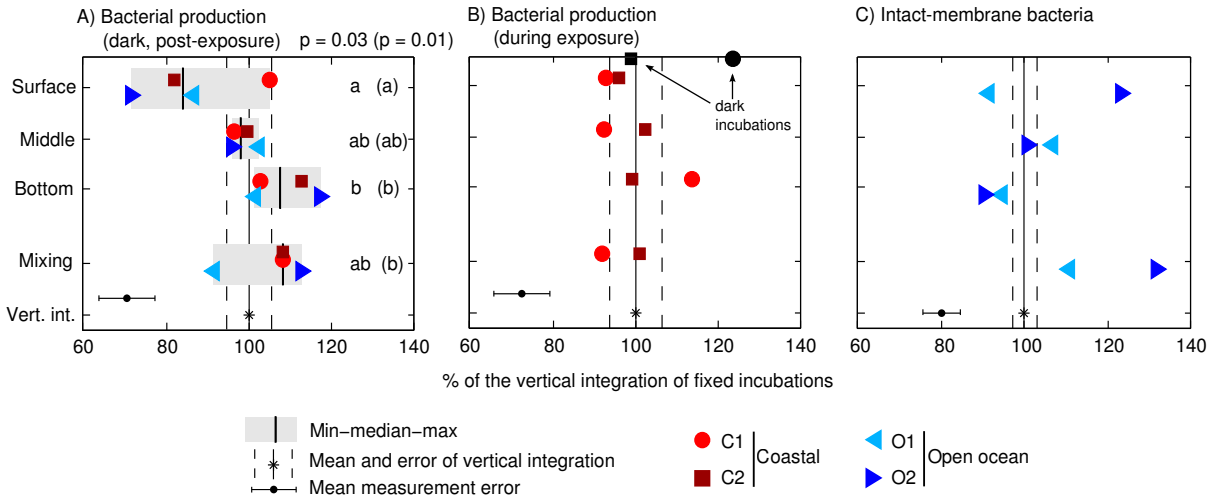

Figure 5. Response of heterotrophic bacteria to irradiance gradients in static and vertically moving incubations. Leucine incorporation rates in (A) post-exposure dark incubations and (B) in situ light and dark incubations; (C) proportion of intact-membrane ("live") bacteria as deduced from the nucleic acid double-staining (NADS) protocol. Statistical comparisons as in Figure 4. In (A), a test was performed on a subset of experiments (C2, O1 and O2) that exhibited a more coherent response, and the resulting p value and multiple comparisons are shown in parentheses.

not significantly) than those in middle bottles and the vertical integral. This suggests that fast mixing favored recovery and photorepair over photodamage. It is well known that photolyase enzymes use UVA and blue light to repair damaged DNA. According to Kaiser and Herndl (1997), optimal photoreactivation occurs in a certain window of UVA/UVB that, in our experiments, would roughly correspond to the bottom half of the UML (Figure 1B). This interpretation is supported by the higher proportions of intact-membrane bacteria found in mixing bottles at the end of the incubations with respect to the surface bottles (O1 and O2 only; Figure 5C). Yet, the vertical trend shown by this cytometric indicator in fixed bottles contradicts this view, especially in O2, where the proportion of intact-membrane bacteria decreased with depth.

In addition to the post-exposure dark incubations, in C1 and C2 we measured LIRs during the sunlit incubations, i.e., with the ^{3}H-leucine added into exposed bottles (Figure 5B). In these "in situ" incubations, surface and mixing bottles displayed more similar degrees of inhibition, and the trends of bacterial production with depth did not match those found in post-exposure dark incubations. We also measured LIRs in aluminum-foil-darkened bottles placed in the in situ incubation basket. Dark LIR was 22% higher than the vertical integral of sunlit bottles in C1, but no differences were observed in C2 (Figure 5B). The discrepancies between in situ and post-exposure leucine incorporation may be due to distinct photoinhibition and photorepair dynamics, and each approach has advantages and disadvantages. The tendency of in situ leucine incorporation to display less photoinhibition may be due to substrate incorporation at the beginning of the incubation, before the onset of severe photoinhibition. On the other hand, post-exposure LIRs reflect the photoinhibition state at the end of the exposure, resulting from the net balance between damage and repair in sunlight as well as from the net repair that might occur during the 2 h post-exposure dark incubation. These methodological issues might be overcome with the development of more sensitive methods that allow a faster determination of bacterial heterotrophic production, which

is particularly challenging in oligotrophic waters with low activity.

Different explanations have been invoked to explain the responses of bacterial activity under sunlight, for instance, the occurrence of photoheterotrophic metabolisms in some bacterial groups, or the exudation of labile organic matter by phytoplankton at high irradiance (reviewed by Ruiz-González et al., 2013). Unfortunately, we did not investigate the phylogenetic composition of the bacterial communities in our experiments. No obvious patterns linking the response of LIR and PPp were found, perhaps because phytoplankton–bacteria interactions through the dissolved carbon pool are complex and group-specific (Sarmento and Gasol, 2012). Despite the numerous uncertainties, our study adds valuable information to the only previous study of bacterial production under dynamic light exposure (Bertoni et al., 2011), and agrees with that work in that the effect of mixing was neutral to positive compared to fixed incubations.

Response of community DMS production

Gross DMS production (GP_{DMS}) showed the strongest vertical gradient among the three processes, and increased significantly by about three-fold between the bottom and the surface of the UML in fixed incubations (Figure 6A). Gross DMS production in mixing bottles was not significantly different from that in middle bottles, nor from the vertical integral, although a slight trend towards lower GP_{DMS} in mixing bottles occurred in C1 and C2.

Gross DMS production results from the addition and interaction of several processes, namely exudation of DMS by phytoplankton, bacterial degradation of DMSP released by phytoplankton as a result of grazing, viral infection, or cell death, and even the reduction of dimethylsulfoxide (Spiese et al., 2009; Asher et al., 2011). Galí et al. (2013a) showed that UVR stimulates GP_{DMS} in a spectral irradiance-dependent manner, a result that is confirmed by our present study. They also demonstrated that the stimulation is more effective at shorter and more energetic UVR wavelengths, with a spectral peak around 330 nm, and attributed the stimulation effect to phytoplankton DMS release caused by the additive effects of excess

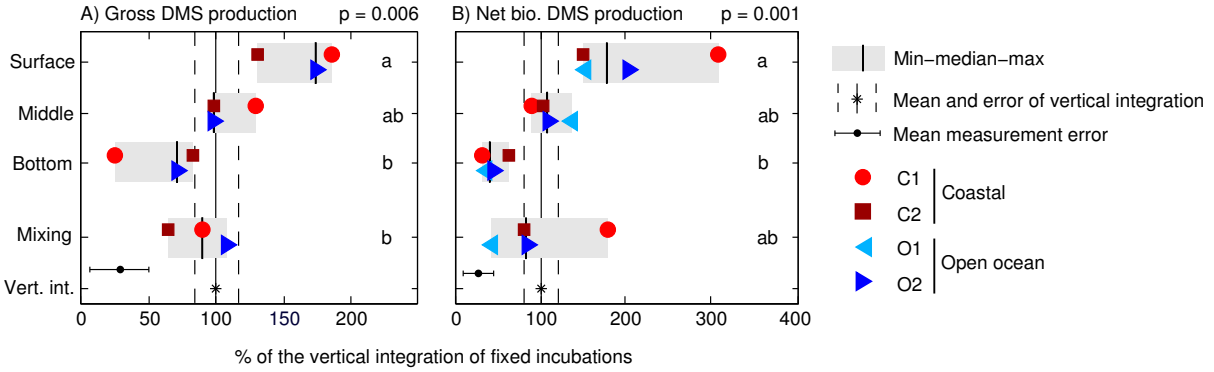

Figure 6. Response of community DMS production to irradiance gradients in static and vertically moving incubations. (A) Gross DMS production (GP_{DMS}, DMDS-amended incubations); (B) net biological DMS production (non-amended incubations; equivalent to GP_{DMS} minus bacterial DMS consumption). Statistical comparisons as in Fig. 4. In (B), a test was performed on a subset of experiments (C2, O1 and O2) that exhibited a more coherent response. Multiple comparisons did not show different patterns from those in the entire data set, although the p value decreased (p =0.0008).

PAR (Stefels, 2000) and UVR stress (Sunda et al., 2002). Furthermore, it was suggested that lethal UVR exposure could promote DMS production as a result of phytoplankton cell lysis and subsequent DMSP release. This mechanism would make more DMSP available to bacteria and to algal DMSP cleavage enzymes ("lyases") released along with algal DMSP.

In the ensemble of all the experiments, experiment-normalized PPp and GP_{DMS} were negatively correlated (Pearson's r = −0.58; p = 0.018; Spearman's p = −0.51; p = 0.044). Moreover, the response of GP_{DMS} to radiative stress was generally consistent with the patterns of photoinhibition and photoprotection (Archer et al., 2010). Whether or not this response was the result of active physiological regulation of phytoplankton cells remains to be elucidated. Clearly, better methods are needed to study the relative weight of different DMS production processes and their modulation by spectral irradiance (Galí et al., 2013a). Sunda et al. (2002) suggested that intracellular DMSP cleavage to DMS plus acrylate and further oxidation products might help phytoplankton cells coping with oxidative stress. If we assume that the UV-driven increase in GP_{DMS} arose completely from up-regulated intracellular DMSP cleavage, which is very unlikely, our data suggest that this antioxidant mechanism would still not be enough to counteract short-term photoinhibition and ameliorate photosynthetic performance, even if working in tandem with other photoprotection mechanisms.

DMSPt concentrations displayed only moderate changes (< 5% variation in 13 out of 16 incubations) and no clear trends were found across treatments (data not shown). A strong DMSPt depletion in surface bottles was only found in O2 (21 %). The stability of the DMSPt concentration across spectral irradiance treatments is notable, given that (1) a lower amount of fixed carbon was available for DMSP synthesis in surface and mixing samples, and (2) higher amounts of DMSP were lost as DMS (and perhaps as dimethylsulfoxide (DMSO)) at higher irradiance. The quotient of GP_{DMS} to DMSPt was 0.42 d^{-1}, 0.29 d^{-1}, 0.18 d^{-1}, and 0.21 d^{-1} on average in surface, middle, bottom and mixing bottles, respectively. These data suggest that faster DMSP synthesis was required to sustain DMSPt concentrations at high irradiance. Gross DMSP synthesis rates were not measured in our experiments, but, interestingly, experiment-normalized net DMSP synthesis rates and PPp were correlated (Pearson's r = 0.50; p = 0.048; Spearman's p = 0.65; p = 0.006). Recent results suggest that DMS can be produced intracellularly in phytoplankton through DMSP cleavage by OH radicals, without the need for DMSP cleavage enzymes (D. J. Kieber, personal communication, 2012). In addition, some algal strains can reduce dimethylsulfoxide back to DMS, potentially enhancing their antioxidant protection (Spiese et al., 2009). Since DMS is membrane-permeable, it is reasonable to assume that a significant fraction will escape the cell without being oxidized, so that DMSP will play a more direct and role in antioxidant protection than in the original antioxidant hypothesis formulated by Sunda et al. (2002).

The similar short-term behavior of DMSPt in all the experiments contrasts with the differences in the ratios of total DMSP (DMSPt) to Chl*a* between the coastal (DMSPt / Chl*a* of 77–92 μmol g^{-1}) and the oceanic (196–315 μmol g^{-1}) settings. These differences may be explained by the presence of strong DMSP producers in O1 and O2, such as dinoflagellates and haptophytes. Besides taxonomy, also nutrient availability (particularly nitrogen) and the longer-term acclimation to elevated UVR and PAR contribute to regulate the DMSP content of phytoplankton (Bucciarelli and Sunda, 2003; Sunda et al., 2007; Archer et al., 2010). While the irradiance doses of the four upper mixed layers sampled were not significantly

different (Table 1), lower nitrate concentrations in the open ocean waters might have contributed to set the higher DMSPt / Chl*a* ratios found in O1 and O2 by simultaneously decreasing Chl*a* and increasing DMSP cell quotas. Intriguingly, the DMSPt / Chl*a* ratios at the end of the experiments showed an opposite pattern in C1 and C2 compared to O1 and O2 (Figure 4G). Overall, these results indicate that it is crucial to distinguish between short-term (hours) and long-term (days, weeks) responses if we are to correctly understand the photo-physiological mechanisms that drive DMS and DMSP cycling in phytoplankton cells and at the community level.

Net biological DMS production (NPbio, DMS) showed a pattern similar to that of GP_{DMS} (Figure 6B). NPbio, DMS is interesting in that it tells the net effect of sunlight on biological DMS cycling, that is, on the difference between GP_{DMS} and bacterial DMS consumption. Bacterial DMS consumption rates, calculated by subtracting NPbio, DMS from GP_{DMS}, consumed on average 11 %, 31 %, 43% and 14% of GP_{DMS} in surface, middle, bottom and mixing bottles, respectively. Thus, the imbalance between GP_{DMS} and bacterial DMS consumption increased with spectral irradiance due to UV and/or PAR inhibition of bacterial DMS consumption and stimulation of GP_{DMS}, making the vertical gradient of NPbio, DMS even larger than that of GP_{DMS} (Figure 6B). The net stimulating effect of sunlight on biological DMS production was largely compensated by DMS photolysis, so that net overall DMS concentration changes were close to zero in all treatments, as already observed by Galí et al. (2013a) with other experimental settings.

Bacterial DMS consumption, expressed as the % of vertically integrated rates, was 49 %, 79 %, 125% and 78% in surface, middle, bottom and mixing bottles, respectively. Although these results suffer from a large uncertainty due to error propagation, they suggest that bacterial DMS consumption was more strongly inhibited than bulk LIR, and that it was photoinhibited in a dose-dependent manner. Severe photoinhibition was already observed by Toole et al. (2006), who reported a similar response of bacterial DMS consumption and LIR. Since only a portion of the bacterial community is able to consume DMS through oxidation, it is likely that the photoresponse of bacterial DMS consumers and that of bulk heterotrophic bacteria differ

(as suggested by Galí and Simó, 2010) and also that the photoresponse of different metabolic activities differs in a given cell or strain. Clearly, these issues deserve further investigation.

Differential irradiance- and dose-response among biogeochemical processes

The experiment-normalized PPp, LIRs and community DMS production rates were plotted against the mean (UVB, UVA, PAR) incubation irradiance in the ensemble of all the experiments, and the points corresponding to fixed bottles were fitted with a linear regression (Figure 7). We also calculated the Pearson correlation coefficient between the experiment-normalized process rates and (1) mean irradiance and (2) total irradiance dose

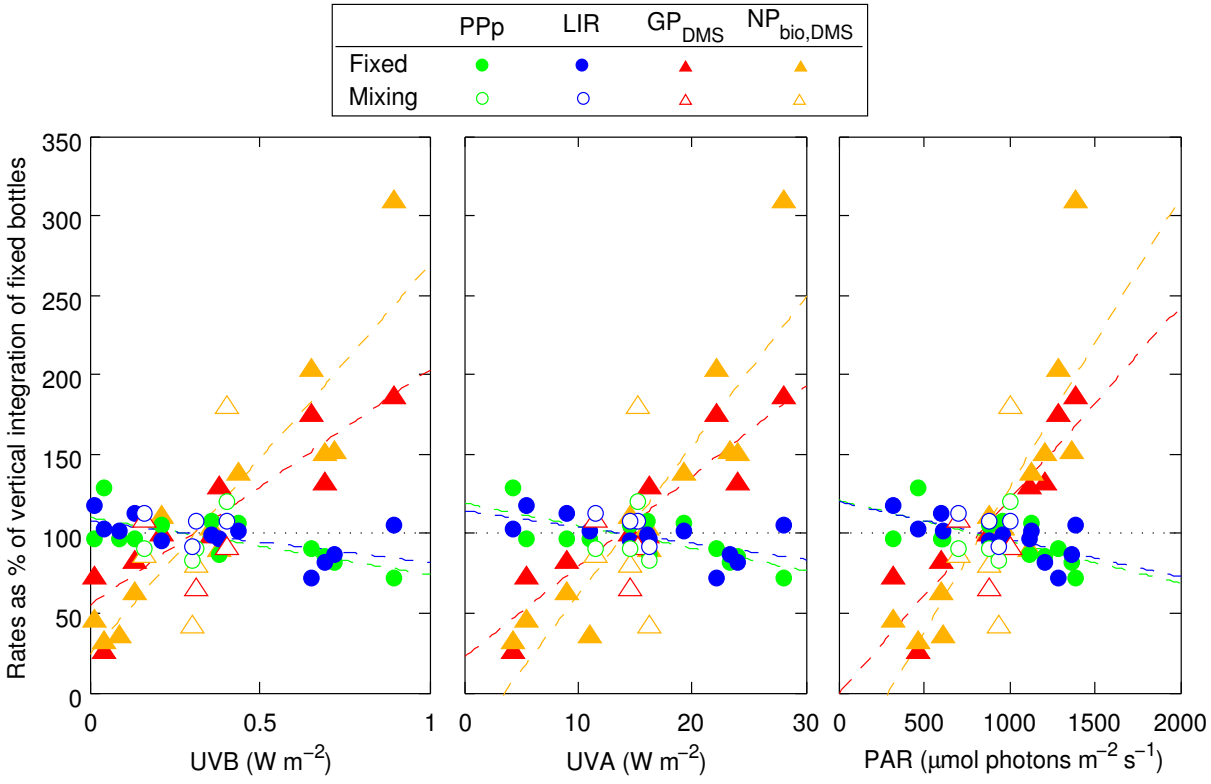

Figure 7. Relationship between mean UVB, UVA and PAR irradiance during the incubations and particulate primary production (PPp), leucine incorporation rates (LIRs), gross DMS production (GP_{DMS}) and net biological DMS production (NPbio,DMS). The rates have been normalized to the vertical integral of fixed-depth incubations (see text). The lines represent linear least squares fits to the fixed-depth incubations only (filled symbols). Vertically moving incubations ("mixing", open symbols) have not been included in the regressions.

for each radiation band (Figure 8). The aim of this exercise was to identify whether a process was more dose-dependent or irradiance ("dosage-rate")-dependent, following the rationale exposed in the Introduction. Note that in our experimental setting it is hard to discriminate between the effects of each band of the spectrum, since the proportion of shortwave UV decreases along with total (or PAR) irradiance as we move deeper in the water column.

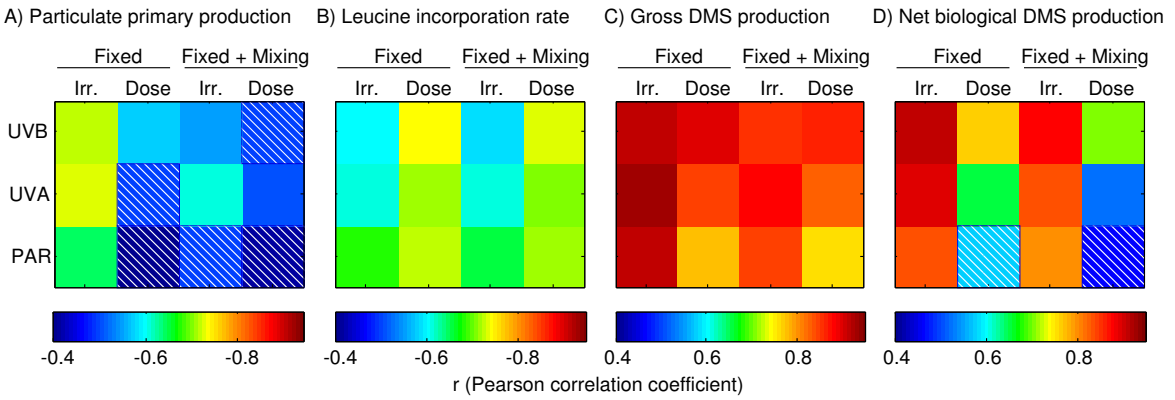

Figure 8. Pearson's correlation coefficient (r) between biogeochemical process rates and mean incubation irradiance (Irr.) or cumulative dose in different radiation bands (UVB, UVA and PAR), in fixed bottles only and in the ensemble of fixed + mixing bottles. Note that r is negative in (A) and (B) and positive in (C) and (D). The diagonal stripe pattern indicates non-significant r ($p > 0.05$).

PPp showed a slight negative trend with respect to irradiance in fixed bottles in the three radiation bands, which was mainly driven by photoinhibition in surface bottles. In fact, the response was rather flat below an irradiance threshold of ca. 0.4 Wm^{-2} UVB, 16 W m^{-2} UVA and 1000 µmol photons m^{-2} s^{-1}. The correlation with irradiance was higher than that with dose (Figure 8A), suggesting that some balance between inhibition and protection/repair could be attained in the different exposure regimes. The highest linear correlation was found with UVA irradiance, perhaps indicating that this band drives photoinhibition in UV-transparent waters. In concordance with this suggestion, some studies have shown that the spectral peak of UV photoinhibition occurs in the UVA, due to the combination of increasing irradiance and decreasing UV effectiveness as we move towards longer wavelengths (Neale and Kieber, 2000).

LIR decreased with increasing UVB, UVA and PAR with a slope very similar to that of PPp. Contrary to the other processes examined, the photoinhibition of LIR was more strongly correlated to the dose than to irradiance, particularly in the UVB band, suggesting that cumulative UVB-induced DNA damage occurred in bacterial cells in fixed incubations (Buma et al., 2001). This fits with the general idea that the radiation bands causing damage (UVB) elicit more dose-dependent responses than the radiation bands that are used by the cells to conduct physiological processes (PAR and longwave UVA).

Community DMS production rates showed a strong response to variations in spectral irradiance, with a steeper slope observed for NPbio,DMS than for GP_{DMS} (Figure 7C, 7D). The strongest correlations were found between GP_{DMS} and irradiance in the three bands, particularly in the UVA. This agrees with previous studies that suggested, using distinct approaches, that the spectral peak of sunlight-induced DMS production occurs in the 330–340 nm region in surface UV-transparent waters (Toole et al., 2008; Levine et al., 2012; Galí et al., 2013a). Finally, note that among all process and radiation combinations (Figure 8) the correlation was stronger when mixing bottles were excluded. This illustrates in a loose way that mixing subtly disrupted the photoacclimation and photodamage processes, as thoroughly discussed in previous Sections. 3.2–3.4.

The results presented here on the enhancement of DMS production by increased irradiance and relative UVB exposure agree with those recently reported by our group using a variety of approaches, from light spectrum manipulation with optical filters (Galí et al., 2013a) to the study of diel cycles at sea (Galí et al., 2013b). They all provide mechanistic bases to the role of solar radiation as the main driver of DMS production and concentration in the surface ocean (Vallina and Simó, 2007). In the short term (hours) sunlight directly affects the cellular machineries of DMS producers and DMS consumers, and favors DMSP-to-DMS conversion pathways; in the longer term (days to months) sunlight shapes the seasonality of the dynamics in upper-ocean physics

and plankton succession, favoring DMSP producers. As a resulting emergent property, DMS tends to increase in summer even in regions where phytoplankton biomass is at its annual minimum. This phenomenon was termed the "DMS summer paradox" (Simó and Pedrós-Alió, 1999) and suggested to be at the base of a "seasonal CLAW" hypothesis by which plankton respond to higher summer irradiances by increasing the production of cloud-brightening DMS (Vallina and Simó, 2008). Whether this seasonal feedback will also operate efficiently at the longer timescale of anthropogenic global warming or Earth climate cycles cannot be easily predicted from short-term observations. Indeed, projections point to an enhancement, expansion and longer duration of stratification by global warming, with shallower mixed layers during longer periods (Sarmiento et al., 1998), which would result in increased exposures of plankton to UVR (Diaz et al., 2000). In view of our results, this might lead to increased DMS concentrations/emissions. However, the likely substitution of plankton species and communities by ones more adapted to the evolving conditions, and the development of protection strategies against environmental stress, hamper the straightforward applicability of our short-term observations to long-term trends.

Conclusions

The photoresponse of phytoplankton, bacterioplankton, and community DMS production displayed clear trends in bottles incubated at fixed depths in the UML (Figure 7) despite the relatively small gradient in spectral irradiance. The irradiance dose response in mixing bottles was distinct (though subtle) in each of the processes measured, as well as for different physiological indicators. In the oligotrophic waters investigated, dynamic light exposure generally caused, compared to the middle bottles receiving the same cumulative exposure, (1) an adverse though non-significant effect on particulate primary production, concomitant with reduced cell-specific fluorescence in most experiments and phytoplankton groups; (2) a slightly alleviating effect on bacterial production photoinhibition, related to an increase in the proportion of intact-membrane, or live, heterotrophic bacteria in two of the experiments; and (3) a neutral effect or slight reduction in gross DMS production. These responses translated, in some experiments, into measurable deviations with respect to the vertically integrated rates in the water column; in others, the effects were close to neutral or too small to be reliably detected. Incubating the samples at a fixed intermediate optical depth appears as a reasonable and convenient solution for measuring GP_{DMS} and leucine incorporation, at least in UVR-transparent stratified UML waters. However, this solution might not be optimal for measuring UML-integrated primary production. Our results call for a more systematic assessment of the consequences of dynamic light exposure of microbial plankton in different oceanic regimes. This way, the photobiological processes governing, among other important processes, the ocean–atmosphere exchange of long-lived (CO_2) and short-lived (DMS) gases of climatic relevance will be better understood.

Acknowledgements

We thank the staff at Port Olímpic de Barcelona for their collaboration, and the crew and scientists aboard R/V García del Cid for their invaluable help in setting up the experiments during the SUMMER-I cruise. We also thank D. J. Kieber for his insightful comments on an earlier version of the manuscript, R. Bertoni for sharing his expertise, and two anonymous reviewers for their constructive suggestions. M. G. acknowledges the receipt of a CSIC JAE scholarship. This work was supported by the (former) Spanish Ministry of Science and Innovation through the project SUMMER (CTM2008-03309/MAR). This is a contribution of the Research Groups on Marine Biogeochemistry and Global Change and on Aquatic Microbial Food Webs, supported by the Generalitat de Catalunya.

References

Aas, P., Lyons, M., Pledger, R., Mitchell, D., and Jeffrey, W.: Inhibition of bacterial activities by solar radiation in nearshore waters and the Gulf of Mexico, Aquat. Microb. Ecol., 11, 229–238, doi:10.3354/ame011229, 1996.

Agogué, H., Joux, F., Obernosterer, I., and Lebaron, P.: Resistance of Marine Bacterioneuston to Solar Radiation, Appl. Environ. Microb., 71, 5282–5289, doi:10.1128/AEM.71.9.5282, 2005.

Alonso-Sáez, L., Gasol, J. M., Lefort, T., Hofer, J., and Sommaruga,R.: Effect of natural sunlight on bacterial activity and differential sensitivity of natural bacterioplankton groups in northwestern Mediterranean coastal waters, Appl. Environ. Microb., 72, 5806–5813, doi:10.1128/AEM.00597-06, 2006.

Archer, S. D., Cummings, D., Llewellyn, C., and Fishwick, J.: Phytoplankton taxa, irradiance and nutrient availability determine the seasonal cycle of DMSP in temperate shelf seas, Mar. Ecol. Prog. Ser., 394, 111–124, doi:10.3354/meps08284, 2009.

Archer, S. D., Ragni, M., Webster, R., Airs, R. L., and Geider, R. J.: Dimethyl sulfoniopropionate and dimethyl sulfide production in response to photoinhibition in Emiliania huxleyi, Limnol. Oceanogr., 55, 1579–1589, doi:10.4319/lo.2010.55.4.1579, 2010.

Asher, E. C., Dacey, J. W. H., Mills, M. M., Arrigo, K. R., and Tortell, P. D.: High concentrations and turnover rates of DMS, DMSP and DMSO in Antarctic sea ice, Geophys. Res. Lett., 38, 1 –5, doi:10.1029/2011GL049712, 2011.

Barbieri, E. S., Villafañe, V. E., Helbling, E. W., and Nov, N.: Experimental assessment of UV effects on temperate marine phytoplankton when exposed to variable radiation regimes, Limnol. Oceanogr., 47, 1648–1655, 2002.

Béjà, O., Aravind, L., Koonin, E. V., Suzuki, M. T., Hadd, A.,Nguyen, L. P., Jovanovich, S. B., Gates, C. M., Feldman, R. A., Spudich, J. L., Spudich, E. N., and DeLong, E. F.: Bacterial Rhodopsin: Evidence for a New Type of Phototrophy in the Sea, Science, 289, 1902–1906, doi:10.1126/science.289.5486.1902, 2000.

Bertoni, R., Jeffrey, W. H., Pujo-Pay, M., Oriol, L., Conan, P., and Joux, F.: Influence of water mixing on the inhibitory effect of UV radiation on primary and bacterial production in Mediterranean coastal water, Aquat. Sci., 73, 377–387, doi:10.1007/s00027-011-0185-8, 2011.

Brainerd, K. E. and Gregg, M. C.: Surface mixed and mixing layer depths, Deep Sea Res. Pt. I, 42, 1521–1543, 1995.

Bricaud, A., Babin, M., Morel, A., and Claustre, H.: Variability in the chlorophyll-specific absorption coefficients of natural phytoplankton, Analysis and parameterization, J. Geophys. Res., Oceans, 100, 13321–13332, doi:10.1029/95JC00463, 1995.

Brunet, C. and Lavaud, J.: Can the xanthophyll cycle help extract the essence of the microalgal functional response to a variable light environment? J. Plankton Res., 32, 1609–1617.

Bucciarelli, E. and Sunda, W. G.: Influence of CO2, nitrate, phosphate, and silicate limitation on intracellular dimethylsulfoniopropionate in batch cultures of the coastal diatom Thalassiosira pseudonana, Limnol. Oceanogr., 48, 2256–2265, doi:10.4319/lo.2003.48.6.2256, 2003.

Buma, A. G., Helbling, E. W., de Boer, M. K., and Villafañe, V. E.: Patterns of DNA damage and photoinhibition in temperate South-Atlantic picophytoplankton exposed to solar ultraviolet radiation, J. Photoch. Photobio. B, 62, 9–18, 2001.
Campbell, D., Eriksson, M. J., Oquist, G., Gustafsson, P., and Clarke, A. K.: The cyanobacterium Synechococcus resists UVB by exchanging photosystem II reaction-center D1 proteins, P. Natl. Aca. Sci. USA, 95, 364–9, 1998.

Carpenter, L. J., Archer, S. D., and Beale, R.: Ocean-atmosphere trace gas exchange, Chem. Soc. Rev., 41, 6473–6506, 2012. Church, M. J., Ducklow, H. W., and Karl, D. M.: Light dependence of [3H] leucine incorporation in the oligotrophic North Pacific ocean, Appl. Environ. Microb., 70, 4079–87, doi:10.1128/AEM.70.7.4079-4087.2004, 2004.

Denman, K. L. and Gargett, A. E.: Time and space scales of vertical mixing in the upper ocean, Limnol. Oceanogr., 28, 801–815, 1983.

Diaz, S. B., Morrow, J. H., and Booth, C. R.: UV physics and optics, The effects of UV radiation in the marine environment, 35–71, 2000.

Galí, M. and Simó, R.: Occurrence and cycling of dimethylated sulfur compounds in the Arctic during summer receding of the ice edge, Mar. Chem., 122, 105–117, doi:10.1016/j.marchem.2010.07.003, 2010.

Galí, M., Saló, V., Almeda, R., Calbet, A., and Simó, R.: Stimulation of gross dimethylsulfide (DMS) production by solar radiation, Geophys. Res. Lett., 38, 1–5, doi:10.1029/2011GL048051, 2011.

Galí, M., Ruiz-González, C., Lefort, T., Gasol, J. M., Cardelús, C., Romera-Castillo, C., and Simó, R.: Spectral irradiance dependence of sunlight effects on plankton dimethylsulfide production, Limnol. Oceanogr., 58, 489–504, 2013a.

Galí, M., Simó, R., Vila-Costa, M., Ruiz-González, C., Gasol, J. M., and Matrai, P.: Diel patterns of oceanic dimethylsulfide (DMS) cycling: Microbial and physical drivers, Glob. Biogeochem. Cy., 2013b.

Gallegos, C. L. and Platt, T.: Vertical advection of phytoplankton and productivity estimates: a dimensional analysis, Mar. Ecol. Prog. Ser., 26, 125–134, 1985.

Grégori, G., Citterio, S., Ghiani, A., Labra, M., Sgorbati, S., Brown, S., and Denis, M.: Resolution of viable and membrane compromised bacteria in freshwater and marine waters based on analytical flow cytometry and nucleic acid double staining, Appl. Environ. Microb., 67, 4662–4670, 2001.

Harada, H., Vila-Costa, M., Cebrian, J., and Kiene, R. P.: Effects of UV radiation and nitrate limitation on the production of biogenic sulfur compounds by marine phytoplankton, Aquat. Bot., 90, 37–42, 2009.

Hefu, Y. and Kirst, G. O.: Effect of UV- radiation on DMSP content and DMS formation of Phaeocystis antarctica, Polar Biol., 18, 402–409, doi:10.1007/s003000050206, 1997.

Helbling, E. W., Carrillo, P., Medina-Sánchez, J. M., Durán, C., Herrera, G., Villar-Argaiz, M., and Villafañe, V. E.: Interactive effects of vertical mixing, nutrients and ultraviolet radiation: in situ photosynthetic responses of phytoplankton from high mountain lakes in Southern Europe, Biogeosciences, 10, 1037–1050, doi:10.5194/bg-10-1037-2013, 2013.

Helbling, E. W., Gao, K., Gonçalves, R., Wu, H., and Villafañe, V. E.: Utilization of solar UV radiation by coastal phytoplankton assemblages off SE China when exposed to fast mixing, Mar. Ecol. Prog. Ser., 259, 59–66, doi:10.3354/meps259059, 2003.

Kaiser, E. and Herndl, G. J.: Rapid Recovery of Marine Bacterioplankton Activity after Inhibition by UV Radiation in Coastal Waters, Appl. Environ. Microb., 63, 4026–4031, 1997.
Kirchman, D., K'nees, E., and Hodson, R.: Leucine incorporation and its potential as a measure of protein synthesis by bacteria in natural aquatic systems, Appl. Environ. Microbiol., 49, 599–607, 1985.

Kirchman, D. L. and Hanson, T. E.: Bioenergetics of photoheterotrophic bacteria in the oceans, Environ. Microbiol. Rep., 5, 188–199, doi:10.1111/j.1758-2229.2012.00367.x, 2012.

Kolber, Z., Van Dover, C., Niederman, R., and Falkowski, P.: Bacterial photosynthesis in surface waters of the open ocean, Nature, 407, 177–179, 2000.

Lana, A., Bell, T. G., Simó, R., Vallina, S. M., Ballabrera-Poy, J., Kettle, A. J., Dachs, J., Bopp, L., Saltzman, E. S., Stefels, J., Johnson, J. E., and Liss, P. S.: An updated climatology of surface dimethlysulfide concentrations and emission fluxes in the global ocean, Global Biogeochem. Cy., 25, 1–17, doi:10.1029/2010GB003850, 2011.

Levine, N. M., Varaljay, V. A., Toole, D. A., Dacey, J. W. H., Doney, S. C., and Moran, M. A.: Environmental, biochemical and genetic drivers of DMSP degradation and DMS production in the Sargasso Sea, Environ. Microbiol., 14, 1210–1223, doi:10.1111/j.1462-2920.2012.02700.x, 2012.

MacIntyre, H. L., Kana, T. M., Anning, T., and Geider, R. J.: Photoacclimation of photosynthesis irradiance response curves and photosynthetic pigments pigments in microalgae and cyanobacteria, J. Phycol., 38, 17–38, 2002.

Marie, D. and Partensky, F.: Analyse de micro-organismes marins, in: La cytométrie en flux, edited by: Ronot, X., Grunwald, D., Mayol, J. F., and Boutonnat, J., Lavoisier, 211–233, 2006.

Mitchell, B., Bricaud, A., Carder, K., Cleveland, J. S., F., G. M., and Gould, R.: Determination of spectral absorption coefficients of particles, dissolved material and phytoplankton for discrete water samples, in: Ocean Optics Protocols for Satellite Ocean Color Sensor Validation, Revision 2, edited by: Fargion, G., Mueller, J., and McClain, C., NASA, 125–153, 2000.

Mitchell, B. G. and Kiefer, D. A.: Determination of absorption and fluorescence excitation spectra for phytoplankton, in: Marine Phytoplankton and Productivity, edited by: Holm-Hansen, O., Bolis, L., and Giles, R., 157–169, Springer, 1984.

Morán, X. A. G., Gasol, J. M., Arin, L., and Estrada, M.: A comparison between glass fiber and membrane filters for the estimation of phytoplankton POC and DOC production, Mar. Ecol. Prog. Ser., 187, 31–41, 1999.

Morán, X. A. G., Massana, R., and Gasol, J. M.: Light Conditions Affect the Measurement of Oceanic Bacterial Production via Leucine Uptake, Appl. Environ. Microb., 67, 3795–3801, doi:10.1128/AEM.67.9.3795-3801.2001, 2001.

Neale, P. J. and Kieber, D. J.: Assessing Biological and Chemical Effects of UV in the Marine Environment: Spectral Weighting Functions, Issues in Environmental Science and Technology, 2000.

Neale, P. J., Helbling, E. W., and Zagarese, H. E.: Modulation of UVR exposure and effects by vertical mixing and advection, in: UV effects in aquatic organisms and ecosystems, The Royal Society of Chemistry Cambridge, 107–134, 2003.

Quinn, P. K. and Bates, T. S.: The case against climate regulation via oceanic phytoplankton sulphur emissions, Nature, 480, 51–6, doi:10.1038/nature10580, 2011.

Ross, O. N., Geider, R. J., Berdalet, E., Artigas, M. L., and Piera, J.: Modelling the effect of vertical mixing on bottle incubations for determining in situ phytoplankton dynamics. I. Growth rates, Mar. Ecol. Prog. Ser., 435, 13–31, doi:10.3354/meps09193, 2011a.

Ross, O. N., Geider, R. J., and Piera, J.: Modelling the effect of vertical mixing on bottle incubations for determining in situ phytoplankton dynamics Pt.II., Primary production, Mar. Ecol. Prog. Ser., 435, 33–45, doi:10.3354/meps09194, 2011b.

Roy, S.: The strategies for minimization of UV damage, in: The Effects of UV Radiation in the Marine Environment, edited by: de Mora, S. J., Demers, S., and Vernet, M., chap. 3, 177–205, Cambridge Uni. Press, Cambridge, 2000.

Ruiz-González, C., Galí, M., Lefort, T., Cardelús, C., Simó, R., and Gasol, J. M.: Annual variability in light modulation of bacterial heterotrophic activity in surface northwestern Mediterranean waters, Limnol. Oceanogr., 57, 1376–1388, doi:10.4319/lo.2012.57.5.1376, 2012.

Ruiz-González, C., Simó, R., Sommaruga, R., and Gasol, J. M.: Away from darkness: A review on the effects of solar radiation on heterotrophic bacterioplankton activity, Front. Microbiol., 4, 131, doi:10.3389/fmicb.2013.00131, 2013.

Saló, V., Simó, R., and Calbet, A.: Revisiting the dilution technique to quantify the role of microzooplankton in DMS(P) cycling: laboratory and field tests, J. Plankton Res., 32, 1255–1267, doi:10.1093/plankt/fbq041, 2010.

Sarmento, H. and Gasol, J. M.: Use of phytoplankton-derived dissolved organic carbon by different types of bacterioplankton., Environ. Microb., 14, 2348–60, doi:10.1111/j.1462- 2920.2012.02787.x, 2012.

Sarmiento, J. L., Hughes, T. M., Stouffer, R. J., and Manabe, S.: Simulated response of the ocean carbon cycle to anthropogenic climate warming, Nature, 393, 245–249, 1998.

Shick, J. M. and Dunlap, W. C.: Mycosporine-like amino acids and related Gadusols: biosynthesis, acumulation, and UV-protective functions in aquatic organisms, Ann. Rev. Physiol., 64, 223–62, doi:10.1146/annurev.physiol.64.081501.155802, 2002.

Simó, R.: From cells to globe : Approaching the dynamics of DMS(P) in the ocean at multiple scales, Can. J. Fish. Aquat. Sci., 61, 673–684, doi:10.1139/F04-030, 2004.

Simó, R. and Pedrós-Alió, C.: Role of vertical mixing in controlling the oceanic production of dimethyl sulphide, Nature, 402, 396– 399, 1999.

Simó, R., Pedrós-Alió, C., Malin, G., and Grimalt, J. O.: Biological turnover of DMS, DMSP and DMSO in contrasting open-sea waters, Mar. Ecol. Prog. Ser., 203, 1–11, doi:10.3354/meps203001, 2000.

Simó, R., Vila-Costa, M., Alonso-Sáez, L., Cardelús, C., Guadayol, O., Vázquez-Domínguez, E., and Gasol, J.: Annual DMSP contribution to S and C fluxes through phytoplankton and bacterioplankton in a NW Mediterranean coastal site, Aquat. Microb. Ecol., 57, 43–55, doi:10.3354/ame01325, 2009.

Slezak, D. and Herndl, G.: Effects of ultraviolet and visible radiation on the cellular concentrations of dimethylsulfoniopropionate (DMSP) in Emiliania huxleyi (strain L), Mar. Ecol. Prog. Ser., 246, 61–71, doi:10.3354/meps246061, 2003.

Smith, D. C. and Azam, F.: A simple, economical method for measuring bacterial protein synthesis rates in seawater using 3Hleucine, Marine Microbial Food Webs, 6, 107–114, 1992.

Sommaruga, R., Hofer, J. S., Alonso-Saez, L., and Gasol, J. M.: Differential sunlight sensitivity of picophytoplankton from surface Mediterranean coastal waters, Appl. Environ. Microb., 71, 2154–2157, 2005.

Spiese, C., Kieber, D. J., Nomura, C., and Kiene, R. P.: Reduction of dimethylsulfoxide to dimethylsulfide by marine phytoplankton, Limnol. Oceanogr., 54, 560–570, 2009.

Stefels, J.: Physiological aspects of the production and conversion of DMSP in marine algae and higher plants, J. Sea Res., 43, 183– 197, doi:10.1016/S1385-1101(00)00030-7, 2000.

Sunda, W., Kieber, D. J., Kiene, R. P., and Huntsman, S.: An antioxidant function for DMSP and DMS in marine algae., Nature, 418, 317–20, doi:10.1038/nature00851, 2002.

Sunda, W. G., Hardison, R., Kiene, R. P., Bucciarelli, E., and Harada, H.: The effect of nitrogen limitation on cellular DMSP and DMS release in marine phytoplankton: climate feedback implications, Aquat. Sci., 69, 341–351, doi:10.1007/s00027-007-0887-0, 2007.

Toole, D. A., Slezak, D., Kiene, R. P., Kieber, D. J., and Siegel, D. A.: Effects of solar radiation on dimethylsulfide cycling in the western Atlantic Ocean, Deep Sea Res. Pt. I, 53, 136–153, 2006.

Toole, D. A., Siegel, D. A., and Doney, S. C.: A lightdriven, one-dimensional dimethylsulfide biogeochemical cycling model for the Sargasso Sea, J. Geophys. Res., 113, 1–20, doi:10.1029/2007JG000426, 2008.

Vallina, S. M. and Simó, R.: Strong relationship between DMS and the solar radiation dose over the global surface ocean., Science, 315, 506–508, doi:10.1126/science.1133680, 2007.

Vallina, S. M. and Simó, R.: Re-visiting the CLAW hypothesis, Environ. Chem., 4, 384–387, 2008.

van de Poll,W. H. and Buma, A. G. J.: Does ultraviolet radiation affect the xanthophyll cycle in marine phytoplankton? Photochem. Photobiol. Sci., 8, 1295–1301, doi:10.1039/B904501E, 2009.

van Rijssel, M. and Buma, A.: UV radiation induced stress does not affect DMSP synthesis in the marine prymnesiophyte Emiliania huxleyi, Aquat. Microb. Ecol., 28, 167–174, doi:10.3354/ame028167, 2002.

Vila-Costa, M., Kiene, R. P., and Simó, R.: Seasonal variability of the dynamics of dimethylated sulfur compounds in a coastal northwest Mediterranean site, Limnol. Oceanogr., 53, 198–211, 2008.

Vincent, W. F. and Neale, P. J.: Mechanisms of UV damage to aquatic organisms, in: The Effects of UV Radiation in the Marine Environment, edited by de Mora, S. J., Demers, S., and Vernet, M., chap. 6, 149–176, Cambridge University Press, Cambridge, 2000.

Wolfe, G. and Kiene, R. P.: Radioisotope and chemical inhibitor measurements of dimethyl sulfide consumption rates and kinetics in estuarine waters, Mar. Ecol. Prog. Ser., 99, 261–269, 1993.

Woodhouse, M. T., Mann, G. W., Carslaw, K. S., and Boucher, O.: Sensitivity of cloud condensation nuclei to regional changes in dimethyl-sulphide emissions, Atmos. Chem. Phys., 13, 2723– 2733, doi:10.5194/acp-13-2723-2013, 2013.

Yang, G., Li, C., and Sun, J.: Influence of salinity and nitrogen content on production of dimethylsulfoniopropionate (DMSP) and dimethylsulfide (DMS) by Skeletonema costatum, Chin. J. Oceanol. Limn., 29, 378–386, 2011.

Zapata, M., Rodríguez, F., and Garrido, J. L.: Separation of chlorophylls and carotenoids from marine phytoplankton: a new HPLC method using a reversed phase C8 column and pyridinecontaining mobile phases, Mar. Ecol. Prog. Ser., 195, 29–45, doi:10.3354/meps195029, 2000.

Chapter 3

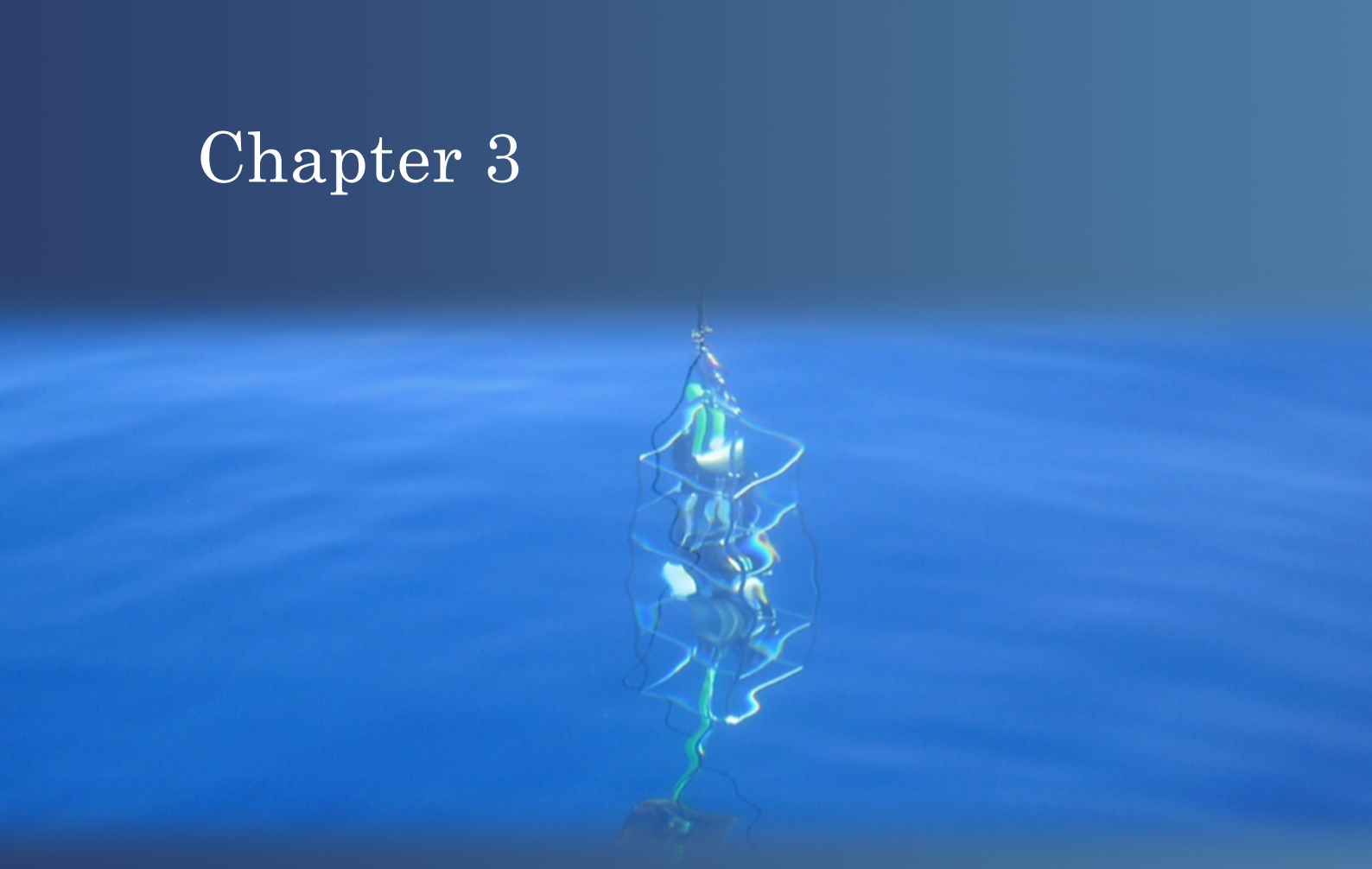

Development and validation of a shipboard system for measuring high-resolution vertical profiles of aqueous dimethylsulfide concentrations using chemical ionisation mass spectrometry

---

Environmental Chemistry, V11, p.309-317, 2014

Sarah-Jeanne Royer, Martí Galí, Eric Saltzman,Cyril McCormick,
Thomas Bell and Rafel Simó

Abstract

A sampling and analytical system has been developed for shipboard measurements of high-resolution vertical profiles of the marine trace gas dimethylsulfide (DMS). The system consists of a tube attached to a CTD with a peristaltic pump on deck that delivers seawater to a membrane equilibrator and atmospheric pressure chemical ionization mass spectrometer (Eq-APCIMS). This allows profiling DMS concentrations to a depth of 50 m, with a depth resolution of 1.3-2 m and a detection limit of nearly 0.1 nmol L^{-1}. The seawater is also plumbed to allow parallel operation of additional continuous instruments, and simultaneous collection of discrete samples for complementary analyses. A valve alternates delivery of seawater from the vertical profiler and the ship's underway intake, thereby providing high-resolution measurements in both the vertical and horizontal dimensions. Tests conducted on various cruises in the Mediterranean Sea, Atlantic, Indian, and Pacific Oceans show good agreement between the Eq-APCIMS measurements and purge and trap gas chromatography with flame photometric detection (GC-FPD) and demonstrate that the delivery of seawater from the underway pump did not significantly affect endogenous DMS concentrations. Combination of the continuous flow DMS analysis with high-frequency hydrographic, optical, biological and meteorological measurements will greatly improve the spatial/temporal resolution of seagoing measurements and improve our understanding of DMS cycling.

Introduction

Dimethylsulfide (DMS) is ubiquitous in the pelagic ocean and plays a key role in the global sulfur cycle (Bates et al., 1992; Berresheim et al., 1990; Simó, 2001). The knowledge gained in recent decades about this volatile sulfur compound and its precursor dimethylsulfoniopropionate (DMSP) is of such extent that they are some of the best-studied organic substances in the world's ocean. The global surface seawater DMS concentration database (Kettle et al., 1999; Lana et al., 2011) is the third largest oceanic trace gas database behind those of CO_2 and N_2O. DMS plays a significant role in the formation, growth and chemistry of marine aerosols (Clarke, 1998), the long-term return of sulfur from the oceans to the continents via atmosphere (Lovelock, 1972), and the chemical ecology of many marine living beings (Kiene et al., 2000; Raina et al., 2013; Seymour et al., 2010; Stefels, 2000). It has been argued that DMS plays a central role in a plankton-climate regulatory feedback loop, but this remains controversial (Charlson et al., 1987; Iizuka et al., 2012; Quinn and Bates, 2011).

The analytical methods most used to determine aqueous DMS concentrations over the last 40 years consist of gas chromatography (GC) with flame photometric or chemiluminescence detectors (e.g., refs. Andreae and Barnard, 1983; Bates et al., 1987; Dacey et al., 1998; Simó, 1998; Turner and Liss, 1985) on samples collected with Niskin bottles or shipboard pumping systems. Most of the reported oceanic DMS observations are from near-surface samples (1 to 10 m depth) or from unequally spaced and sparse samples collected from vertical profiles. The limited vertical resolution of the sampling technique (usually Niskin bottles attached to a CTD rosette), together with the time needed for the analysis of discrete samples, result in a poor resolution of the obtained vertical concentration profiles.

Today, mass spectrometric (MS) techniques with high sensitivity and fast response allow the determination of DMS without pre-concentration. These techniques, supplied

with seawater pumped continuously from the ocean and coupled to either bubbling or membrane equilibration to remove the volatiles from their aqueous matrix, provide high-frequency measurements of seawater DMS concentrations. Recently, a number of systems that involve coupling of water/gas equilibrators to electron impact, chemical ionization, and proton transfer mass spectrometers have been developed (Kameyama et al., 2009; Saltzman et al., 2009; Tortell, 2005). These systems have the potential to dramatically increase the collection of surface ocean DMS data. The 30+ year global DMS database contains nearly 50,000 data points (Lana et al., 2011). Today, a single cruise of 20 days with one of these systems working continuously provides ca. 10,000 measurements for 5 minute averaged data. These systems are suited to resolve sub-mesoscale and short-term variability features (Asher et al., 2011; Kameyama et al., 2013; Tortell and Long, 2009). However, before thousands of new data are archived into the global database, it is important to inter-compare the new techniques with each other and with the traditional GC methods (Bell et al., 2012). To our knowledge, only one study (Tortell et al., 2011) has reported a comparison exercise of a high-frequency mass spectrometric technique (membrane inlet mass spectrometry (MIMS)) with purge and trap GC. The results showed good consistency in capturing DMS variability but exhibited a variable offset.

The increasing resolution on the horizontal and temporal scales has not yet been matched in the vertical scale, because the aforementioned instruments have been coupled to shipboard underway intake systems that pump water from a single depth. To date, vertical profiles of DMS concentration are obtained from discrete samples and measured manually using non-automated instruments (e.g., GC), with a depth resolution of several meters and a time resolution of hours between casts. This lack of high-resolution concentration profiles limits description of DMS dynamics on short temporal scales and understanding of the complex biogeochemical interactions that drive oceanic DMS cycling across the water column.

Here we present the development of a technique for sampling and analyzing DMS concentrations at high frequency through the upper water column along with parallel measurements of physical and biological variables. The technique consists of a profiling sampler, connected to a membrane equilibrator and atmospheric pressure chemical ionization mass spectrometer (Eq-APCIMS). We describe the system components and its operation, and compare the results with those from the purge and trap, gas chromatograph with flame photometric detection (GC-FPD) technique. To our knowledge, this is the first time that a continuous sampling technique has enabled vertical DMS concentration profiles at high resolution over depth and time.

Experimental

The analytical system

This study used a tubular counter-flow membrane equilibrator. Details of equilibrator design, construction, and operating conditions are given in Saltzman et al., (2009) and Table 1. The equilibrator consists of a porous hydrophobic Teflon-membrane tube mounted inside a coiled larger internal diameter tube. Seawater flows through the annular space between the porous membrane and outer tubes and high purity (zero) air counter-flows through the porous inner tube. Dissolved gases, including DMS, diffuse across the pores in the inner tube wall into the air stream, such that the exiting air reaches equilibrium with the seawater DMS. The air exiting the equilibrator is mixed with a larger dilution flow of zero air and directed to the source of the APCIMS. The residence time of seawater and zero air in the equilibrator are approximately 10 and 20 seconds, respectively.

DMS was detected using an atmospheric pressure chemical ionization mass spectrometer. The instrument used in this study is the “mini-CIMS”, developed and described in detail in Saltzman et al., (2009). The mini-CIMS is a single quadrupole

Table 1. Equilibrator and atmospheric pressure chemical ionization mass spectrometer (APCIMS) operating parameters used in this study.

EQUILIBRATOR		
		Flow rates (mL min^{-1})
Seawater flow		1800-2100
Air flow		60
NON-EQUILIBRATOR GAS LINES		
		Flow rates (mL min^{-1})
Dilution (bypass) air		600
CH_3SCD_3 standard in air		70
APCIMS		
Region	*Lens*	*Lens potential (V DC)*
Ion source (760 Torr)	pinhole	65
Collision region (1 Torr)	cone 1	34
	cone 2	8
Analyzer region (10^{-5} Torr)	mesh 1	-110
	aperture 2	12
	aperture 3	-4
	aperture 4	-90
	focus plate	50
		Temperature (^{o}C)
Ion source		350

mass spectrometer based on the Stanford Research Systems residual gas analyzer, with a heated ^{63}Ni radioactive source. DMS is ionized by proton transfer from protonated water ($H_2O \cdot H^+$), declustered, mass filtered, and detected by an electron multiplier. Table 1 reports the lens potentials, ion source temperature and gas flow rates used to obtain optimal sensitivity for DMS. Figure 1A shows a mass scan of the equilibrator outflow using the shipboard system on board the *R/V* Garcia del Cid in May 2012.

DMS is quantified by monitoring the ratio of signals from ambient DMS (CH_3SH_3 H+, m/z 63) and an isotopically-labeled internal standard (triple-deuterated DMS, CH_3SCD_3 H^+, m/z 66). During regular operation in the field, data were recorded continuously by single ion monitoring (SIM) of $(H_20)H^+$ (m/z 19), $(H_2O)_2H^+$ (m/z 37), DMS (m/z 63), CH_3SCD_3 (m/z 66) and isoprene (m/z 69), (Figure 1B). The internal standard was provided by a CH_3SCD_3 permeation tube (0.78 ng min^{-1}; Dynacal, VICI Metronics) maintained at 30°C in a permeation chamber diluted in a flow of 70 mL min^{-1} of zero air. The permeation rate was monitored in the laboratory before the cruises using high precision weight measurements, and validated on GC-FPD by cross calibration with a higher permeation rate DMS standard (183 ng min^{-1}) that in turn had been calibrated by high precision weighing and displayed a constant weight loss rate over a period of 4 years (R^2 = 0.9999). The output from the CH_3SCD_3 permeation tube was added to the air stream exiting the equilibrator. The level of DMS (m/z 63) impurity in the CH_3SCD_3 standard (m/z 66) corresponded to about 1.9 % of the signal at m/z 66 and was corrected from the raw m/z 63 data. Blank measurements in the dilution air were also run, but were typically negligible. Figure 1B shows the raw signals typically acquired in SIM mode.

The molar mixing ratio of ambient DMS (X_{DMS}) in the gas stream exiting the equilibrator is calculated as follows:

$$X_{DMS} = (C_{63}/C_{66}) * (P/F_{eq})$$

where C_{63} and C_{66} are the blank corrected-signals (in amps) for m/z 63 and 66, P is the permeation rate in mol s^{-1}, and F_{eq} is air flow rate in the equilibrator (mol s^{-1}) determined from the measured mass flow and ideal gas law. The gas phase DMS mixing ratio (X_{DMS}) was converted to a seawater concentration, using the temperature- and salinity-dependent Henry's law constant for DMS (H_{DMS}, M atm^{-1}; Dacey et al., 1984):

$$DMS_{sw} = X_{DMS} * P_{atm} * H_{DMS}$$

(A)

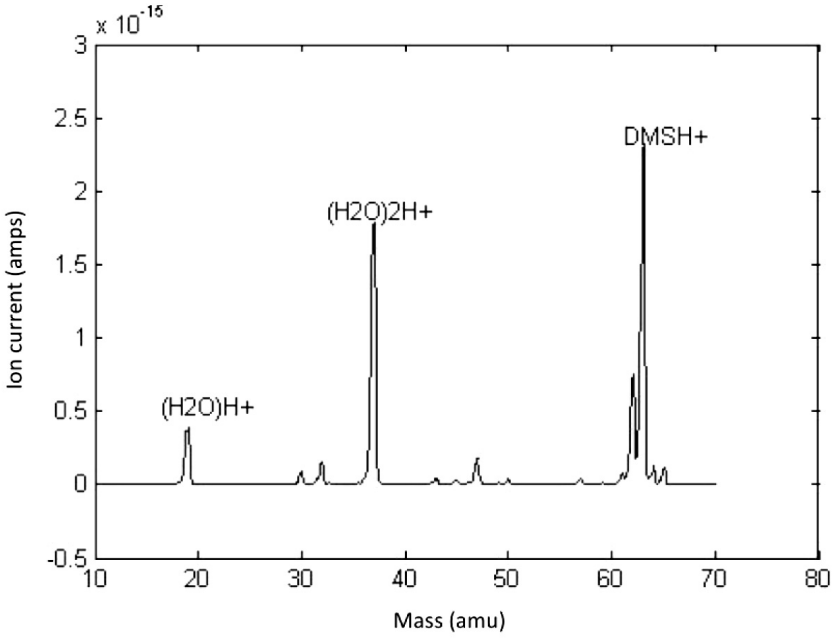

(B)

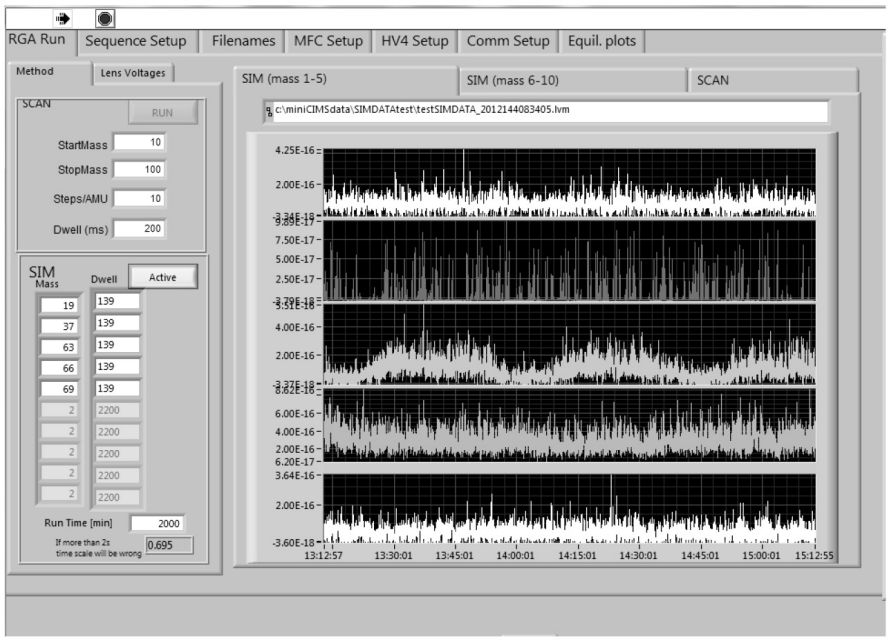

Figure 1: (A) Ion scan from the Eq-APCIMS instrument running a seawater sample with no standard on-line. Sample collected with the underway-pumping system aboard the R/V Garcia del Cid in the Mediterranean Sea, May 2012. (B) A screen capture of the signal acquisition on the Eq-APCIMS; from top to bottom, raw signal for water molecules (m/z 19 - $H_2O(H^+)$), clustered water molecules (m/z 37 – $(H_2O)_2(H^+)$), DMS (m/z 63 – $(CH_3)_2S(H^+)$), trideuterated DMS standard (m/z 66 – $CH_3SCD_3(H^+)$), and isoprene (m/z 69 – $C_5H_8(H^+)$).

The instrument was operated in an automated operational cycle consisting typically of a 12-hour seawater data collection period (in SIM mode), followed by equilibrator blanks (no internal standard; 5 minutes SIM, 10 full scans), and standard-only blanks (equilibrator bypassed; 5 minutes SIM, 10 full scans). The blanks were used to account for the contribution of non-isotope DMS in the internal standard and to detect DMS contamination in the system tubing and electronic noise. These were very small corrections (1.9%), and are minor contributors to the overall uncertainty of the measurement. It is important to note that these blanks do not account for any contamination of the equilibrator itself. The regular ambient data acquisition accounted for 95% of the operation time.

The zero air for both the equilibrator and the internal standard was supplied either from a pressurized cylinder or by an ultra-zero air generator (model GT6000, LNI Schmidlin) fed by the compressed air supply of the ship.

The overall shipboard system layout

A schematic of the whole system on board is presented in Figure 2. The setup allowed alternation between the underway intake while steaming, and vertical profiling when the ship is on station. The Eq-APCIMS was located in one of the ship laboratories, next to the outlet of the clean underway intake system. A valve allowed switching between the underway and profiler seawater supplies. A multitap set divided the incoming water flow into three parallel flows directed to: (1) the equilibrator of the Eq-APCIMS, (2) a Fast Repetition Rate fluorometer (FRRf; FASTracka, Chelsea Instruments) recording in continuous mode, and (3) a tube for filling bottles for discrete measurements.

The underway seawater intake system

The underway seawater intake system uses the ship's clean water intake pump, which provides an uncontaminated (non-toxic), continuous source of near-surface seawater.

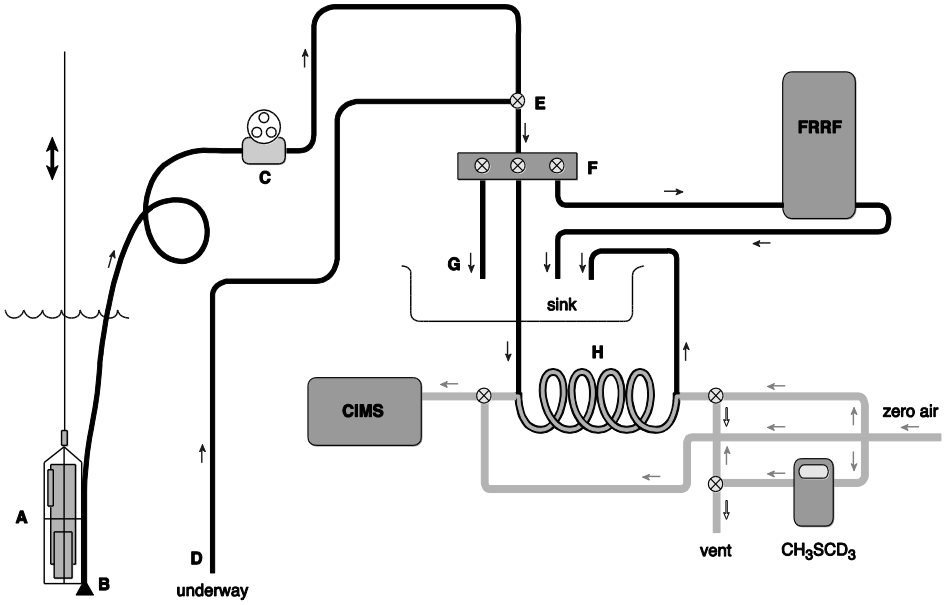

Figure 2: Diagram of the system designed for either underway or vertically profiled high-resolution measurements of DMS aboard an oceanographic vessel. Black circuit represents the water flow; grey circuit corresponds to the air flow. A: CTD sensors in a protected cage (the double arrow indicates operation from the winch in yo-yo mode); B: hose inlet; C: peristaltic pump on board; D: silicone pipe from the ship's underway pump; E: switch tap; F: multitap; G: flow outlet into the sink; H: equilibrator loop; CH_3SCD_3: standard permeation device. CIMS stands for Atmospheric Pressure Chemical Ionization Mass Spectrometer. FRRf stands for Fast Repetition Rate Fluorometer. Small arrows signal the direction of the flow. In the circuit for the zero air supply to the equilibrator, filled arrows indicate the flow in normal conditions. The open arrows indicate operation through a bypass of the equilibrator and venting of the standard to check for blanks.

The water is brought to the laboratories through epoxide-free silicone pipes. A branch of the flow is directed through continuously logged thermo-salinograph, fluorometer and temperature sensors. The data reported in the present study were collected on three cruises: one conducted aboard the *R/V* Hesperides across the Atlantic, Indian and Pacific oceans (Malaspina cruise, January-June 2011), and the other two aboard the *R/V* Garcia del Cid in the northwestern Mediterranean Sea (SUMMER cruises, September 2011 and May 2012). On the *R/V* Hesperides, the water intake is located 5 m below sea level, and the parts of the centrifugal pump (BKMKC-10.11, Tecnium) in contact with the fluid are made of polypropylene and glass. On the *R/V* Garcia del Cid, the intake is located 4 m below sea level and the interior of the pump (BKMKC-8.10, Tecnium) is also made of polypropylene.

The vertical profiling system

The system developed for measuring high-resolution vertical profiles consisted of a CTD operated manually in up and down motion, with a tied hose through which water was pumped to the ship's laboratory. The device used for drawing seawater was an in-lab peristaltic pump (model 620UN**,** Watson-Marlow), which is free of valves, seals or glands to avoid clogging or corrosion. The pumped seawater flow contacts only the bore of the tube (Marprene, inert thermoplastic elastomer, Watson-Marlow), eliminating the risk of sample contamination. The pump flow rate was 3.5 L min^{-1}. The pump intake tubing was a 50-70 m non-toxic latex hose reinforced with polyester thread mesh (model Mallalatex, Espiroflex), with inner and outer diameters of 15 and 21 mm, respectively. A 10 cm diameter plastic funnel was mounted at the hose inlet and covered with 5 mm nylon mesh to avoid drawing large jellyfish that might clog the system. The first meter of the hose was tied to the cage of the CTD probe with the aid of a segment of semi-rigid plastic tubing that prevented bending of the hose. The CTD (SBE-19, Seabird) was manually controlled to cycle from 1 to 35 or 50 m depth at a speed of about 2.5-4 m min^{-1}. A complete cycle from the surface to 35 m and back took about 20-25 minutes. Profiling to 50 m and back took 30 minutes. Vertical profiles of conductivity and temperature were measured with the CTD sensors as seawater was drawn through the hose for DMS measurements.

Parallel DMS analysis by gas chromatography with flame photometric detection (GC-FPD)

A traditional purge and trap GC-FPD, was used to analyze discrete DMS samples on the cruises in parallel with the Eq-APCIMS (Galí et al., 2013; Simó et al., 1996). Samples were collected in glass vials either from Niskin bottles attached to a CTD rosette or from the underway-pumped flow using the open tap. In all cases, some overflow was allowed to avoid headspace and bubbles while sampling and filling the vials. Subsamples of

3-10 mL were gently filtered through GF/F, purged for 3-5 min with ultra-high purity helium, and the stripped DMS was cryogenically trapped in liquid nitrogen. The trapped volatiles were desorbed by dipping the trap in water at room temperature. Gases were separated on a Carbopack 60/80 mesh column (Supelco) at 170ºC. A Shimadzu GC14A gas chromatograph and flame photometric detection were used. All samples were processed shortly after collection. DMS concentrations were determined by comparison with a standard curve constructed by injecting different volumes of gas standards from a DMS permeation device (183 ng min^{-1}, Dynacal, VICI Metronics) maintained at a constant temperature and diluted in zero air (Simó et al., 1996). The detection limit was 3 pmol DMS (0.3 nmol L^{-1} aqueous DMS in a 10 mL seawater sample). All samples were analyzed in duplicate and the coefficient of variation between the duplicates was generally ≤ 5%.

Results

Eq-APCIMS data averaging, measurement precision and sensitivity

The Eq-APCIMS instrument acquired data for each ion for 139 milliseconds with a frequency of 0.5 Hz but, as depicted by Figure 1B, time averaging (binning) of the data was required to improve the signal to noise ratio. In order to determine the optimal averaging time we used 6.2 hours of continuous, near-surface underway measurements conducted in the Mediterranean Sea on the *R/V* Garcia del Cid, with the ship closely following a pair of surface Lagrangian drifters. Because we stayed in a coherent water patch, the DMS concentration underwent only a small and smooth drift during the sampling period. Raw data (63:66 ratios) were binned into increasing intervals between 4 and 400 s, bin averages were computed and the standard deviation of the mean of all bins over the 6.2 h period was calculated. Figure 3 illustrates the effect of averaging (binning) time on the variance of the signal. Increasing the averaging time rapidly

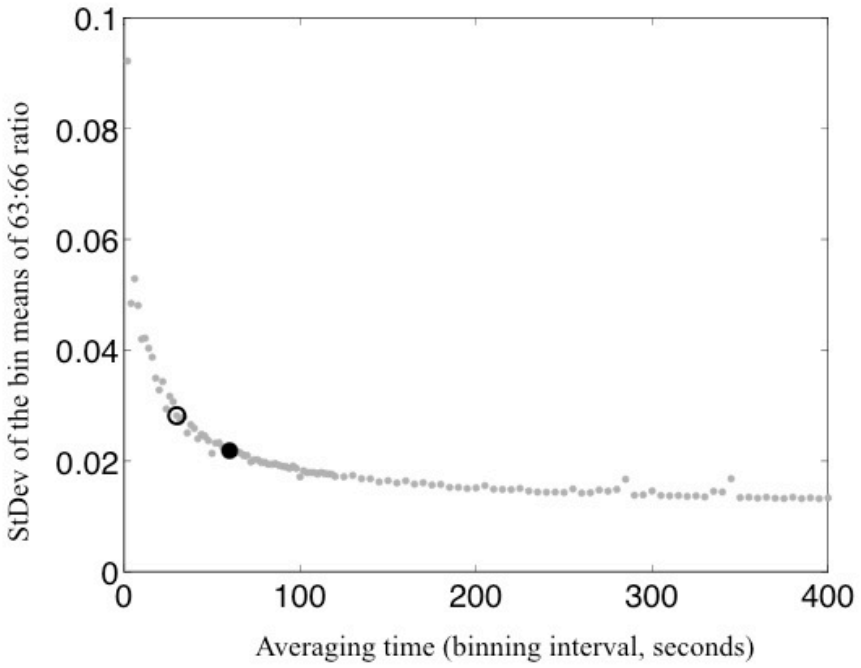

Figure 3: Standard deviation of averaged bin means of Eq-APCIMS data vs. binning time. Data are the values of the ratio of ion 63 ($DMS(H^+)$) to ion 66 ($CH_3SCD_3(H^+)$), which is the ratio used to calculate the aqueous DMS concentration, over a period of 6.2 hours. Binning times increase by 2 seconds until 120 seconds and then by 5 seconds up to 400 seconds. The filled circle shows the optimal averaging (binning) time chosen for surface underway data (60 seconds); the open circle shows the optimal averaging (binning) time selected for vertical profiles (30 seconds). See text for details.

reduces the standard deviation essentially because it increases the signal to noise ratio, until a point where further lengthening the bins does not significantly reduce the variance, as shown by the flattening of the curve in the figure. Based on these results, an averaging time of 60 seconds was used to process underway data. With the ship steaming at 10 knots, a 60 second averaging time yields a datum every 300 m. When profiling at an ascent/descent speed of 2.5-4 m min^{-1}, averaging every 60 seconds would yield a vertical resolution of 2.5-4 m, which was deemed too coarse to observe DMS gradients. Therefore, an averaging time of 30 seconds (equivalent to 1.3-2 m) was used for vertical profiles.

An estimate of the overall uncertainty in the DMS analysis was obtained using the same Lagrangian data series. This included the error associated to the mean of the 63:66 ratio within each bin, and the uncertainty in solubility associated with the variance in equilibrator seawater temperatures. Assuming these uncertainties are

uncorrelated, the resulting coefficient of variation of DMS concentration in 60 seconds bins was 8%. This can be regarded as the experimental error or precision of the underway DMS concentration measurements. For vertical profile DMS measurements, which used a binning time of 30 seconds, the experimental error was 11%.

As for instrument's sensitivity, the detection limit of the Eq-APCIMS is estimated as 220 ppt in the equilibrated air stream (Saltzman et al., 2009). Based on the solubility of DMS in seawater, this is equivalent to aqueous concentrations of 0.12, 0.10, and 0.08 nmol L^{-1} at temperatures of 15, 20, and 25°C, respectively.

Eq-APCIMS vs. GC-FPD measurements

On the *R/V* Hesperides 2011 cruise across oligo- and mesotrophic regions of the world's oceans, discrete DMS samples were collected from the underway pumped flow, using the open outlet of the multitap system throughout the day. These samples were analyzed

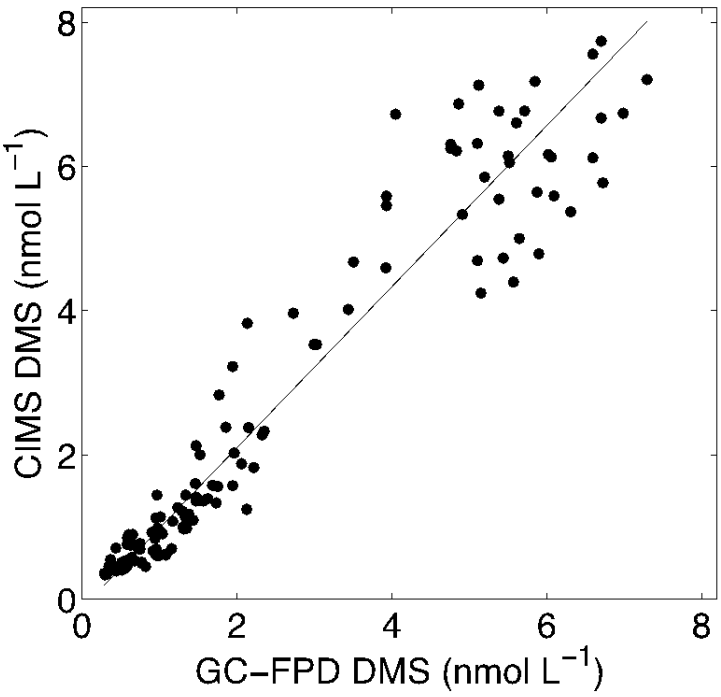

Figure 4: Model II regression for Eq-APCIMS against GC-FPD DMS concentrations in 125 samples; y = 1.12 (±0.03)*x – 0.13 (±0.09); $R^2 = 0.92$; $p < 0.0001$.

by purge and trap GC-FPD as described above. The exact time of discrete sampling was noted and matched to the corresponding one-minute averaged Eq-APCIMS datum. On Lagrangian cruises aboard the *R/V* Garcia del Cid, discrete GC samples were collected from several depths using the open outlet of the multitap system while measuring vertical profiles with the profiler. The corresponding time and depth were matched to the 30 second averaged Eq-APCIMS data. All of these GC-FPD and Eq-APCIMS data are compared in Figure 4. Each of the two techniques was calibrated with its own permeation standard.

A Model II linear regression of the Eq-APCIMS vs. GC data yields a significant relationship, with $R^2 = 0.92$ ($p < 0.0001$), slope of 1.12 ± 0.03 and intercept of -0.13 ± 0.09. This average discrepancy between the Eq-APCIMS and GC-FPD measurements is within the experimental error of the Eq-APCIMS (ca. ±10%), and also within the estimated inherent variability of other DMS measurement methods (Bell et al., 2012). The agreement is reasonably good given the independent calibrations, the differences in sample handling (e.g., the GC-FPD requires filtration, the Eq-APCIMS does not; the Eq-APCIMS method equilibrates the sample with air and measures the equilibrated fraction only, while the GC-FPD method sparges the sample), and the fact that GC-FPD is run on a discrete 3-10 mL sample whereas the Eq-APCIMS datum is the average of 30-60 seconds of acquisition and therefore averages DMS concentration over 1.5-2 m of water column or 300 m of horizontal track.

Test for potential pumping artifacts

Possible concerns associated with measuring DMS using the underway intake pumping system include: (1) damage to phytoplankton cells and associated DMS release or production through enzymatic cleavage of DMSP, (2) loss of DMS due to bacterial metabolism associated with biofilms in the system, or (3) loss of analytes through volatilization or wall losses. To validate the use of underway pumping systems for

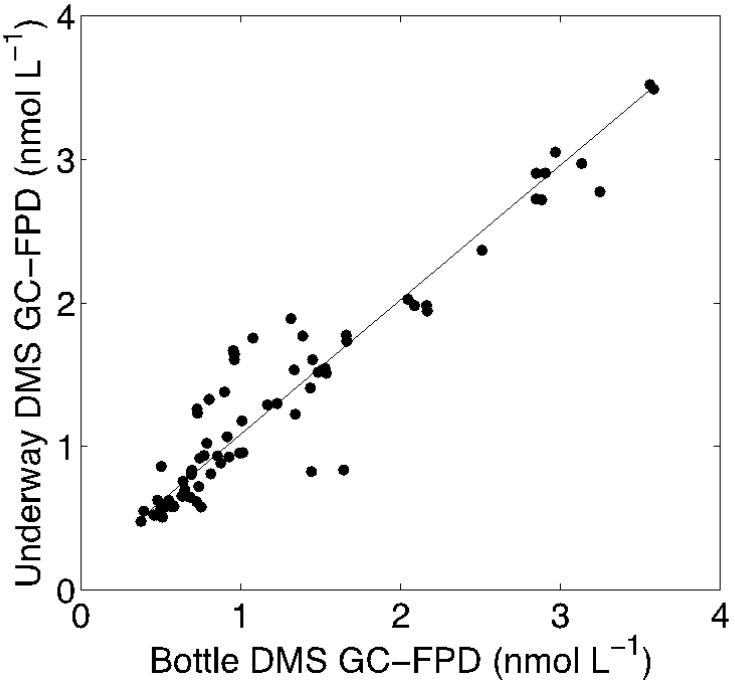

Figure 5: Model II regression for underway DMS sampling against co-located overboard bottle sampling using GC-FPD for the analysis of all 75 samples; y = 0.94 (±0.024)*x + 0.15 (±0.036); $R^2 = 0.91$; $p < 0.0001$.

DMS, we compared discrete samples collected from the underway intake system with samples collected simultaneously at a similar depth (3 m) using Go-Flo bottles launched overboard. Both sets of samples were analyzed by GC-FPD using identical method (Figure 5). There is good agreement between the two series. Model II linear regression gives a strong and significant relationship ($R^2 = 0.91$ $p < 0.0001$), with an underway/ bottle slope of 0.94 ± 0.024 and an intercept of 0.15 ± 0.036, i.e., the agreement is almost within the measurement uncertainty of the GC-FPD method (±5%).

Vertical profiles at sea

The profiler / Eq-APCIMS system was field tested for high-resolution vertical profiles of DMS concentrations during the two cruises in the Mediterranean Sea on board the *R/V* Garcia del Cid in September 2011 and May 2012. As a token example, data collected during a 2.5 hour run in the evening of September 14th, 2011, are shown in Figure 6 to

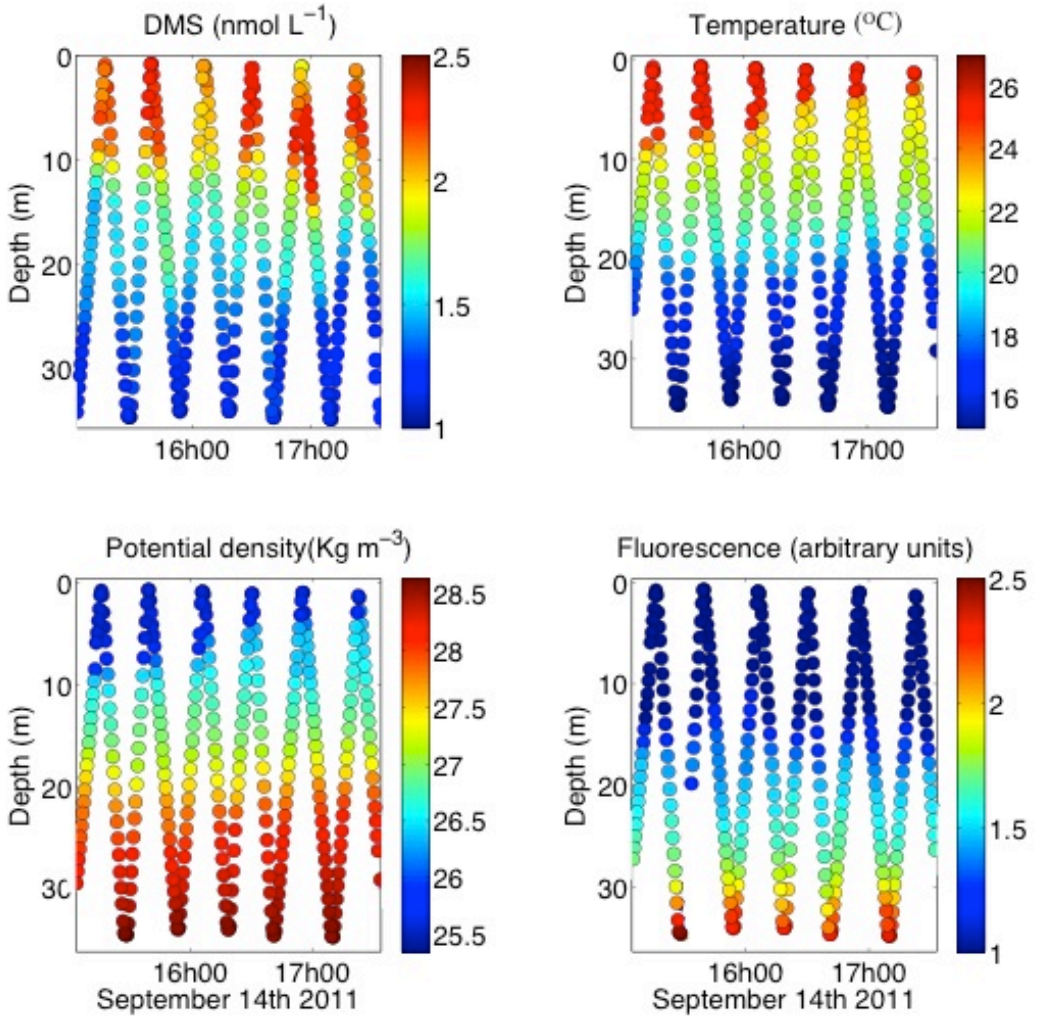

Figure 6: Repeated depth profiles of DMS, seawater temperature and potential density, and chlorophyll a fluorescence measured for 2.5 hours during a Mediterranean cruise aboard the R/V Garcia del Cid on September 14, 2011. The profiler was cycled from the near surface to 35 m and DMS and fluorescence were measured using the Eq-APCIMS and the FRRF (see text for details). Temperature and potential density were measured and calculated, respectively, from the CTD sensors of the profiler. The X axis is GMT time. Half minute average data are shown.

illustrate the performance of the profiling technique. The depth vs. time plot shown here corresponds to 6 complete up/down cycles from the surface water to about 35 m depth. In a later cruise, the technique was proven to work well up to a depth of 50 m.

Figure 6 also shows profiles of seawater temperature and potential density derived from the CTD probe of the profiler, and chlorophyll *a* fluorescence measured with the

FRRf installed in parallel to the Eq-APCIMS. It clearly illustrates that steep gradients with depth occur for all variables, with DMS showing maximum concentrations near the warmer surface, completely decoupled from the deeper fluorescence maximum that occurs in the colder waters at the bottom of the pycnocline. It also reveals a rapid change in stratification, with the upper mixed layer turning shallower as the sun approached sunset (ca. 18:00 GMT). This rapid change in water physics was not matched at the same pace by significant changes in the DMS concentration profile. The full dataset from the cruises will be presented and discussed elsewhere.

The pressure sensor of the CTD probe provided the sampling depth at any time. However, attributing each Eq-APCIMS measurement to its corresponding depth was not trivial because the sampled water took 3.5 minutes to flow from the hose inlet to the Eq-APCIMS. There were some slight variations in time lag due to changes in flow rate associated with transitory bending of the hose under water. Since the Eq-APCIMS equilibrator was equipped with a temperature data-logging sensor, we matched the temperature profiles of the equilibrator and CTD sensors to determine the depth at which the equilibrator seawater was sampled.

One concern of any profiler working from a floating platform is the effect that platform motion (primarily ship roll) may have on the depth accuracy of the measured profile. In this sense, having a depth (pressure) probe continuously recording at the mobile sampling point (hose inlet) allows accounting for variations in the sampling depth due to ship roll. Another concern relates to the potential smearing or homogenization of the target analyte(s) in the sampled water owing to mixing in the profiler pipe. Calculations for our hose dimensions and pumping rate following Taylor (1953) give an e-folding mixing length along the hose of about 1 m or a mixing time scale of about 3 seconds (i.e., 13-20 cm depth resolution at speeds of 2.5-4 m min^{-1}). Laboratory experiments indicate that the response time constant for the Eq-APCIMS to a step change in seawater concentration is approximately 10 seconds due to mixing within the equilibrator

and equilibration time. When these two sources of uncertainty are added together in a nonlinear way, the resulting response time of the system is SQRT(3^2 + 10^2) = 10.4 seconds. Therefore, the effects of the tubing and equilibrator response times limit the best depth resolution achievable with the profiling system to approximately 0.4-0.7 m for profiling speeds of 2.5-4 m min^{-1}. Nonetheless, the aforementioned need for averaging the signal in 30-seconds bins sets the actual depth resolution of the profiler to 1.3-2 m.

Discussion

The profiling system described here achieved DMS depth profiles with a time resolution of 30 seconds, a depth resolution of 1.3-2 m, a measurement precision of 11%, and a detection limit of nearly 0.1 nmol L^{-1}. The resolution of the profiling system can be improved by varying the pumping and profiling rates, and improving the time response of the Eq-APCIMS and its sensitivity. The mini-CIMS used in this study is a relatively low cost, low sensitivity instrument, and a more sensitive Eq-APCIMS such as that used by Bell et al., (2013) would increase signal to noise by roughly an order of magnitude. However, theoretical time resolution limits of 3 seconds and 10 seconds are imposed by the mixing in the pumping pipeline and the mixing and equilibration response in the equilibrator. Even at the resolution presented here, the profiling approach represents a significant advance in data coverage from the use of Niskin bottles on CTD casts followed by purge and trap analysis.

Hales and Takahashi (2002) developed a vertical profiler by which water was pumped from a SeaSoar CTD through a 750-m tube, while undulating from near the surface to depths near 200 m. Even though the Lamont Pumping SeaSoar (LPS) allows deeper profiles, it has to be operated while steaming and its launch and recovery is far from quick and easy. This prevents its use on station, either at a fixed location or in Lagrangian drift. Our profiler, conversely, is used with the ship stopped on site, and

it is very easy to recover from water, which makes it particularly suited for on-station or Lagrangian studies. As for depth resolution, the LPS is less affected by ship's vertical motion and more affected by mixing in the longer pipe. The authors (Hales and Takahashi, 2002) estimated a mixing time constant of 7.5-10 seconds, which corresponded to a vertical resolution of 1.9-2.5 m when used at dive and climb rates of 15 m min^{-1}. These figures are similar to and even coarser than our aforementioned resolution of 1.3-2 m.

This study provides validation for the continuous flow measurement of DMS by Eq-APCIMS. The method used here involves use of an internal gas standard added after the equilibrated gas stream. This approach assumes complete equilibration in the membrane equilibrator. It does not correct for possible clogging of membrane pores in the equilibrator due to fouling. Extensive use of this equilibrator in prior studies suggests that the porous Teflon tube membrane does not experience biofouling in oligo- and mesotrophic conditions (Bell et al., 2013; Marandino et al., 2007, 2008, 2009; Saltzman et al., 2009). However, during the Malaspina cruise aboard the *R/V* Hesperides, abundant jellyfish in the Benguela current region caused some clogging of the equilibrator, which had to be dismounted and cleaned with 10% hydrochloric acid. Bell et al., (2013) recently modified the technique to introduce the isotopically labeled internal standard as an aqueous solution at the inlet of the equilibrator. This method corrects for any loss of signal in the event of fouling or incomplete equilibration. Neither standardization technique accounts for possible artefact production of DMS in the equilibrator resulting from growth on the tube interior or mechanical stress to organisms in the pump/tubing. However, the observed agreement between the Eq-APCIMS and the GC-FPD methods (Figure 5) across a broad DMS concentration range (0.3 to 8 nmol L^{-1}) suggests that under most typical oceanic conditions (Lana et al., 2011) the equilibrator provides accurate and repeatable measurements.

The agreement of GC-FPD measurements in seawater from Go-Flo bottles and

underway intake indicates that the underway systems did not have a significant impact on endogenous DMS concentrations during this study. Bell et al., (2013) carried out a similar comparison using the Eq-APCIMS, with similar results. However, the results of these studies do not necessarily apply to all ships due to variations in shipboard underway pump types, pipe materials, and maintenance procedures. The fact that some respiratory activity (oxygen consumption) has been measured in underway seawater lines of several ships (Juranek et al., 2010) calls for caution regarding microbial activity that might consume DMS. Likewise, the tests in the present study were conducted with picophytoplankton-dominated waters; phytoplankton assemblages more susceptible to mechanical stress or damage by pumping and/or filtration (e.g., those with colonial *Phaeocystis*) may yield larger differences between underway and bottle-derived measurements.

One of the strengths of the continuous flow DMS measurement is that it can be coupled with other instruments that also provide continuous measurements. For instance, our system was coupled via a multitap split of the seawater flow to a FRRf, which provides fluorescence of organisms and data on the performance of photosystem II (Kolber et al., 1998). This is an interesting complement to DMS measurements, since DMS has been linked to algal physiological stress (Sunda et al., 2002). Like the Eq-APCIMS, the FRRf was used to either record fluorescence response in surface waters while steaming or in vertical profiles when coupled to the profiling sampler. In addition, the CTD probe of the profiler provided physical data such as salinity, temperature and the derived density profiles. Figure 6 shows the importance of getting high-resolution measurements over depth and time to study the dynamics of DMS within its biophysical context. The setup can easily be complemented by adding further sensors to the probe, thereby obtaining high-resolution vertical profiles of variables such as oxygen, underwater light, beam transmission, organic matter fluorescence, turbidity or nitrate, which will provide a more comprehensive context for the DMS profiles.

In summary, high-resolution vertical profiles and near surface underway measure-ments of DMS demonstrate that membrane equilibrator-APCIMS is a valuable new tool to describe short-term DMS variability and its relationship to other physical and biogeochemical parameters. This approach facilitates the study of DMS distribution, cycling and environmental forcing at unprecedented resolution, also along the vertical dimension.

Acknowledgements

We thank the marine technicians (UTM) and the crews aboard the *R/V* Hesperides and Garcia del Cid for their assistance and cooperation. We also thank Anoop S. Mahajan for invaluable assistance with data processing codes. The insightful comments of three anonymous reviewers helped improve the manuscript. This work was supported by the former Spanish Ministry of Science and Innovation through projects Consolider-Ingenio Malaspina (CSD2008–00077), SUMMER (CTM2008-03309/MAR) and PRISMA (CTM2009-10193), and through a PhD scholarship to S.J.R.. Support was also provided by the U.S. National Science Foundation (grants 0851472 and 1143709).

References

Andreae, M. O. and Barnard, W. R.: Determination of trace quantities of dimethyl sulfide in aqueous solutions, Anal. Chem., 55(20), 608–612, 1983.

Asher, E. C., Merzouk, A. and Tortell, P. D.: Fine-scale spatial and temporal variability of surface water dimethylsufide (DMS) concentrations and sea–air fluxes in the NE Subarctic Pacific, Mar. Chem., 126(1-4), 63–75, 2011.

Bates, T. S., Cline, J. D., Gammon, R. H. and Kelly-Hansen, S. R.: Regional and seasonal variations in the flux of oceanic dimethylsulfide to the atmosphere, J. Geophys. Res., 92(C3), 2930, 1987.

Bates, T. S., Lamb, B. K., Guenther, A., Dignon, J. and Stoiber, R. E.: Sulfur Emissions to the Atmosphere from Natural Sources, J. Atmos. Chem., 14, 315–337, 1992.

Bell, T. G., De Bruyn, W., Miller, S. D., Ward, B., Christensen, K. and Saltzman, E. S.: Air–sea dimethylsulfide (DMS) gas transfer in the North Atlantic: evidence for limited interfacial gas exchange at high wind speed, Atmos. Chem. Phys., 13(5), 11073–11087, doi:10.5194/acp-13-11073-2013, 2013.

Bell, T. G., Malin, G., Lee, G. A., Stefels, J., Archer, S., Steinke, M. and Matrai, P.: Global oceanic DMS data inter-comparability, Biogeochemistry, 110(1-3), 147–161, 2012.

Berresheim, H., Andreae, M. O., Ayers, G. P., Gillett, R. W., Merrill, J. T., Davis, V. J. and Chameides, W. L.: Airborne Measurements of Dimethylsulfide , Sulfur Dioxide , and Aerosol Ions over the Southern Ocean South of Australia, J. Atmos. Chem., 10, 341–370, 1990.

Charlson, J. R., Lovelock, J. E., Andreae, M. O. and Warren, S. G.: Oceanic phytoplankton, atmospheric sulphur, cloud albedo and climate., Nature, 326, 655–661, 1987.

Clarke, A. D.: Particle nucleation in the tropical boundary layer and its coupling to marine sulfur sources, Science (80-.)., 282(5386), 89–92, 1998.

Dacey, J. W. H., Howse, F. A., Michaels, A. F. and Wakeham, S. G.: Temporal variability of dimethylsulfide and dimethylsulfoniopropionate in the Sargasso Sea, Deep Sea Res. Part I Oceanogr. Res. Pap., 45, 2085–2104, 1998.

Dacey, J. W. H., Wakeham, G. and Howes, B. L.: Henry's law constants for dimethylsulfide in freshwater and seawater, Geophys. Res. Lett., 11(10), 991–994, 1984.

Galí, M., Ruiz-González, C., Lefort, T., Gasol, J. M., Cardelús, C., Romera-Castillo, C. and Simó, R.: Spectral irradiance dependence of sunlight effects on plankton dimethylsulfide production, Limnol. Oceanogr., 58(2), 489–504, doi:10.4319/lo.2013.58.2.0489, 2013.

Hales, B. and Takahashi, T.: The Pumping SeaSoar : A High-Resolution Seawater Sampling Platform, J. Atmos. Ocean. Technol., 1096–1104, 2002.

Iizuka, Y., Uemura, R., Motoyama, H., Suzuki, T., Miyake, T., Hirabayashi, M. and Hondoh, T.: Sulphate-climate coupling over the past 300,000 years in inland Antarctica., Nature, 490(7418), 81–4, 2012.

Juranek, L. W., Hamme, R. C., Kaiser, J., Wanninkhof, R. and Quay, P. D.: Evidence of O2 consumption in underway seawater lines: Implications for air-sea O2 and CO2 fluxes, Geophys. Res. Lett., 37(1), 1–5, 2010.

Kameyama, S., Tanimoto, H., Inomata, S., Tsunogai, U., Ooki, A., Yokouchi, Y., Takeda, S., Obata, H. and Uematsu, M.: Equilibrator inlet-proton transfer reaction-mass spectrometry (EI-PTR-MS) for sensitive, high-resolution measurement of dimethyl sulfide dissolved in seawater., Anal. Chem., 81(21), 9021–6, doi:10.1021/ac901630h, 2009.

Kameyama, S., Tanimoto, H., Inomata, S., Yoshikawa-Inoue, H., Tsunogai, U., Tsuda, A., Uematsu, M., Ishii, M., Sasano, D., Suzuki, K. and Nosaka, Y.: Strong relationship between dimethylsulfide and net community production in the western subarctic Pacific, Geophys. Res. Lett., 40, 3986–3990, doi:10.1002/grl.50654, 2013.

Kettle, A. J., Andreae, M. O., Amouroux, D., Andreae, T. W., Bates, T. S., B, H., Boniforti, R., Curran, M. A. J., Ditullio, G. R., Helas, G., Jones, G. B., Keller, M. D., Kiene, R. P., Leck, C., Levasseur, M., Malin, G., Maspero, M., Matrai, P., Mctaggart, A. R., Mihalopoulos, N., Nguyen, B. C., Novo, A., Putaud, J. P., Rapsomanikis, S., Roberts, G., Schebeske, G., Sharma, S., Sim, R., Staubes, R., Turner, S., Uher, G., Boothbay, W. and Planck, M.: A global database of sea surface dimethylsulfide (DMS) measurements and a procedure to predict sea surface DMS as a function of latitude , longitude , and month TM grazing, Global Biogeochem. Cycles, 13(2), 399–444, 1999.

Kiene, R. P., Linn, L. J. and Bruton, J. a.: New and important roles for DMSP in marine microbial communities., J. Sea Res., 43(3-4), 209–224, 2000.

Kolber, Z., Prasil, O. and Falkowski, P. P. G.: Measurements of variable chlorophyll fluorescence using fast repetition rate techniques: defining methodology and experimental protocols, Biochim. Biophys. Acta, 1367(1-3), 88–106, doi:10.1016/S0005-2728(98)00135-2., 1998.

Lana, a., Bell, T. G., Simó, R., Vallina, S. M., Ballabrera-Poy, J., Kettle, a. J., Dachs, J., Bopp, L., Saltzman, E. S., Stefels, J., Johnson, J. E. and Liss, P. S.: An updated climatology of surface dimethlysulfide concentrations and emission fluxes in the global ocean, Global Biogeochem. Cycles, 25(1), 1–17, doi:10.1029/2010GB003850, 2011.

Lovelock, J. E.: Atmospheric Dimethyl Sulphide and the Natural Sulphur Cycle, Nature, 237, 452–453, 1972.

Marandino, C. A., Bruyn, W. J. De, Miller, S. D. and Saltzman, E. S.: DMS air/sea flux and gas transfer coefficients from the North Atlantic summertime coccolithophore bloom, Geophys. Res. Lett., 35, 1–5, doi:10.1029/2008GL036370, 2008.

Marandino, C. A., Bruyn, W. J. De, Miller, S. D. and Saltzman, E. S.: Open ocean DMS air/sea fluxes over the eastern South Pacific Ocean, Atmos. Chem. Phys., 9, 1–12, 2009.

Marandino, C., De Bruyn, W. J., Miller, S. D. and Saltzman, E. S.: Eddy correlation measurements of the air/sea flux of dimethylsulfide over the North Pacific Ocean, J. Geophys. Res., 112, D03301, 2007.

Quinn, P. K. and Bates, T. S.: The case against climate regulation via oceanic phytoplankton sulphur emission., Nature, 480, 51–56, doi:10.1038/nature10580, 2011.

Raina, J.-B., Tapiolas, D. M., Forêt, S., Lutz, A., Abrego, D., Ceh, J., Seneca, F. O., Clode, P. L., Bourne, D. G., Willis, B. L. and Motti, C. a.: DMSP biosynthesis by an animal and its role in coral thermal stress response, Nature, doi:10.1038/nature12677, 2013.

Saltzman, E. S., De Bruyn, W. J., Lawler, M. J., Marandino, C. and McCormick, C.: A chemical ionization mass spectrometer for continuous underway shipboard analysis of dimethylsulfide in near-surface seawater, Ocean Sci., 6(2), 1569–1594, 2009.

Seymour, J. R., Simó, R., Ahmed, T. and Stocker, R.: Chemoattraction to dimethylsulfoniopropionate throughout the marine microbial food web., Science (80-.)., 329, 342–5, 2010.

Simó, R.: Trace chromatographic analysis of dimethyl sulfoxide and related methylated sulfur compounds in natural waters., J. Chromatogr., 807(A), 151–64, 1998.

Simó, R.: Production of atmospheric sulfur by oceanic plankton: biogeochemical, ecological and evolutionary links., Trends Ecol. Evol., 16(6), 287–294, 2001.

Simó, R., Grimalt, J. O. and Albaigés, J.: Sequential method for the field determination of nanomolar concentrations of dimethyl sulfoxide in natural waters., Anal. Chem., 68(9), 1493–8, 1996.

Stefels, J.: Physiological aspects of the production and conversion of DMSP in marine algae and higher plants., J. Sea Res., 43, 183–197, 2000.

Sunda, W., Kieber, D. J., Kiene, R. P. and Huntsman, S.: An antioxidant function for DMSP and DMS in marine algae., Nature, 418(6895), 317–20, 2002.

Taylor, G.: Dispersion of soluble matter in solvent flowing slowly through a tube, Proc. R. Soc. London, 219(1137), 186–203, 1953.

Tortell, P. D.: Dissolved gas measurements in oceanic waters made by membrane inlet mass spectrometry, Limnol. Oceanogr. Methods, 2, 24–37, 2005.

Tortell, P. D., Guéguen, C., Long, M. C., Payne, C. D., Lee, P. and DiTullio, G. R.: Spatial variability and temporal dynamics of surface water pCO2, ΔO2/Ar and dimethylsulfide in the Ross Sea, Antarctica, Deep Sea Res. Part I Oceanogr. Res. Pap., 58(3), 241–259, doi:10.1016/j.dsr.2010.12.006, 2011.

Tortell, P. D. and Long, M. C.: Spatial and temporal variability of biogenic gases during the Southern Ocean spring bloom, Geophys. Res. Lett., 36, L01603, 2009.

Turner, S. M. and Liss, P. S.: Measurements of various sulphur gases in a coastal marine environment, J. Atmos. Chem., 2, 223–232, 1985.

Chapter 4

A high resolution time-depth view of dimethylsulfide cycling in the surface sea

Sarah-Jeanne Royer, Anoop Sharad Mahajan, Martí Galí, Gonzalo Pérez, Eric Saltzman, Oliver Ross and Rafel Simó

Abstract

The emission of volatile dimethylsulfide (DMS) has important implications for aerosol formation and growth over the oceans. Whether this emission sets a two-way connection between oceanic plankton and climate through cloud seeding is the subject of considerable debate. Some of the fundamental questions that remain unanswered are whether DMS emission responds to meteorological forcing and through which short-term drivers. Here we report continuous underway measurements of seawater DMS concentrations made by mass spectrometry during two Lagrangian studies in the Mediterranean Sea. Use of an underway vertical profiler provided DMS distribution with depth at unprecedented resolution. In September 2011, surface DMS concentrations showed a remarkable coupling with atmospheric physical forcing, with accumulation in sunny days and substantial loss by ventilation and vertical mixing during the course of a windstorm. They also showed consistent 24 h periodicity, with daytime increase and nighttime decrease. This diel oscillation was initially lost after the windstorm, but recovered in a few sunny days. Diel oscillation in May 2012 had the opposite sign: daytime decrease and nighttime increase. In both cases, inflection points occurred around dawn and dusk, coinciding with inflection points for fluorescence markers of phytoplankton photoacclimation. These results suggest that a photo-biological clock drives DMS cycling in the upper mixed layer. Implementation of measurements into a numerical 1D model revealed that net biological DMS production occurs around the hours of maximum insolation. The high-resolution study of DMS presented here supports the strong direct influence of solar radiation onto the DMS cycle.

Introduction

The knowledge gained on the trace gas dimethylsulfide (DMS) and its main biological precursor, the algal osmolyte dimethylsulfoniopropionate (DMSP), over the last 40 years is of such extent that they make some of the best-studied organic substances in the world's oceans (Simó, 2001; Stefels et al., 2007). Although the controversy is on for its hypothesized role in a plankton-clouds-climate feedback loop (Charlson et al., 1987; Iizuka et al., 2012; Quinn and Bates, 2011; Vallina et al., 2007), there is consensus that ocean-leaving DMS plays a fundamental role in aerosol formation and growth (Andreae and Rosenfeld, 2008), and in returning sulfur to continents through the atmosphere (Lovelock et al., 1972). DMS also plays a role in chemical ecology as an aerial olfactory signal sensed by marine mammals (Kowalewsky et al., 2006), turtles (Endres and Lohmann, 2012) and birds (Amo et al., 2013; Cunningham et al., 2008; Debose et al., 2010; Wright et al., 2011), and as an underwater infochemical for marine plankton (Garcés et al., 2013; Steinke et al., 2006), with important ecological consequences (Pohnert et al., 2007; Savoca and Nevitt, 2014; Seymour et al., 2010).

The flux of DMS from the ocean to the atmosphere is a function of the DMS concentration in surface waters and, because of its environmental roles, it is important to be able to understand and predict surface ocean DMS distribution and dynamics. DMS is produced mainly by enzymatic degradation of the phytoplankton osmolyte DMSP with involvement of the entire planktonic food web (Simó, 2001). DMS ventilation into air generally represents a non-dominant sink compared to competing underwater DMS consumption pathways: bacterial DMS catabolism and photochemical oxidation (Simó, 2004; Toole et al., 2006). Thus, it follows that the interplay between biotic and abiotic DMS sinks and gross community DMS production determines how much DMS ends up in the marine troposphere. Several studies have been conducted to understand DMS seasonality in relation to solar radiation, vertical mixing, nutrients and associated biological succession over the seasons (e.g., Archer et al., 2009; Dacey et al., 1998;

Herrmann et al., 2012; Lizotte et al., 2012; Simó and Pedrós-Alió, 1999; Vallina and Simó, 2007; Vila-Costa et al., 2008). Conversely, few studies have addressed in detail the short-term variability of DMS cycling that occurs over timescales of hours to weeks, except during strong changes across phases of natural and fertilized blooms (e.g., van Duyl et al., 1998; Levasseur et al., 2004; Simó and Pedrós-Alió, 1999; Turner et al., 1995). Studies addressing the variability of DMS coupled to environmental forcing in oligotrophic or non-blooming situations are scarce (Gabric et al., 2008; Galí et al., 2013a; Toole and Siegel, 2004) and this warrants further exploration if we are to gain understanding applicable to the large oligotrophic ocean basins.

Recently, strong evidence has been reported for net and gross biological DMS production being stimulated by solar radiation, particularly in the UV spectral region, through plankton photobiology (Galí et al., 2011, 2013a, 2013b; Toole et al., 2006). Plankton exposure to sunlight largely depends on meteorology, which governs irradiance and upper-ocean mixing. It also depends on the length and amplitude of the day-night cycles, set by latitude and season. It is well known that day-night alternation of the underwater light exposure regime exerts a rhythmic forcing on photochemical and photobiological processes (Doney et al., 1995), which translate into diel oscillations of biogeochemical fluxes. Since light-driven processes are key player in the biogeochemical cycling of DMS and its precursor DMSP (Galí et al., 2011; Lizotte et al., 2012; Miles et al., 2012; Toole et al., 2006), diel and other meteorologically-relevant short-term variability is to be expected.

A recent study reported that DMS cycling process rates showed large regular variation at an hourly timescale over diel cycles, while DMS concentrations show less variation or less harmonic (Galí et al., 2013a). This apparent buffer on DMS concentration may be real or as a result of the effect of low temporal resolution sampling, instrumental noise, or a poor acquaint of vertical variability due to the lack of adequate vertical resolution in the measurements. Also, little is known about the time scale of the

response of the DMS-producing pelagic ecosystem to meteorological perturbation, let alone the time scale for restoration of the pre-perturbation conditions, if any.

Here we report on two Lagrangian studies conducted in the western Mediterranean Sea on the effects of meteorology, solar radiation and day-night cycles on DMS concentration, phytoplankton photobiology and biological DMS production in the upper sea. High frequency mass spectrometric and optical measurements, coupled to continuous vertical sampling with a yoyo profiler allowed a view of the DMS cycling pace at unprecedented resolution.

Materials and experimental methods

Study site and sampling scheme

The two cruises were conducted aboard R/V García del Cid in the Western Mediterranean Sea, in September 2011 and May 2012. Three Lagrangian drifters with underwater sail were deployed to track the movement of the upper water layer. All ship operations were conducted next to the drifters. Both cruises were held in the same region, within the core of a cyclonic eddy (Figure 1). Seawater was withdrawn from 4 m depth using the ship's underway pump, and measured continuously for DMS and phytoplankton fluorescence characteristics. Several times a day, a CTD probe equipped with a Niskin bottle rosette was used to profile the hydrographical properties until 200 m, and to collect discrete water samples along the vertical profile. On three occasions, (09/13-14, 09/21-22 and 05/23-24), intensive studies were conducted over periods of approx. 30-40 hours. These consisted of CTD probing and sampling every 4 hours, and vertical underway profiling during the periods in between. The vertical profiler has been described in detail elsewhere (Royer et al., 2014). Briefly, it consists of a small CTD probe with an attached tube connected to a peristaltic pump on deck. The CTD is operated in yoyo mode between surface and 35-50 m, at a descending-ascending speed of 2.5 to 4 m min^{-1}.

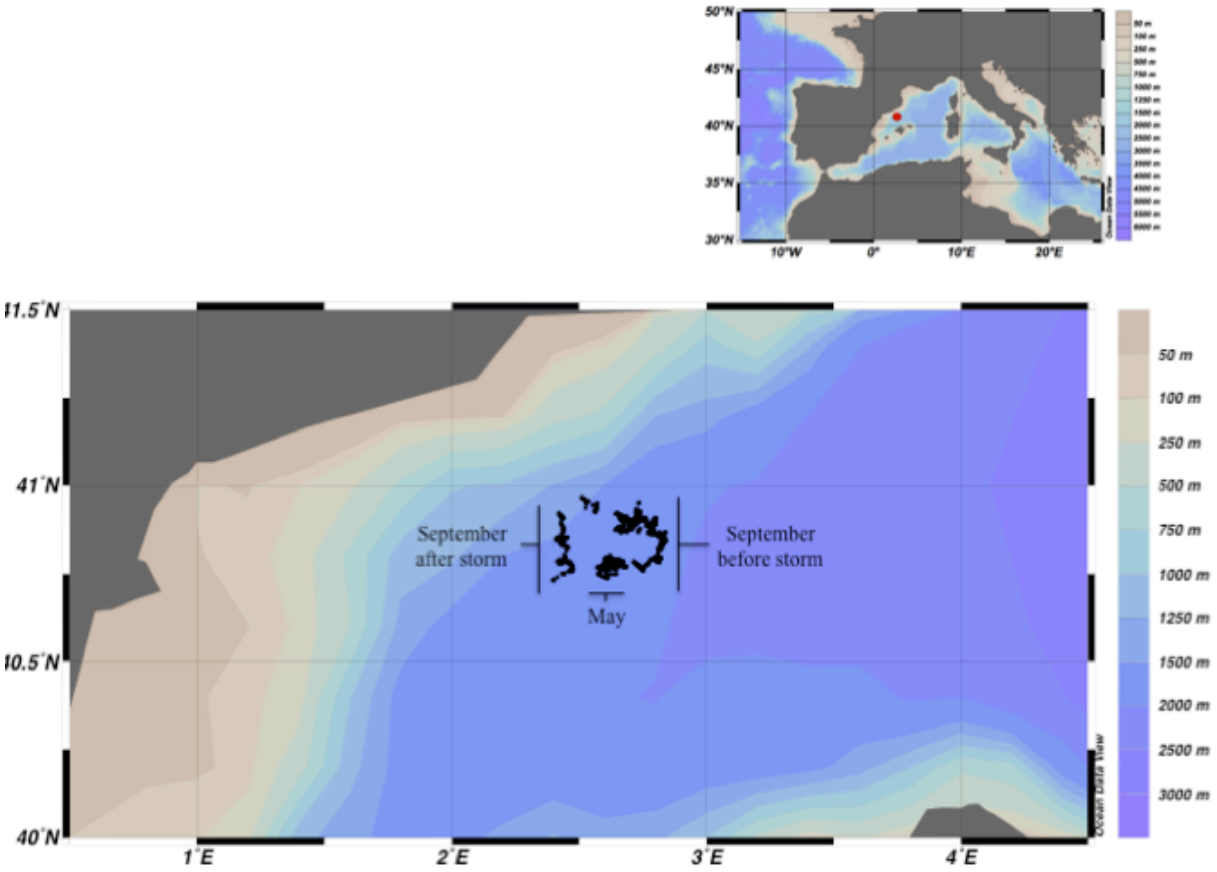

Figure 1. September 2011 (pre- and post-storm) and May 2012 cruise trajectories overlaid on the bathymetric map of the Catalan Sea in the NW Mediterranean. The cruise trajectories were defined by the trajectories of the Lagrangian drifters.

Oceanographic measurements

A membrane equilibrator, atmospheric pressure chemical ionization mass spectrometer (Eq-APCIMS) was used for continuous DMS measurements from surface waters and across the vertical column during intensive studies (Figure 2). The instrument is described in detail by Saltzman et al., (2009) and the complete setup by Royer et al., (2014). Essentially, the Eq-APCIMS provided noise-filtered DMS concentrations every 30 s, which corresponded to depth steps of 1.3-2 m when profiling. The detection limit was nearly 0.1 nmol L^{-1}, and precision was around 10%. Total (particulate and dissolved) DMSP concentration was measured in 3-10 mL discrete samples by gas chromatography (GC) coupled to flame photometric detection (FPD), as described in Galí et al., (2013a). The detection limit was nearly

0.3 nmol L^{-1} and precision was around 5%. Chlorophyll *a* (Chl*a*) concentrations were determined by filtration of 150 mL of seawater through GF/F, extraction in acetone (90% v:v in water, 4ºC, overnight) and measurement in a Turner Designs fluorometer. Samples for dissolved inorganic nutrients were stored frozen and analyzed with a Bran+Loebbe AutoAnalyzer II, using standard methods. Taxonomic pigments were analyzed by HPLC (Spectra SYSTEM, Thermo) after GF/F filtration of 1–2 L of seawater and extraction with methanol (Zapata et al., 2000). A Fast Repetition Rate fluorometer (FRRf, Chelsea Instruments) was used in continuous in the underway and the vertical profiler flows. Chl*a* fluorescence (initial, F_0, maximum, Fm, and variable, Fv=Fm-F_0), the maximum quantum efficiency of photosystem II (FvFm) and the functional cross light absorption ($\boldsymbol{\sigma}_{PSII}$) were derived from the fluorescence induction curve (Kolber et al., 1998). Every day around noon, an APR-UV radiometer (Biospherical PUV 2500) was deployed overboard to profile underwater irradiances in the PAR, UVA and UVB bands and compute the corresponding extinction coefficients. Seawater potential density (σ_t) was calculated using high resolution CTD profile

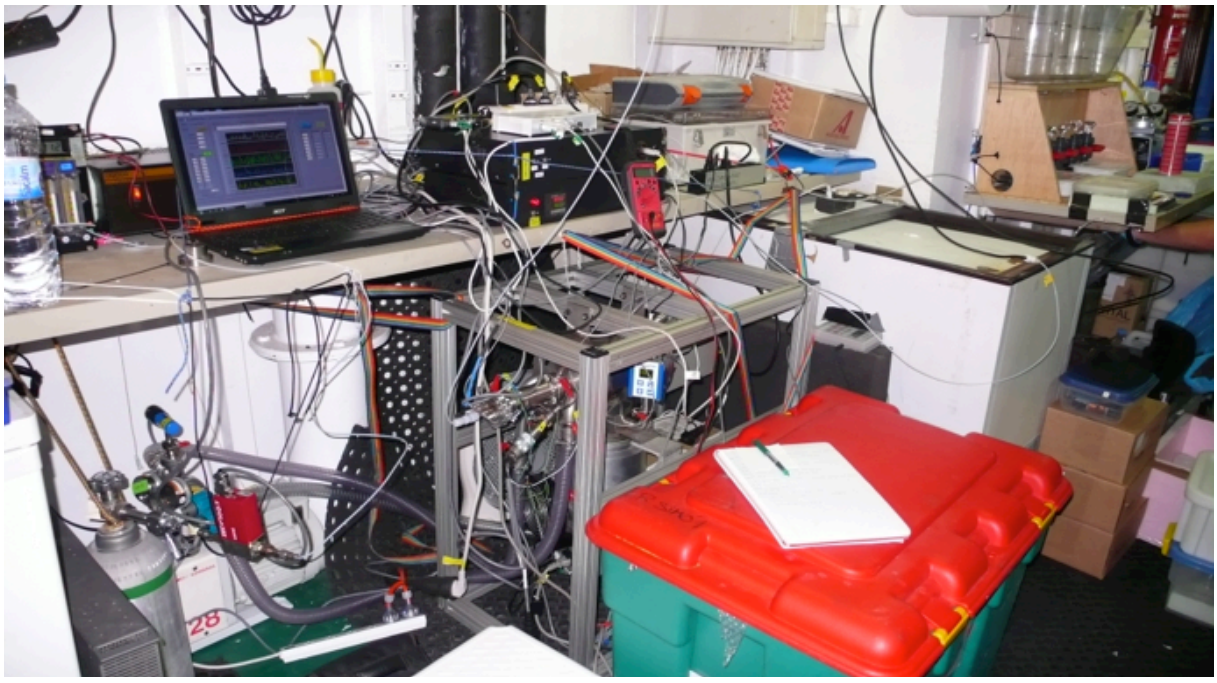

Figure 2. The Eq-APCIMS instrument aboard the *R/V* Garcia del Cid.

data. This was used to compute vertical profiles of the Brunt-Väisälä buoyancy frequency (s^{-1}). High resolution temperature profiles were used to compute the mixing layer depth (mLD), using a temperature criterion of a 0.05°C difference from the reference depth (2 m).

DMS cycling incubation experiments

To determine microbial DMS production and consumption rates, two UV-transparent Teflon bottles were filled with unfiltered seawater and incubated for 9 hours under the light in a black tank flushed with surface sea water to keep in situ temperature. One layer of a neutral mesh was used to simulate the average irradiance of the upper mixed layer. DMS concentration was measured at the beginning and end of the incubation. Changes in DMS concentration, once corrected for photochemical loss, corresponded to net biological production rate (Simó et al., 1995). DMS photolysis rates were determined in surface seawater gravity filtered through 0.2 µm Nylon membrane. The filtrate was kept in the dark for 24 h to exhaust any enzymatic activity left. DMS was then added to concentrations of 50 nM. Six UV transparent Teflon bottles were filled with the filtrate and incubated in the outdoor tank as described above. Two replicates were kept in dark. An APR-UV radiometer (Biospherical PUV 2500) was placed at the center of the incubation tank to keep a continuous record of the solar radiation.

Turbulent diffusivity modelling and budget calculations

The General Ocean Turbulence Model (GOTM, www.gotm.net) was used to compute vertical profiles of turbulent diffusivity during the 3 intensive experiments (Figure 3). Realistic atmospheric forcing was applied using real observations of wind speed and direction, pressure, air temperature and humidity, as well as computed irradiance. Clouds were neglected for lack of data, and there was no precipitation. The 2nd order turbulence closure scheme is used with coefficients from Cheng et al., (2002) and a k-e

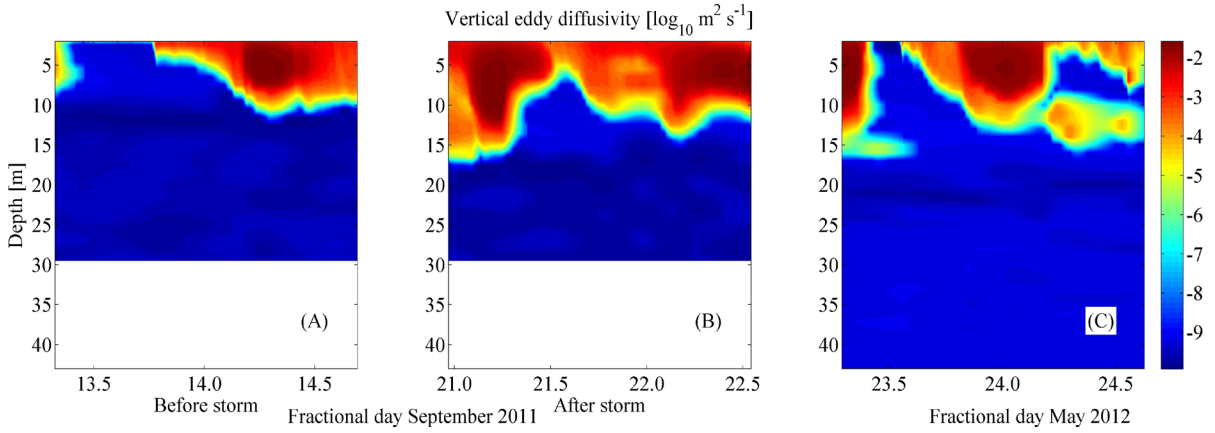

Figure 3. Vertical profiles of turbulent diffusivity as computed with the GOTM model for the three intensive studies.

style equation with a vertical resolution of 1m and a time step of 10 s. The model was allowed to relax toward real in situ observations of temperature and salinity from the CTD of the profiler using a 30 min relaxation time. Observed DMS concentration profiles were gridded onto the model grid by interpolating DMS concentrations to 1 m (vertical) spatial resolution and 1 minute temporal resolution. They were subsequently smoothed using the running average method.

At any time (t) and depth (z), DMS concentration is the net result of production and consumption processes:

$$[DMS]_{z,t+1} = [DMS]_{z,t} + GP_{z,t} - BC_{z,t} - PHOTO_{z,t} - VENT_{z,t} \pm MIXING_{z,t}$$

where, GP = gross DMS production; BC = bacterial DMS consumption; PHOTO = DMS photolysis; VENT = DMS ventilation; MIXING = DMS displacement by vertical turbulent diffusivity.

Ventilation applies only to the very upper water layer, from where its effects are “redistributed” by turbulent diffusion. GP and BC can be merged into a single term called Net Biological DMS production (NPBIO), which is the net balance of the two:

$$NPBIO_{z,t} = GP_{z,t} - BC_{z,t}$$

For the calculation of DMS photolysis (PHOTO), total surface irradiance ($E_{d,o,t}$) and the underwater light extinction coefficients (K_d) were combined to obtain the amount of radiation available at each *t* and *z* ($E_{d,z,t}$):

$$E_{d,z,t} = E_{d,o,t} \cdot \mathbf{e}^{(-Kd*z)}$$

$$PHOTO_{z,t} = [DMS]_{z,t} \cdot \mathbf{K}_{max} \cdot (\mathbf{E}_{d,z,t}/E_{d,o,max})$$

where K_{max}= photolysis rate constant at the water surface, and $E_{d,o,max}$ = maximum irradiance at the water surface. In clear NW Mediterranean waters DMS photolysis reaches its maximum yield in the UML at 340 nm, which had an extinction coefficient of 0.15 m^{-1}. Emission or ventilation fluxes (VENT) were obtained as the product of DMS concentration in seawater and the transfer or piston velocity ($k_{w,DMS}$, cm h^{-1}):

$$VENT = 0.24 \cdot K_{w,DMS} \cdot [DMS]$$

$K_{w,DMS}$ was computed using wind speed data from the ship's meteo station, SST and surface DMS concentrations, following Marandino et al., (2009):

$$K_{w,DMS} = Sc^{-1/2} \cdot (0.51 \cdot u - 0.27)$$

where u_{10}= wind speed at 10 m (m s^{-1}) and Sc = Schmidt number of DMS, calculated from SST (Saltzman et al., 1993). Once all rates needed for budgeting DMS are obtained and distributed according to diffusivity, the final matrix of Net Biological DMS production (NPBIO) was then obtained applying the following equation at a resolution of 1 m (vertical) and 1 minute:

$$NPBIO_{z,t} = [DMS]_{z,t+1} - [DMS]_{z,t} + PHOTO_{z,t} + VENT_{z,t}$$

Results

Sea surface data and meteorological forcing

The continuous data recording over 10 days of tracking a water mass in September showed a remarkable picture of the coupling between atmospheric physical forcing and biogeochemistry of the surface sea (Figure 4). Wind speed showed a half-day cycle underlying stochastic variability. The average wind speed of the cruise was <5 m s^{-1}. It picked up to 7-8 m s^{-1} on 09/14 for almost 12 hours, and again from 09/18 on, this time reaching at least 14 m s^{-1} and lasting about 30 hours. Calm winds followed the storm on the last 2.5 sunny days (Figure 4A). Sea surface temperature (SST) responded to the high diurnal irradiance by showing warming towards the end of every day. It gradually increased over the first 5 calm and sunny days until the storm caused heat loss and mixed surface waters with colder waters below. The result was a SST decrease of almost 2ºC. Surface DMS concentrations (1.5-4 nM) also increased gradually during the first 4 days, except on the windy 09/14. The wind invigoration from 09/18 on rapidly reduced DMS concentrations by ca. 50% (Figure 4B). In subsequent sunny days, DMS recovered gradually the pre-storm levels.

But the most salient feature of the surface DMS concentration series was the consistent 24 h periodicity over day night cycles (Figure 4B). Throughout the days, concentration always increased during the day and decreased during the night. In other words, it was minimum at dawn and maximum at dusk. Before the wind storm, the cycle was so accentuated that the dusk – dawn difference reached 2 nM, i.e., a doubling-halving of the extreme concentration. The storm disrupted or attenuated the cycle, which gradually recovered amplitude as the concentration increased. There is a striking agreement between SST and DMS in how the two evolve through diel cycles and in response to meteorological perturbation and recovery.

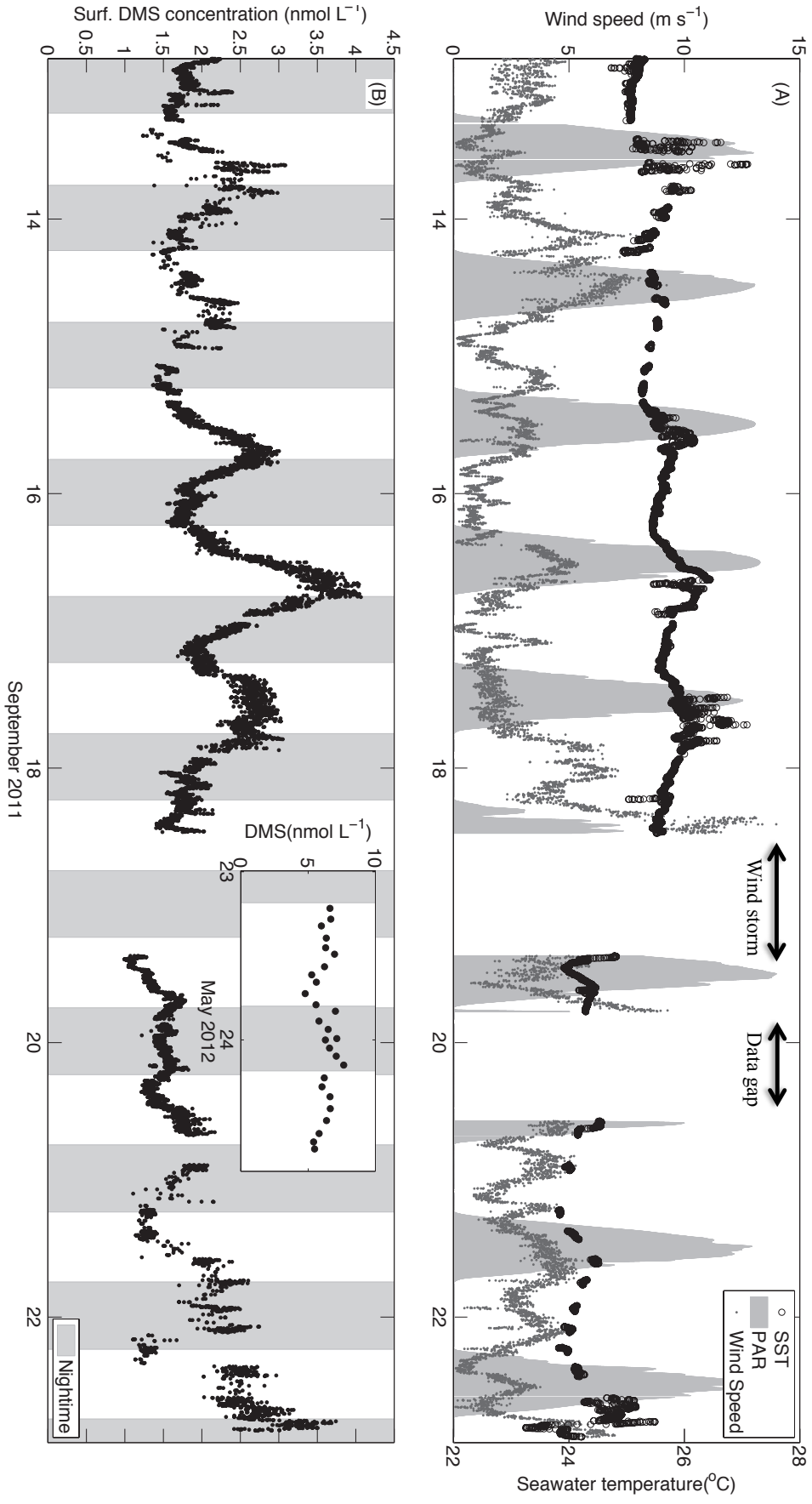

Figure 4. (A) Times series of solar radiation (in light grey in the background, maximum irradiance of 960 W/m^2), sea surface temperature (^{o}C – black circles) and wind speed (m s^{-1} – dark grey) during the September 2011 cruise. (B) Time series of DMS surface concentrations (nmol L^{-1}) during the September 2011 and May 2012 (inset) cruises. The shaded areas represent nighttime. The data gaps in September were due to a wind storm and instrumental problems.

This time series is a remarkable example of the influence of meteorology (mainly irradiance and wind speed) on surface DMS concentrations, seen at a temporal resolution not achievable a few years ago. Prolonged high insolation under weak wind causes gradual DMS accumulation over days. One may think this is a particular situation of a late summer cruise in oligotrophic waters. However, the same phenomenon was observed in an early summer coccolithophore bloom in the North Atlantic (Simó and Pedrós-alió, 1999). In both cases, a wind storm removed most of the accumulated DMS from the surface.

In the May cruise DMS concentrations (5-8 nM) were considerably higher than in September, in agreement with the typical seasonality in the region (Vila-Costa et al., 2008). The two sunny days were also characterized by a strong day-night pattern in surface DMS concentration, with inflexion points at dawn and dusk (Figure 4B, inset). The pace was, however, completely opposite to that of September, with nighttime increase and the maximum concentration around dawn, and daytime decrease and the minimum at dusk.

Vertical profiles of DMS, DMSP and Chl*a*

Observations at the sea surface are only part of the story and reflect the processes occurring simultaneously at the air-sea interface and in the waters of the upper mixing layer and below. Figure 5 shows the dawn-dusk beat of DMS, its precursors DMSP and Chl*a* in the vertical dimension as studied from discrete CTD samples. In September, DMS was higher at surface, and the increase at dusk was noticeable from surface down to 15-20 m deep, i.e., shortly beyond the bottom of the mixing layer into the thermocline. DMSPt concentrations also increased between dawn and dusk (hence during daytime), particularly so at the thermocline above the deep Chl*a* maximum (20-50 m), which the water layer typically occupied by maximum primary production rates. Chl*a* also increased over daytime all throughout the water column. In May, where all concentrations

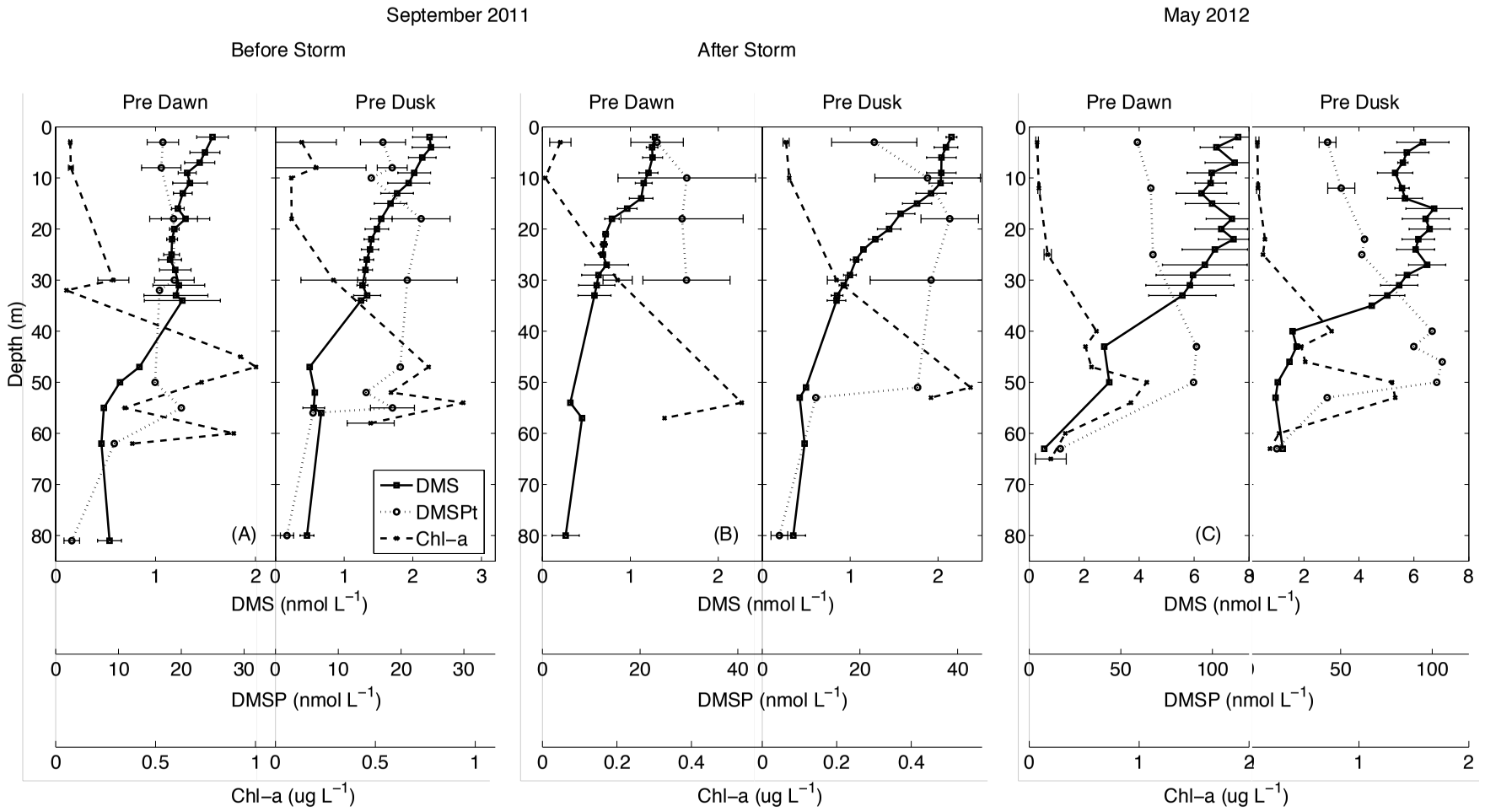

Figure 5. Averaged vertical profiles from the surface to below the deep chlorophyll maximum (DCM) for DMS (nmol L^{-1}), DMSPt (nmol L^{-1}) and Chl-a (5µg L^{-1}). DMSPt and Chl-a measurements, and DMS below 35 m, were done from CTD rosette samples. DMS data above 35 m are 2 h averages of Eq-APCIMS measurements obtained with the vertical profiler. Pre-dawn and pre-dusk profiles are shown for (A) 13th and14th of September before storm, (B) 21st and 22nd September after storm, (C) May. The depth of the mixing layer is indicated in Figure 5.

were much higher, a slight Chl*a* increase from dawn to dusk was only noticeable at the deep maximum. DMSPt behaved similarly at depth but the concentration slightly decreased at surface during daytime. The same happened to DMS in the mixing layer.

The profiles described above portray the typical open ocean vertical distributions in oligotrophic waters (e.g., Dacey et al., 1998), where Chl*a* peaks at depth (at the bottom of the thermocline), DMSPt peaks from right above the Chl*a* peak to right below the mixing layer, and DMS peaks up in the mixing layer, or right below. In spite of this vertical segregation of maxima, the three compounds varied in concert between dawn and dusk near the surface (Figure 5). But is the analysis of aggregated twice a day enough to fully describe and understand the diel pace of DMS?

High resolution time x depth profiles

The use of continuous data recording in yoyo mode permitted monitoring the vertical changes of target variables at far much higher temporal resolution than CTD-rosette sampling profiles. DMS and in vivo fluorescence (as a proxy for Chl*a*) could be recorded, but unfortunately there is no method yet for continuous measurements of DMSPt. Figure 6 shows the 1D x time plots of the former two variables as well as the buoyancy frequency, computed from the yoyo CTD density profiles, as a measure of water column stability in the vertical axis. These bottom plots clearly portray that in the calm days of September before the storm, surface waters were getting mixed to only 5-10 m, beyond which the pycnocline and thermocline began. The wind friction and heat loss during the storm increased surface water turbulence and instability, and deepened the mixing layer. Before the storm, the fluorescence profiles were indicative of a deep Chl*a* that we did not go deep enough to capture. After the storm there was an increase of phytoplankton abundance at shallower depths, which we had not captured in the bottle profiles because of the coarse depth resolution. In both cases, fluorescence confirmed the previous Chl*a* profiles and was higher at depth during the day, with a weak pattern at surface. DMS

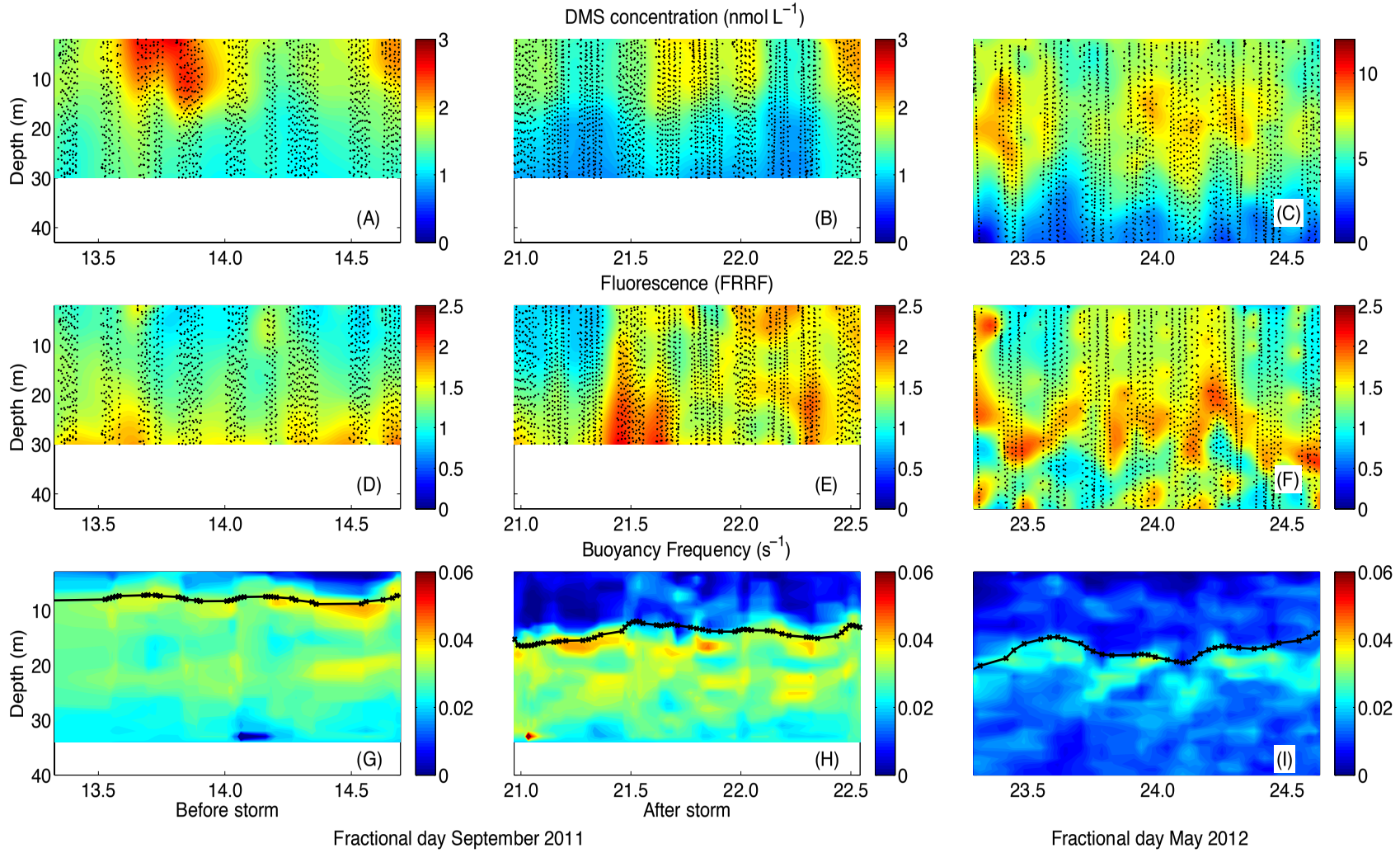

Figure 6. High-resolution vertical profiles during the intensive Lagrangian studies in September (first two colums) and May (third column). The positions of the original data are shown as black dots in the foreground. Colors show data interpolation over 2 m and 30 min. (A-C) DMS concentrations (nmol L^{-1}), (D-F) chlorophyll a fluorescence from the FRRf, (G-I) buoyancy frequency (s^{-1}). Black lines on the buoyancy plots represent the mixing layer depth calculated from a 0.05ºC departure from a reference depth of 5 m.

distributed almost completely opposite to fluorescence: concentrations accumulated at the very top (<20 m) and increased in the afternoon towards dusk. Days after the wind storm, DMS had recovered its pace within the upper 30 m.

In May, the extent of vertical turbulent mixing was deeper (15-20 m). High resolution fluorescence revealed the occurrence of a well-defined maximum at around 30 m, which has been overlooked in the bottle profiles. This Chl*a*-rich layer presented oscillations probably due to internal waves, but no clear diel pattern. At surface, conversely, fluorescence was higher during the night and lower during the day, a phenomenon that might be indicative of phytoplankton photoacclimation cycles. DMS peaked at the very surface and most remarkably right below the mixing layer depth. The diel pattern of nighttime increase and daytime decrease that was observed at surface and with bottle profiles could be examined here in detail and was seen to propagate to a depth of 30-40 m.

Photobiological clock

The fact that the diel variation series of surface DMS concentrations had dawn and dusk as the inflexion points where change reverts direction suggests the involvement of photobiological processes and circadian rythms. Figure 7 compares diel cycles of hourly-averaged DMS and the two PSII efficiency indicators FvFm and sigma. Indeed, the breaking points of the diel DMS pattern did not only coincide with sunrise and sunset but also with the breaking points of these two photophysiological measurements.

Computed turbulent diffusivity and abiotic DMS losses

Runs of GOTM with real atmospheric forcing and relaxation to the CTD data of the yoyo profiler provided vertical fields of the turbulent eddy diffusivity over time for the three intensive studies. Calculation of DMS ventilation fluxes according to wind speed and SST gave values up to 0.27 μmol m^{-2} h^{-1} in September and up to 0.5 μmol m^{-2} h^{-1} in May

(Figure 8). Profiles of DMS photolysis rates were estimated from incubations under controlled conditions and transportation in situ by use of underwater light fields. In September, photolysis rates at noon under the surface were in the order of 0.12 nM h^{-1}, and decreased exponentially with depth to negligible values below 20 m. In May, under-surface photolysis rates at noon were in the order of almost 0.5 nM h^{-1}, and became negligible at around 30 m deep (Figure 8).

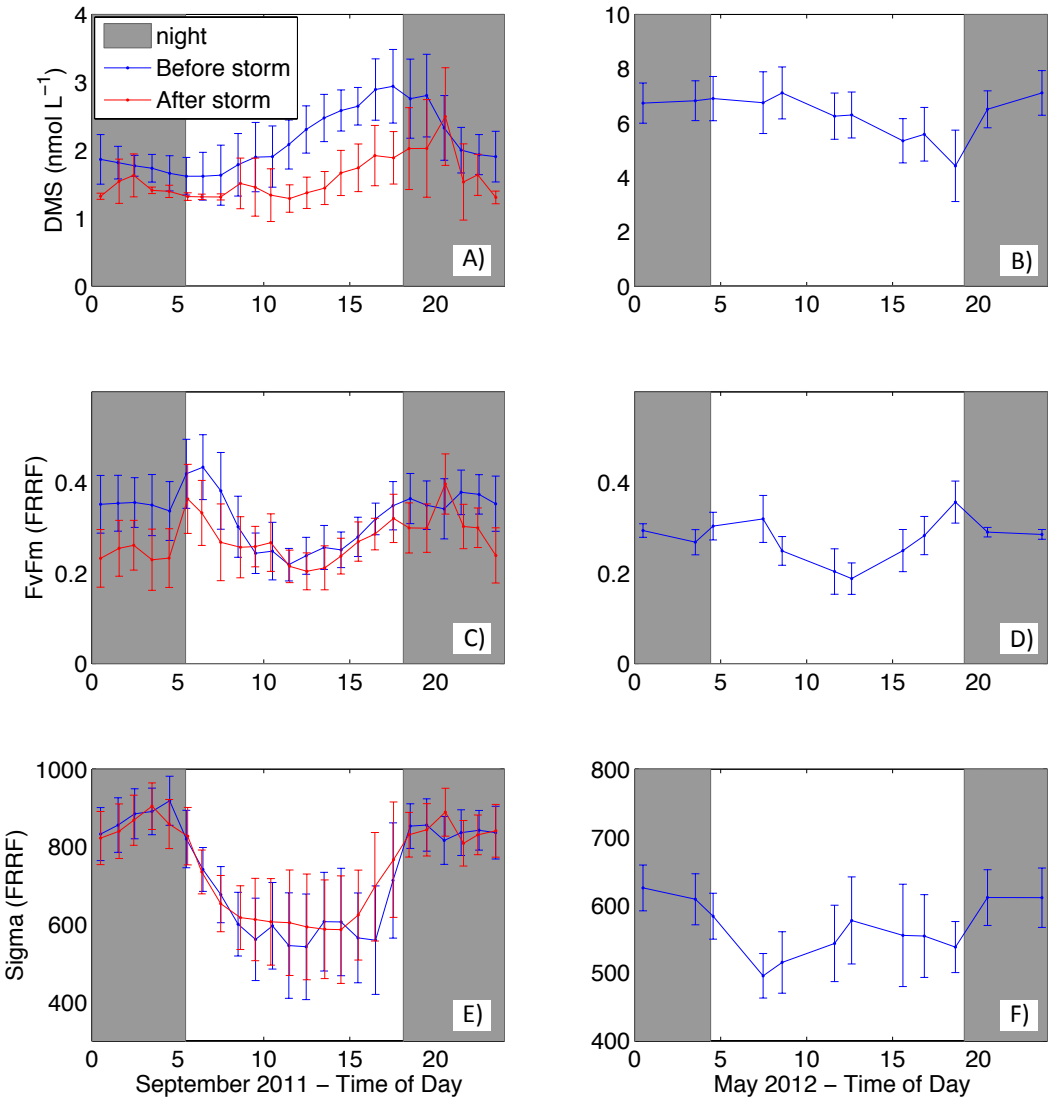

Figure 7. Hourly averages of DMS concentrations, and FRRf-derived FvFm and sigma over characteristic diel cycles in surface waters, as obtained in the three intensive studies. (A-C-E) September 2011, pre-storm (blue) and post-storm (red); (B-D-F) May 2012

Diel cycles of net biological DMS production

The turbulent diffusivity fields and the abiotic DMS loss rates were used to compute time x depth profiles of net biological production of DMS (Figure 8). In September, NPBIO rates (irrespective of the sign) were higher at surface and decreased with depth. Surface values varied approximately between -0.1 and 0.3 nM h^{-1}. They are positive (net production) in the central hours of the day, and negative (net consumption) in the night. In May, vertical gradients were less clear, yet NPBIO rates were still maximum at surface (range -0.03 to 0.7 nM h^{-1}). Interestingly, while the diel cycle is blurred over the 40 m, at the very surface (<5 m) NPBIO is higher during the day, similarly to September.

To validate this computed NPBIO, we compared the obtained rates with those measured by seawater incubations on deck. The results gathered in Table 1 show remarkable agreement, with higher biological production in the morning and across noon, and lower in the afternoon. In the night, biological production is almost zero or even turns into net consumption.

Table 1. Net biological DMS production rates at surface waters in the intensive studies, determined experimentally and computed from modelling and budgeting. September is a combination of before and after storm.

	Period of the day	NBP_{DMS} from model nM h^{-1}	NBP_{DMS} from experiments nM h^{-1}
September	05:00-14:00	0.13	0.05-1
	14:00-22:00	0.04	0-0.05
	22:00-05:00	-0.03	0-0.05
May	05:00-14:00	0.17	0.4
	14:00-22:00	0.06	0.1
	22:00-05:00	0.04	0

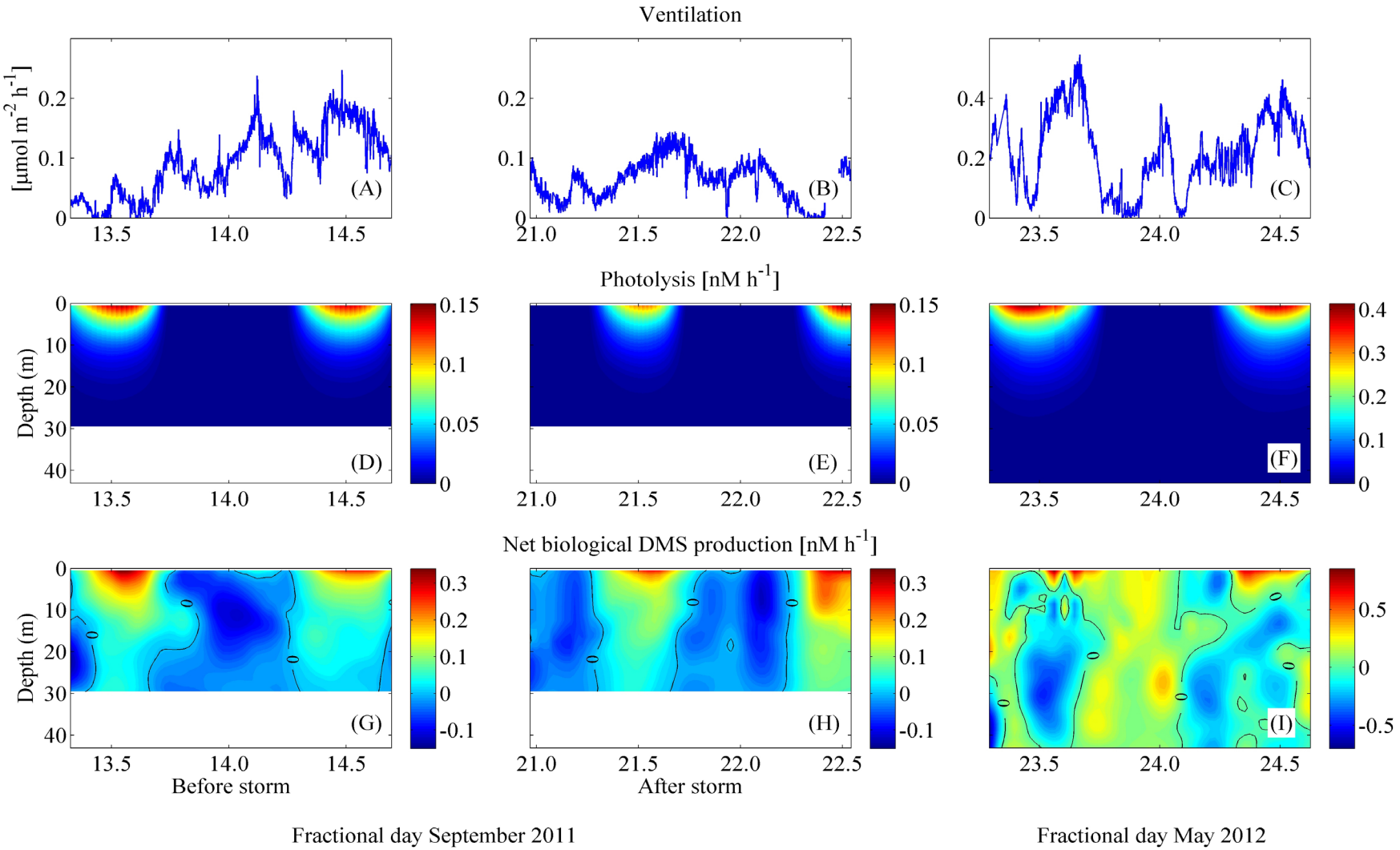

Figure 8. Computed rates for DMS cycling processes in the three intensive studies. (Top) Ventilation rate (µmol m^{-2} h^{-1}). (Middle) Photolysis rate (nmol L^{-1} h^{-1}). (Bottom) Net biological production (nmol L^{-1} h^{-1}).

Discussion

The two cruises in the same region, and the intensive studies conducted on them, provided complementary data on the effects of meteorological forcing and day-night cycles on DMS production and concentration in the surface sea. The two cruises encountered surprisingly similar phytoplankton assemblages, but at very different abundances. According to taxonomic pigments, surface phytoplankton in September were dominated by *Synechococcus*, dinoflagellates and prymnesiophytes. Phytoplankton at the deep Chl*a* maximum (55 m approx.) were dominated by *Prochlorococcus* and dinoflagellates. In May, the surface assemblage was rather similar to that in September, but the deep maximum assemblage was dominated by prymnesiophytes, dinoflagellates, *Synechococcus* and Pelagophytes. Chl*a* concentrations were not so different in the two cruises at the surface (nearly 0.1 μg L^{-1}), but the concentration at the deep maximum was twice as much in May. As a result of specific taxonomic differences that we cannot resolve, the DMSPt concentrations in September and May were around 20-40 nM and 50-100 nM, respectively. Therefore, the May pelagic ecosystem was more prone to DMS production. Indeed, DMS concentration in May was 1.5-5 times higher than that of September.

Another difference between the two cruises was that in September the maximum DMS concentration was near the surface, whereas in May there was a larger maximum below the mixing layer depth. DMS subsurface maximum are quite common and have been measured in the Atlantic Ocean (Bailey et al., 2008; Toole et al., 2006) and in several other marine systems (Andreae and Barnard, 1984; Cline and Bates, 1983; Leck et al., 1990; Matrai and Keller, 1993; Turner et al., 1988; Uzuka et al., 1996; Wakeham and Dacey, 1989; Yang et al., 2000). They may occur when gross DMS production occurs across the photic zone and DMS in the mixed layer is severely downwards regulated by photolysis and ventilation. Their occurrence is important because they can supply new DMS into the mixing layer and during mixing events, thereby building emission fluxes

that could not have been predicted from surface concentrations only. These relatively thin and dynamic layers like the one encountered in May prompt to the need for sampling systems with fine resolution in the vertical dimension, not only the horizontal.

The passage of a wind storm and subsequent return to the previous calm conditions provided the opportunity to monitor the effects of the environemental perturbation and the resilience of the DMS-producing ecosystem in real time. The persistent wind reduced the surface DMS concentration to one third. Probably part of it was lost by turbulent mixing to deeper water, and a big proportion was vented to the atmosphere. Actually, the loss of the integrated column DMS burden was in the order of 30%. Fluorescence profiles 2-3 days after the end of the storm showed enhanced phytoplankton growth. This may be the result of a mixing-induced injection of either nutrients or cells from below. Actually, DMSPt concentrations at intermediate depths increased towards the end of the cruise (data not shown). However, surface DMS did not shift to a different (new) state in terms of concentration ranges and diel pace, but rather returned to the previous state. In order words, even though there was evidence for a week-long shift of biomass and composition of the phytoplankton assemblage, in the short term the DMS-producing system exhibit strong resilience.

This is relevant to understand DMS dynamics in the global oceans. Sometimes it is stated that windy regions are potentially first order emitters of trace gases (and particularly DMS) because emission fluxes are dependent on wind speed. However, persistent wind depletes trace gases from the ocean by ventilation; besides, windy regions generally have deeply mixed waters where trace gases can hardly build up. Therefore, the conundrum of the net sign of wind effects on air-sea exchange of trace gases is somewhat unresolved. Our results indicate that, under conditions favorable for DMS production (e.g., highly irradiated spring and summer waters), short-lived wind events may cause pulses of large emissions if there is enough time between events for the system to recover and DMS concentration to build up.

In the highly irradiated zone of the surface ocean, sunlight not only provides sufficient energy for photosynthetic activities but also modulates the biological activity by causing photobiological stress and damage effects (Harrison and Smith, 2009; Neale et al., 2003). Phytoplankton cells have different tolerance to solar radiation and sunlight-related stress can either affect DMS production positively and activate a defense mechanism in response to oxidative stress, as proposed by Sunda et al., (2002) or negatively through photo-inhibition of photosynthesis and, in extreme cases, cell death (Behrenfeld et al., 1998; Eilers and Peeters, 1988; Long and Humphries, 1994; Ross et al., 2008), which will counter-act the positive effect on DMS production.

Over the last decade, a number of works have suggested that the daily averaged solar radiation dose received in the upper mixed or mixing layer is a key factor governing DMS dynamics at all spatial scales, from the local to the global (Lizotte et al., 2012; Miles et al., 2012; Simó, 2004; Toole and Siegel, 2004; Vallina and Simó, 2007; Vallina et al., 2007). Other works have reported a suite of experimental lines of evidence and hypothetical mechanisms whereby this emergent property occurs (Archer et al., 2010; Galí et al., 2011, 2013a, 2013b; Sunda et al., 2002). In all cases, solar radiation, and particularly UV radiation, is reported to enhance DMS production, to the extent of counteracting and overcoming photolysis. These experimental results align with the field observations that DMS tends to build up in highly irradiated waters and generally has its annual maximum in summer (Lana et al., 2012; Simó and Pedrós-Alió, 1999). The high-resolution study of DMS presented here supports the strong influence of solar radiation onto the DMS cycle. First, DMS concentration was higher near the surface while DMSP and Chl*a* peaked further deep. Second, surface DMS concentration increased gradually in sunny calm days, even after a strong perturbation. Third, net biological DMS production at sea surface occurred mainly during the day (noon and afternoon). All these features were common to two different seasons.

Solar radiation does not intervene only on the DMS production side, it also has important effects on biological DMS consumption. DMS is biologically removed from the water column primarily by bacterial metabolism (e.g., del Valle et al., 2007, 2009). Bacterial activity is susceptible to inhibition by UV light (Ruiz-González et al., 2013). Therefore, suppression of bacterial consumption by high light could have contributed to enhanced net biological DMS production rates at surface during the day in the two cruises.

The high-resolution profiles gave us the rare opportunity to correlate the very dynamic DMS production to physical and biological data measured at the same pace. Lagrangian vertical profiles of DMS clearly reveal short-term response to environmental forcing. The emergent link between net biological DMS production and day/night variability in solar radiation, derived for the first time in the field at unprecedented resolution, suggests that a strong photo-physiological clock (function) influences the temporal cycles of DMS. The Mediterranean Sea represents an excellent natural laboratory to study photochemical and photo-biological processes and our results underscore the need for high resolution underway analysis to fully describe the short-term variability of surface DMS in this region. The newly developed technique used for high resolution vertical profiles presents significant advantages for future studies in more hydrodynamic systems.

Acknowledgements

The authors wish to acknowledge the invaluable assistance and cooperation of the marine technicians (UTM) and the crew aboard the R/V Garcia del Cid. This research has been funded by the successive Spanish Ministries of Science through projects SUMMER (CTM2008-03309/MAR) and PEGASO (CTM2012-37615), and through a PhD scholarship to S.J.R. Support was also provided to E.S. by the U.S. National Science Foundation (grants 0851472 and 1143709). A.S.M. acknowledges support from the Ministry of Earth Sciences, Government of India. This is a contribution of the Research Group on Marine Biogeochemistry and Global Change of the ICM, funded by the Catalan Government.

References

Amo, L., Rodríguez-Gironés, M. and Barbosa, A.: Olfactory detection of dimethylsulphide in a krill-eating Antarctic penguin, Mar. Ecol. Prog. Ser., 474, 277–285, doi:10.3354/meps10081, 2013.

Andreae, M. O. and Barnard, W. R.: The marine chemistry of dimethylsulfide, Mar. Chem., 14, 267–279, 1984.

Andreae, M. O. and Rosenfeld, D.: Aerosol–cloud–precipitation interactions. Part 1. The nature and sources of cloud-active aerosols, Earth-Science Rev., 89(1-2), 13–41, doi:10.1016/j.earscirev.2008.03.001, 2008.

Archer, S. D., Ragni, M., Webster, R., Airs, R. L. and Geider, R. J.: Dimethylsulfoniopropionate and dimethylsulfide production in response to photoinhibition in Emiliania huxleyi, Limnol. Oceanogr., 55(4), 1579–1589, doi:10.4319/lo.2010.55.4.1579, 2010.

Archer, S. S. D., Cummings, D. D. G., Llewellyn, C. A. and Fishwick, J. J. R.: Phytoplankton taxa, irradiance and nutrient availability determine the seasonal cycle of DMSP in temperate shelf seas, Mar. Ecol. Prog. Ser., 394, 111–124, doi:10.3354/meps08284, 2009.

Bailey, K. E., Toole, D. a. D. a., Blomquist, B., Najjar, R. G. R. G., Huebert, B., Kieber, D. J. D. J., Kiene, R. P. R. P., Matrai, P. a., Westby, G. R. and del Valle, D. a.: Dimethylsulfide production in Sargasso Sea eddies, Deep Sea Res. Part II Top. Stud. Oceanogr., 55(10-13), 1491–1504, doi:10.1016/j.dsr2.2008.02.011, 2008.

Behrenfeld, M. J., Prasil, O., Kolber, Z. S., Babin, M. and Paul, G.: Compensatory changes in Photosystem II electron turnover rates protect photosynthesis from photoinhibition, Photosynth. Res., 259–268, 1998.

Charlson, J. R., Lovelock, J. E., Andreae, M. O. and Warren, S. G.: Oceanic phytoplankton, atmospheric sulphur, cloud albedo and climate., Nature, 326, 655–661, 1987.
Cheng, Y., Canuto, V. M. and Howard, M.: An Improved Model for the Turbulent PBL, J. Atmos. Sci., 59, 1550–1565, 2002.

Cline, J. D. and Bates, T. S.: Dimethyl sulfide in the Equatorial Pacific Ocean: A natural source of sulfur to the atmosphere, Geophys. Res. Lett., 10(10), 949–952, 1983.

Cunningham, G. B., Strauss, V. and Ryan, P. G.: African penguins (Spheniscus demersus) can detect dimethyl sulphide, a prey-related odour., J. Exp. Biol., 211(Pt 19), 3123–7, doi:10.1242/jeb.018325, 2008.

Dacey, J. W. H., Howse, F. A., Michaels, A. F. and Wakeham, S. G.: Temporal variability of dimethylsulfide and dimethylsulfoniopropionate in the Sargasso Sea, Deep Sea Res. Part I Oceanogr. Res. Pap., 45, 2085–2104, 1998.

Debose, J. L., Nevitt, G. a and Dittman, A. H.: Rapid communication: experimental evidence that juvenile pelagic jacks (Carangidae) respond behaviorally to DMSP., J. Chem. Ecol., 36(3), 326–8, doi:10.1007/s10886-010-9755-9, 2010.

Doney, S. C., Najjar, R. G. and Stewart, S.: Photochemistry, mixing and diurnal cycles in the upper ocean, J. Mar. Res., 53, 341–369, 1995.

Van Duyl, F. C., Gieskes, W. W. C., Kop, A. J. and Lewis, W. E.: Biological control of short-term variations in the concentration of DMSP and DMS during a Phaeocystis spring bloom, J. Sea Res., 40(3-4), 221–231, doi:10.1016/S1385-1101(98)00024-0, 1998.

Eilers, P. H. C. and Peeters, J. C. H.: A model for the relationship between light intensity and the rate of photosynthesis in phytoplankton., Ecol. Modell., 42, 199–215, 1988.

Endres, C. S. and Lohmann, K. J.: Perception of dimethyl sulfide (DMS) by loggerhead sea turtles: a possible mechanism for locating high-productivity oceanic regions for foraging., J. Exp. Biol., 215(Pt 20), 3535–8, doi:10.1242/jeb.073221, 2012.

Gabric, A. J., Matrai, P. a., Kiene, R. P. R. P., Cropp, R., Dacey, J. W. H. J. W. H., DiTullio, G. R. G. R., Najjar, R. G. R. G., Simó, R., Toole, D. a., DelValle, D. a. and Slezak, D.: Factors determining the vertical profile of dimethylsulfide in the Sargasso Sea during summer, Deep Sea Res. Part II Top. Stud. Oceanogr., 55(10-13), 1505–1518, doi:10.1016/j.dsr2.2008.02.002, 2008.

Galí, M., Ruiz-González, C., Lefort, T., Gasol, J. M., Cardelús, C., Romera-Castillo, C. and Simó, R.: Spectral irradiance dependence of sunlight effects on plankton dimethylsulfide production, Limnol. Oceanogr., 58(2), 489–504, doi:10.4319/lo.2013.58.2.0489, 2013a.

Galí, M., Saló, V., Almeda, R., Calbet, A. and Simó, R.: Stimulation of gross dimethylsulfide (DMS) production by solar radiation, Geophys. Res. Lett., 38(15), 1–5, doi:10.1029/2011GL048051, 2011.

Galí, M., Simó, R., Vila-Costa, M., Ruiz-González, C., Gasol, J. M. and Matrai, P.: Diel patterns of oceanic dimethylsulfide (DMS) cycling: Microbial and physical drivers, Global Biogeochem. Cycles, 27, 1–17, doi:10.1002/gbc.20047, 2013b.

Garcés, E., Alacid, E., Reñé, A., Petrou, K. and Simó, R.: Host-released dimethylsulphide activates the dinoflagellate parasitoid Parvilucifera sinerae., Int. Soc. Microb. Ecol., 7, 1065–1068, doi:10.1038/ismej.2012.173, 2013.

Harrison, J. W. and Smith, R. E. H.: Effects of ultraviolet radiation on the productivity and composition of freshwater phytoplankton communities., Photochem. Photobiol. Sci., 8(9), 1218–32, doi:10.1039/b902604e, 2009.

Herrmann, M., Najjar, R. G., Neeley, A. R., Vila-costa, M., Dacey, J. W. H. H., Ditullio, G. R., Kieber, D. J., Kiene, R. P., Matrai, P. a., Simó, R., Vernet, M. and Simo, R.: Diagnostic modeling of dimethylsulfide production in coastal water west of the Antarctic Peninsula, Cont. Shelf Res., 32, 96–109, doi:10.1016/j.csr.2011.10.017, 2012.

Iizuka, Y., Uemura, R., Motoyama, H., Suzuki, T., Miyake, T., Hirabayashi, M. and Hondoh, T.: Sulphate-climate coupling over the past 300,000 years in inland Antarctica., Nature, 490(7418), 81–4, 2012.

Kolber, Z., Prasil, O. and Falkowski, P. P. G.: Measurements of variable chlorophyll fluorescence using fast repetition rate techniques: defining methodology and experimental protocols, Biochim. Biophys. Acta, 1367(1-3), 88–106, doi:10.1016/S0005-2728(98)00135-2., 1998.

Kowalewsky, S., Dambach, M., Mauck, B. and Dehnhardt, G.: High olfactory sensitivity for dimethylsulphide in harbour seals., Biol. Lett., 2(1), 106–9, doi:10.1098/rsbl.2005.0380, 2006.

Lana, A., Simó, R., Vallina, S. M. and Dachs, J.: Re-examination of global emerging patterns of ocean DMS concentration, Biogeochemistry, 110(1-3), 173–182, doi:10.1007/s10533-011-9677-9, 2012.

Leck, C., Larsson, U., Bågander, L. E., Johansson, S. and Hajdu, S.: Dimethyl sulfide in the Baltic Sea: Annual variability in relation to biological activity, J. Geophys. Res., 95(C3), 3353, doi:10.1029/JC095iC03p03353, 1990.

Levasseur, M., Scarratt, M., Roy, S., Laroche, D., Michaud, S., Cantin, G., Gosselin, M. and Vézina, A.: Vertically resolved cycling of dimethylsulfoniopropionate (DMSP) and dimethylsulfide (DMS in the Northwest Atlantic in spring, Can. J. Fish. Aquat. Sci., 61, 744–757, doi:10.1139/F04-026, 2004.

Lizotte, M., Levasseur, M., Michaud, S., Scarratt, M. G., Merzouk, A., Gosselin, M., Pommier, J., Rivkin, R. B. and Kiene, R. P.: Macroscale patterns of the biological cycling of dimethylsulfoniopropionate (DMSP) and dimethylsulfide (DMS) in the Northwest Atlantic, Biogeochemistry, 110, 183–200, 2012.

Long, S. P. and Humphries, S.: Photoinhibition of photosynthesis in nature, Annu. Rev. Plant Physiol. Plant. Mol. Bio., 45, 633–62, 1994.

Lovelock, J. E., Maggs, R. J. and Rasmussen, R. A.: Atmospheric Dimethyl Sulphide and the Natural Sulphur Cycle, Nature, 237, 452–453, 1972.

Marandino, C. A., Bruyn, W. J. De, Miller, S. D. and Saltzman, E. S.: Open ocean DMS air/sea fluxes over the eastern South Pacific Ocean, Atmos. Chem. Phys., 9, 1–12, 2009.

Matrai, P. a. and Keller, M. D.: Dimethylsulfide in a large-scale coccolithophore bloom in the Gulf of Maine, Cont. Shelf Res., 13(8-9), 831–843, doi:10.1016/0278-4343(93)90012-M, 1993.

Miles, C. J., Bell, T. G. and Suntharalingam, P.: Investigating the inter-relationships between water attenuated irradiance, primary production and DMS(P), Biogeochemistry, 110(1-3), 201–213, doi:10.1007/s10533-011-9697-5, 2012.

Neale, P. J., Helbling, E. W. and Zagarese, H. E.: Modulation of UVR exposure and effects by vertical mixing and advection, in UV effects in aquatic organisms and ecosystems., 2003.

Pohnert, G., Steinke, M. and Tollrian, R.: Chemical cues, defence metabolites and the shaping of pelagic interspecific interactions., Trends Ecol. Evol., 22(4), 198–204, doi:10.1016/j.tree.2007.01.005, 2007.

Quinn, P. K. and Bates, T. S.: The case against climate regulation via oceanic phytoplankton sulphur emission., Nature, 480, 51–56, doi:10.1038/nature10580, 2011.

Ross, O. N., Moore, C. M., Suggett, D. J., MacIntyre, H. L. and Geider, R. J.: A model of photosynthesis and photo-protection based on reaction center damage and repair, Limnol. Oceanogr., 53(5), 1835–1852, doi:10.4319/lo.2008.53.5.1835, 2008.

Royer, S.-J., Galí, M., Saltzman, E. S., McCormick, C. A., Bell, T. G. and Simó, R.: Development and validation of a shipboard system for measuring high-resolution vertical profiles of aqueous dimethylsulfide concentrations using chemical ionisation mass spectrometry, Environ. Chem., 1–9, doi:http://dx.doi.org/10.1071/EN13203, 2014.

Ruiz-González, C., Simó, R., Sommaruga, R. and Gasol, J. M.: Away from darkness: a review on the effects of solar radiation on heterotrophic bacterioplankton activity., Front. Microbiol., 4(May), 131, doi:10.3389/fmicb.2013.00131, 2013.

Saltzman, E. S., De Bruyn, W. J., Lawler, M. J., Marandino, C. and McCormick, C.: A chemical ionization mass spectrometer for continuous underway shipboard analysis of dimethylsulfide in near-surface seawater, Ocean Sci., 6(2), 1569–1594, 2009.

Saltzman, E. S., King, D. B., Holmen, K. and Leck, C.: Experimental determination of the diffusion coefficient of dimethylsulfide in water, J. Geophys. Res., 98(C9), 16481, doi:10.1029/93JC01858, 1993.

Savoca, M. S. and Nevitt, G. a: Evidence that dimethyl sulfide facilitates a tritrophic mutualism between marine primary producers and top predators., Proc. Natl. Acad. Sci., 111(11), 4157–4161, doi:10.1073/pnas.1317120111, 2014.

Seymour, J. R., Simó, R., Ahmed, T. and Stocker, R.: Chemoattraction to dimethylsulfoniopropionate throughout the marine microbial food web., Science (80-.)., 329, 342–345, 2010.

Simó, R.: Production of atmospheric sulfur by oceanic plankton: biogeochemical, ecological and evolutionary links., Trends Ecol. Evol., 16(6), 287–294, 2001.

Simó, R.: From cells to globe : approaching the dynamics of DMS (P) in the ocean at multiple scales., Can. J. Fish. Aquat. Sci., 684(September 2002), 673–684, doi:10.1139/F04-030, 2004.

Simó, R., Grimalt, J. O., Pedros-Alió, C. and Albaigés, J.: Occurrence and transformation of dissolved dimethyl sulfur species in stratified seawater (western Mediterranean Sea), Mar. Ecol. Prog. Ser., 127, 291–299, 1995.

Simó, R. and Pedrós-Alió, C.: Role of vertical mixing in controlling the oceanic production of dimethyl sulphide., Nature, 402(November), 1999.

Simó, R. and Pedrós-alió, C.: Short-term variability in the open cycle of dimethylsulfide., Global Biogeochem. Cycles, 13(4), 1173–1181, 1999.

Stefels, J., Steinke, M., Turner, S., Malin, G. and Belviso, S.: Review: Environmental constraints on the production and removal of the climatically active gas dimethylsulphide (DMS) and implications for ecosystem modelling., Biogeochemistry, 83(1-3), 245–275, doi:10.1007/s10533-007-9091-5, 2007.

Steinke, M., Stefels, J. and Stamhuis, E.: Dimethyl sulfide triggers search behavior in copepods, Limnol. Oceanogr., 51(4), 1925–1930, 2006.

Sunda, W., Kieber, D. J., Kiene, R. P. and Huntsman, S.: An antioxidant function for DMSP and DMS in marine algae., Nature, 418(6895), 317–20, 2002.

Toole, D. a. and Siegel, D. A.: Light-driven cycling of dimethylsulfide (DMS) in the Sargasso Sea: Closing the loop, Geophys. Res. Lett., 31(9), 5–8, doi:10.1029/2004GL019581, 2004.

Toole, D. a., Slezak, D., Kiene, R. P., Kieber, D. J. and Siegel, D. a.: Effects of solar radiation on dimethylsulfide cycling in the western Atlantic Ocean, Deep Sea Res. Part I Oceanogr. Res. Pap., 53(1), 136–153, doi:10.1016/j.dsr.2005.09.003, 2006.

Turner, S. M., Malin, G., Liss, P. S., Harbour, D. S. and Holligan, P. M.: The seasonal variation of dimethyl sulfide and dimethylsulfoniopropionate concentrations in nearshore waters, Limnol. Oceanogr., 33(3), 364–375, doi:10.4319/lo.1988.33.3.0364, 1988.

Turner, S. M., Nightingale, P. D., Broadgate, W. and Liss, P. S.: The distribution of dimethyl sulphide and dimethylsulphoniopropionate in Antarctic waters and sea ice, Deep Sea Res. Part II Top. Stud. Oceanogr., 42(4-5), 1059–1080, doi:10.1016/0967-0645(95)00066-Y, 1995.

Uzuka, N., Watanabe, S. and Tsunogai, S.: Dimethylsulfide in Coastal Zone of the East China Sea, J. Oceanogr., 52, 313–321, 1996.

Del Valle, D. A., Kieber, D. J., Bisgrove, J. and Kiene, R. P.: Light-stimulated production of dissolved DMSO by a particle-associated process in the, Limnol. Oceanogr., 52(6), 2456–2466, 2007.

Del Valle, D. A., Kieber, D. J., Toole, D. A., Brinkley, J. and Kiene, R. P.: Biological consumption of dimethylsulfide (DMS) and its importance in DMS dynamics in the Ross Sea, Antarctica, Limnol. Oceanogr., 54(3), 785–798, doi:10.4319/lo.2009.54.3.0785, 2009.

Vallina, S. M. and Simó, R.: Strong relationship between DMS and the solar radiation dose over the global surface ocean., Science (80-.)., 315(5811), 506–8, doi:10.1126/science.1133680, 2007.

Vallina, S. M., Simó, R. and Manizza, M.: Weak response of oceanic dimethylsulfide to upper mixing sholaing induced by global warming, Proc. Natl. Acad. Sci., 104(41), 16004–16009, 2007.

Vila-Costa, M., Kiene, R. P. and Simó, R.: Seasonal variability of the dynamics of dimethylated sulfur compounds in a coastal northwest Mediterranean site, Limnol. Oceanogr., 53(1), 198–211, doi:10.4319/lo.2008.53.1.0198, 2008.

Wakeham, S. G. and Dacey, J. W. H.: Biogeochemical cycling of dimethylsulfide in marine environments., in Biogenic sulfur in the environement, edited by A. C. Society, pp. 152–166, Washington DC., 1989.

Wright, K. L. B., Pichegru, L. and Ryan, P. G.: Penguins are attracted to dimethyl sulphide at sea., J. Exp. Biol., 214(Pt 15), 2509–11, doi:10.1242/jeb.058230, 2011.

Yang, G., Zhang, J., Li, L. and Qi, J.: Dimethylsulfide in the surface water of the East China Sea, Cont. Shelf Res., 20, 69–82, 2000.

Zapata, M., Rodriguez, F. and Garrido, J. L.: Separation of chlorophylls and carotenoids from marine phytoplankton : a new HPLC method using a reversed phase C8 column and pyridine- containing mobile phases, Mar. Ecol. Prog. Ser., 195, 29–45, 2000.

Chapter 5

Small-scale variability patterns of DMS and phytoplankton in surface waters of the tropical and subtropical Atlantic, Indian and Pacific oceans

Geophysical Research Letters doi: 10.1002/2014GL062543

Sarah-Jeanne Royer, Anoop Sharad Mahajan, Martí Galí, Eric Saltzman and Rafel Simó

Abstract

High-resolution surface measurements of dimethylsulfide (DMS), chlorophyll a fluorescence and the efficiency of photosystem II were conducted together with temperature and salinity along five eastwards sections in the tropical and subtropical Atlantic, Indian and Pacific Oceans. Analysis of variability length scales revealed that much of the variability in DMS concentrations occurs at scales between 15 and 50 km, that is, at the lower edge of mesoscale dynamics, decreasing with latitude and productivity. DMS variability was found to be more commonly related to that of phytoplankton-related variables than to that of physical variables. Unlike phytoplankton physiological data, DMS did not show any universal diel pattern when using the normalized solar zenith angle as a proxy for solar time across latitudes and seasons. The study should help better design sampling and computing schemes aimed at mapping surface DMS and phytoplankton distributions, taking into account latitude and productivity.

Introduction

Dimethylsulfide (DMS) is a biogenic gas produced by the microbial food web within the photic layer of the ocean. Oceanic emission of DMS is important because it plays a crucial role for the recycling of sulfur to continents through the atmosphere (Lovelock et al., 1972) and because DMS serves as a precursor for the formation and growth of atmospheric sulfate aerosols (Andreae and Barnard, 1984; Hegg et al., 1991). This has important implications for cloud microphysics in marine regions remote from continental emissions (Andreae and Rosenfeld, 2008; Lana et al., 2012; Vallina et al., 2007). Sea surface DMS concentration and emission result from a complex web of ecological, chemical and biogeochemical processes interacting with the physics of the environment (Kiene et al., 2000; Malin and Kirst, 1997; Simó, 2001).

Resolving the spatial/temporal pattern of DMS variability and its relationships to other biogeochemical and biophysical variables is important in order to understand the factors controlling DMS cycling. Analyses of remotely sensed global ocean color have demonstrated that mesoscale (10-200 km) variability occurs similarly for biological and physical variables, dominates over most of the oligotrophic regimes, and contributes up to a third of the total variability of high productivity regions (Doney et al., 2003). The database of DMS measurements used for the DMS climatology (Lana et al., 2011) shows that large-scale spatial and temporal variability occurs in the surface oceans, but coverage is insufficient to resolve the fine-scale dynamics (Belviso et al., 2004; Tortell et al., 2011).

Most of seawater DMS measurements to date have been obtained using standard purge and trap - gas chromatography (GC) methods, with a measurement frequency typically of a few measurements per hour at the best (Bell et al., 2012). As a result, the distribution of DMS is still coarse considering the number of field campaigns targeted at this compound. The development of high frequency, DMS analysis mass spectrometers over the last decade has the potential to greatly expand the coverage and resolution of surface ocean DMS observations and their relationship to other oceanographic variables

(Kameyama et al., 2009, 2013; Royer et al., 2014; Saltzman et al., 2009; Tortell, 2005a).

Tortell, (2005b) reported significant small-scale heterogeneity in the distribution of DMS across oceanic regimes, and suggested that previous field studies might have under-estimated the true spatial variability of DMS in dynamic marine systems. Subsequent work by the same group in the northeast subarctic Pacific (Asher et al., 2011; Nemcek et al., 2008) used decorrelation and variability length scales to show that DMS concentration varied over shorter distances (ca. 7 km) compared to sea-surface temperature (SST) and salinity (11-14 km), and shorter or longer than that of chlorophyll *a* (Chl*a*; 3.5-12.5 km). On the western side of the subarctic North Pacific, Kameyama et al., (2009) observed elevated DMS peaks associated with patches of high biological activity. In the eastern Atlantic, Zindler et al., (2014) observed variability in DMS and isoprene concentrations across mesoscale hydrographic eddies that was related to

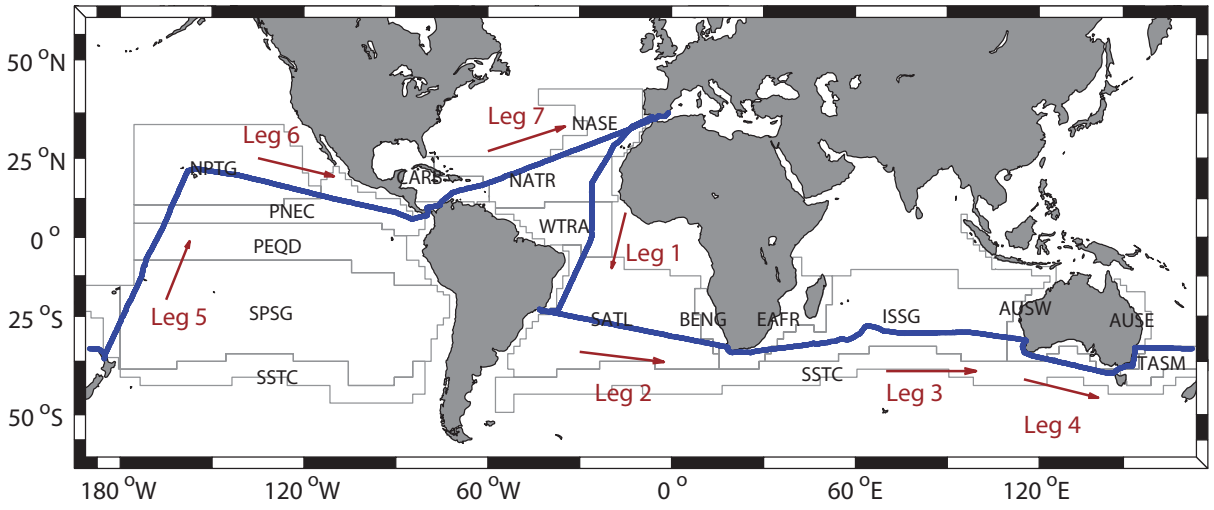

Figure 1: Circumnavigation track and leg numbers of the Malaspina 2010 expedition. Continuous DMS data exist for parts of legs 2, 3, 4, 5 and 6. The background shows the biogeographical (Longhurst) provinces visited during the expedition. The acronyms refer to Longhurst's biogeographical provinces: SPSG is South Pacific Subtropical Gyre; PEQD is Pacific Equatorial Divergence; PNEC is North Pacific Equatorial Countercurrent; NPTG is North Pacific Tropical Gyre; SATL is South Atlantic Gyre; EAFR is East Africa Coastal; ISSG is Indian South Subtropical Gyre; AUSW is Australia-Indonesia Coastal; SSTC is South Subtropical Convergence; AUSE is East Australian Coastal; TASM is Tasman Sea.

nitrogen-phosphorous limitation. Studies of this kind are scattered and mostly regional, hence not necessarily representative of most of the world's oceans.

Here we use atmospheric pressure chemical ionization mass spectrometry (APCIMS) to explore DMS concentration and some of the hydrographic and biophysical variables that may influence it at very fine scale within the low latitude oceans. We collected continuous underway data across the tropical and subtropical Atlantic, Indian and Pacific oceans over spring, summer and fall during the seven-month circumnavigation expedition Malaspina 2010. Analysis of variability length scales (VLS) for DMS, along with potential hydrographic and biological drivers in surface waters, provides insight into how DMS distributes on the map of the physics and biology of the surface oceans.

Methods

Sampling scheme

This study was conducted on board the R/V *Hespérides* from January to July 2011 during the Malaspina 2010 Circumnavigation Expedition. The expedition covered 22 biogeochemical provinces (Longhurst, 1998) and a total distance of 58,890 km across the Atlantic, Indian and Pacific oceans, mostly within latitudes ranging between 30ºN and 30ºS (Figure 1). DMS was measured continuously in near-surface seawater along a total distance of ca. 21,300 km, when the analytical system was operative (Figure 2). Seawater was sampled using the underway pump of the ship (4 m inlet) and supplied continuously for DMS and Fast Repetition Rate Fluorometer (FRRf) measurements. A third tap allowed discrete sampling for manual analyses. Details of the underway sampling setup can be found elsewhere (Royer et al., 2014). Go-Flo sampling bottles (General Oceanics, Miami, FL, USA) were also used to collect seawater samples overboard from a depth of 3 m, with the purpose of intercomparison with the underway pump.

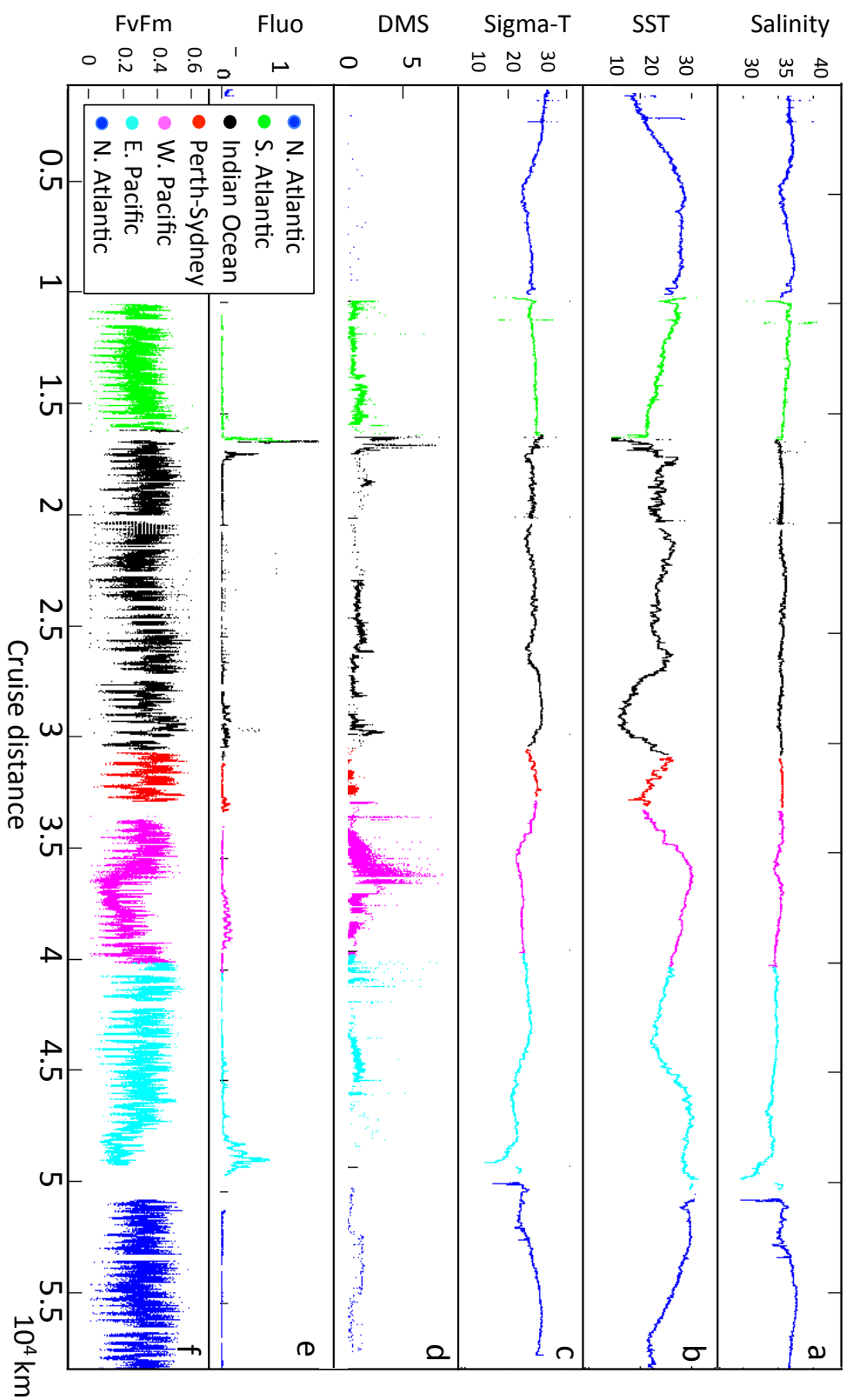

Figure 2: Variables measured at high frequency during the Malaspina 2010 Expedition.A: Salinity (kg m^{-3}); B: SST (°C); C: Sigma-T (potential density, (kg m^{-3}); D: DMS concentration (nmol L^{-1}); E: Chlorophyll a fluorescence (Fluo, arbitrary units); and F: efficiency of photosystem II (FvFm). Colors indicate broad oceanic regions. The instrument measuring Fluo and FvFm was not operative during the first leg in the North Atlantic. Note that there are sections where no continuous but discrete DMS measurements exist. These are shown to provide the circumnavigation results context, but have not been used for the variability analysis.

Analytical instruments and methods

Continuous DMS measurements were performed with a gas equilibrator APCIMS (Eq-APCIMS) as described by Saltzman et al., (2009) and Royer et al., (2014). In brief, aqueous DMS is equilibrated with air across using a hydrophobic Teflon membrane with seawater and clean air flowing in opposite directions. The resulting air stream is diluted with air containing an isotope-labeled CD_3SCH_3 internal standard from a permeation tube and directed towards the mass spectrometer inlet. DMS molecules are ionized via proton transfer from H_3O^+, and subsequently declustered, quadrupole mass filtered and detected by an ion multiplier. Seawater DMS (m/z 63) is quantified from the ratio to the isotope-labeled internal standard (m/z 66). Details of the calculation required to convert the raw data into ambient concentrations are given elsewhere (Royer et al., 2014). For data collected every 2 s and averaged every minute, the sensitivity of the instrument was equivalent to 0.1 nmol L^{-1}, and the precision was 8%. The Eq-APCIMS measurements were matched with the ship geo-referenced position system, meteorological data, and salinity and SST measurements.

Purge and trap and gas chromatography (GC) coupled to flame photometric detection (FPD) was also used through the entire cruise for DMS measurements in discrete samples. This instrument had a detection limit equivalent to 0.3 nmol L^{-1} and a precision better than 5% (Galí et al., 2013b). Inter-comparison exercises between the Eq-APCIMS and the GC-FPD gave satisfactory results (slope = 1.12; R^2 = 0.92; $p < 0.0001$). Further tests demonstrated that the delivery of seawater from the underway pump did not significantly affect endogenous DMS concentrations (Royer et al., 2014).

A FRRf (FASTracka, Chelsea Technologies, Surrey, UK) was used in parallel for underway measurements of phytoplankton photophysiology, including the maximum quantum efficiency of photosystem II photochemistry (FvFm). Seawater flowed continuously through dark tubes for ca. 3 minutes before reaching the dark chamber of the FRRf. The fluorescence induction protocol consisted of 100 saturation flashlets

(1.3 μs duration, 2.8 μs interflash delay) followed by 20 relaxation flashlets (separated by 50 μs). Different physiological parameters such as initial fluorescence (F_0), maximum fluorescence (Fm), variable fluorescence (Fv = Fm-F_0), and the ratio of variable to maximum fluorescence (FvFm = Fv/Fm = (Fm-F_0)/Fm) were derived from the curve of fluorescence induction in the photosystem II (PSII) according to Kolber et al., (1998). Blank calibrations with 0.2 μm filtered seawater were performed before and after instrument deployment. No significant bio-fouling was observed during the cruise. The data were processed using the Chelsea FRS Software (v.1.8), with reference and baseline corrections.

Data processing and VLS

All high frequency data (DMS, FRRf-derived parameters, SST, salinity and derived potential density – sigma-T) were processed using MATLAB. First, the data were quality controlled and calculations were made to find the optimum averaging time for improving the signal-to-noise ratio. Based on these results for DMS, an averaging time of 60 s was used to process underway data, which yields a datum every 300 m for a ship steaming speed of 10 knots (18.5 km h^{-1}; Royer et al., (2014)). Data acquired during oceanographic sampling stations were discarded, and only measurements obtained during steaming were used. These yielded analyzable transects ranging between 115 km to 1132 km. To assess the spatial scale at which underway variables undergo critical variations, we chose the VLS over several other similar analyses for its flexibility in using unequally spaced data and transects of different lengths. The VLS can be regarded as the minimum spatial resolution necessary to fully describe the distribution of a variable along a data series. We followed an analytical approach similar to that described by Asher et al., (2011). Each transect's high-resolution data series over distance was first binned with increasing distance bin sizes. The data were then interpolated linearly to the resolution of the original measurements. A mean squared error (MSE) between the real and

the interpolated data was calculated for each binning scheme. The MSE by default increases proportionally with increasing distance bin size, since data in close proximity are more related to one another than distant data. The VLS is identified as the binning or interpolation distance at which there is a change in slope in the relationship between MSE and interpolation distance (inset in Figure 3). We defined a continuous transect as one with a maximum gap distance of 1 km between two consecutive data points. Only transects with lengths of continuous data >100 km were analyzed. We computed the VLS for each variable in each transect, and then calculated regional averages in the 11 biogeochemical provinces in which the study was conducted (Longhurst, 1998).

Solar zenith angle computation

The solar zenith angle (SZA) is the angle of the sun away from vertical. It is 0 at noon at the equinox in the Equator, and at the solstice in the tropics; on the same dates and latitudes, it is 180º at midnight. The time at which the sun reaches a given SZA varies according to the latitude and the seasons, except for the fact that, by definition, the sun always rises at SZA -90º and sets at 90º, no matter where and what season the data are collected. The SZA corresponding to each 60 second-average of high-resolution data was computed according to date, local time, and latitude. A normalization of the SZA was applied to make it vary between -180º or +180º (midnight) and 0º (noon) through the diel cycle regardless of date and latitude. The normalized SZA (SZAn) was computed using the following equations:

$$SZAn = ((SZA + SZAmin)/(90 - SZAmin))*90 \quad \text{for } -90<SZA<0;$$

$$SZAn = ((SZA - SZAmin)/(90 - SZAmin))*90 \quad \text{for } 0<SZA<90;$$

$$SZAn = (((SZA + 90)/(SZAmax - 90)) - 1)*90 \quad \text{for } -180<SZA<-90;$$

$$SZAn = (((SZA - 90)/(SZAmax - 90)) + 1)*90 \quad \text{for } 90<SZA<180.$$

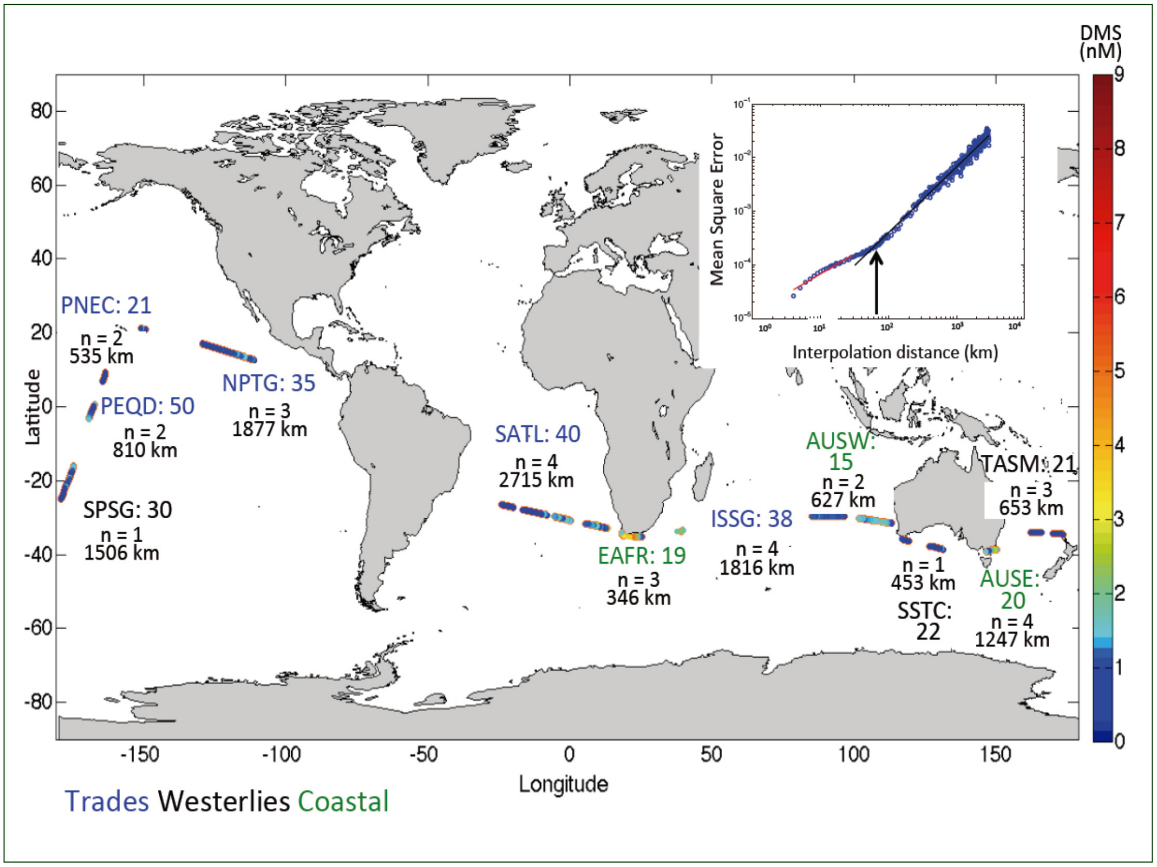
DMS (nM)
Latitude
Longitude
Mean Square Error
Interpolation distance (km)
PNEC: 21
n = 2
535 km
PEQD: 50
n = 2
810 km
NPTG: 35
n = 3
1877 km
SPSG: 30
n = 1
1506 km
SATL: 40
n = 4
2715 km
EAFR: 19
n = 3
346 km
ISSG: 38
n = 4
1816 km
AUSW: 15
n = 2
627 km
n = 1
453 km
SSTC: 22
TASM: 21
n = 3
653 km
AUSE: 20
n = 4
1247 km
Trades Westerlies Coastal

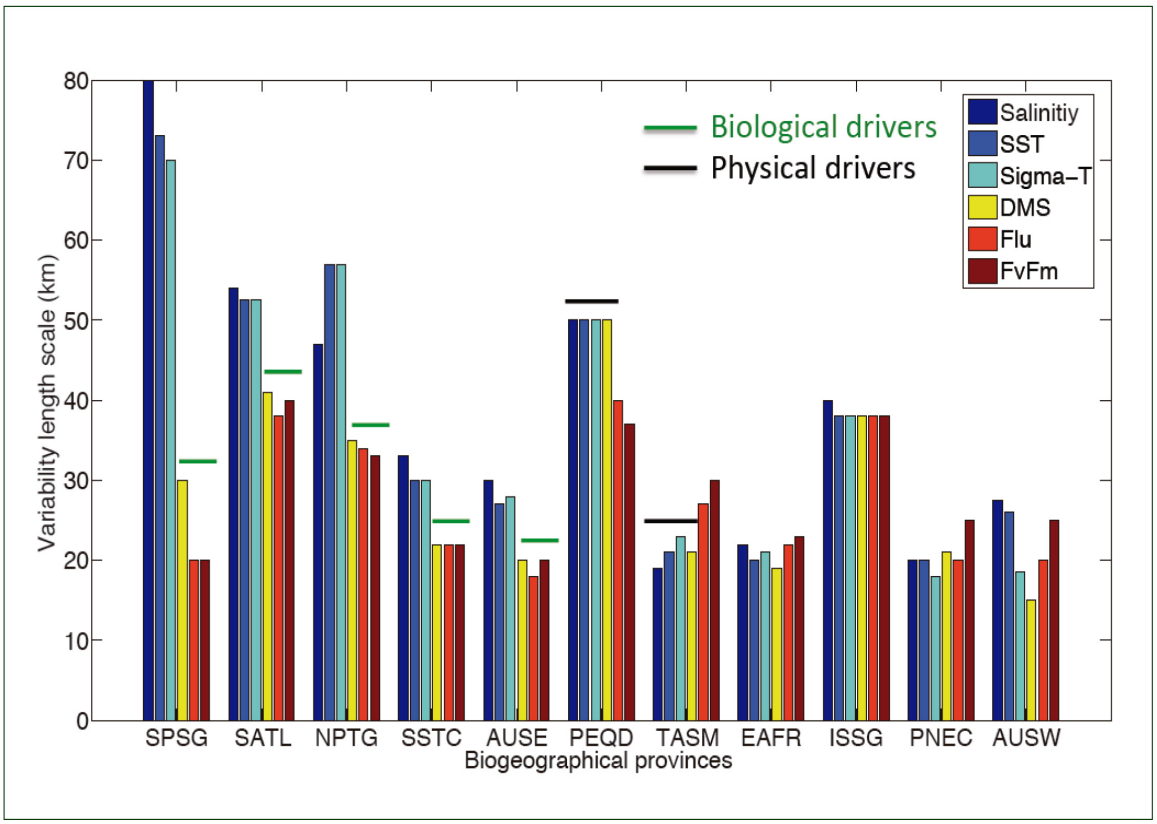
Biological drivers
Physical drivers
Salinitiy
SST
Sigma–T
DMS
Flu
FvFm
Variability length scale (km)
SPSG SATL NPTG SSTC AUSE PEQD TASM EAFR ISSG PNEC AUSW
Biogeographical provinces

← **Figure 3:** Distribution of high-resolution DMS concentrations and DMS VLS across provinces along the track of the Malaspina 2010 Expedition. Top: Dots on the map are surface DMS concentrations (nmol L^{-1}) as measured with the Eq-APCIMS. Concentration is depicted by the color bar on the right. The acronyms refer to Longhurst's biogeographical provinces: SPSG is South Pacific Subtropical Gyre; PEQD is Pacific Equatorial Divergence; PNEC is North Pacific Equatorial Countercurrent; NPTG is North Pacific Tropical Gyre; SATL is South Atlantic Gyre; EAFR is East Africa Coastal; ISSG is Indian South Subtropical Gyre; AUSW is Australia-Indonesia Coastal; SSTC is South Subtropical Convergence; AUSE is East Australian Coastal; TASM is Tasman Sea. The colors of province acronyms refer to the following biogeographical domains: blue = trades, black = westerlies, green = coastal. The number next to the province acronym is the mean VLS (km) of DMS. The number of transects analyzed per province is termed n, and the number of km comprised by all transects in an individual province is indicated below. The inset graph shows an example of how the VLS is calculated: it represents the measurement interpolation errors as a function of interpolated distance (km) within the SPSG province; the VLS is marked by the arrow. Bottom: Province-averaged VLS (km) for salinity, SST, sigma-T, DMS, Fluo and FvFm. The green or black line above bars identifies the provinces where DMS VLS is similar to that of biological or physical variables, respectively.

where SZAmin and SZAmax are the daily minimum and maximum SZA at a particular date and location. Every 60 second-average of every measured variable was matched to its SZAn, thus allowing exploring their variability over a universal diel cycle irrespective of season and latitude.

Results and Discussion

DMS distribution patterns

Most of the circumnavigation took place across oligotrophic waters of the central oceanic gyres, where Chl*a* concentrations were very low. Cruise mean Chl*a* was 0.14 μg L^{-1} with a range of 0.015-0.693 μg L^{-1} (data not shown). Cruise mean DMS concentration, including the regions with discrete sampling, was 1.1 nmol L^{-1}, with a minimum value below 0.1 nmol L^{-1} observed in the ultra-oligotrophic waters of the South Atlantic and Pacific oceans (SATL and SPSG), and a maximum value of 9.6 nmol L^{-1} near the South African coast (Figure 2).

Over the total length of the expedition DMS appeared to change sharply at salinity and SST gradients in localized areas (for example in the Equatorial Pacific, around km 35,000), suggesting a direct or indirect physical influence on DMS concentrations. Such harmonious

changes also occurred occasionally with Chl*a* fluorescence: peaks were coincident in the Agulhas-Benguela region (around km 17,000) and in the Western Australian current (around km 29,000), which suggested DMS production associated with biological drivers. However, for the full dataset, neither salinity nor SST nor fluorescence were good predictors of DMS concentration. Simó and Dachs (2002) successfully combined biological and physical variables to predict broad regional and seasonal DMS distributions using low resolution measurements of the mixed-layer depth (MLD) and the Chl*a*/MLD ratio. Unfortunately, our high frequency DMS dataset was not paralleled with same resolution MLD and Chl*a* measurements as to be able to explore the behavior of the Simó and Dachs (2002) relationship at the high resolution. The lack of covariance between DMS and biophysical variables over most of the cruise (Figure 2) resulted in no significant statistical relationship of global applicability.

VLS across biogeographical provinces

In order to better understand DMS distribution and its drivers, the dataset was divided into biogeographical domains (Trades, Westerlies and Coastal) and subdivided further into 11 biogeographical provinces (Longhurst, 1998). Province averages of the VLS of DMS, salinity, SST, sigma-T, in situ fluorescence (F_0 from the FRRf, hereafter Fluo) and FvFm are shown in Figure 3 and Table 1. In general, the VLS of salinity, SST and sigma-T were similar to each other, an expected feature that depicts the physical structure of the surface ocean. The VLS of these physical properties ranged 18-80 km across provinces (Table 1), with a circumnavigation average of 38 km. Biological variables related to phytoplankton biomass and physiology generally showed shorter VLS: across province range of 18-40 km (mean of 27 km) for Fluo, and 20-40 km (mean of 28 km) for FvFm (Table 1). These scales of variability of physical and biological properties are in agreement with the typical ranges for cross-stream widths of ocean's swift currents (10-100 km) and about $1/4^{th}$ of the typical radii of surface eddies as revealed by satellite altimetry (60-200 km; Fu et al.,

Table 1. List of biogeographical (Longhurst) provinces visited during Malaspina 2010, ordered by date, number and mean length of the transects analyzed per province, and the corresponding mean variability length scale (VLS - km) for salinity, sea-surface temperature (SST), potential density (sigma-T), DMS, phytoplankton fluorescence (Fluo) and the efficiency of photosystem II (FvFm).

Longhurst provinces						Variability length scale (km)					
Province #	Acronym	Province name	# transects analyzed	Date 2011	Mean transect length (km)	Salinity	SST	Sigma-T	DMS	Fluo	FvFm
10	SATL	Trades: S Atlantic Gyral	4	21/01-03/02	679	54±1	53±4	53±4	40±1	38	40
24	EAFR	Coastal: E Africa Coastal	3	05/02-15/02	115	22±3	20	21±1	19±1	22	23±2
23	ISSG	Trades: Indian S Subtropical Gyre	4	17/02-05/03	400	40	38±3	38±1	38±1	38	38
29	AUSW	Coastal: Australia-Indonesia Coastal	2	07/03-12/03	314	28±4	26±1	19±2	15	20	25
51	SSTC	Westerlies: S Subtropical Convergence	1	21/03-23/03	453	33	30	30	22	22	22
49	AUSE	Coastal: E Australian Coastal	4	24/03-26/03	312	30	27	28	20	18±2	20
36	TASM	Westerlies: Tasman Sea	3	12/04-14/04	218	19±1	21±1	23±5	21±1	27±6	30
37	SPSG	Westerlies: S Pacific Subtropical Gyre	1	20/04-24/04	1132	80	73	70	30	20	20
40	PEQD	Trades: Pacific Equatorial Divergence	2	29/04-04/05	503	50	50	50	50	40±1	37±2
39	PNEC	Trades: N Pacific Equatorial Countercurrent	2	05/05-19/05	268	20	20	18±3	21	20	25
38	NPTG	Trades: N Pacific Tropical Gyre	3	22/05-28/05	626	47±1	57±2	57±2	35±1	34	33

Errors represent standard deviations; when absent, it means all sections had the same VLS.

Table 2: Pearson's correlation coefficients between province-averaged variability length scales (VLS) of DMS and phytoplankton fluorescence (Fluo), and the magnitudes of several variables.

Provinces	VLS	Salinity	SST	Sigma-T	DMS	Fluo	FvFm	Latitude
All[a]	DMS	0.26	0.48 *	(-)0.27	(-)0.04	(-)0.17	(-)0.69 **	(-)0.71 ***
	Fluo	0.36	0.29	(-)0.07	(-)0.21	(-)0.22	(-)0.47 *	(-)0.50*
DMS VLS biologically driven[b] (n=5)	DMS	0.34	0.66	(-)0.40	(-)0.42	(-)0.86 **	(-)0.89 **	(-)0.64
	Fluo	0.31	0.33	(-)0.14	(-)0.65 *	(-)0.61 *	(-)0.61 *	(-)0.43

a Correlations using all biogeographical provinces.
b Correlations using only the biologically driven provinces highlighted in Figure 3.
Probabilities of significance are: *** > 99%; ** > 95%; * > 90%.

(2010)). Examining the VLS by provinces, the VLS of Fluo and FvFm are generally equal or smaller than those of salinity, SST and sigma-T. This was already observed by Strutton et al., (1997) as an indication that the Chl*a* spatial variability is not always associated with the physical heterogeneity of the environment. It is also consistent with the notion that faster responding tracers develop smaller scales of variability, or more patchiness, than slower or more conservative tracers (Mahadevan, 2004).

The VLS of DMS was similar to those of physical and biological variables, ranging from 15 to 50 km (mean of 28 km; Table 1). These values are consistently larger than those reported with similar methodologies in the North Pacific (Asher et al., 2011; Nemcek et al., 2008). Interestingly, DMS VLS exhibited a significant inverse correlation with latitude (Pearson's $r=-0.71$, $P<0.05$; Table 2). This correlation remains significant after including the VLS reported by the aforementioned studies at 50ºN and the VLS reported by Tortell et al., (2011) in the Ross Sea ($r=-0.74$, $P<0.005$). This decrease in the VLS with increasing latitude is consistent with the parallel decrease of the Rossby deformation radius and eddy size with latitude (Chelton et al., 1998), and stresses the dependence of DMS variability on surface mesoscale features.

By comparing the VLS of DMS to those of physical and biological variables in all individual transects across different provinces, we aim to obtain insight into the relative roles

of the two types of variables in driving spatial DMS variability. The DMS VLS was more similar to that of the biological parameters (Fluo and FvFm) than to that of the physical parameters in 65% of the transects (Figure 3). This occurred mainly in the oligotrophic gyres of the Atlantic and Pacific oceans (SATL, SPSG, NPTG) as well as the waters south of Australia (SSTC and AUSE). DMS VLS more closely matched that of the physical variables in only 15% of the analyzed transects. This occurred in the Equatorial Pacific (PEQD) and Tasman Sea (TASM). In most of the remaining 20% of the transects (within EAFR, ISSG and PNEC), all of the VLS were similar. In those waters, the relative influences of physics and biology on DMS could not be discerned. Only in AUSW, was the DMS VLS smaller than any of the other variables' VLS.

In general, the coastal domain presented the smallest VLS for biological variables and DMS (Figure 3; Table 1), while oligotrophic waters showed the largest. In support of this emerging pattern, a significant anti-correlation was observed between DMS VLS and Fluo across the regions where DMS variability is driven by biology ($r=-0.86$, $P<0.05$; Table 2). In other words, more productive waters, usually associated with the coastal domain, tend to be patchier for both biological and biogenic tracers. Again, this pattern is consistent with the previous studies by Nemcek et al., (2008) and Asher et al., (2011), where much smaller DMS

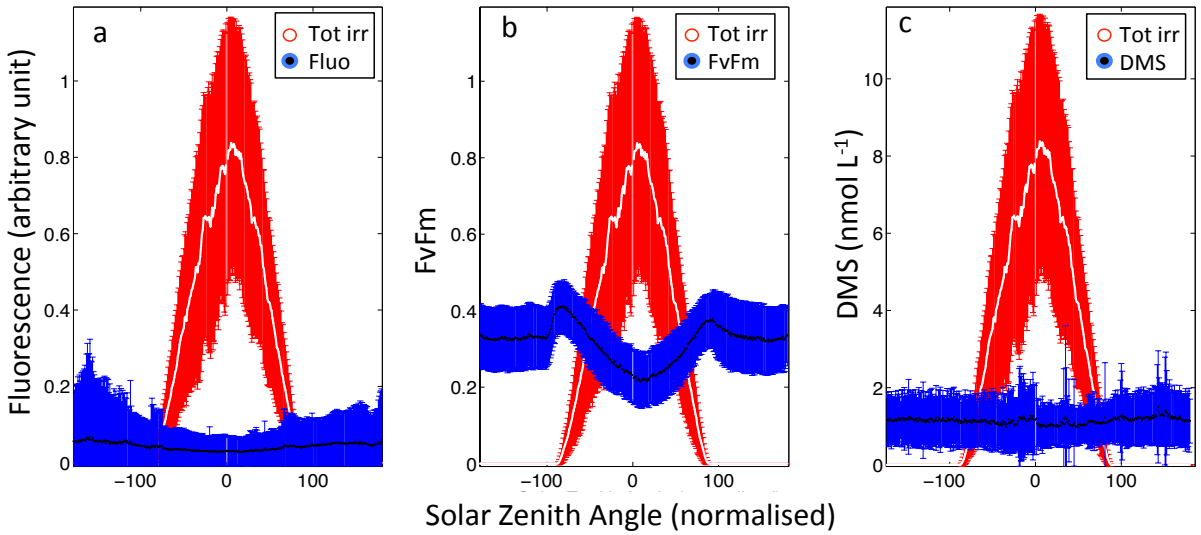

Figure 4: Normalized solar zenith angle (SZAn) dependence across the entire circumnavigation for: A: Fluorescence (Fluo), B: FvFm, and C: DMS. Total surface irradiance is given in red. Means and standard deviations are shown for each SZAn.

VLS (ca. 7 km) was associated with highly productive waters (Chl*a* up to 33 μg L^{-1}) in coastal domain waters off British Columbia.

DMS and phytoplankton physiology over the normalized diel cycle

Diel oscillations in solar irradiance are an additional potential source of DMS variability encountered during this study. The day-night alternation and the hourly underwater light regime exert an obvious rhythmic forcing on biological circadian rhythms, photochemical and photobiological processes, and potentially on biogeochemical fluxes as well (Doney et al., 1995; Ottesen et al., 2014; Poretsky et al., 2009). Our dataset is not particularly well suited for assessing diel oscillations because spatial variability occurred simultaneously to temporal variability, and the cruise covered a number of latitudes and seasons. To overcome this limitation, we examined our data as a function of SZAn (Figure 4), which allows collapsing all data into a single solar diel cycle.

A photoacclimation process was apparent for fluorescence (Figure 4A), with lower Fluo at daytime and higher at nighttime following the need for less or more efficient photosynthetic antenna. An even more remarkable diel pattern was found for the maximum photosystem II photochemical efficiency, FvFm (Figure 4B). As in Behrenfeld et al., (2006), photoinhibition of phytoplankton (translated into low FvFm values) appeared at low SZAn while higher FvFm occurred at dawn and dusk. The sudden increase in FvFm at dawn results from the oxidation of the plastoquinone pool by the photosystem I electron turnover, and higher FvFm at dusk results from complete recovery after the depressing effect of high light during daytime, due to non-photochemical quenching and photodamage to PSII. This common pattern across latitudes and seasons indicates that time of the day, and not only the instantaneous or daily-integrated irradiance, is more important for phytoplankton physiology.

Interestingly, DMS concentration did not show a significant relationship to SZAn (Figure 4C). Strong diel cycles have been reported for gross community DMS

production in Lagrangian studies conducted in highly irradiated and stratified waters at sea (Galí et al., 2013a). Suggested causes are the diel oscillations of UV radiation exposure and grazing (Galí et al., 2013a, 2013b). As for DMS losses, photolysis follows an obvious oscillation that parallels irradiance. Weaker yet significant cycles have also been observed for microbial DMS consumption. Although these processes tend to cancel each other and buffer DMS concentration changes, clear diel variability is often encountered. Using the Eq-APCIMS in two Lagrangian studies, we recently observed repeated day-night DMS oscillations in the Mediterranean Sea (results not shown); however, the diel pace in September was in anti-phase of that in May. Therefore, the absence of a pattern in Figure 4c is not to be interpreted as the lack of diel patterns in DMS concentration and cycling processes, but the absence of a *universal* diel cycle of global applicability similar to those of Fluo and FvFm.

Implications

Broad spatial coverage with high frequency measurements is essential to decipher the scales of variability and patchiness of DMS. In some instances, high-resolution measurements showed strong gradients; e.g., an abrupt change from 1 to 8 nmol L^{-1} was observed within 1.5 km in the Benguela (BENG) province. Tortell (2005b) observed an increase of 30 nmol L^{-1} over 750 m along the Queen Charlotte Islands. In contrast, traditional field sampling and measurement protocols, with sampling and analysis times in the order of 10–20 min at the shortest, would clearly fail to resolve this level of spatial heterogeneity. These results emphasize the need for high frequency DMS measurements that match the resolution of sensor-based physical and biological data, in order to better understand the mechanisms driving DMS distribution. The VLS analysis revealed that most spatial DMS variability occurs at the low mesoscale (15-50 km). Nemcek et al., (2008) and Asher et al., (2011) had already reported even shorter scales of variability with similar methods. However, these works were conducted in highly

productive temperate waters across two biogeographical provinces, one coastal. Our study covers 11 biogeographical provinces in 3 domains, mostly low latitude oligotrophic waters. Thus, we largely expand the variability analysis to the tropical and subtropical regions that make up the most of the world's oceans in terms of area.

Our study shows that, similarly to what occurs with phytoplankton, the DMS variability scale is smaller in productive waters, and larger in oligotrophic waters. This, along with its dependence on latitude, should be considered when designing sampling schemes in future field studies aimed at describing DMS distribution and its drivers. The spatial coverage and gridding of sampling (when analysis is to be done on discrete samples) should be designed to, at the least, cover the low mesoscale, taking into account that this contracts as we move pole wards. Satellite imagery can assist with sampling design: both Chl*a* patchiness from ocean color as well as physical structure information based on satellite altimetry and infrared radiation can be helpful; we strongly recommend increase the sampling grid density at high latitudes and in highly productive waters. Similar criteria should apply when we aim to construct regional to global maps of surface ocean DMS concentration using objective analysis schemes (Lana et al., 2011). Our results indicate that distance-weighted interpolations steps (e.g., Barnes (1964)) should scale to latitude-dependent sizes of mesoscale variability.

The lack of correlation of DMS with SZAn revealed that there is no such a thing as a *universal* diel pattern of global applicability for DMS. Only Lagrangian studies in representative oceanic regions provide the proper strategy to investigate the mechanisms of short-term DMS dynamics. However, the absence of a unique diel cycle, along with the observation that DMS tracks spatial variability in patchy or abruptly-varying environments, increases the difficulty in extrapolating from local studies when developing prognostic numerical modeling for this trace gas at the global scale. Global models are close to resolve mesoscale DMS variability (Chu et al., 2004), but will still have a hard time to reproduce the lower-edge mesoscale and submesoscale variability presented here.

Acknowledgements

Data can be requested to Sarah-Jeanne Royer (royer@icm.csic.es). Data supporting Figure 3 are available in Table 1. We wish to acknowledge the assistance and cooperation of the marine technicians (UTM) and crew aboard the R/V Hesperides, as well as the leadership of C.M. Duarte. This research has been funded by the Spanish Ministry of Economy and Competitiveness through projects Malaspina Expedition 2010 (INGENIO 2010 CONSOLIDER program, CSD2008-00077) and PEGASO (CTM2012-37615) and through a PhD scholarship to S.J.R. Support was also provided by the U.S. National Science Foundation (grants 0851472 and 1143709). The Indian Institute of Tropical Meteorology is funded by the Ministry of Earth Sciences, Government of India.

References

Andreae, M. O. and Barnard, W. R.: The marine chemistry of dimethylsulfide, Mar. Chem., 14, 267–279, 1984.

Andreae, M. O. and Rosenfeld, D.: Aerosol–cloud–precipitation interactions. Part 1. The nature and sources of cloud-active aerosols, Earth-Science Rev., 89(1-2), 13–41, doi:10.1016/j.earscirev.2008.03.001, 2008.

Asher, E. C., Merzouk, A. and Tortell, P. D.: Fine-scale spatial and temporal variability of surface water dimethylsufide (DMS) concentrations and sea–air fluxes in the NE Subarctic Pacific, Mar. Chem., 126(1-4), 63–75, 2011.

Barnes, S. L.: A technique for maximizing details in numerocal weather map analysis, J. Appl. Meteorol., 3, 396–409, 1964.

Behrenfeld, M. J., Worthington, K., Sherrell, R. M., Chavez, F. P., Strutton, P., McPhaden, M. and Shea, D. M.: Controls on tropical Pacific Ocean productivity revealed through nutrient stress diagnostics., Nature, 442(7106), 1025–8, doi:10.1038/nature05083, 2006.

Bell, T. G., Malin, G., Lee, G. A., Stefels, J., Archer, S., Steinke, M. and Matrai, P.: Global oceanic DMS data inter-comparability, Biogeochemistry, 110(1-3), 147–161, 2012.

Belviso, S., Moulin, C., Bopp, L. and Stefels, J.: Assessment of a global climatology of oceanic dimethylsulfide (DMS) concentrations based on SeaWiFS imagery (1998 – 2001), Can. J. Fish. Aquat. Sci., 61(September 2002), 804–816, doi:10.1139/F04-001, 2004.

Chelton, D. B., DeSzoeke, A. and Schlax, M. G.: Geographical Variability of the First Baroclinic Rossby Radius of Deformation, J. Phys. Oceanogr., 28(1984), 1998.

Chu, S., Elliott, S. and Maltrud, M.: Ecodynamic and Eddy-Admitting Dimethyl Sulfide Simulations in a Global Ocean Biogeochemistry / Circulation Model, Earth Interact., 8, 11, 2004.

Doney, S. C., Glover, D. M. and Mccue, S. J.: Mesoscale variability of Sea-viewing Wide Field-of-view Sensor (SeaWiFS) satellite ocean color: Global patterns and spatial scales., J. Geophys. Res., 108(C2), 3024, doi:10.1029/2001JC000843, 2003.

Doney, S. C., Najjar, R. G. and Stewart, S.: Photochemistry, mixing and diurnal cycles in the upper ocean, J. Mar. Res., 53, 341–369, 1995.

Fu, L.-L., Chelton, D. B., Le Traon, P.-Y. and Morrow, R.: Eddy dynamics from satellite altimetry, Oceanography, 23(4), 14–25, 2010.

Galí, M., Ruiz-González, C., Lefort, T., Gasol, J. M., Cardelús, C., Romera-Castillo, C. and Simó, R.: Spectral irradiance dependence of sunlight effects on plankton dimethylsulfide production, Limnol. Oceanogr., 58(2), 489–504, doi:10.4319/lo.2013.58.2.0489, 2013a.

Galí, M., Simó, R., Vila-Costa, M., Ruiz-González, C., Gasol, J. M. and Matrai, P.: Diel patterns of oceanic dimethylsulfide (DMS) cycling: Microbial and physical drivers, Global Biogeochem. Cycles, 27, 1–17, doi:10.1002/gbc.20047, 2013b.

Hegg, A., Radke, F. and Hobbs, V.: Measurements of Aitken nuclei and cloud condensation nuclei in the marine atmosphere and their relation to the DMS-Cloud-climate hypothesis., J. Geophys. Res., 96(10), 727–733, 1991.

Kameyama, S., Tanimoto, H., Inomata, S., Tsunogai, U., Ooki, A., Yokouchi, Y., Takeda, S., Obata, H. and Uematsu, M.: Equilibrator inlet-proton transfer reaction-mass spectrometry (EI-PTR-MS) for sensitive, high-resolution measurement of dimethyl sulfide dissolved in seawater., Anal. Chem., 81(21), 9021–6, doi:10.1021/ac901630h, 2009.

Kameyama, S., Tanimoto, H., Inomata, S., Yoshikawa-Inoue, H., Tsunogai, U., Tsuda, A., Uematsu, M., Ishii, M., Sasano, D., Suzuki, K. and Nosaka, Y.: Strong relationship between dimethylsulfide and net community production in the western subarctic Pacific, Geophys. Res. Lett., 40, 3986–3990, doi:10.1002/grl.50654, 2013.

Kiene, R. P., Linn, L. J. and Bruton, J. a.: New and important roles for DMSP in marine microbial communities., J. Sea Res., 43(3-4), 209–224, 2000.

Kolber, Z., Prasil, O. and Falkowski, P. P. G.: Measurements of variable chlorophyll fluorescence using fast repetition rate techniques: defining methodology and experimental protocols, Biochim. Biophys. Acta, 1367(1-3), 88–106, doi:10.1016/S0005-2728(98)00135-2., 1998.

Lana, a., Bell, T. G., Simó, R., Vallina, S. M., Ballabrera-Poy, J., Kettle, a. J., Dachs, J., Bopp, L., Saltzman, E. S., Stefels, J., Johnson, J. E. and Liss, P. S.: An updated climatology of surface dimethlysulfide concentrations and emission fluxes in the global ocean, Global Biogeochem. Cycles, 25(1), 1–17, doi:10.1029/2010GB003850, 2011.

Lana, A., Simó, R., Vallina, S. M. and Dachs, J.: Potential for a biogenic influence on cloud microphysics over the ocean: a correlation study with satellite-derived data, Atmos. Chem. Phys., 12(17), 7977–7993, doi:10.5194/acp-12-7977-2012, 2012.

Longhurst, A.: Ecological geography of the sea Longhurst, Academy Pr., London., 1998.

Lovelock, J. E., Maggs, R. J. and Rasmussen, R. A.: Atmospheric Dimethyl Sulphide and the Natural Sulphur Cycle, Nature, 237, 452–453, 1972.

Mahadevan, A.: Spatial Heterogeneity and Its Relation to Processes in the Upper Ocean, in Ecosystem Function in Heterogeneous Landscape, edited by G. M. Lovett, C. G. Jones, M. G. Turner, and K. C. Weathers, pp. 165–182., 2004.

Malin, G. and Kirst, G. O.: Algal production of dimethyl sulfide and its atmospheric role., J. Phycol., 33, 889–896, 1997.

Nemcek, N., Ianson, D. and Tortell, P. D.: A high-resolution survey of DMS, CO2, and O2 /Ar distributions in productive coastal waters, Global Biogeochem. Cycles, 22(2), 1–13, doi:10.1029/2006GB002879, 2008.

Ottesen, E. a, Young, C. R., Gifford, S. M., Eppley, J. M., Marin, R., Schuster, S. C., Scholin, C. a and DeLong, E. F.: Ocean microbes. Multispecies diel transcriptional oscillations in open ocean heterotrophic bacterial assemblages., Science (80-.)., 345(6193), 207–12, doi:10.1126/science.1252476, 2014.

Poretsky, R. S., Hewson, I., Sun, S., Allen, A. E., Zehr, J. P. and Moran, M. A.: Comparative day/night metatranscriptomic analysis of microbial communities in the North Pacific subtropical gyre., Environ. Microbiol., 11(6), 1358–75, doi:10.1111/j.1462-2920.2008.01863.x, 2009.

Royer, S.-J., Galí, M., Saltzman, E. S., McCormick, C. A., Bell, T. G. and Simó, R.: Development and validation of a shipboard system for measuring high-resolution vertical profiles of aqueous dimethylsulfide concentrations using chemical ionisation mass spectrometry, Environ. Chem., 1–9, 2014.

Saltzman, E. S., De Bruyn, W. J., Lawler, M. J., Marandino, C. and McCormick, C.: A chemical ionization mass spectrometer for continuous underway shipboard analysis of dimethylsulfide in near-surface seawater, Ocean Sci., 6(2), 1569–1594, 2009.

Simó, R.: Production of atmospheric sulfur by oceanic plankton: biogeochemical, ecological and evolutionary links., Trends Ecol. Evol., 16(6), 287–294, 2001.

Simó, R. and Dachs, J.: Global ocean emission of dimethylsulfide predicted from biogeophysical data, Global Biogeochem. Cycles, 16(4), 1–10, doi:10.1029/2001GB001829, 2002.

Strutton, P. G., Mitchell, J. G., Parslow, J. S. and Greene, R. M.: Phytoplankton patchiness: quantifying the biological contribution using Fast Repetition Rate Fluorometry, J. Plankton Res., 19(9), 1265–1274, doi:10.1093/plankt/19.9.1265, 1997.

Tortell, P. D.: Dissolved gas measurements in oceanic waters made by membrane inlet mass spectrometry, Limnol. Oceanogr. Methods, 2, 24–37, 2005a.

Tortell, P. D.: Small-scale heterogeneity of dissolved gas concentrations in marine continental shelf waters, Geochemistry Geophys. Geosystems, 6(11), 1–16, 2005.

Tortell, P. D., Guéguen, C., Long, M. C., Payne, C. D., Lee, P. and DiTullio, G. R.: Spatial variability and temporal dynamics of surface water pCO2, ΔO2/Ar and dimethylsulfide in the Ross Sea, Antarctica, Deep Sea Res. Part I, 58(3), 241–259, doi:10.1016/j.dsr.2010.12.006, 2011.

Vallina, S. M., Simó, R., Gassó, S., de Boyer-Montégut, C., del Río, E., Jurado, E. and Dachs, J.: Analysis of a potential "solar radiation dose–dimethylsulfide–cloud condensation nuclei" link from globally mapped seasonal correlations, Global Biogeochem. Cycles, 21(2), 1–16, doi:10.1029/2006GB002787, 2007.

Zindler, C., Marandino, C. a., Bange, H. W., Schütte, F. and Saltzman, E. S.: Nutrient availability determines dimethylsulfide (DMS) and isoprene distribution in the eastern Atlantic Ocean, Geophys. Res. Lett., 1–8, doi:10.1002/2014GL059547, 2014.

Chapter 6

Sea surface DMS distribution patterns and environmental and biological drivers across the tropical and subtropical oceans

Sarah-Jeanne Royer, Martí Galí, Anoop Sharad Mahajan, Antonio Delgado Huertes, Dolors Blasco, Marta Estrada, Susana Agustí, Antonio Bode, Ricardo Sánchez-Leal, Mikel Latasa, Emilio Marañón and Rafel Simó

Abstract

We present an extensive collection of data for sea surface dimethylsulfide (DMS; n=500) and dimethylsulfoniopropionate (DMSP; n=488) concentrations from the circumnavigation cruise Malaspina 2010. These data are compared with simultaneous measurements of a wide range of accompanying variables, such as mixed layer depth (MLD) and solar radiation dose (SRD) index (which characterizes the prevailing physical and optical conditions), chlorophyll a (Chl*a*), in situ fluorescence, taxonomic and photoprotection pigments and microscopic phytoplankton counts (which characterizes the phytoplankton assemblages and their capacity to cope with light and nutrient stresses). DMS concentrations were generally lower than the corresponding monthly values of the latest DMS climatology. The highest concentrations were observed in productive regions characterized by upwelling hydrographic structures: the Agulhas Current in the South Atlantic, the Equatorial currents and the Costa Rica Dome in the Pacific. No significant paired correlations were obtained for the complete dataset but relations between DMS and MLD, SRD index in the upper mixed layer, Chl*a* and chromophoric dissolved organic matter (CDOM) were observed in some of the biogeochemical provinces. DMS and DMSP generally increased where pigments revealed relatively high abundances of dinoflagellates and haptophytes, or with photoprotection. Principal component analysis using data from all regions showed that while DMSP is more closely related to the biological components of the pelagic ecosystem, DMS aligns positively with SRD and negatively with CDOM, MLD and the performance of photosystem II (FvFm), thus stressing the importance of the physico-chemical setting in driving DMS variability in the open ocean.

Introduction

Dimethylsulfide (DMS) is a climate-active volatile compound biologically produced by the marine food web and also the most important form of reduced sulfur emitted from the ocean into the atmosphere. Globally, oceanic DMS accounts for 80% of the natural emission and 25% of total emissions of sulfur (Simó 2001). DMS is produced in the marine food web from the algal osmolyte dimethylsulfoniopropionate (DMSP), a compatible solute that occurs in a wide variety of phytoplankton phyla (Keller 1989). One would think that phytoplankton biomass should be a good indicator of total DMSP concentrations in seawater, but intracellular DMSP concentrations vary up to five orders of magnitude across phytoplankton species and physiological states (Stefels et al., 2007). Most of the high DMSP producers are small phytoplankton cells (Keller 1989; Belviso et al. 2003), amongst them the small coccolithophores, including *Emiliana huxleyi*, the species of the colony-forming phytoplankton *Phaeocystis* (Stefels and van Boekel 1993), and dinoflagellates (Bucciarelli et al. 2003). On the other hand, diatom species are known to be more abundant in nutrient-replete waters and are low DMSP producers (Keller 1989; Vila-Costa et al. 2006). DMSP is suggested to play a number of roles within the algal cells such as osmoregulation, cryoprotection (Malin and Kirst 1997), methyl donation in metabolic reactions (Kiene et al. 1999), overflow of reduced power (Stefels 2000), and oxygen radical scavenger (Sunda et al. 2002). Therefore, because of the taxonomic and physiological dependence of DMSP production, co-linearity (cause-effect) relationship between DMSP and proxies of total phytoplankton biomass, such as chlorophyll *a* (Chl*a*), is hardly observed.

Being a labile compound associated mainly with plankton microbes, DMSP undergoes rapid cycling and is involved in important ecological functions like chemotaxis (e.g., DeBose et al. 2008; Seymour et al. 2010; Garren et al. 2013) and sulfur transfer among trophic levels of the food web (Kiene et al. 2000; Simó 2004; Vila-Costa et al. 2006; Simó et al. 2009). The composition and structure of the plankton community ultimately

governs the production rate of DMSP, the release of DMSP and DMS into the water column via algal leakage, exudation and mortality, the bacterial catabolism of DMSP and its enzymatic transformation into DMS (Stefels et al. 2007). Once in seawater, the fate of most DMS is to be photo-oxidized or utilized by bacteria (Simó 2004). Only a minor fraction is vented to the atmosphere, where, upon oxidation, it can affect the formation and growth of secondary aerosols (Andreae and Crutzen 1997). Atmospheric DMS also acts as an olfactory signal sensed by marine mammals (Kowalewsky et al. 2006), turtles (Endres and Lohmann 2012) and birds (DeBose et al. 2008; Wright et al. 2011).

Still today, no single method for predicting realistic global DMS distribution is completely satisfactory due to the complexity and the different variables involved in its cycle (Belviso et al. 2004; Le Clainche et al. 2004, 2010). Recent studies have tried to understand the global distribution of DMS by studying the emerging patterns of its concentration (Lana et al. 2012b) and the processes regulating its cycling (Galí and Simó, submitted). Lana et al. (2012b) re-examined the previously described latitudinal effect on the relative seasonality of DMS and phytoplankton Chl*a* (Vallina et al. 2007), and found that they are positively correlated in latitudes higher than 40º, but negatively correlated in the 20º-40º latitudinal bands of both hemispheres. Over the last 15 years, amongst the several bio-physical parameters influencing seawater DMS concentrations, Chl*a* and specific pigment concentrations, MLD, solar radiation, phosphate limitation, gross primary production and net community production have been statistically explored for their predictive capabilities of large-scale surface ocean DMS distribution and dynamics, with irregular success (Kettle et al. 1999; Aranami and Tsunogai 2004; Vallina and Simó 2007; Bell et al. 2010; Miles et al. 2012; Belviso et al. 2012; Lana et al. 2012b; Kameyama et al. 2013). Also chromophoric dissolved organic matter (CDOM) and nitrate have been suggested to play a role since they act as photosensitizers of DMS

photolysis (Toole and Siegel 2004; Bouillon and Miller 2005), but they have not yet been used in diagnostic models aimed to predict DMS concentration distribution.

Several prognostic numerical models have been developed with the aim to predict DMS concentrations in the global ocean from the full representation of its production and removal processes (Chu et al. 2003; Cropp 2004; Le Clainche et al. 2004; Kloster et al. 2006; Six and Maier-Reimer 2006; Bopp et al. 2008; Gabric et al. 2008; Elliott 2009; Vogt et al. 2010). However, models can only be as good as our knowledge is of the processes and players involved, and important parts of the DMS cycle are not yet fully resolved. It is worth stressing the difficulties encountered by prognostic models to reproduce the vertical dynamics of DMS and the lags between annual maxima of phytoplankton biomass, DMSP and DMS concentrations at low latitudes (Le Clainche et al. 2010).

In order to better understand DMS and DMSP (hereafter named together as DMS(P)) concentrations in the world's oceans as well as the processes and bio-physical agents responsible for their variability, we participated in the Malaspina circumnavigation expedition (Malaspina 2010) from December 2010 to July 2011, where we studied the DMS(P) distribution across different biogeographical regions. The expedition covered a total of 31,832 nautical miles (NM) mostly across tropical and subtropical oceans over spring, summer and fall. DMS(P) were measured daily (total of 147 morning stations) in the water column using a standard gas chromatography (GC) technique. To get insight into the biotic and abiotic factors that regulate DMS production in the surface ocean, comparisons of DMS(P) with ancillary physico-chemical data, plankton biomass, and phytoplankton physiological response to environmental stressors were conducted across biogeographical provinces.

Methods

Sampling scheme

This study was conducted during the Malaspina Circumnavigation Expedition on board the R/V *Hespérides* from December 2010 to July 2011. The expedition was composed of seven transects across the Atlantic, Indian and Pacific Oceans (Figure 1). A total of 147 stations were sampled, one every morning of the cruise, each separated by about 200 NM. The cruise crossed 22 biogeographical provinces (Longhurst 1998), along 31,832 NM (58,890 km; see Table 1).

Go Flo sampling bottles (General Oceanics) were used to collect seawater samples at 3 m depth every morning at 7 AM and 9AM local time. Water was also sampled from 10 m depth using Niskin bottles attached to a CTD-rosette at 9 AM and occasionally at 5 m depth around 11 AM. DMS(P) and FRRf samples were collected using dark bottles to avoid light stress and processed immediately on board.

Figure 1: World map of the Longhurst provinces and the ship track of the circumnavigational expedition Malaspina 2010.

Additional measurements were also made using the underway pumping system of the ship (4 m depth) in parallel to the above sampling points as well as outside of station periods. Parallel sampling allowed inter-comparison between underway pumping and Niskin and Go Flo bottles (Royer et al. 2014).

Table 1: List of provinces visited during the circumnavigational expedition Malaspina 2010.

			Longhurst provinces	
#	Acronym	Biogeochemical domain	Province name	station per provinces
7	NATR	Trades	North Atlantic Tropical Gyral	6+8
8	WTRA	Trades	Western Tropical Atlantic	7
9	ETRA	Trades	Eastern Tropical Atlantic *	none
10	SATL	Trades	South Atlantic Gyral	25
12	CNRY	Coastal	Canary Coastal *	none
14	GUIA	Coastal	Guianas Coastal *	none
16	MEDI	Westerlies	Mediterranean Sea, Black Sea *	none
17	CARB	Trades	Caribbean	5
18	NASE	Westerlies	North Atlantic Subtropical Gyral	4+8
19	BRAZ	Coastal	Brazil Current Coastal *	none
21	BENG	Coastal	Benguela Current Coastal	1
23	ISSG	Trades	Indian South Subtropical Gyre	19
24	EAFR	Coastal	East Africa Coastal	3
29	AUSW	Coastal	Australia-Indonesia Coastal	4
36	TASM	Westerlies	Tasman Sea *	none
37	SPSG	Westerlies	South Pacific Subtropical Gyre	10
38	NPTG	Trades	North Pacific Tropical Gyre	15+3
39	PNEC	Trades	North Pacific Equatorial Countercurrent	2+11
40	PEQD	Trades	Pacific Equatorial Divergence	6
45	CAMR	Coastal	Central American Coastal *	none
49	AUSE	Coastal	East Australian Coastal	2
51	SSTC	Westerlies	South Subtropical Convergence	6

* Data from these provinces are not including in the analysis since there were no morning station on site.

Oceanographic instrumentation and analyses

DMS and DMSP analysis

DMS(P) were analyzed using a purge-and-trap system coupled to sulfur-specific gas chromatography (Shimadzu GC14A) with flame photometric detection (Galí et al. 2013a). For DMS analysis, 3–10 mL of GF/F filtered seawater were sparged 3–6 min with 60 mL min^{-1} of high-purity helium (He). Volatiles were trapped at the temperature of liquid nitrogen and revolatilized in hot water. Sulfur compounds were separated using a packed CarbopackH 60/80 mesh column (Sigma-Aldrich) at 170ºC. The estimated detection limit was 3 pmol, and analytical precision was within 5%. Calibration was performed by injections of known volumes of a gaseous mixture of He and DMS released by a weight-calibrated permeation tube (Dynacal, Valco Instruments Co. Inc.; Simó 1998). For DMSPt analysis, a larger volume of unfiltered sample (30-40 mL) was stored in crimp glass vials after adding two NaOH pellets (45 mg each, 0.2 mol L^{-1} final concentration, pH ≈ 12). The DMSPt + DMS pool was analyzed as evolved DMS after undergoing alkaline hydrolysis for at least 24 h (and always within 3 weeks). The DMSPt concentration was calculated by subtraction of the previously determined DMS concentration.

Dissolved inorganic nutrients (only nitrate + nitrite and phosphate are reported here) were analyzed in a Skalar autoanalyzer with spectrophotometric detection, using standard methods. Depth profiles were measured from bottles sampled with the CTD rosette. The slope of the nutricline was computed for each nutrient, and the ratio of the slopes of nitrate and phosphate was taken as an indicator of the stoichiometry of the diffusive fluxes into the photic layer. Chl*a* concentrations were determined by filtration of 150 mL of seawater through GF/F, extraction in acetone (90% v:v in water, 4ºC, overnight) and measurement in a Turner Designs fluorometer. Picocyanobacteria (Prochlorococcus and Synechococcus) and picoeukaryotic phytoplankton populations were enumerated in live samples by flow cytometry (FACScalibur, Beckton Dickinson;

Marie and Partensky 2006). Microphytoplankton species (dinoflagellates and diatoms) were identified and counted with an inverted microscope in samples preserved with formalin-hexamine (0.4% final concentration) and kept at 4ºC. In order to calculate the zooplankton biomass vertical hauls plankton net of 40 μm were launched overboard and sent to 200 m depth for the integration of the water column. Size-fractionation for 200, 500, 1000, 2000 and 5000 μm fractions were collected using nylon sieves. The samples were dried at 50ºC for a 24 h period, and weighted with a dry-weight accuracy of ±0.001 mg.

For pigment quantification, 2.0 L of seawater were filtered onto 25 mm glass fiber filters (Whatman GF/F) with low vacuum (0.03 MPa) to prevent cells from breaking. Each filter was folded, blotted dry, placed in a criotube and frozen at -80 °C until their analysis by HPLC. For pigment extraction, filters were placed in 10 mL polypropylene tubes with 2.5 mL acetone 90% with trans-ß-apo-8'-carotenal as internal standard and stored at -20 °C. After 24 h, the individual 10 mL tubes were placed in a beaker filled with crunched ice and sonicated. The sonicator tip was slightly introduced into the extract. The sonicator was set at 50% power for 30 s with on: off intervals at 8:2 rate. The tubes were then tightly closed and stored at -20°C After 24 h the extract was cleared with a cleaning system following the procedures of Wright and Jeffrey (1997). A 10 uL pipette tip was clogged with ¼ of a 25 mm GFF filter previously washed with distilled water and dried at 60 °C overnight. This tip was tightly inserted in a 5 mL pipette tip inserted, in turn, in a 10 mL polypropylene centrifuge tube. The extract (including the filter) was transferred into this cleaning column and closed. This system was centrifuged at 3000 rpm for 3 min. A 1 mL of clean extract from the bottom of the centrifuge tube was transferred to an autosampler vial. A large volume (720-840 μL) of extract was injected onto an Agilent 1200 HPLC system and analyzed following the procedure of Latasa (2014).

Maximum quantum efficiency of photosystem II photochemistry (FvFm) was measured using a Fast Repetition Rate fluorometer (FRRf; Fasttracka, Chelsea Marine

Systems). Underway-pumped water flowed through a dark tube for 3 minutes to allow phytoplankton to recover from short-term photoinhibition by opening the photoreaction centers, before entering the dark chamber of the FRRf. The measurement protocol consisted of 100 saturation flashlets (1.3 ms duration, 2.8 ms inter flash delay) followed by 20 relaxation flashlets (separated by 50 ms). Thirty acquisitions were averaged, and the resulting saturation curve was fitted using the version 5 (v5) Matlab software (Laney 2003), which allows correcting for 0.2 mm filtered water blanks and for the instrument's response function. Different physiological parameters (F_0, Fm, ΦPSII = FvFm) were derived from the fluorescence induction curve in PSII and assessed the photosynthetic performance of phytoplankton (Kolber et al. 1998). F_0 was taken as in situ fluorescence. No significant bio-fouling was observed over the circumnavigation.

MLD and SRD calculations

Vertical profiles, 200 m deep, of the morning CTD sampling (10 AM) were used for the calculations of the MLD, which we defined as the depth at which the potential density differs by 0.125 kg m^{-3} from that at a near-surface reference depth. After a thorough inspection of individual CTD profiles in the different oceanic regions of the cruise, 7 m depth was set as the reference depth. To help determine the MLD, the SEASOFT software (Seabird) was first used to calculate seawater potential density and Matlab routines were then used to bin the profiles at 1 m intervals and to compute the MLD calculations.

The station SRD index was estimated using the exponential decay of the daily-averaged surface solar irradiance with depth (z; Vallina and Simó 2007). Surface irradiance (W m^{-2}) was measured continuously by the meteo station on the ship; we averaged it over the 24 hrs previous to sampling. Light extinction coefficients (Kd) used for the calculations were determined from the downward photosynthetically active radiation (PAR) profiles measured with the CTD sensor for the everyday 200 m cast and was calculated as the regres-

sion slope between –ln (PAR(z)) and z, for z comprised within the corresponding daily MLD.

Satellite data

Level-3 data from the Aqua MODIS remote sensing reflectance were downloaded from the Ocean Color website (http://oceancolor.gsfc.nasa.gov). Data corresponded to Chl*a* (443 nm, 480 nm, or 510 nm bands), CDOM (412 nm band) and calcite (590 nm band), corresponding to the reflectance of visible light from coccolithophore cells and detached coccoliths (Holligan et al. 1983; Balch et al. 1991). The concentrations of each variable was derived from the 4 km^2 resolution data that was closest to each sampling station or geographical position of the vessel. When available, the daily product corresponding to the sampling date was used; otherwise we used the nearest 3-day, 8-day or monthly composite, subsequently.

Statistical analyses

Principal component analysis (PCA) was conducted on a correlation matrix composed of 19 variables and 147 data rows (sampling stations). Only primary and methodologically independent variables were included in the PCA. Variables that were continuously recorded (PAR, salinity, SST, wind speed) were averaged over the duration of the stay on station. Before performing the analysis, selected environmental variables were log10-transformed and standardized, in order to normalize the distribution and harmonize differences in units and scales within observations (see selected variables in Table 3).

Results and Discussion

Biogeographical provinces

The 147 stations sampled during the seven-month cruise were located in 15 different Longhurst biogeographical provinces (Figure 1; Table 1). Most of the stations were in

oligotrophic waters and in provinces that fall within the "Trades", the "Westerlies" and the "Coastal" domains. The number of stations per province varied between 1 (BENG) and 25 (SATL). The most visited provinces were SATL, ISSG, NPTG and PNEC (Table 1).

Table 2: Mean and range of the different variables measured on station during the circumnavigational expedition Malaspina 2010.

List of variables used for the PCA analysis	Sources
Latitude	Ship met data
Wind speed	Ship met data
SST	Ship thermosalinometer data
DMS *	Measured: Simó et al.,
DMSP *	Measured: Simó et al.,
Fluorescence *	Measured: Simó et al.,
Fv:Fm *	Measured: Simó et al.,
Mixed Layer Depth *	CTD data; calculations Simó et al.,
Extracted chl-a *	Measured: Estrada et al.,
Total PP *	Measured: Marañón et al.,
Prochlorococcus *	Measured: Agusti et al.,
Synechococcus *	Measured: Agusti et al.,
Picoeukaryotes *	Measured: Agusti et al.,
SRD in the UML *	CTD/Ship met data; calculations Simó et al.,
CDOM satellite *	Satellite: Aqua-MODIS
POC satellite *	Satellite: Aqua-MODIS
Calcite Satellite *	Satellite: Aqua-MODIS
Δ NO3/Δ PO4 *	Measured: Blasco et al.,
Zooplankton total biomass *	Measured: Bode et al.,

* Log transformed and standardized variable.

DMS, DMSP and phytoplankton fluorescence along the circumnavigation: the general picture

Surface DMSP varied between 1.78 nM and 17.65 nM and the average value for the entire cruise was 7.9 nM (Table 2). The highest DMSP concentration was found in the Agulhas Current, in the Western Boundary Current along the eastern coast of South Africa (EAFR; Figure 2A), an oceanic convergence zone that results in the upwelling of cold and nutrient rich water and thus is an area of enhanced primary productivity. High-end DMSP concentrations were also found in the Pacific equatorial upwelling

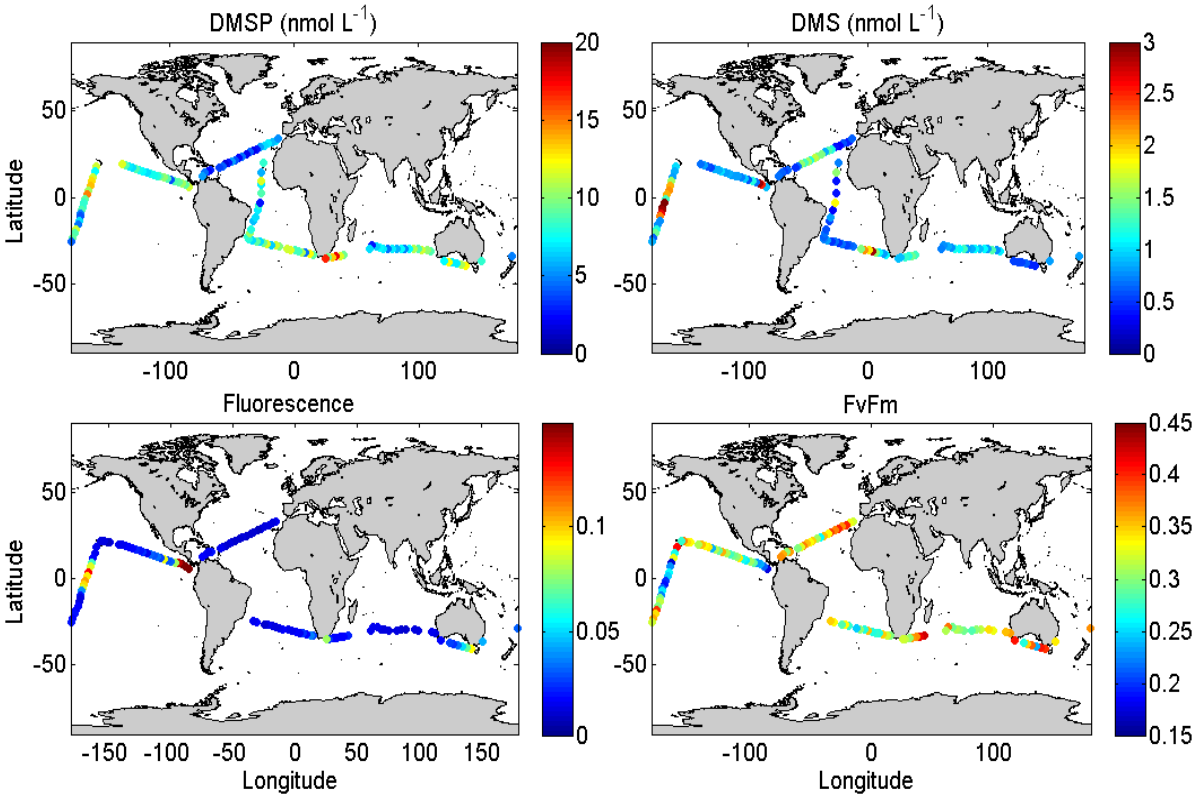

Figure 2: Distribution of DMS(P) and related variables throughout the 147 stations sampled during the circumnavigational expedition Malaspina 2010. (A) DMSP concentration (nmol $^{-1}$); (B) DMS concentration (nmol $^{-1}$); (C) fluorescence from FRRf; note that the parameter Fo (from dark-adapted samples) is used here as a proxy for bulk chlorophyll (chl) and; (D) FvFm from FRRf; note that FvFm is used as a measure for the efficiency of photosystem II.

province (PEQD), a region known to be "high nutrient low chlorophyll" (HNLC), where phytoplankton growth is limited by low iron bioavailability (Martin et al. 1994). Although no taxonomic data were available at the closure of this thesis, the most likely explanation for high DMSP in this region is due to the adaptation skills of small phytoplankton cells (high DMSP producers) to low iron conditions.

DMS varied between 0.34 nM and 3.58 nM across the stations (Table 2). The average concentration for the entire cruise was 1.15 nM, similar to the partial averages in the various open ocean regions explored. This value is significantly lower than the previously reported global annual mean (close to 2 nM; Lana et al. (2011a), reflecting that most stations were in oligotrophic waters (Figure 2B). Similarly to DMSP, higher DMS concentrations were found in PEQD with a maximum value of 3.58 nM, while the lowest value (0.34 nM) was measured in the North Atlantic Gyre (NASE). High concentrations were also seen on two consecutive days in the North Pacific Equatorial Counter-current (PNEC), in the region known as the Costa Rica dome, where a cyclonic eddy is responsible for bringing up colder and nutrient-rich waters close to the surface. Additionally, high DMS levels (3 nM and 8 nM - measured off station using samples supplied by the underway pump of the ship) were observed close to the western coast of South Africa (BENG), where the meteorological and hydrographical conditions create a continuous system that pumps cold, nutrient-rich water to the surface, resulting in an intense phytoplankton growth regardless of the season.

In some of the regions, such as PEQD and BENG, there is agreement between DMSP and DMS concentrations where both increase. However, in other regions such as NATR, there is a clear mismatch, which illustrates the complex dynamics between the two compounds. To investigate the potential drivers of DMS dynamics and its variability, fluorescence data from the FRRf were used as a proxy for bulk Chl*a* (Figure 2C). In the NATR region, lower summer levels of Chl*a* and DMSP co-occurred with moderate concentrations of DMS (Figure 2). This phenomenon, already described for the Sargasso

Sea and named the "summer DMS paradox" (Simó and Pedrós-Alió 1999), results from the taxonomic dependence of DMSP production and the decoupling of the different actors involved in the conversion of DMSP to DMS.

The minimum fluorescence was found in the Pacific Ocean, south of the equatorial upwelling (NPTG; Figure 2C), where the clearest oceanic waters of the circumnavigation were observed (Agustí et al., *in preparation*). High intensity and deep penetration of UV radiation, along with scarce nutrient availability, may be responsible for the low photosynthetic activity in the region. The highest level of fluorescence was measured in nutrient-richer waters in the vicinity of the Costa Rica dome in PNEC. Other fluorescence-rich regions were the Equatorial Pacific upwelling region (PEQD), the Tasman Sea (TASM) and the South African West Coast (BENG; Figure 2C).

FRRf-derived FvFm was used as an indicator of photosystem II efficiency (Figure 2D). The lower the ratio, the less efficient is the phytoplankton community at converting the energy in the photosystem II. This may be interpreted as physiological stress caused by micronutrient scarcity or excess irradiance. The minimum photosynthetic efficiency was found in PEQD (0.17), where the fluorescence reached close to its maximum value (Figure 2C). In this dynamic region, low FvFm values might be indicative of Fe limitation, as suggested by a 12-year study (Behrenfeld et al. 2006). Low FvFm values were also observed in the nutrient rich waters of the Costa Rica dome (PNEC). Since Fe limitation is not known in this region, the most likely factor that caused low FvFm is the shallow MLD (12 m). This would have resulted in high solar radiation exposure for the phytoplankton cells trapped within the upper mixed layer, which would have reduced their PSII efficiency through photoacclimation. In the two aforementioned regions (PEQD, PNEC), it is plausible that low FvFm and relative high DMS are mechanistically linked. Exposure to high SRD, especially of UVR, has been shown to promote DMS production (Galí et al. 2013b). Sunda et al. (2002) suggested that oxidative stressors, such as solar ultraviolet radiation and Fe limitation, increase cellular DMSP

production and/or its lysis to DMS as a way of coping with oxygen radicals. On the other hand, the maximum FvFm (0.42) was found in the Agulhas region (EAFR), where the nutrients are fully replenished and the deep MLD (73 m) results in a low SRD index (59 W m^{-2}). Both nutrient availability and low average sunlight exposure favour a higher efficiency of the PSII.

Short-term DMS(P) variability at stations

Several studies have explored the effects of sunlight exposure and spectral characteristics on DMS(P) metabolism and processes (Archer et al. 2010; Galí et al. 2011, 2013a). We measured DMS(P) and other variables at the same depth (3 m) at different times in the morning (7 AM, 9 AM and 11 AM) while being at stations. This was repeated throughout the circumnavigation cruise (Figure 3A). For most of the expedition, DMSP showed no change or an increase (up to 9 nM) with increasing solar radiation in the course of the morning. The outstanding exceptions were around the Equatorial Pacific upwelling and the NPTG in the vicinity of Hawaii, where decreases of up to 5 nM were observed. Short-term (few hours) DMSP changes can result from various processes such as a physiological response of phytoplankton to light stress, algal biosynthesis and mortality, zooplankton grazing, microbial consumption and bacterial carbon/sulfur demands (Stefels et al. 2007 and references therein). Microbial DMS consumption is inhibited by UV radiation (Slezak et al. 2001; Toole et al. 2006), and it is probably affected by other factors that regulate general bacterial activity, such as temperature or dissolved organic matter availability. Recently, Ruiz-González et al. (2012) reported that under increased UVR exposure, DMSPd-sulfur assimilation was inhibited in heterotrophic bacteria in the oligotrophic Mediterranean Sea. The inhibition of bacterial consumption, therefore, could help explain the increase in DMSP in the morning. However, since we measured DMSPt and this is mostly contributed by DMSPp (probably by 80-90%, Kiene and Slezak 2006), the observed changes in DMSP are thought to be essentially

due to changes in the cellular pool. DMSPp increases must be related to biosynthesis being decoupled from loss through in-cell breakdown, exudation and algal mortality and the opposite must occur for DMSPp decreases. Neither zooplankton biomass nor zooplankton over Chl*a* were higher at the stations where DMSP decreased. However, this was mesozooplankton, and most grazing in the oligotrophic ocean is mediated by microzooplankton (Calbet and Landry 2004), which were not quantified in our study.

DMS is a breakdown product of DMSP metabolism, either in the phytoplankton cell, from where it leaks across membranes, or by the action of bacteria and free enzymes

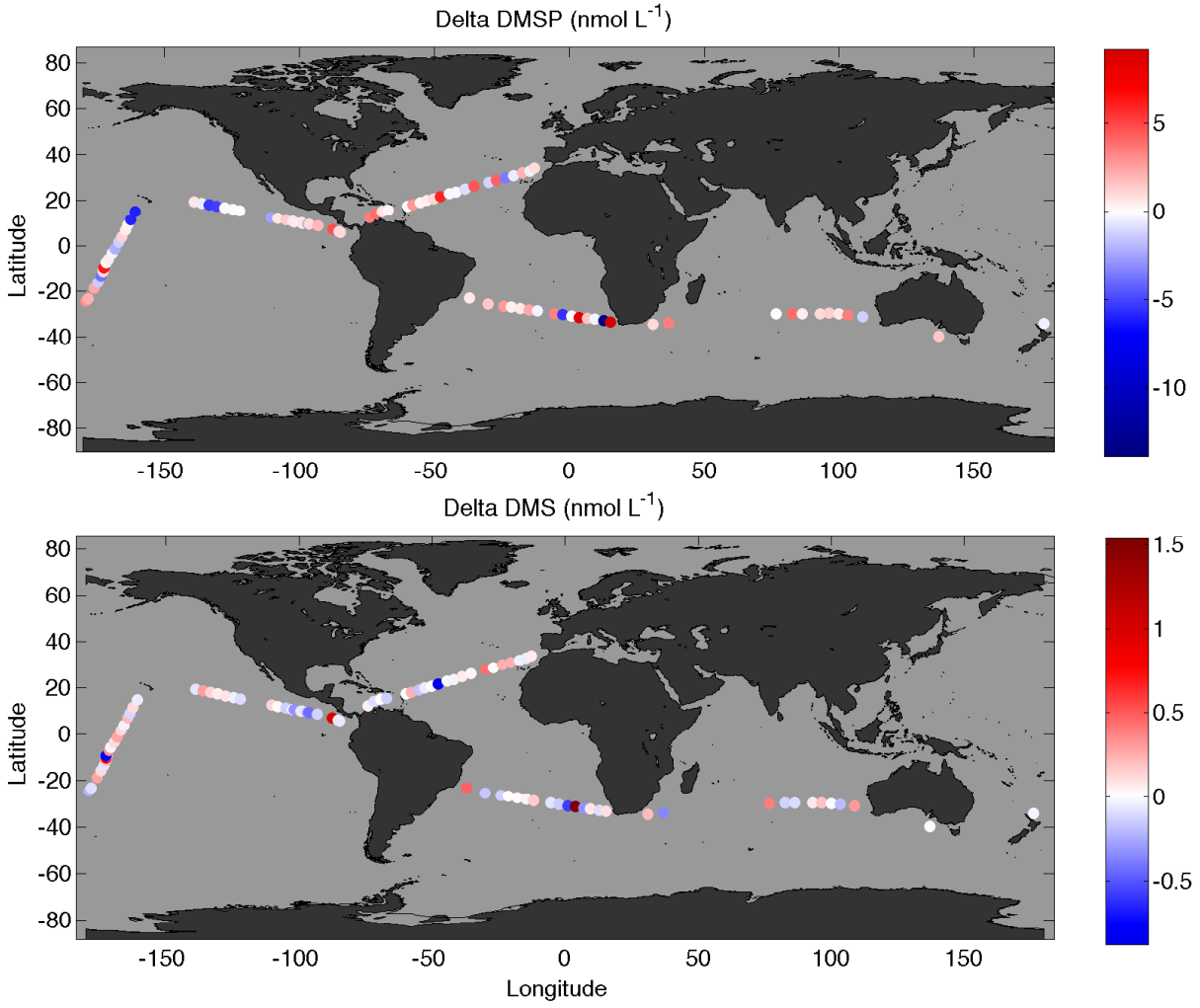

Figure 3: DMS and DMSP delta (nmol $^{-1}$) between 7AM and 9AM using seawater sampled on station from 3 m depth. (A) DMSP (B) DMS. Red color means increase and blue means decrease.

in seawater. Controls on bacterial DMS production from DMSPd are not well understood, and bacterial sulfur requirements are suggested to play a role (Kiene and Linn 2000; Pinhassi et al. 2005). Once produced in seawater, DMS is consumed by heterotrophic bacteria, ventilation and photo-oxidation mediated principally by CDOM. Gross DMS production, microbial DMS consumption and photo-oxidation are all influenced by sunlight in different manners. As a consequence of this complex interplay of actors and environmental factors, differing diel cycle patterns in DMS concentrations have been observed (Royer et al. Ch.4 this thesis), including the absence of any clear pattern (Galí et al. 2013b). In general, DMS is considered to be a buffered variable, for which production and loss processes tend to be in equilibrium (Galí and Simó, submitted). In the present study, changes in DMS between early and late morning were generally small and no clear geographical pattern could be described (Figure 3B).

Geographical variability across oceanographic features

Disentangling the coupling between biological, chemical, hydrographic and optical factors is crucial to understand the dynamics of dimethylated sulfur compounds in the ocean and their role in the global sulfur cycle. Phytoplankton abundance and taxonomic composition, grazing, bacterial activity, photophysiology, nutrient availability and stoichiometry, solar radiation, vertical and horizontal mixing, wind speed, CDOM, etc. are all factors that determine the ultimate distribution of DMS in the surface ocean. Teasing these factors apart and establishing their relative importance is a complex but essential task, if we are to understand and eventually model the occurrence of DMS in the marine environment. In the following sections we will thoroughly examine the variability of DMS(P) along with those of other potentially linked variables (Figure 4). We will also examine the main currents crossed during the navigation and their hydrographic borders, since they portray the movement of different water masses and all the unique physico-chemical characteristics they contain.

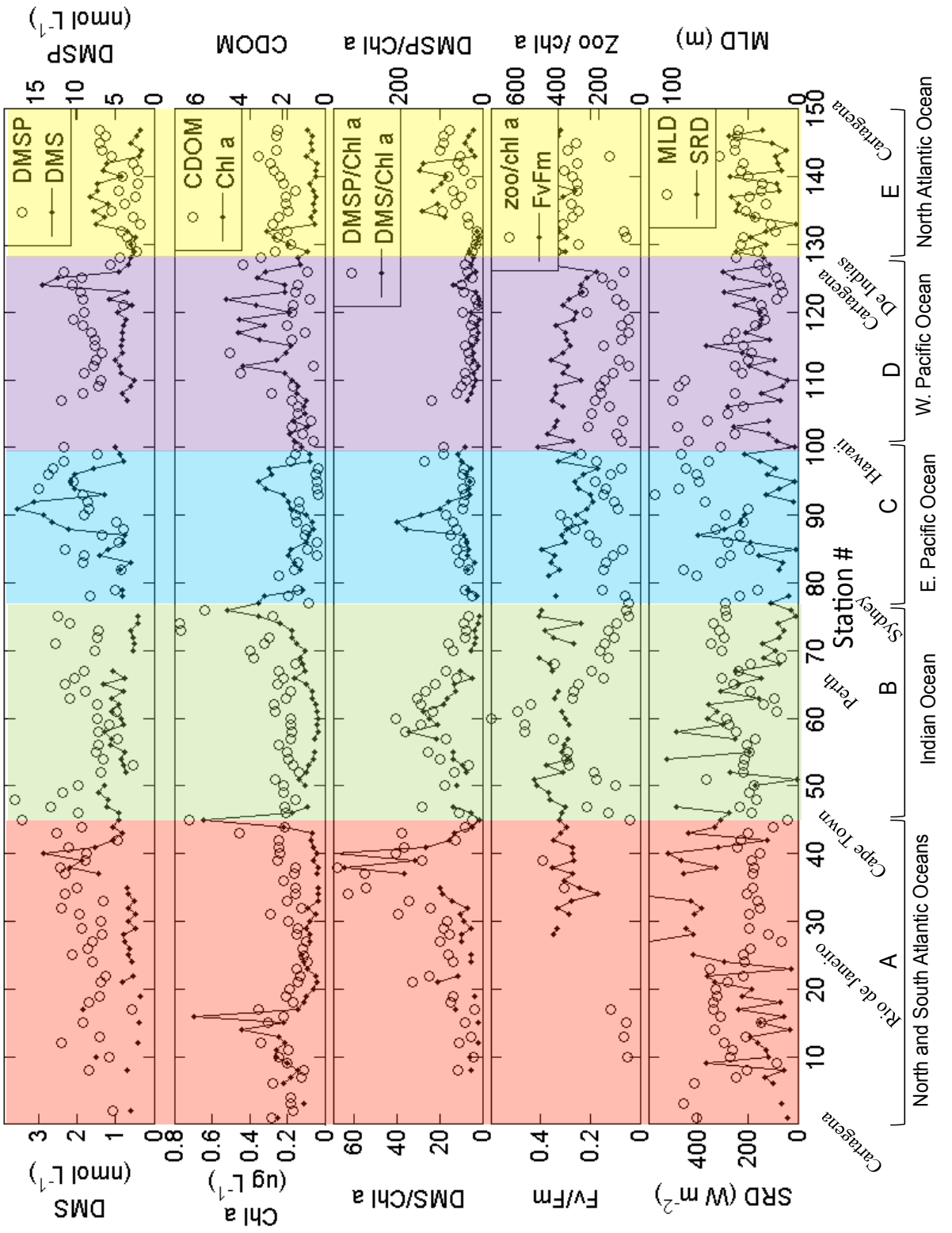

Figure 4: Surface measurements of DMS and DMSP and selected environmental variables throughout stations during the circumnavigational expedition Malaspina 2010. Station number, the port cities and the oceans studied are indicated on the primary x-axis.

North Atlantic Ocean: winter – Leg 1

The meridional Atlantic transect from Cartagena (Spain) to Rio de Janeiro (Brasil) was navigated between 16th of December 2010 and 11th of January 2011. DMS levels were low, with values around 0.5 nM, except for station 10 close to the Equator (WTRA, 1.5 nM). DMSP did not vary much even across the productive waters around the Equator and those of the oligotrophic southern subtropical gyre. Abrupt changes in Chl*a* and CDOM were closely linked to the Equatorial current (stations 15-18) transporting upwelled nutrients that stimulate the flourishing of phytoplankton. Nutrient and Chl*a* poorer waters further south were relatively richer in pigments of dinoflagellates and haptophytes, and photoprotective pigments (Latasa et al., in preparation). This rendered DMSP concentrations similar to those of the productive waters.

South Atlantic Ocean: summer – Leg 2

The eastwards transect between Rio de Janeiro and Cape Town (South Africa) was navigated from 19th of January to 5th of February 2011. DMS concentrations were below 1 nM until the South Atlantic Current (stations 37-40), where it increased from 1.5 to 3 nM. The pigments in these stations showed a clear dominance of markers of *Prochlorococcus* (ratios of divinyl to Chl*a* and zeaxanthin to Chl*a*). This cyanobacterium does not produce DMSP nor DMS, but it may co-occur with small algae that do. DMSP showed moderate concentrations (ca. 10 nM) in the central stations of the transect, those corresponding to the subtropical gyre. There, the DMSP:Chl *a* ratios were very high (>200 nmol/μg) and coincided with an increase in the pigment signature for dinoflagellates (peridinin:Chl *a*), phytoplankters with high intracellular DMSP concentrations and high DMSP:Chl*a* ratios (Stefels et al. 2007). A strong coupling between DMSP:Chl*a* and the solar radiation dose (SRD) index was observed along these two first Atlantic transects (R^2 = 0.55), supporting the hypothetical involvement of intracellular DMSP upregulation on coping with oxidative stress induced by large doses of solar radiation (Sunda et al. 2002). Close to the African continent, in the

Agulhas Current region, Chl*a* levels increased to 0.2 μg L^{-1} while DMSP concentrations remained moderate (ca. 7-9nM). The resulting intermediate DMSP:Chl*a* values (30-50 nmol/μg) are indicative of moderate DMSP producing phytoplankton, albeit pigments did not provide any univocal signature.

Indian Ocean, Australia and Tasman Sea: fall – Legs 3-4

The eastwards transect across the subtropical Indian Ocean (ca. 30ºS), from Cape Town to Perth (Australia) to Sydney, was navigated between 13th of February and 28th of March 2011. Upon departure, the coastal province EAFR, largely influenced by the Agulhas Current, had the highest levels of Chl*a* of the entire navigation (>0.6 μg L^{-1}). Although they were accompanied with some of the highest DMSP concentrations (>16 nM), the low DMSP:Chl*a* (<30 nmol/μg), low DMS, and high relative concentrations of fucoxanthin, all indicate that diatoms dominated in these high-Chl*a* region. Diatoms are known to grow better under nutrient rich coastal regions but generally prevent the build-up of DMS, because they do not possess DMSP lyases (Stefels et al. 2007). Very high levels of CDOM were also observed, which may have further contributed to keep DMS levels low by favouring photo-oxidation. Moving eastwards into Chl*a* poorer waters of the Indian Ocean (stations 47-50), the dominance of dinoflagellates maintained high DMSP levels (with DMSP:Chl*a* values around 100) and increased DMS concentrations.

As we entered the central gyre (the ultraoligotrophic province ISSG, stations 52 to 64), DMS and DMSP concentrations were low, but their ratios to Chl*a* showed a remarkable increase. Dinoflagellates and haptophytes increased to the Chl*a*-poor waters as indicated by the relative contributions of peridinin and 19'-hexanoyloxyfucoxanthin. Also diadinoxanthin, a photoprotective pigment of eukaryotes, increased in the gyre. This is consistent with the fact that, as shown in Figure 4, the mixed layer SRD index (which results from combining surface irradiance, water transparency and vertical mixing depth) showed a hump shape at the centre of the gyre transect, parallel to the shapes of the DMSP:Chl*a* and DMS:Chl*a*

ratios. Another variable that followed the same pattern was the mesozooplankton:Chl*a* ratio (Figure 4). This may have contributed further to the increase of DMS:Chl*a*, since grazing on DMSP-containing algae favours DMS production (Stefels et al. 2007).

Further east, DMSP concentrations along the transect south of Australia were moderate, and DMS concentrations were low. This coincided with deeper mixing and lower SRD. In the Tasman Sea, Chl*a* increased remarkably while none of the sulfur compounds did; CDOM reached its circumnavigation maximum, which may have helped keep DMS concentrations low. Consistently, the contributions of photoprotective pigments decreased. Overall, the full transect from Cape Town to Sydney showed a negative relationship between Chl*a* and DMS ($R^2 = 0.4$, $p < 0.001$). This reflects the dependence of DMSP and DMS production on the taxonomic composition and physiology of the phytoplankton assemblages (Keller 1989) and that (Lana et al. 2012b) already reported widespread negative correlation between DMS and Chl*a* over seasons in most of the global oceans within the 20º-40º latitudinal bands in both hemispheres. A negative correlation was also observed between DMS:Chl*a* and MLD ($R^2 = 0.56$, $p < 0.001$). They may be related through nutrient availability, since rich DMSP-producers that are dominated by small algal cells with high surface-to-volume ratio are better adapted to low nutrient conditions.

Hence, shallow mixing promotes phytoplankton succession to DMSP producing species (Simó and Pedrós-Alió 1999). They may also be related through exposure to solar radiation, since exposure is larger in shallow upper mixed layers. Indeed, a positive relationship was seen between DMSP:Chl*a* and SRD ($R^2 = 0.57$, $p < 0.001$) and DMS: Chl*a* and SRD ($R^2 = 0.53$, $p < 0.001$). This is in agreement with the hypothesis of Sunda et al. (2002), who suggested that stressors such as light and nutrient limitation might favour cellular DMS(P) production. A positive relationship to SRD ($R^2 = 0.52$, $p < 0.001$) was also observed for DMS and is in agreement with Vallina and Simó (2007), who showed a significant positive correlation between DMS and SRD over most of the global ocean.

In summary, the central gyre waters of the transect were characterised by physiological stresses associated with shallow mixed layers, lack of nutrients and high UVR, resulting in lower Chl*a* and higher DMS, DMS:Chl*a* and DMSP:Chl*a*. On the contrary, the coastal domain waters of the transect was characterised by high biomass (high Chl*a* and high CDOM) accompanied with higher DMSP but moderate-to-low DMS, and low DMSP:Chl*a* and DMS:Chl*a* ratios. This points to dominance of diatom cells in nutrient rich waters. Following the nomenclature proposed by Toole and Siegel (2004), the central Indian Ocean gyre would correspond to the 'stress-forced regime' where the DMS stock is driven by physico-chemical stressors more than by total productivity, while coastal domain waters belong in the productivity-driven eutrophic regime.

West and Equatorial Pacific Ocean: summer – Leg 5

A northwards latitudinal transect from Sydney and Auckland (New Zealand) to Hawaii was navigated between 17th of April and 7th of May 2011. The Eastern Pacific Ocean is characterized by warm, well-stratified and nutrient-poor waters separated by a major upwelling plume of nutrient-rich water near the Equator extending from roughly the dateline to the eastern boundary. Upon departure, the crossing of the Eastern Australian Current (station 78; AUSE) was characterised by DMS levels below average (ca. 0.7 nM) and DMSP and Chl*a* similar to the cruise average (8 nM and 0.13 μg L^{-1}, respectively). DMS concentrations were much lower than previously reported in the region (up to 12 nM; Walker et al. 2000). Deep mixing (MLD of 80 m), low SRD and high efficiency of phytoplankton PSII are all plausible causes for the low DMS.

Shortly after entering the Subtropical Gyre (from station 82 on; SPSG), we encountered Chl*a* richer waters (0.2 μg L^{-1}) near Tonga (stations 84-86). According to their pigment signature, these were characterized by likely dominance of *Synechococcus* over dinoflagellates and haptophytes. Microscopic observations, however, revealed abundant cells of *Scrippsiella*, a DMSP-producing dinoflagellate. Both DMSP and DMS were higher

in these waters than in the immediate surroundings, although their ratios to Chl*a* were not. Further north, near the border between SPSG and PEQD, we crossed some of the most transparent waters in the world's oceans (Agustí et al., in preparation). These waters (stations 88-92) were characterised by high DMS concentrations co-occurring with low DMSP (5 nM) and Chl*a* (0.1 μg L^{-1}). DMS levels increased from 0.7 nM to 3.6 nM, the latter being the highest DMS value recorded at stations during the entire circumnavigation. Other variables that increased were DMS:Chl*a*, the DMS:DMSP ratio (data not shown), the zoo:Chl*a* ratio, and, in some stations, SRD (see Figure 4). Microscopic counts and pigment analysis identified small dinoflagellates and haptophytes, and larger contributions of photoprotective pigments. Given the low productivity in the region, grazing and solar radiation exposure acting on DMSP producing phytoplankton, plus reduced photolysis due to low CDOM, seem the most plausible explanations for the high DMS concentrations.

Physical borders or frontal zones among provinces where physico-chemical conditions change more or less abruptly also seemed to have played a role while cruising from PEQD to PNEC (stations 94 to 97). A second DMS peak, lower in concentration (2.1 nM), occurred with a close coupling to increased Chl*a* (0.3 μg L^{-1}) and DMSP (ca. 12 nM), deeper MLD (c.a. 100 m), increased zooplankton biomass (60 mg/m^3), increased nutrients (phosphate, silicate and nitrite-nitrate; data not shown), and reduced CDOM (Figure 4). In this case, SRD was low throughout the DMS peak and hence could not act as a stressor for DMS production. Indeed, photoprotective pigments were less important. Large abundances of haptophytes, and particularly small coccolithophores, were recorded. Therefore, higher productivity, a DMSP-producing assemblage, potentially active grazing, and low CDOM-mediated photolysis could be responsible for high DMS levels.

It is also important to mention that for both DMS peaks described above, the FvFm values (ca. 0.2) were amongst the lowest recorded during the circumnavigation. This may seem contradictory with high phytoplankton biomass and primary production. The reason is to be found in the low Fe concentrations of the region, which have been previously reported

to reduce FvFm (Behrenfeld et al. 2006). Lack of Fe to fully utilise nutrients in photosynthesis is a cause of oxidative stress, and has been related to enhance DMS production (Bucciarelli et al. 2013).

Finally, the transition from PNEC to NPTG (stations 97 to 100) was the last hydrographical border crossed before reaching Hawaii, and coincided with a decrease in DMS (1.5 nM to 0.8 nM) occurring along with low Chl*a*, high DMSP:Chl*a*, slightly higher CDOM and the maintenance of the deep MLD.

Overall, in this transect across the Pacific Ocean, DMS was positively correlated to Chl*a* (R^2 = 0.8; n=15; high DMS and high Chl*a* values excluded). DMSP also showed positive correlation to Chl*a*, yet weaker (R^2 = 0.5; n=15). In spite of this apparently simple emergent pattern, the different water masses behaved differently as for the potential factors controlling DMS. For instance, the two DMS peaks occurring in the vicinity of the equator were fairly similar in terms of concentrations but the interplay between the actors was very different. This is a good example of the complexity of the DMS cycle and the interplay among controlling processes.

East Pacific Ocean: summer – Leg 6

The transect from Hawaii to Cartagena de Indias (Colombia) was navigated between the 14th of May and the 10th of June 2011. At first, we crossed oligotrophic waters of the NPTG province, with moderate DMSP and low DMS concentrations. DMSP reached ca. 12 nM at station 107, going down to ca. 6.5 nM close to the border of PNEC (station 114; Figure 4). Later on, it increased from ca. 7 nM to 10 nM (station 119). DMS remained low (c.a. 0.6 nM) despite DMSP variability and the Chl*a* peaks at stations 112, 117, 119 and 121 (ca. 0.4 μg L^{-1}). Unfortunately, we do not have information on the phytoplankton present in surface waters along most of this transect. Severely anoxic waters occurred at a depth of 200-400 m, but there were no identifiable effects at surface. Microscopic counts identified coccolithophores at the stations. An important increase in DMS

(to ca. 3 nM) occurred at stations 124 and 125, under the influence of a large cyclonic eddy known as the Costa Rica Dome, which brings colder and nutrient-richer waters close to the surface. The DMS peak co-occurred with DMSP values of about 10 nM and high Chl*a* concentrations. MLD were the shallowest of the circumnavigation (12 m) and the SRD (240 Wm^{-2}) was well above average. Consequently, FvFm was low (0.2). Oxidative stress, therefore, may have acted in accordance to high productivity to render high DMS concentrations. The phytoplankton was dominated by diatoms, with high abundances of *Thalassiossira* sp., a genus that contains moderate DMSP producers (Keller 1989). The occurrence of abundant faecal pellets in microscopic preparations also pointed at grazing as an extra source of DMS.

After the crossing of the dome, the ship steamed through the warm waters of the North Equatorial Current where the levels of DMS decreased drastically to values below 1 nM although DMSP (11 nM) and Chl*a* (0.3 µg L^{-1}) remained high and FvFm was still low (0.17 – lowest value measured during the entire cruise). A potential explanation for the low DMS values might be related to the very high CDOM levels and moderate SRD, which would have favoured photo-oxidation.

North Atlantic Ocean: summer – Leg 7

The last transect of the circumnavigation, from Cartagena de Indias to Cartagena (Spain) across the subtropical North Atlantic, was navigated between 19th of June and 14th of July 2011. Here we explored 3 different biogeographical provinces: CARB, NATR and NASE. In CARB (stations 127 to 131) Chl*a*, DMS(P) were low while CDOM varied from very high to moderate. At the border going into the NATR province, Chl*a* increased from 0.1 to 0.3 μg L^{-1} (station 132) and decreased dramatically to 0.07 μg L^{-1}at station 134 to stay low across the central oligotrophic gyre until station 142. There was a presence of coccolithophores, but nano- and microplankton counts were very low. DMSP remained below average with a mean value of 3.2 nM. These values contrasted with those of DMS,

which were in anti-phase with Chl*a*: they increased to 1.5 nM upon entrance into the gyre. This region is in the vicinity of the Sargasso Sea, which has been the object of several studies discussing the effect of high SRD on DMS cycle under oligotrophic conditions (e.g., Toole and Siegel 2004; Vallina and Simó 2007; Vallina et al. 2008). The well-known summer DMS paradox (Simó and Pedrós-Alió 1999) was named after realisation that there was a time lag among the annual maxima of Chl*a* (spring), DMSP (early summer) and DMS (late summer). This is rather counter intuitive given the strong bond between the three compounds, and was the start of the study of the influence of solar radiation exposure and vertical mixing on DMS dynamics. Since we visited the region only in summer, we cannot prove or reject the hypothesis that solar radiation drives most of DMS seasonality, but still it is interesting to see that, under relatively high summer SRD, DMS levels were high despite relatively low DMSP and low Chl*a*.

The idea that solar radiation is the base for the DMS paradox has been challenged (Belviso and Caniaux 2009; Polimene et al. 2011), but no solid experimental proof for an alternative mechanistic explanation of the summer paradox has been given. One hypothesis is that phosphorus limitation is actually causing the summer DMS build-up. Nutrient concentrations were measured during the circumnavigation; however, methodological limitations impede the use of surface concentrations because they are too noisy at most stations. To get an idea about the limiting nutrient, we computed the ratio of the slopes of nitrate and phosphate across their respective nutriclines (data not shown). Slope ratios >16 indicate P deficiency, whereas slope ratios <16 indicate N deficiency. In a large portion of the transect, from station 127 to station 148, the slope ratio was indeed >16 (around 20), indicative of phosphorus limitation. However, no direct link can be made between this feature and DMS concentration, because the breaking points for DMS increase and decrease were stations 134 and 142, respectively, and do not correspond to any change in the nutrient slope ratios.

The last region visited was the North Atlantic Subtropical Gyre (NASE) where DMS stayed at ca 1.3 nM and decreased at station 143 (0.3 nM) in parallel to the DMS: Chl*a*. Conversely, DMSP was low (3 nM) and increased to ca. 7 nM from station 143, in parallel to DMSP:Chl*a*, indicating an increase in number of DMSP-richer cells. These changes with respect to the central gyre were accompanied by a deepening of MLD from 20-30 m to 40-50 m. Accordingly, SRD decreased and FvFm remained high (average 0.35), reflecting the growth of phytoplankton cells under low stress conditions. As in previous transects, high CDOM levels may have prevented the build-up of DMS.

Global multivariant relationships

Having explored the possible drivers of DMS and DMSP distribution along each individual transect, here we investigate whether there are common controlling factors for the entire circumnavigation. The complete dataset was subjected to PCA analysis to quantify the proximity (distance) between the variables (Figure 5). The 2-D PCA uses a total of 19 variables for 147 stations and explains a total of 52% of the variability while the 3-D PCA explains 64% (data not shown). The first component of the PCA explains 34 % of the variability and is mostly driven by biological productivity (green arrow), which contains 10 biological variables. The second component explains 18% of the variability and is contributed by DMS and mostly physical and optical variables. The third one explains 12% of the variability (data not shown).

DMSP, the precursor of DMS synthesized by certain groups of phytoplankton algae is partially related to general biological productivity but deviates slightly from most of the productivity indicators, including Chl*a*. It is oppositely aligned with the nutrient slope ratio (deltaN/deltaP), and similarly with FvFm. The information we can extract is that DMSP is obviously linked to phytoplankton abundance but, because both taxonomy and physiology affect it, it tends to increase in response to high light or nutrient deficiency. Remarkably, DMSP tends to abound where there is a deficiency in N supply. This is consistent with

the suggestion that its role as osmolyte in the algal cell can be fulfilled by N-containing osmolytes, which are energetically cheaper to synthesize, when N is not limiting (Simó 2001). Some authors have suggested that smaller eukaryotic phytoplankton carry most of the DMSP (Belviso et al. 1993), but the PCA shows little alignment of DMSP and picoeukaryote counts. Indeed, pigment analyses and microscopic counts confirmed abundance of dinoflagellates and haptophytes.

DMS shows a 90º angle with the productivity component and thus does not contribute to its variance, confirming that it is largely independent of phytoplankton biomass and productivity in the oligotrophic ocean. DMS is mostly aligned positively with SRD and negatively with CDOM, FvFm, MLD and wind speed. These results support the prominent role of solar radiation and vertical mixing as a drivers of DMS dynamics (Simó and Pedrós-Alió 1999; Vallina and Simó 2007; Galí et al. 2013a), the importance of CDOM as photosynthetizer (Toole et al. 2003) and the impact of nutrient

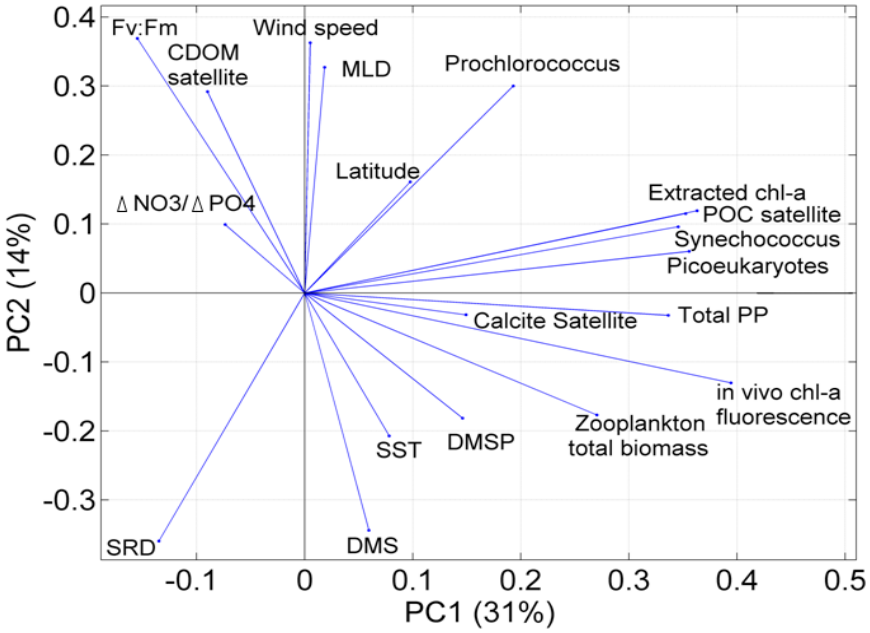

Figure 5: Two-dimensional PCA analysis using averaged station data (147 stations) for 19 variables (see Table 2 for data sources). Note that the selected environmental variables (* in Table 2) were first log transformed and standardized.

and light stress on phytoplankton physiology resulting in DMS production. DMS does not align with satellite-derived calcite. Even though coccolitophore blooms are hotspots for DMS concentration and emission (Malin et al. 1993), they occur mainly at latitudes higher that those visited by our expedition, and low abundances of coccolithophores do not render a traceable signature from satellite. DMS does not align either with ^{14}C-based measurements of primary production. Miles et al. (2012) recently reported positive correlation between these two variables across the Atlantic, but their statistical analysis included vertical profiles. Finally, DMS did not correlate with zooplankton biomass in the upper 200 m, despite the fact that zooplankton is a known DMS source (Dacey and Wakeham 1986). In these waters dominated by small phytoplankton, mesozooplankton do not seem to play a major role in producing DMS, probably because the main herbivores in these waters are microzooplankton (Calbet and Landry 2004).

The PCA also shows the role of wind speed as the main actor in DMS ventilation to the atmosphere. The PCA also depicts positive correlation between FvFm and MLD (confirmed by direct Pearson's correlation, $R^2 = 0.44$) and negative correlation between FvFm and SRD ($R^2 = 0.40$), showing the importance of solar radiation within the MLD on the photophysiology of phytoplankton cells.

As a whole, the PCA analysis reveals interesting features of the influencing factors DMS(P) highlighting a striking difference between the factors that play a role in the distribution of DMS and that of its precursor DMSP (Figure 5). In summary, if we consider the two major axes driving surface dimethylated sulfur as phytoplankton productivity, on the one hand, and solar radiation, nutrients and photophysiology on the other hand, DMSP and DMS fall between the two, being DMSP closer to the former and DMS closer to the latter. In other words, DMSP conversion to DMS and subsequent DMS loss process make it deviate from productivity (Vila-Costa et al. 2008). We should note, however, that these results apply to the low latitude, mainly oligotrophic oceans, and inclusion of higher latitude, more eutrophic waters would probably change the general picture.

Conclusions

DMS distribution and dynamics have proven difficult to fully comprehend because of the numerous variables involved in its cycle and their complex interplay. A lot of progress has been made in terms of understanding the physiological, ecological, bacterial and chemical drivers behind DMS cycling in planktonic food webs (e.g., Stefels et al. 2007 and reference therein). Nonetheless, there is no numerical parameterization yet that can successfully predict DMS distribution across all oceanographic conditions. The question of how climate and climatic variables affect DMS concentrations in the surface ocean still remains largely unanswered. Our results, over 32,000 NM of the world's oceans, provide some insights in specific biogeographical regions and help understand the interplay between variables. We observed that the abiotic factors related to physical and optical properties of the upper mixed layer estimate DMS variability better than phytoplankton production and biomass. Conversely, DMSP concentrations can be better predicted from phytoplankton taxonomic composition, particularly if it is tuned using physiological indicators. Physiological stresses associated with shallow mixed layers and solar radiation are the first order determinant of biological production of DMS, indicating that DMS cycling in the vast oceanic deserts is fundamentally different from that in productive regions where phytoplankton biomass and taxonomy provide the conditions for elevated DMS concentrations.

Acknowledgements

Data can be requested to Sarah-Jeanne Royer (royer@icm.csic.es). The authors wish to acknowledge the assistance and cooperation of the marine technicians (UTM) and crew aboard the R/V Hesperides, as well as the leadership of C.M. Duarte. We would also like to thank the NASA Aqua-MODIS project team (http://modis.gsfc.nasa.gov/). Ocean Color data used in this study (http://oceancolor.gsfc.nasa.gov/) were produced by the Aqua-MODIS project. This research has been funded by the Spanish Ministry of Economy and Competitiveness through projects Malaspina Expedition 2010 (INGENIO 2010 CONSOLIDER program, CSD2008-00077) and PEGASO (CTM2012-37615) and through a PhD scholarship to S.J.R. Support was also provided by the U.S. National Science Foundation (grants 0851472 and 1143709). The Indian Institute of Tropical Meteorology is funded by the Ministry of Earth Sciences, Government of India.

References

Andreae, M. O., and P. J. Crutzen. 1997. Atmospheric Aerosols: Biogeochemical Sources and Role in Atmospheric Chemistry. Science (80-.). **276**: 1052–1058.

Aranami, K., and S. Tsunogai. 2004. Seasonal and regional comparison of oceanic and atmospheric dimethylsulfide in the northern North Pacific : Dilution effects on its concentration during winter. J. Geophys. Res. **109**: 1–15.

Archer, S. D., M. Ragni, R. Webster, R. L. Airs, and R. J. Geider. 2010. Dimethylsulfoniopropionate and dimethylsulfide production in response to photoinhibition in Emiliania huxleyi. Limnol. Oceanogr. **55**: 1579–1589.

Balch, M., P. M. Holligan, S. G. Ackleson, and K. J. Voss. 1991. Biological and optical properties of mesoscale coccolithophore blooms in the Gulf of Maine. Limnol. Oceanogr. **36**: 629–643.

Behrenfeld, M. J., K. Worthington, R. M. Sherrell, F. P. Chavez, P. Strutton, M. McPhaden, and D. M. Shea. 2006. Controls on tropical Pacific Ocean productivity revealed through nutrient stress diagnostics. Nature **442**: 1025–8.

Bell, T. G., A. J. Poulton, and G. Malin. 2010. Strong linkages between dimethylsulphoniopropionate (DMSP) and phytoplankton community physiology in a large subtropical and tropical Atlantic Ocean data set. Global Biogeochem. Cycles **24**: n/a–n/a.

Belviso, S., P. Buat-mrnard, J. Putaud, B. C. Nguyen, and H. Claustre. 1993. Size distribution of dimethylsulfoniopropionate (DMSP) in areas of the tropical northeastern Atlantic Ocean and the Mediterranean Sea. Mar. Chem. **44**: 55–71.

Belviso, S., and G. Caniaux. 2009. A new assessment in North Atlantic waters of the relationship between DMS concentration and the upper mixed layer solar radiation dose. Global Biogeochem. Cycles **23**: 1–12.

Belviso, S., I. Masotti, A. Tagliabue, L. Bopp, P. Brockmann, C. Fichot, G. Caniaux, L. Prieur, J. Ras, J. Uitz, H. Loisel, D. Dessailly, S. Alvain, N. Kasamatsu, and M. Fukuchi. 2012. DMS dynamics in the most oligotrophic subtropical zones of the global ocean. Biogeochemistry **110**: 215–241.

Belviso, S., C. Moulin, L. Bopp, and J. Stefels. 2004. Assessment of a global climatology of oceanic dimethylsulfide (DMS) concentrations based on SeaWiFS imagery (1998 – 2001). Can. J. Fish. Aquat. Sci. **61**: 804–816.

Belviso, S., A. Sciandra, and C. Copin-Montégut. 2003. Mesoscale features of surface water DMSP and DMS concentrations in the Atlantic Ocean off Morocco and in the Mediterranean Sea. Deep Sea Res. Part I Oceanogr. Res. Pap. **50**: 543–555.

Bopp, L., O. Aumont, S. Belviso, and S. Blain. 2008. Modelling the effect of iron fertilization on dimethylsulphide emissions in the Southern Ocean. Deep Sea Res. Part II Top. Stud. Oceanogr. **55**: 901–912.

Bouillon, R.-C., and W. L. Miller. 2005. Photodegradation of dimethyl sulfide (DMS) in natural waters: laboratory assessment of the nitrate-photolysis-induced DMS oxidation. Environ. Sci. Technol. **39**: 9471–7.

Bucciarelli, E., C. Ridame, W. G. Sunda, C. Dimier-Hugueney, M. Cheize, S. Belviso, and N. Carolina. 2013. Increased intracellular concentrations of DMSP and DMSO in iron-limited oceanic phytoplankton Thalassiosira oceanica and Trichodesmium erythraeum. Limnol. Oceanogr. **58**: 1667–1679.

Bucciarelli, E., W. G. Sunda, N. O. Service, P. I. Road, and N. Carolina. 2003. Influence of CO2, nitrate, phosphate, and silicate limitation on intracellular dimethylsulfoniopropionate in batch cultures of the coastal diatom Thalassiosira pseudonana. Limnol. Oceanogr. **48**: 2256–2265.

Calbet, A., and M. R. Landry. 2004. Phytoplankton growth, microzooplankton grazing, and carbon cycling in marine systems. Limnol. Oceanogr. **49**: 51–57.

Chu, S., S. Elliott, and M. E. Maltrud. 2003. Global eddy permitting simulations of surface ocean nitrogen, iron, sulfur cycling. Chemosphere **50**: 223–35.

Le Clainche, Y., M. Levasseur, A. Vézina, J. W. H. Dacey, and F. J. Saucier. 2004. Behaviour of the ocean DMS (P) pools in the Sargasso Sea viewed in a coupled physical – biogeochemical ocean model. Can. J. Fish. Aquat. Sci. **803**: 788–803.

Clainche, Y. Le, A. Vézina, M. Levasseur, R. A. Cropp, J. R. Gunson, S. M. Vallina, M. Vogt, C. Lancelot, J. I. Allen, S. D. Archer, L. Bopp, C. Deal, S. Elliott, M. Jin, G. Malin, V. Schoemann, R. Simó, K. D. Six, and J. Stefels. 2010. A first appraisal of prognostic ocean DMS models and prospects for their use in climate models. Global Biogeochem. Cycles **24**: 1–13.

Cropp, R. a. 2004. Modeling dimethylsulphide production in the upper ocean. Global Biogeochem. Cycles **18**: GB3005.

Dacey, J. W. H., and S. G. Wakeham. 1986. Oceanic Dimethylsulfide: Production During Zooplankton Grazing on Phytoplankton. Science (80-.). **233**, doi:10.1126/science.233.4770.1314

DeBose, J. L., S. C. Lema, and G. A. Nevitt. 2008. Dimethylsulfoniopropionate as a foraging cue for reef fishes. Science (80-.). **319**: 1356.

Elliott, S. 2009. Dependence of DMS global sea□air flux distribution on transfer velocity and concentration field type. J. Geophys. Res. **114**: G02001.

Endres, C. S., and K. J. Lohmann. 2012. Perception of dimethyl sulfide (DMS) by loggerhead sea turtles: a possible mechanism for locating high-productivity oceanic regions for foraging. J. Exp. Biol. **215**: 3535–8.

Gabric, A. J., P. a. Matrai, R. P. R. P. Kiene, R. Cropp, J. W. H. J. W. H. Dacey, G. R. G. R. DiTullio, R. G. R. G. Najjar, R. Simó, D. a. Toole, D. a. DelValle, and D. Slezak. 2008. Factors determining the vertical profile of dimethylsulfide in the Sargasso Sea during summer. Deep Sea Res. Part II Top. Stud. Oceanogr. **55**: 1505–1518.

Galí, M., C. Ruiz-González, T. Lefort, J. M. Gasol, C. Cardelús, C. Romera-Castillo, and R. Simó. 2013a. Spectral irradiance dependence of sunlight effects on plankton dimethylsulfide production. Limnol. Oceanogr. **58**: 489–504.

Galí, M., V. Saló, R. Almeda, A. Calbet, and R. Simó. 2011. Stimulation of gross dimethylsulfide (DMS) production by solar radiation. Geophys. Res. Lett. **38**: 1–5.

Galí, M., R. Simó, M. Vila-Costa, C. Ruiz-González, J. M. Gasol, and P. Matrai. 2013b. Diel patterns of oceanic dimethylsulfide (DMS) cycling: Microbial and physical drivers. Global Biogeochem. Cycles **27**: 1–17.
Garren, M., K. Son, J.-B. Raina, R. Rusconi, F. Menolascina, O. H. Shapiro, J. Tout, D. G. Bourne, J. R. Seymour, and R. Stocker. 2013. A bacterial pathogen uses dimethylsulfoniopropionate as a cue to target heat-stressed corals. Int. Soc. Microb. Ecol. 1–9.

Holligan, P. M., M. Viollier, D. S. Harbour, P. C. Camus, and M. Philippe. 1983. Satellite and ship studies of coccolithophore production along a continental shelf. Nature **304**.

Kameyama, S., H. Tanimoto, S. Inomata, H. Yoshikawa-Inoue, U. Tsunogai, A. Tsuda, M. Uematsu, M. Ishii, D. Sasano, K. Suzuki, and Y. Nosaka. 2013. Strong relationship between dimethylsulfide and net community production in the western subarctic Pacific. Geophys. Res. Lett. **40**: 3986–3990.

Keller, M. D. 1989. Dimethyl sulfide production in marine phytoplankton., p. 167–182. *In* W.J. Saltzman, E. S. and Cooper [ed.], Biogenic sulfur in the environment. ACS symposium Series.

Kettle, A. J., M. O. Andreae, D. Amouroux, T. W. Andreae, T. S. Bates, H. B, R. Boniforti, M. A. J. Curran, G. R. Ditullio, G. Helas, G. B. Jones, M. D. Keller, R. P. Kiene, C. Leck, M. Levasseur, G. Malin, M. Maspero, P. Matrai, A. R. Mctaggart, N. Mihalopoulos, B. C. Nguyen, A. Novo, J. P. Putaud, S. Rapsomanikis, G. Roberts, G. Schebeske, S. Sharma, R. Sim, R. Staubes, S. Turner, G. Uher, W. Boothbay, and M. Planck. 1999. A global database of sea surface dimethylsulfide (DMS) measurements and a procedure to predict sea surface DMS as a function of latitude , longitude , and month TM grazing. Global Biogeochem. Cycles **13**: 399–444.

Kiene, R. P., and L. J. Linn. 2000. Distribution and turnover of dissolved DMSP and its relationship with bacterial production and dimethylsulfide in the Gulf of Mexico. Limnol. Oceanogr. **45**: 849–861.

Kiene, R. P., L. J. Linn, and J. a. Bruton. 2000. New and important roles for DMSP in marine microbial communities. J. Sea Res. **43**: 209–224.

Kiene, R. P., L. J. Linn, J. González, M. a Moran, and J. a Bruton. 1999. Dimethylsulfoniopropionate and methanethiol are important precursors of methionine and protein-sulfur in marine bacterioplankton. Appl. Environ. Microbiol. **65**: 4549–58.

Kiene, R. P., and D. Slezak. 2006. Low dissolved DMSP concentrations in seawater revealed by small volume gravity filtration and dialysis sampling. Limnol. Oceanogr. Methods **4**: 80–95.

Kloster, S., J. Feichter, K. D. Six, P. Stier, and P. Wetzel. 2006. Biogeosciences DMS cycle in the marine ocean-atmosphere system – a global model study. Biogeosciences **3**: 29–51.

Kolber, Z., O. Prasil, and P. P. G. Falkowski. 1998. Measurements of variable chlorophyll fluorescence using fast repetition rate techniques: defining methodology and experimental protocols. Biochim. Biophys. Acta **1367**: 88–106.

Kowalewsky, S., M. Dambach, B. Mauck, and G. Dehnhardt. 2006. High olfactory sensitivity for dimethylsulphide in harbour seals. Biol. Lett. **2**: 106–9.

Lana, A., R. Simó, S. M. Vallina, and J. Dachs. 2012a. Potential for a biogenic influence on cloud microphysics over the ocean: a correlation study with satellite-derived data. Atmos. Chem. Phys. **12**: 7977–7993.

Lana, A., R. Simó, S. M. Vallina, and J. Dachs. 2012b. Re-examination of global emerging patterns of ocean DMS concentration. Biogeochemistry **110**: 173–182.

Laney, S. R. 2003. Assessing the error in photosynthetic properties determined by fast repetition rate fluorometry. Limnol. Oceanogr. **48**: 2234–2242.

Latasa, M. 2014. A simple method to increase sensitivity for RP-HPLC phytoplankton pigment analysis. Limnol. Oceanogr. Methods **12**: 46–53.

Longhurst, A. 1998. Ecological geography of the sea Longhurst, Academy Pr.
Malin, G., and G. O. Kirst. 1997. Algal production of dimethyl sulfide and its atmospheric role. J. Phycol. **33**: 889–896.

Malin, G., S. Turner, S. L. Peter, P. M. Holligan, and D. S. Harbour. 1993. Dimethyisulphide and dimethyisulphoniopropionate in the Northeast Atlantic during the summer coccolithophore bloom. Deep Sea Res. Part I Oceanogr. Res. Pap. **40**: 1487–1508.

Marie, D., and F. Partensky. 2006. Analyse de micro-organismes marins, p. 211–233. *In* La cytométrie en flux.

Martin, J. H., K. H. Coale, K. S. Johnson, S. E. Fitzwater, R. M. Gordon, S. Tanner, C. N. Hunter, V. A. Elrod, and J. L. Nowicki. 1994. Testing the iron hypothesis in ecosystems of the equatorial Pacific Ocean. Nature 123–129.

Miles, C. J., T. G. Bell, and P. Suntharalingam. 2012. Investigating the inter-relationships between water attenuated irradiance, primary production and DMS(P). Biogeochemistry **110**: 201–213.

Pinhassi, J., R. Simo, M. Gonza, M. Vila, L. Alonso-sa, R. P. Kiene, M. A. Moran, and C. Pedro. 2005. Dimethylsulfoniopropionate Turnover Is Linked to the Composition and Dynamics of the Bacterioplankton Assemblage during a Microcosm Phytoplankton Bloom. Appl. Environ. Microbiol. **71**: 7650–7660.

Polimene, L., S. D. Archer, M. Butenschön, and J. I. Allen. 2011. A mechanistic explanation of the Sargasso Sea DMS "summer paradox." Biogeochemistry **110**: 243–255.

Royer, S.-J., M. Galí, E. S. Saltzman, C. A. McCormick, T. G. Bell, and R. Simó. 2014. Development and validation of a shipboard system for measuring high-resolution vertical profiles of aqueous dimethylsulfide concentrations using chemical ionisation mass spectrometry. Environ. Chem. 1–9.

Ruiz-González, C., M. Galí, E. Sintes, G. J. Herndl, J. M. Gasol, and R. Simó. 2012. Sunlight effects on the Osmotrophic uptake of DMSP-sulfur and leucine by polar phytoplankton. PLoS One **7**: 1–14.

Seymour, J. R., R. Simó, T. Ahmed, and R. Stocker. 2010. Chemoattraction to dimethylsulfoniopropionate throughout the marine microbial food web. Science (80-.). **329**: 342–5.

Simó, R. 1998. Trace chromatographic analysis of dimethyl sulfoxide and related methylated sulfur compounds in natural waters. J. Chromatogr. **807**: 151–64.

Simó, R. 2001. Production of atmospheric sulfur by oceanic plankton: biogeochemical, ecological and evolutionary links. Trends Ecol. Evol. **16**: 287–294.

Simó, R. 2004. From cells to globe : approaching the dynamics of DMS (P) in the ocean at multiple scales. Can. J. Fish. Aquat. Sci. **684**: 673–684.

Simó, R., and C. Pedrós-Alió. 1999. Role of vertical mixing in controlling the oceanic production of dimethyl sulphide. Nature **402**.

Simó, R., M. Vila-Costa, L. Alonso-Sáez, C. Cardelús, Ò. Guadayol, E. Vázquez-Domínguez, and J. Gasol. 2009. Annual DMSP contribution to S and C fluxes through phytoplankton and bacterioplankton in a NW Mediterranean coastal site. Aquat. Microb. Ecol. **57**: 43–55.

Six, K. D., and E. Maier-Reimer. 2006. What controls the oceanic dimethylsulfide (DMS) cycle? A modeling approach. Global Biogeochem. Cycles **20**: 1–12.

Slezak, D., A. Brugger, and G. J. Herndl. 2001. Impact of solar radiation on the biological removal of dimethylsulfoniopropionate and dimethylsulfide in marine surface waters. Aquat. Microb. Ecol. **25**: 87–97.

Stefels, J. 2000. Physiological aspects of the production and conversion of DMSP in marine algae and higher plants. J. Sea Res. **43**: 183–197.

Stefels, J., and W. H. M. van Boekel. 1993. Production of DMS from dissolved DMSP in axenic cultures of the marine phytoplankton species Phaeocystis sp. Mar. Ecol. Prog. Ser. **97**: 11–18..

Stefels, J., M. Steinke, S. Turner, G. Malin, and S. Belviso. 2007. Review: Environmental constraints on the production and removal of the climatically active gas dimethylsulphide (DMS) and implications for ecosystem modelling. Biogeochemistry **83**: 245–275.

Sunda, W., D. J. Kieber, R. P. Kiene, and S. Huntsman. 2002. An antioxidant function for DMSP and DMS in marine algae. Nature **418**: 317–20.

Toole, D. A., D. J. Kieber, R. P. Kiene, D. A. Siegel, B. Norman, and N. B. Nelson. 2003. Photolysis and the dimethylsulfide (DMS) summer paradox in the Sargasso Sea. Limnol. Oceanogr. **48**: 1088–1100.

Toole, D. a., and D. A. Siegel. 2004. Light-driven cycling of dimethylsulfide (DMS) in the Sargasso Sea: Closing the loop. Geophys. Res. Lett. **31**: 5–8.

Toole, D. a., D. Slezak, R. P. Kiene, D. J. Kieber, and D. a. Siegel. 2006. Effects of solar radiation on dimethylsulfide cycling in the western Atlantic Ocean. Deep Sea Res. Part I Oceanogr. Res. Pap. **53**: 136–153.

Vallina, S. M., and R. Simó. 2007. Strong relationship between DMS and the solar radiation dose over the global surface ocean. Science (80-.). **315**: 506–8.

Vallina, S. M., R. Simó, T. R. Anderson, A. J. Gabric, R. Cropp, and J. M. Pacheco. 2008. A dynamic model of oceanic sulfur (DMOS) applied to the Sargasso Sea: Simulating the dimethylsulfide (DMS) summer paradox. J. Geophys. Res. **113**: 1–23.

Vallina, S. M., R. Simó, and M. Manizza. 2007. Weak response of oceanic dimethylsulfide to upper mixing sholaing induced by global warming. Proc. Natl. Acad. Sci. **104**: 16004–16009.

Vila-Costa, M., R. P. Kiene, and R. Simó. 2008. Seasonal variability of the dynamics of dimethylated sulfur compounds in a coastal northwest Mediterranean site. Limnol. Oceanogr. **53**: 198–211.

Vila-Costa, M., R. Simó, H. Harada, J. M. Gasol, D. Slezak, and R. P. Kiene. 2006. Dimethylsulfoniopropionate uptake by marine phytoplankton. Science **314**: 652–4.

Vogt, M., S. M. Vallina, E. T. Buitenhuis, L. Bopp, and C. Le Quéré. 2010. Simulating dimethylsulphide seasonality with the Dynamic Green Ocean Model PlankTOM5. J. Geophys. Res. **115**: C06021.

Walker, C. ., M. . Harvey, S. . Bury, and F. . Chang. 2000. Biological and physical controls on dissolved dimethylsulfide over the north-eastern continental shelf of New Zealand. J. Sea Res. **43**: 253–264.

Wright, K. L. B., L. Pichegru, and P. G. Ryan. 2011. Penguins are attracted to dimethyl sulphide at sea. J. Exp. Biol. **214**: 2509–11.

Wright, S. W., S. W. Jeffrey, and R. F. C. Mantoura. 1997. Guidelines for collecting and pigment analysis of field samples, p. 429–445. *In* Phytoplankton Pigments in Oceanography: Guidelines to Modern Methods.

Summary of Results

Chapter 1 presented photophysiological community-level responses of plankton to light in the short-term (minutes) in the Western Mediterranean Sea and in the Canadian Arctic. Seawater samples from different depths (surface and ca. 35 m) were incubated under PAR-only and FULL light (UV-Inclusive) irradiances. The kinetics of the fluorescence quantum yield of PSII (ΦPSII) was measured as a proxy for phytoplankton photosynthesis efficiency using a Fast Repetition Rate fluorometer (FRRf). Incubation-induced changes in ΦPSII were different depending on the radiation regimes, the depth and the sampling region. Exposure to near-surface irradiance resulted in photodamage (photoinhibition) in all experiments, regardless of the phytoplankton assemblage composition and irradiance levels. For deep samples, exposure to FULL and PAR produced lower ΦPSII values compared to surface samples. Following early strong photoinhibition (ca. 30 minutes), quasi steady state was observed in both light treatments. Mediterranean experiments showed similar photosynthetic responses under PAR and FULL treatments. Arctic experiments depicted little effects of PAR and slight-to-moderate photoinhibiton under FULL light exposure. DMSP concentration generally showed no net change or a slight upregulation in the Mediterranean under PAR, and no net upregulation under FULL sunlight, while DMS concentration showed a consistent increase and on occasions UV enhancement. In the Arctic, we found contrasting responses, with no clear relationship to photoinhibition patterns, including PAR- or UVR-enhanced or suppressed DMSP and DMS production. This is attributed to the heterogeneous set of Arctic samples in terms of photoacclimation and phytoplankton composition.

In order to further assess the effect of cumulative response to short-term varying light conditions at the community level, in situ incubation experiments were conducted in the Western Mediterranean Sea and have been described in **Chapter 2.** The results of UV-transparent bottles incubated at three different depths and on a vertically moving basket across the same depth range helped us understand the impact of vertical mixing and changing solar irradiance on DMS(P) variability in the MLD. Our results

showed that dynamic light exposure caused a subtle disruption of the photoinhibition and photoacclimation processes associated with UVR, which slightly alleviated bacterial photoinhibition but did not favor primary production. Gross DMS production also decreased sharply with depth in parallel to shortwave UVR, and displayed a dose-dependent response that mixing did not significantly disrupt.

This far, observations were made with seawater enclosed in transparent vessels and incubated over time. We wanted to know whether these mechanistic observations have a translation into phytoplankton photophysiology indicators and dimethylated sulfur concentrations in the real environment. In order to be able to resolve the fine scale structure of the water column along with fine changes across time, a sampling and analytical system was developed for shipboard measurements of high-resolution vertical profiles of DMS and photophysiological variables. This has been presented in **Chapter 3**. The high-resolution system consists of a tube attached to a CTD with a peristaltic pump on deck that delivers seawater to a membrane equilibrator and atmospheric pressure chemical ionization mass spectrometer (Eq-APCIMS). This allows profiling DMS concentrations to a depth of 50 m, with a depth resolution of 1.3-2 m and a detection limit of nearly 0.1 nmol L^{-1}. The seawater is also plumbed to allow parallel operation of additional continuous instruments, and simultaneous collection of discrete samples for complementary analyses. A valve alternates delivery of seawater from the vertical profiler and the ship's underway intake, thereby providing high-resolution measurements in both the vertical and horizontal dimensions. Inter-calibration tests conducted on various cruises in the Mediterranean Sea, Atlantic, Indian, and Pacific Oceans show good agreement between the Eq-APCIMS measurements and purge and trap gas chromatography with flame photometric detection (GC-FPD) and demonstrate that the delivery of seawater from the underway pump did not significantly affect endogenous DMS concentrations. High-resolution vertical profiles and near surface underway measurements of DMS demonstrate that Eq-APCIMS is a valuable new tool to describe short-term DMS

variability and its relationship to other physical and biogeochemical parameters.

This analytical system was applied in two Lagrangian cruises conducted in the Western Mediterranean. The studies aimed at investigating the ecosystem level dynamics of DMS over diel, weekly and seasonal time scales, in coupling with meterorological forcing and phytoplankton photophysiology. Results have bee fully reported and discussed in **Chapter 4.** Briefly, in September 2011, surface DMS concentrations showed a remarkable coupling with atmospheric physical forcing, with accumulation in sunny days and substantial loss by ventilation and vertical mixing during the course of a windstorm. The data also showed consistent 24 h periodicity, with daytime increase and nighttime decrease. This diel oscillation was initially lost after the windstorm, but recovered in a few sunny days. Diel oscillation in May 2012 had the opposite sign: daytime decrease and nighttime increase. In both cases, inflection points occurred around dawn and dusk, coinciding with inflection points for fluorescence markers of phytoplankton photoacclimation. These results suggest that a photo-biological clock drives DMS cycling in the upper mixed layer. Finally implementation of measurements into a numerical 1D model revealed that net biological DMS production occurs around the hours of maximum insolation.

To further describe the very fine scale distribution of DMS in the surface ocean and understand its relationship to other physical and biogeochemical parameters, the Eq-APCIMS was taken on a 7-month circumnavigation cruise across the tropical and subtropical oceans.

Chapter 5 explained the association of the variability length scale of DMS to physical and biological drivers within specific biogeographical regions. The analysis revealed that much of the variability in DMS concentrations occurs at scales between 15 km and 50 km, that is, at the lower edge of mesoscale dynamics, decreasing with latitude and productivity. DMS variability was also found to be more commonly related to that of phytoplankton-related variables than to that of physical variables. Unlike phytoplankton physiological data, DMS did not show any universal diel pattern when using the normalized

solar zenith angle as a proxy for solar time across latitudes and seasons. The study should help better design sampling and computing schemes aimed at mapping surface DMS and phytoplankton distributions, taking into account latitude and productivity.

During the same circumnavigation cruise, daily DMS measurements were taken at sampling stations along with many other variables. This provided a unique data set that we used to explore the factors and actors potentially driving DMS distribution in the surface ocean.

Chapter 6 showed the highest DMS concentrations were observed in productive regions characterized by upwelling hydrographic structures: the Agulhas Current in the South Atlantic, the Equatorial currents and the Costa Rica Dome in the Pacific. No significant paired correlations were obtained for the complete dataset but relations between DMS and MLD, SRD index in the upper mixed layer, Chl*a* and chromophoric dissolved organic matter (CDOM) were observed in some of the biogeochemical provinces. DMS and DMSP generally increased where pigments revealed relatively high abundances of dinoflagellates and haptophytes, or with photoprotection. Principal component analysis (PCA) using data from all regions showed that while DMSP is more closely related to the biological components of the pelagic ecosystem, DMS aligns positively with SRD and negatively with CDOM, MLD and the performance of photosystem II (FvFm), thus stressing the importance of the physico-chemical setting in driving DMS variability in the open ocean.

General Discussion

Overview

This thesis presents an integrated vision of biological, physical and chemical variables influencing oceanic DMS production under different spatio-temporal regimes (scales). Adding to the well documented complexity of DMS dynamics, the present work confirmed the presence of important variability in DMS(P) concentrations across a vast panoply of oceanic regimes and temporal scales. Beyond describing the natural variability, the central aim of the thesis was to determine the variability of change in DMS and parallel environmental factors as a function of the spatial and temporal resolution. The results tell us that DMS is strongly influenced by biological and physical variables but the weight of their influence will depend on the environmental conditions that are affected by the geographical location and the time of the year (seasons). The resolution of the data collection is also an important factor to consider in order to elucidate the individual effect of the multiple variables affecting DMS(P) cycling.

Scale characterization

From the previous chapters we can undoubtedly affirm that environmental conditions and the scale and resolution at which the data are presented have an impact on the conclusions drawn on DMS(P) cycling. To be able to understand, and even predict, the dynamics of DMS successfully along with its production and consumption processes, several questions need to be answered. First, key factors that play an important role and influence on DMS dynamics need to be clearly defined and brought down to the relevant details. Second, the biological and non-biological pathways (direct or indirect) that link DMS to key factors need to be identified. Third, the weight that each factor plays in DMS dynamics needs to be elucidated. As mentioned previously, solving the complexity of DMS accumulation in the surface ocean does not solely rely on the knowledge about the key players but depends on the environmental forcing factors that also impact on DMS emissions and its relationship to climate.

The 'environmental forcing factors' concept refers to the measurable or predictable physico-chemical variables that drive the action of the actors in any time frame, by initiating, enhancing, limiting, or suppressing it. Amongst the possible forcing factors, solar irradiance reaching the earth's surface at a given geographical position is responsible for dictating the length of the day (day/night fluctuation) as well as the changes in season. Meteorological conditions also play an important temporal role scaling from sporadic short-term events (i.e. tides, storms) to long-term overturning events (i.e. El Niño, yearly). Environmental forcing factors can be used as dividers for drawing borders amongst the different temporal scales, which can be interpreted as short and long-term scales including the: - minute - hour - day - week - month - season - year and inter-annual scales.

The scale of variability does not only include the temporal dimension but also spatial, which are not necessarily mutually exclusive. The spatial scale can be represented by the following divisions: - global - oceanic biomes - Longhurst provinces - mesoscale and sub-mesoscale, - microscale and the vertical dimension that is represented by the variability within the water column. Once the key players and the temporal/ spatial scale of variability are clearly identified, one needs to establish which of these variables will be more critically shaping the DMS(P) cycle. The aim of the thesis was to understand the processes that control the oceanic DMS concentrations and the links associated to phytoplankton physiology and other abiotic and biotic variables through different temporal and spatial scales.

In **Chapter 1**, we explored the short-term response (temporal scale - minutes) of the microplankton community under changing light conditions. We tried detailing the very fine and fast response at the local community level following light exposure with and without UVR through experiments conducted in polar and sub-tropical environments. **Chapter 2** assesses the cumulative response at the community level of short-term light changes through vertical mixing. The physiological response following variable light

exposure is described with a "slower" temporal scale where samples were measured at lower frequency over a longer period of time resulting in the measurement of the cumulative response rather than punctual transition measurements. An extra dimension is included, the vertical dimension, introducing an additional level of complexity where changing light irradiance is applied to the surface samples by moving them up and down in the mixing layer. These first two chapters take a closer look to the fast biological response of phytoplankton cells following induced stress, and hence this places the studies at the fastest level on the temporal scale. The spatial scale is represented here by the use of two contrasting environments (Mediterranean and Arctic) in **Chapter 1** and using the vertical column in the Mediterranean Sea in **Chapter 2**.

Chapter 3 consists of a methodology paper describing the development of a technique to measure DMS continuously at high frequency in surface waters and across the upper water column. This technique helped achieve the objectives of **Chapters 4 and 5**. **Chapter 4** shows the role of solar radiation on daily and seasonal (summer and spring) cycles, in addition to the impact of a meteorological forcing events (storm) on the DMS dynamic over a few days. This permitted the assessment of several forcing factors and the responses of the ecosystem dynamics in the vertical dimension over daily, sub-weekly and seasonal time scales.

Chapters 5 and 6 mainly address the broad spatial scale since they belong to a circumnavigation cruise where the tropical and sub-tropical oceans were surveyed. **Chapter 5** explores the spatial dimension at the meso and sub-mesoscale levels given the availability of high-resolution measurements, and reports DMS variability length scales along with those of proxies of phytoplankton biomass and physiology and those of physical variables. **Chapter 6** explores daily data of DMS and several bio-physico-chemical variables along the circumnavigation, and, for the sake of facilitating interpretation, groups the data using the biogeographic province classification (Longhurst, 1995). The most productive regions in terms of DMS were in the vicinity

of highly productive upwelling regions such as the Benguela current, the Equatorial Pacific and the Costa Rica Dome. We used principal component analysis (PCA) to show that DMSP is more closely related to the biological productivity component, while DMS is better explained by the solar radiation dose index, the depth of the mixed layer, the physiological state of phytoplankton (as represented by FvFm), and the abundance of the DMS photolysis sensitizer coloured dissolved organic matter (CDOM).

Factors regulating DMS cycling

In this section we evaluate how environmental factors and the interplay between them modulate DMS dynamics. For the sake of representing the main controlling factors as a whole, an overview scheme of the principal environmental forcing factors influencing the DMS(P) cycle in a spatio-temporal context is shown in Figure 1. Here, sunlight plays a role at short and long-term temporal scales driving the daily and seasonal cycles, while the meteorological events (clouds, winds) influence at the very short (passage of a cloud, minutes to hours) and moderate (sub-weekly passage of storms) temporal scales to very long (interannual, decadal) overturning events (such as El Niño). The latter might also have an influence on DMS variability, but they have not been examined here. The Earth in Figure 1 represents the spatial scale ranging from local to multi-regional to global studies. The vertical scale also contributes to the spatial scale and is represented by the 3D vision of the water column. The inter-play between the three main players, namely physics, chemistry and biology is distinct across latitudes and seasons, influencing and shaping the DMS(P) cycle in different ways.

The microscale picture of DMS production is far more complex than the schematic representation in Figure 1 and involves multiple interactions between bacteria, phytoplankton cells of varied taxonomical, morphological and physiological characteristics, and grazers (Stocker et al., 2008). In fact, from the results of this thesis it is not possible to conclude whether one actor is more important in shaping DMS than the

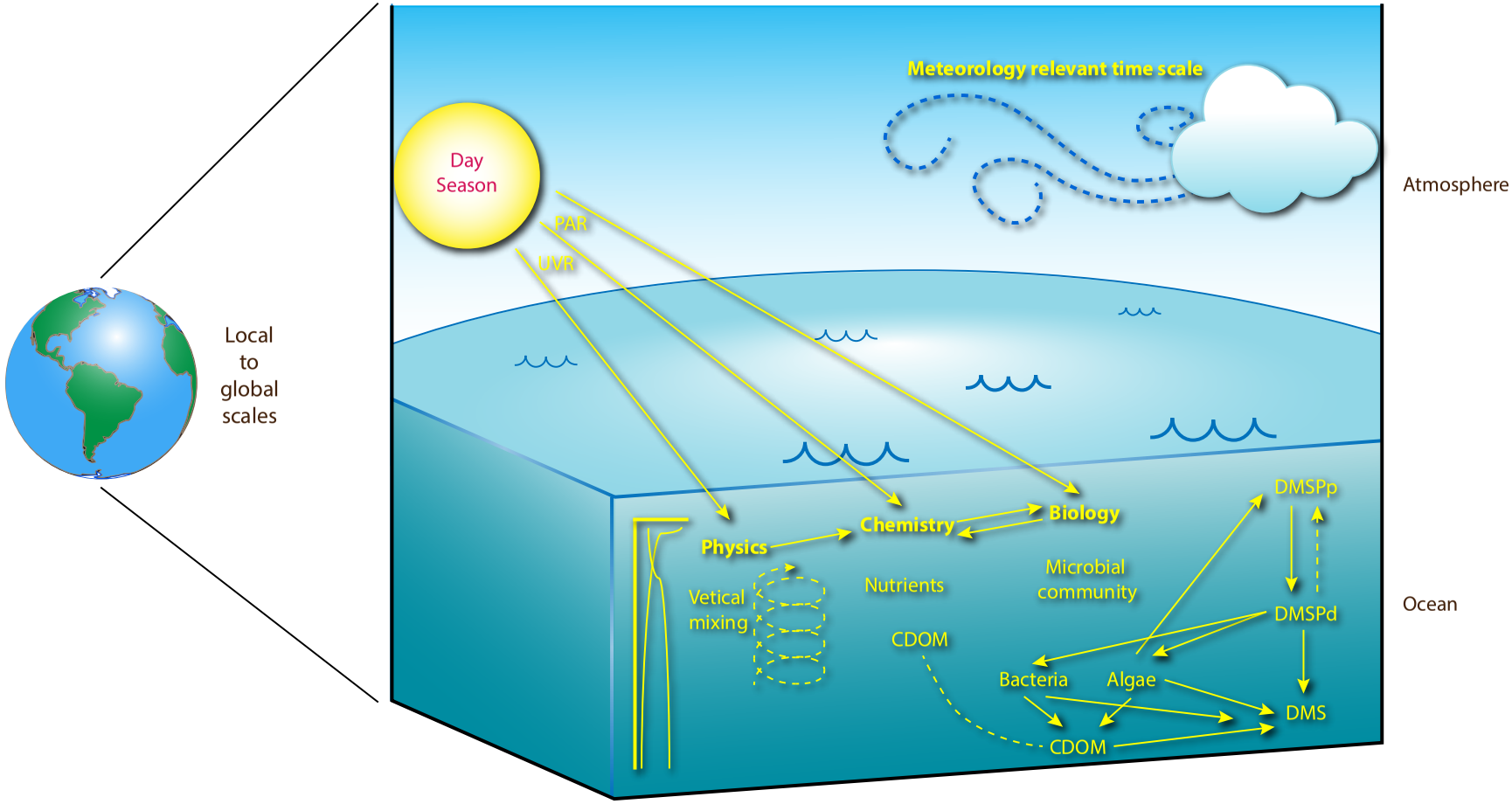

Figure 1: Overview of the principal environmental forcing factors and spatio-temporal scales influencing the DMS(P) cycle. The sun plays a role at short and long-term temporal scales driving the daily and seasonal cycles while the meteorological events (cloud-wind) influence at the very short to moderate temporal scales (e.g., passage of clouds in minutes-hours or passage of storm in quasi-weekly cycles). The Earth represents the spatial scale ranging from local to multi-regional to global studies. The vertical scale is represented by the 3D vision of the water column and the physical profiles. The inter-play between the three main players, physics, chemistry and biology, is distinct across latitudes and seasons, influencing and shaping the DMS(P) cycle in different ways. Note that the arrows do not mean fluxes but influence.

other at a global scale because all of them are closely related. From what we have learned in the different sections of the thesis, certain bio-physico-chemical variables impact on DMS cycle under certain environmental conditions and specific spatio-temporal scales. In addition to such a broad range of possible environmental drivers affecting DMS cycling, the inherent variability of DMS processes adds some more layers of complexity. However, this inherent variability is palpable only if the right measurement frequency is used and is easily hidden or misinterpreted if the instrumentation does not permit to isolate the signal or does not permit to reveal the real trend. Apart from the frequency, the scale measured also need to be defined and taken into account. As shown in this work, studies conducted over short spatio-temporal scale (**Chapters 1, 2 and 4**) are not applicable for global conclusions and vice-versa where a circumnavigation cruise (large spatial scale; **Chapters 5 and 6**) cannot discern the short-scale local processes (e.g., the diel cycles). For these reasons, one should not exclude the presence of a pattern because of its absence in the dataset.

Under specific scales, abiotically/biologically driven DMS(P) patterns can be present or "hidden". A good example is given in **Chapter 5** where the data measured at very high frequency do not exhibit any clear diel pattern even though the need of required instrumentation was satisfied. One of the most plausible reason for this "absence" of diel trends in the dataset is the "moving" spatial scale imposed over the temporal one, where the ship was cruising through different water masses preventing the proper assessment of the local dynamics. To try and remove the spatial effect from the temporal trends, the data were homogenized into a common diel cycle using the normalized solar zenith angle (SZAn). Despite the strong diel cycles observed in the Mediterranean cruises presented in **Chapter 4** and in previous studies of DMS production and consumption rates (Galí et al. 2013), no common diel DMS pattern was observed during the circumnavigation expedition. Since the circumnavigation dataset comes from a combination of diverse communities and physico-chemical conditions across seasons and provinces it resulted

in the absence of a single emerging diel pattern in surface DMS concentration. This illustrates the need of resolving the effect of the temporal and spatial variability when assessing the importance of the drivers on DMS cycles as they may have an influence but their impact is hidden behind stronger forces.

Additionally, physico-chemical forcing factors potentially operate at all stages of the DMS(P) cycle and some act in contrary ways. For instance, opposite diel patterns in surface DMS concentrations were observed during the two Lagrangian studies in the Mediterranean (**Chapter 4**). In September 2011, DMS increased with cumulative exposure to solar radiation and decreased over night, consistent with sunlight-mediated stimulation of DMS production and inhibition of DMS consumption. In May, surface DMS increased at night and decreased during the day because strong photolysis overcame the photobiological stimulation of DMS production.

Another example of factors impacting the DMS dynamics, which was not measured in this thesis, is the effect of bacterial DNA damage by UV-B, which may reduce both DMS production and consumption (Ruiz-Gonzalez et al., 2013). Depending on the environmental conditions, nutrient limitations can also impact in opposite ways on the release of DMSP by the phytoplankton cells (Sunda et al., 2002; Stefels et al., 2007). The involvement of the plankton diversity and ecophysiology, interacting with sunlight, hydrodynamics, nutrients, organic matter and wind speed illustrates the complexity of the biogeochemical DMS cycle, which becomes even more complex when integrating the several spatio-temporal scales.

DMS variability across temporal and spatial scales

DMS has been the subject of hundreds of studies over the past 30 years. Examining the DMS data from these past studies, the scientific community agrees that there is a homogeneous variability range among latitudes. Indeed, DMS concentrations can be buffered over diel cycles (Gabric et al., 2008; Simó et al., unpublished results) and DMS variability increases

when influenced by the dynamics of the ecosystems. The variability can occur on weekly time scales that can be driven by more stochastic events (i.e. high winds) than seawater physical, chemical and biological characteristics (as revealed by Lagrangian observations: Gabric et al., 2008; Levasseur et al., 2006; Simó & Pedrós-Alió, 1999). The largest amplitude in DMS concentrations has been reported on a seasonal scale, which is wider than the inter-annual variability scale. Here we dress a portrait of the variation (change) factors of DMS encountered across various spatial and temporal scales covered during the several oceanographic studies presented in this work (Table 1).

Table 1: Variation factors (max/min) of DMS concentration encountered across spatial and temporal scales over several oceanographic studies.

Thesis Sections	Temporal Scale	Spatial Scale	Longhurst provinces	Variation factor
Chapter 1	Short-term exposure to UV (min)	Local	Westerlies: MEDI	1,1
			Polar: ARCT	1.5-5.8
Chapter 2	Short-term exposure to variable light (hr)	Local	Westerlies: MEDI	1,1
Chapter 4	Daily	Local	Westerlies: MEDI	1.5-1.8
	Sub-weekly			2,3
	Seasonally			5,16
Chapter 5	Minutes to days	Sub-mesoscale to region	Trades: SATL	68
			Trades: ISSG	8
			Trades: NPTG	59
			Trades: PNEC	52
			Trades: PEQD	29
			Westerlies: TASM	9
			Westerlies: SPSG	96
			Westerlies: SSTC	4
			Coastal: EAFR	15
			Coastal: AUSW	11
			Coastal: AUSE	6
			Global	97
Chapter 6	Multi-daily (2 to 25 days)	Region	Trades: SATL	9,9
			Trades: ISSG	2,2
			Trades: NPTG	2,4
			Trades: PNEC	7,0
			Trades: PEQD	3,1
			Westerlies: TASM	-
			Westerlies: SPSG	5,1
			Westerlies: SSTC	2,2
			Coastal: EAFR	1,4
			Coastal: AUSW	2,2
			Coastal: AUSE	1,8
			Global	10,7

In view of the reported complexity, it can be seen that common trends among experiments will not be easily found. Through the different studies presented in the thesis, DMS is shown to exhibit a change factor ranging from 1.1 to 96, corresponding to an increase of 11.4% to 9534%. The reason for such a wide range is because of the different types of instrumentations used for collecting the data and the several combinations between temporal and spatial scales. Here, we try to relate the change factor with the variability scale(s) exploited during the given study. The shorter temporal scale studied in this work is presented in **Chapter 1**, where fast physiological response was assessed following experimental exposure to UV. These changes are believed to be shown over a minute-scale and potentially attributed to physiological response of the local phytoplankton community to solar radiation. In the Mediterranean Sea, the change factor for DMS is low (1.1) while in the Arctic the change factor is relatively higher with a range from 1.5 to 5.8, potentially due to a more extreme response of the phytoplankton community under UV stress. In other words, when submitted to strong changes in light conditions, plankton communities can increase seawater DMS concentration by a factor of up to 6 in minutes to hours. In **Chapter 2**, a further step to realism was applied by varying light levels simulating vertical mixing in the upper mixed water column. The cumulative response of the plankton community in a few hours resulted in a change factor in DMS concentration of 1.1, that is, similar to the factor reported in the same cruise for fixed-light short-term incubations.

The study reported in **Chapter 4** combines a range of temporal scales. High frequency measurements were used to describe clear diel DMS patterns during the summer and spring cruises, resulting in change factors between 1.5 and 1.8 for 24 hr periods. On top of this day/night variability, a 20 hours storm event caused a decrease in DMS concentrations and broadened the change factor of the 2 weeks study to 2.3. Since both Mediterranean cruises were located at the same geographical position, the assessment of the change factor due to the two seasons was possible and happened to be the largest experienced during this work (5.2). This is not surprising since seasonal variability carries fundamental changes in

physical, chemical and biological properties of the marine ecosystem, such as the depth of the mixing layer, the light regime, nutrient availability, or plankton community succession. This inter-variability in environmental forcing factors leads to important changes in DMS production and cycling, and the resulting net effects on DMS concentration, generally larger than to the daily and sub-weekly variability discussed above.

Measurements along the circumnavigation cruise Malaspina (**Chapters 5 and 6**) using high-frequency or daily data showed an overall change factor of 96 or 10, respectively, depending on whether it is computed. Also change factors within each of the 11 biogeographical provinces are always larger for high-frequency data. High frequency instrumentation measures DMS concentration within minutes, i.e., at a spatial resolution of hundreds of meters. Conversely, daily data at sampling stations were separated from each other by 150-200 NM. High frequency measurements reveal patchiness and strong concentration gradients that occur over small spatial scales, on top of the better known gradients at the larger scales. Amplitude factors as high as 96 were found in the SPSG province. This does not necessarily reflect that such a high factor occurred at a single location, but within a province. In this case, this factor arose from within-province extremes as low as 0.1 nM and as high as 9.6 nM. From daily station data (**Chapter 6**), this same SPSG province had a factor of 5.1 with a minimum concentration of 0.58 nM and a maximum concentration of 2.97 nM. Overall the maximum change factor observed for daily stations (9.9) is ten times lower than that obtained with high-frequency data (96), and belongs in a different province (SATL compared to SPSG). To further emphasize the importance of measurement frequency, in **Chapter 5** the variability length scale of DMS was shown to vary between 15 km and 50 km whereas in **Chapter 6** the distance between 2 stations was 150-200 km and the determination of its variability is not possible.

How do these change or amplitude factors observed in the overall circumnavigation compare with the amplitude of DMS measurements in global and historical datasets? The Global Surface Seawater Dimethylsulfide (DMS) Database at PMEL (http://saga.pmel.

noaa.gov/dms/) has a minimum concentration of 0.01 nM and a maximum of 420 nM, even in one single season, hence rendering an amplitude factor of 42000. In the region mostly covered by the Malaspina circumnavigation (30ºN to 30ºS), and the seasonal period (January to June), the range is 0.01 to 220 nM, amplitude factor 22000.

Are data measured over different spatio-temporal scales using different sampling resolution comparable?

As discussed in the previous section, the way the environmental factors affect and shape DMS distribution varies broadly among regions, seasons and oceanographic settings. This is partly due to the inherent variability of each individual environmental factor. This effect of the inherent variability of a given factor on DMS variability is hardly detectable if the measurement frequency is lower than the actual variability. Ideally, the characterization of the potential influence that an individual actor plays on DMS dynamic should be obtained by measuring both, DMS and the actor, at the same frequency or resolution. This is rarely the case during oceanographic cruises, where generally DMS is measured in discrete samples at much lower resolution than sensor-based physical, chemical and biological variables. With the emergence of fast DMS analyzers, the situation is reversing, to the extent that now DMS can be measured continuously at higher resolution than many biological variables of interest. In **Chapter 5**, we faced sampling limitation for most of the chemical and biological variables and because of that we could only relate the variability length of DMS with fast sampling resolution given by the FRRf and the physical sensors connected to the underway. In **Chapter 6**, even though we had a considerable amount of DMS data available, we could only use the daily station data given the low resolution sampling of most of the chemical and biological variables used to interpret DMS distribution.

On top of such a broad range of possible environmental drivers affecting DMS cycling, temporal and spatial scales are also present. This means that the inherent

variability of DMS and environmental factors will also depend on the temporal and spatial scales we are looking at, adding a layer of complexity to the matter. In this work, most of the datasets are not looking at the same spatio-temporal scale, which makes the different analysis hard to compare. The first chapter looks at the variability in the physiological response of the phytoplankton over c.a. 2 hr experiments where the data are measured every 5 to 10 min. In **Chapter 2**, measurements are conducted twice over the length of the experiment, which hides shorter variability that is present within the 6 hr resolution. This is also the case with **Chapter 6** where the data used are only measured daily.

In **Chapter 4**, the data were collected during a Lagrangian study and measured at very high frequency (every 2 sec) and averaged every 30 sec for the vertical profiles and every 60 sec for the surface data. This helped deducing a clear diel cycle with a daily increase and decrease over night in September and an opposite pattern in May. This pattern could have been detected with lower data resolution (i.e. CTD every 4 hrs) but would not have been measurable for a non-Lagrangian study or for daily sampling. High-resolution data is necessary for the vertical profiling where we looked at the DMS vertical variability, with short sampling times to cope with strong vertical gradients. Measurements in the Mediterranean in May showed an important subsurface maximum that could have been easily missed using low resolution Rosette-Niskin bottle sampling. In **Chapters 5 and 6**, the temporal scale could not be assessed because of the movement of the ship across different water masses. The spatial dimension was the base of the circumnavigation studies where different information was conveyed through different oceanic provinces. For the high-resolution data analyzed in **Chapter 5**, the meso and sub-mesoscale variability of DMS and bio-physical variables could be resolved while only broad patterns, yet with many more variables, were discussed using the low resolution data of **Chapter 6**.

Putting research into context

Given the several scenarios presented here, one could wonder at which point we start missing temporal and/or spatial variability because of limited resources. To help identify the type of data resolution required and the type of instrumentation needed, specific questions should be asked: What is the question we want to answer or the hypothesis proposed? This will help directing the type of measurements to make. Of course in an ideal world, high frequency measurements would be preferred over low frequency one, but its availability is very rare and costly. Additionally, the use of high-frequency data is not always compulsory to answer the hypothesis and low frequency data might be sufficient. Also, high-frequency instruments generally require large water volumes or flow rates, which limit their applicability to cultures or enclosed incubation experiments.

What are the variables needed to help answer the questions/hypothesis and what would be the frequency resolution needed? Given the above-explained impact of the resolution scale on data, DMS data should be compared to ancillary data with the same sampling resolution to avoid any types of artifacts and bias imposed because of the different sampling resolution and instrumentations used.

It is often the case that scientists on oceanographic campaigns face limitations in data resolution because of instrumental reasons. Indeed, it is not possible to have the manpower and the state of the art technology or to afford high-resolution measurements in every study. For this reason the above questions should be taken into account while designing experimental setup.

The ocean in a bottle

There is still an unresolved debate on whether "*in vitro*" incubations lasting from hours to days reproduce reliable estimates of DMS(P) processes and realistic *in situ*

rates due to the possible artefacts generated by the "bottle effects" (e.g. Serret et al. 2009, Calvo-Díaz et al. 2011). Nevertheless, incubation experiments under realistic environmental conditions, either under surface irradiance at ambient SST (**Chapter 1**) or exposed to vertical mixing in the water column (**Chapter 2**) are still one of the best approaches for reproducing process rates and exploring the relative roles of environmental factors that can be manipulated (for example UV doses). Several of the individual processes that constitute the DMS(P) cycle have been and are still part of "isolated" studies. This allows us to explore in a more controlled environment how each of these processes responds to external forcing or perturbation (e.g., how the intracellular DMSP concentration changes with changes in solar radiation intensity and spectrum). Each of these processes generates short-term oscillations in net properties like DMS concentration, which are associated to individual variables and superimposed on each other in the oceanic environment. This super-imposition results in trends that vary according to the period of the year (**Chapter 4**), the geographical location (**Chapter 6**), and even the solar time in the day-night cycle (**Chapters 4 and 5**). Therefore, experiments in laboratory or during fieldwork campaigns are crucial for the understanding of process dynamics and environmental factors that govern DMS variability.

We still understand little about how and why marine algae and bacteria make DMS, how it moves through the food web in the upper ocean, or how much of it gets into the lower atmosphere and whether it can make a difference in global climate change. Because of the complicated web of individual processes and the tight interconnection of these processes driving DMS distribution and dynamics, the variable responses of the system becomes a maze that is hard to resolve by measurement and even more challenging for mechanistic modeling (Gabric et al. 2001). For this reason, a combination of measurements from laboratory work to world-wide data collection is necessary, with lab work inspiring the design of field studies and viceversa.

Conclusions

Chapter 1

Phytoplankton assemblages responded to an experimental change in spectral irradiance (PAR vs. FULL LIGHT) by expanding or reducing their light-harvesting complexes. Depending on their photosynthetic physiological state, they also responded by enhancing or reducing DMS and DMSP production. Production of the two compounds did not necessarily respond in concert to light treatments, which reflects the diversity of environmental factors influencing phytoplanktonic and bacterial DMSP-to-DMS conversion and the fate of DMS.

Chapter 2

In the oligotrophic waters of the Mediterranean, dynamic light exposure experiments compared to fixed depth experiments receiving the same cumulative exposure showed a different dynamic where a slight reduction in gross DMS production was observed along with an effect on particulate primary production, concomitant with reduced cell-specific fluorescence.

Chapter 3

High-resolution vertical profiles and near surface underway measurements of DMS demonstrate that membrane equilibrator-APCIMS is a valuable new tool to describe short-term DMS variability and its relationship to other physical and biogeochemical parameters.

Chapter 4

Lagrangian vertical profiles of DMS clearly reveal short-term response to environmental forcing. The emergent link between net biological DMS production and day/night variability in solar radiation, derived for the first time in the field at unprecedented resolution, suggests that a strong photo-physiological clock influences the temporal cycles of DMS.

Chapter 5

In the open-ocean the variability of DMS concentrations occurs at the low mesoscale between 15 and 50 km and decreasing with latitude and productivity. DMS variability was found to be more commonly related to that of phytoplankton-related variables than to that of physical variables. Comparison of DMS with the solar zenith angle across latitudes and seasons revealed that there is no universal diel pattern of global applicability for DMS

Chapter 6

Abiotic factors related to physical and optical properties of the upper mixed layer estimate DMS variability better than phytoplankton production and biomass. Conversely, DMSP concentrations can be better predicted from phytoplankton taxonomic composition. Physiological stresses associated with shallow mixed layers and solar radiation are the first order determinant of biological production of DMS, indicating that DMS cycling in the vast oceanic deserts is fundamentally different from that in productive regions where phytoplankton biomass and taxonomy provide the conditions for elevated DMS concentrations.

References

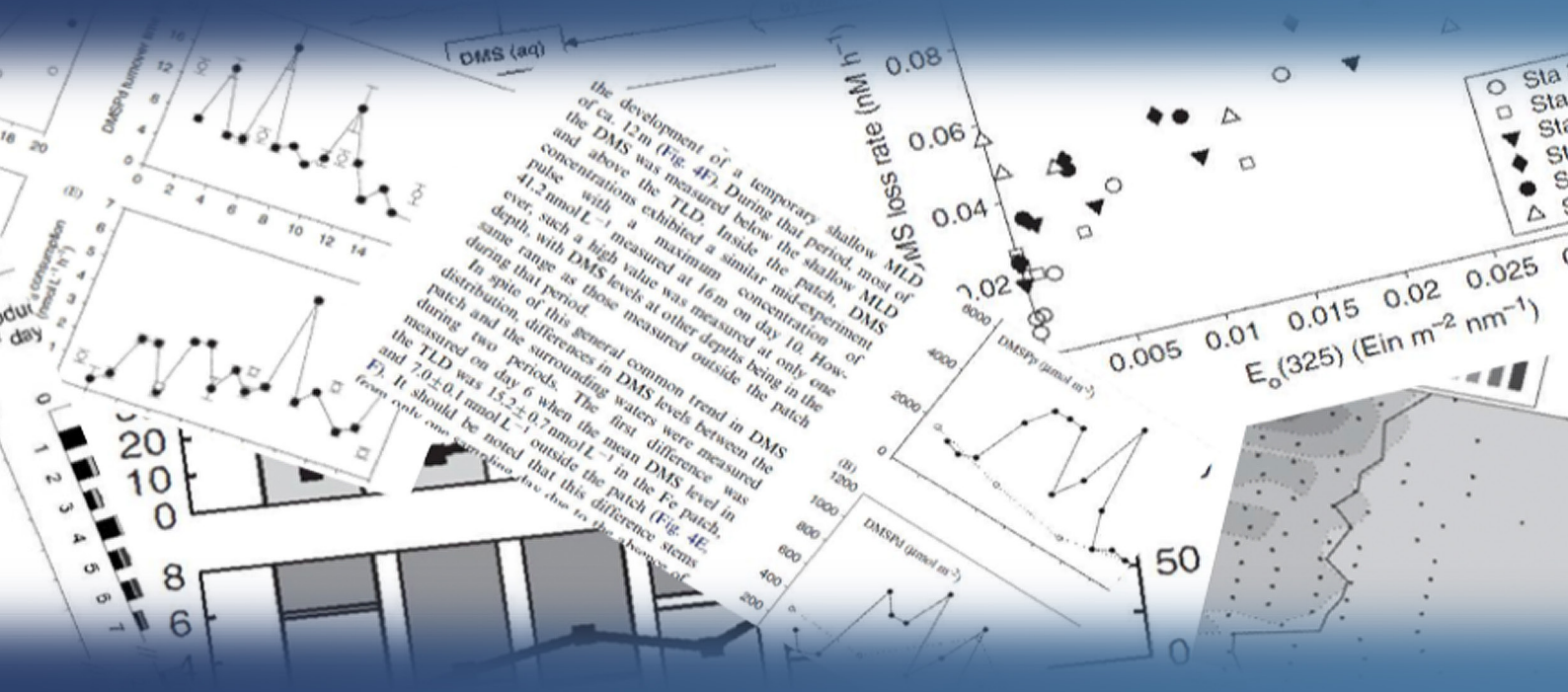
DMS (aq)
DMSPd turnover
DMSPd consumption (nmol L⁻¹ h⁻¹)
DMS loss rate (nM h⁻¹)
0.08
0.06
0.04
0.02
0.005
0.01
0.015
0.02
0.025
E0(325) (Ein m⁻² nm⁻¹)
DMSPp (μmol m⁻³)
DMSPd (μmol m⁻³)
20
10
0
8
6
50
0
1200
1000
800
600
400
200
4000
2000

References (from the General Introduction and Discussion)

Anderson, T. R., S. a. Spall, a. Yool, P. Cipollini, P. G. Challenor, and M. J. R. Fasham. 2001. Global fields of sea surface dimethylsulfide predicted from chlorophyll, nutrients and light. J. Mar. Syst. **30**: 1–20.

Andreae, M. O., and W. R. Barnard. 1984. The marine chemistry of dimethylsulfide. Mar. Chem. **14**: 267–279.

Andreae, M. O., and D. Rosenfeld. 2008. Aerosol–cloud–precipitation interactions. Part 1. The nature and sources of cloud-active aerosols. Earth-Science Rev. **89**: 13–41.

Archer, S. D., M. Ragni, R. Webster, R. L. Airs, and R. J. Geider. 2010. Dimethylsulfoniopropionate and dimethylsulfide production in response to photoinhibition in Emiliania huxleyi. Limnol. Oceanogr. **55**: 1579–1589.

Archer, S. S. D., D. D. G. Cummings, C. A. Llewellyn, and J. J. R. Fishwick. 2009. Phytoplankton taxa, irradiance and nutrient availability determine the seasonal cycle of DMSP in temperate shelf seas. Mar. Ecol. Prog. Ser. **394**: 111–124.

Asher, E. C., A. Merzouk, and P. D. Tortell. 2011. Fine-scale spatial and temporal variability of surface water dimethylsufide (DMS) concentrations and sea–air fluxes in the NE Subarctic Pacific. Mar. Chem. **126**: 63–75.

Aumont, O., S. Belviso, and P. Monfray. 2002. Dimethylsulfoniopropionate (DMSP) and dimethylsulfide (DMS) sea surface distributions simulated from a global three-dimensional ocean carbon cycle model. J. Geophys. Res. **107**.

Ayers, G. P., and R. W. Gillett. 2000. DMS and its oxidation products in the remote marine atmosphere : implications for climate and atmospheric chemistry. J. Sea Res. **43**: 275–286.

Bailey, K. E., D. a. D. a. Toole, B. Blomquist, R. G. R. G. Najjar, B. Huebert, D. J. D. J. Kieber, R. P. R. P. Kiene, P. a. Matrai, G. R. Westby, and D. a. del Valle. 2008. Dimethylsulfide production in Sargasso Sea eddies. Deep Sea Res. Part II Top. Stud. Oceanogr. **55**: 1491–1504.

Behrenfeld, M. J., K. H. Halsey, and A. J. Milligan. 2008a. Evolved physiological responses of phytoplankton to their integrated growth environment. Philos. Trans. R. Soc. Lond. B. Biol. Sci. **363**: 2687–703.

Behrenfeld, M. J., T. K. Westberry, E. S. Boss, R. T. O. Malley, D. A. Siegel, J. D. Wiggert, and B. A. Franz. 2009. Satellite-detected fluorescence reveals global physiology of ocean phytoplankton. Biogeosciences **6**: 779–794.

Behrenfeld, M. J., T. K. Westberry, E. S. Boss, R. T. O'Malley, D. a. Siegel, J. D. Wiggert, B. a. Franz, C. R. McClain, G. C. Feldman, S. C. Doney, J. K. Moore, G. Dall'Olmo, a. J. Milligan, I. Lima, and N. Mahowald. 2008b. Satellite-detected fluorescence reveals global physiology of ocean phytoplankton. Biogeosciences Discuss. **5**: 4235–4270.

Behrenfeld, M. J., K. Worthington, R. M. Sherrell, F. P. Chavez, P. Strutton, M. McPhaden, and D. M. Shea. 2006. Controls on tropical Pacific Ocean productivity revealed through nutrient stress diagnostics. Nature **442**: 1025–8.

Bell, T. G., G. Malin, G. A. Lee, J. Stefels, S. Archer, M. Steinke, and P. Matrai. 2012. Global oceanic DMS data inter-comparability. Biogeochemistry **110**: 147–161.

Bell, T. G., A. J. Poulton, and G. Malin. 2010. Strong linkages between dimethylsulphoniopropionate (DMSP) and phytoplankton community physiology in a large subtropical and tropical Atlantic Ocean data set. Global Biogeochem. Cycles **24**: 1–12.

Belviso, S., L. Bopp, C. Moulin, J. C. Orr, T. R. Anderson, O. Aumont, S. Chu, S. Elliott, M. E. Maltrud, and R. Simó. 2004a. Comparison of global climatological maps of sea surface dimethylsulfide. Global Biogeochem. Cycles **18**: 1–10.

Belviso, S., and G. Caniaux. 2009. A new assessment in North Atlantic waters of the relationship between DMS concentration and the upper mixed layer solar radiation dose. Global Biogeochem. Cycles **23**: 1–12.

Belviso, S., I. Masotti, A. Tagliabue, L. Bopp, P. Brockmann, C. Fichot, G. Caniaux, L. Prieur, J. Ras, J. Uitz, H. Loisel, D. Dessailly, S. Alvain, N. Kasamatsu, and M. Fukuchi. 2012. DMS dynamics in the most oligotrophic subtropical zones of the global ocean. Biogeochemistry **110**: 215–241.

Belviso, S., C. Moulin, L. Bopp, and J. Stefels. 2004b. Assessment of a global climatology of oceanic dimethylsulfide (DMS) concentrations based on SeaWiFS imagery (1998 – 2001). Can. J. Fish. Aquat. Sci. **61**: 804–816.

Van Bergeijk, S., K. Schönefeldt, L. Stal, and J. Huisman. 2002. Production and consumption of dimethylsulfide (DMS) and dimethylsulfoniopropionate (DMSP) in a diatom-dominated intertidal sediment. Mar. Ecol. Prog. Ser. **231**: 37–46.

Boyd, P. W., a J. Watson, C. S. Law, E. R. Abraham, T. Trull, R. Murdoch, D. C. Bakker, a R. Bowie, K. O. Buesseler, H. Chang, M. Charette, P. Croot, K. Downing, R. Frew, M. Gall, M. Hadfield, J. Hall, M. Harvey, G. Jameson, J. LaRoche, M. Liddicoat, R. Ling, M. T. Maldonado, R. M. McKay, S. Nodder, S. Pickmere, R. Pridmore, S. Rintoul, K. Safi, P. Sutton, R. Strzepek, K. Tanneberger, S. Turner, a Waite, and J. Zeldis. 2000. A mesoscale phytoplankton bloom in the polar Southern Ocean stimulated by iron fertilization. Nature **407**: 695–702.

De Boyer Montégut, C. 2004. Mixed layer depth over the global ocean: An examination of profile data and a profile-based climatology. J. Geophys. Res. **109**: 1–20.

Brainerd, K.E. and M. C. Gregg. 1995. Surface mixed and mixing layer depths. Deep Sea Res. Part I Oceanogr. Res. Pap. **42**: 1521–1543.

Brimblecombe, P., and D. Shooter. 1986. Photo-oxidation of dimethylsulphide in aqueous solution. Mar. Chem. **19**: 343–353.

Broadbent, A. D., and G. B. Jones. 2004. DMS and DMSP in mucus ropes, coral mucus, surface films and sediment pore waters from coral reefs in the Great Barrier Reef. Mar. Freshw. Res. **55**: 849.

Brugger, A., D. Slezak, I. Obernosterer, and G. J. Herndl. 1998. Photolysis of dimethylsulfide in the northern Adriatic Sea: Dependence on substrate concentration, irradiance and DOC concentration. Mar. Chem. **59**: 321–331.

Bucciarelli, E., C. Ridame, W. G. Sunda, C. Dimier-Hugueney, M. Cheize, S. Belviso, and N. Carolina. 2013. Increased intracellular concentrations of DMSP and DMSO in iron-limited oceanic phytoplankton Thalassiosira oceanica and Trichodesmium erythraeum. Limnol. Oceanogr. **58**: 1667–1679.

Bucciarelli, E., W. G. Sunda, N. O. Service, P. I. Road, and N. Carolina. 2003. Influence of CO2, nitrate, phosphate, and silicate limitation on intracellular dimethylsulfoniopropionate in batch cultures of the coastal diatom Thalassiosira pseudonana. Limnol. Oceanogr. **48**: 2256–2265.

Carey, C. C., B. W. Ibelings, E. P. Hoffmann, D. P. Hamilton, and J. D. Brookes. 2012. Eco-physiological adaptations that favour freshwater cyanobacteria in a changing climate. Water Res. **46**: 1394–407.

Carr, N. G., and N. H. Mann. 1994. The oceanic cyanobacterial picoplankton, p. 27–48. *In* D.A. Bryant [ed.], The molecular biology of cyanobacteria.

Charlson, J. R., J. E. Lovelock, M. O. Andreae, and S. G. Warren. 1987. Oceanic phytoplankton, atmospheric sulphur, cloud albedo and climate. Nature **326**: 655–661.

Le Clainche, Y., M. Levasseur, A. Vézina, J. W. H. Dacey, and F. J. Saucier. 2004. Behaviour of the ocean DMS (P) pools in the Sargasso Sea viewed in a coupled physical – biogeochemical ocean model. Can. J. Fish. Aquat. Sci. **803**: 788–803.

Coale, K. H., K. S. Johnson, S. E. Fitzwater, R. M. Gordon, S. Tanner, F. P. Chavez, L. Ferioli, C. Sakamoto, P. Rogers, F. Millero, P. Steinberg, P. Nightingale, D. Cooper, W. P. Cochlan, M. R. Landry, J. Constantinou, G. Rollwagen, A. Trasvina, and R. Kudela. 1996. A massive phytoplankton bloom induced by an ecosystem-scale iron fertilization experiment in the equatorial Pacific Ocean. Nature **383**: 495–501.

Cullen, J. J. 2009. Interactive comment on " Satellite-detected fluorescence reveals global physiology of ocean phytoplankton " by M . J . Behrenfeld et al. Biogeosciences Discuss. **5**: 2646–2655.

Dacey, J. W. H., F. A. Howse, A. F. Michaels, and S. G. Wakeham. 1998. Temporal variability of dimethylsulfide and dimethylsulfoniopropionate in the Sargasso Sea. Deep Sea Res. Part I Oceanogr. Res. Pap. **45**: 2085–2104.

DeBose, J. L., S. C. Lema, and G. A. Nevitt. 2008. Dimethylsulfoniopropionate as a foraging cue for reef fishes. Science (80-.). **319**: 1356.

Decelle, J., I. Probert, L. Bittner, Y. Desdevises, S. Colin, C. de Vargas, M. Galí, R. Simó, and F. Not. 2012. An original mode of symbiosis in open ocean plankton. Proc. Natl. Acad. Sci. U. S. A. **109**: 18000–5.

Doney, S. C., D. M. Glover, and S. J. Mccue. 2003. Mesoscale variability of Sea-viewing Wide Field-of-view Sensor (SeaWiFS) satellite ocean color: Global patterns and spatial scales. J. Geophys. Res. **108**: 3024.

Van Duyl, F. C., W. W. C. Gieskes, A. J. Kop, and W. E. Lewis. 1998. Biological control of short-term variations in the concentration of DMSP and DMS during a Phaeocystis spring bloom. J. Sea Res. **40**: 221–231.

Endres, C. S., and K. J. Lohmann. 2012. Perception of dimethyl sulfide (DMS) by loggerhead sea turtles: a possible mechanism for locating high-productivity oceanic regions for foraging. J. Exp. Biol. **215**: 3535–8.

Field, C. B. 1998. Primary Production of the Biosphere: Integrating Terrestrial and Oceanic Components. Science (80-.). **281**: 237–240.

Gabric, A. J., P. a. Matrai, R. P. R. P. Kiene, R. Cropp, J. W. H. J. W. H. Dacey, G. R. G. R. DiTullio, R. G. R. G. Najjar, R. Simó, D. a. Toole, D. a. DelValle, and D. Slezak. 2008. Factors determining the vertical profile of dimethylsulfide in the Sargasso Sea during summer. Deep Sea Res. Part II Top. Stud. Oceanogr. **55**: 1505–1518.

Galí, M., C. Ruiz-González, T. Lefort, J. M. Gasol, C. Cardelús, C. Romera-Castillo, and R. Simó. 2013a. Spectral irradiance dependence of sunlight effects on plankton dimethylsulfide production. Limnol. Oceanogr. **58**: 489–504.

Galí, M., R. Simó, M. Vila-Costa, C. Ruiz-González, J. M. Gasol, and P. Matrai. 2013b. Diel patterns of oceanic dimethylsulfide (DMS) cycling: Microbial and physical drivers. Global Biogeochem. Cycles **27**: 1–17.

Glover, H. E., B. Barbara, and M. Wyman. 1988. Pico- and ultraplankton Sargasso Sea communities : variability and comparative distributions of Synechococcus spp . and algae. Mar. Ecol. Prog. Ser. **49**: 127–139.
Hatton, A. D. 2002. DMSP removal and DMSO production in sedimenting particulate matter in the northern North Sea. Deep Sea Res. Part II Top. Stud. Oceanogr. **49**: 3053–3065.

Hegg, A., F. Radke, and V. Hobbs. 1991. Measurements of Aitken nuclei and cloud condensation nuclei in the marine atmosphere and their relation to the DMS-Cloud-climate hypothesis. J. Geophys. Res. **96**: 727–733.

Iizuka, Y., R. Uemura, H. Motoyama, T. Suzuki, T. Miyake, M. Hirabayashi, and T. Hondoh. 2012. Sulphate-climate coupling over the past 300,000 years in inland Antarctica. Nature **490**: 81–4.

Kameyama, S., H. Tanimoto, S. Inomata, H. Yoshikawa-Inoue, U. Tsunogai, A. Tsuda, M. Uematsu, M. Ishii, D. Sasano, K. Suzuki, and Y. Nosaka. 2013. Strong relationship between dimethylsulfide and net community production in the western subarctic Pacific. Geophys. Res. Lett. **40**: 3986–3990.

Kara, A. B., P. A. Rochford, and H. E. Hurlburt. 2003. Mixed layer depth variability over the global ocean. J. Geophys. Res. **108**: 3079.

Karsten, U., K. Kück, C. Vogt, and G. O. Kirst. 1996. Dimethylsulfoniopropionate production in phototrophic organisms and its physiological function as a cryoprotectant., p. 143–153. *In* R.P. Kiene, P. Visscher, M.D. Keller, and G.O. Kirst [eds.], Biological and environmental chemistry of DMSP and related sulfonium compounds.

Keller, A. a. 1989. Modeling the effects of temperature, light, and nutrients on primary productivity: An empirical and a mechanistic approach compared. Limnol. Oceanogr. **34**: 82–95.

Kettle, A. J., and M. O. Andreae. 2000. Flux of dimethylsulfide from the oceans: A comparison of updated data sets and flu models. J. Geophys. Res. **105**: 793–808.

Kettle, A. J., M. O. Andreae, D. Amouroux, T. W. Andreae, T. S. Bates, H. B, R. Boniforti, M. A. J. Curran, G. R. Ditullio, G. Helas, G. B. Jones, M. D. Keller, R. P. Kiene, C. Leck, M. Levasseur, G. Malin, M. Maspero, P. Matrai, A. R. Mctaggart, N. Mihalopoulos, B. C. Nguyen, A. Novo, J. P. Putaud, S. Rapsomanikis, G. Roberts, G. Schebeske, S. Sharma, R. Sim, R. Staubes, S. Turner, G. Uher, W. Boothbay, and M. Planck. 1999. A global database of sea surface dimethylsulfide (DMS) measurements and a procedure to predict sea surface DMS as a function of latitude , longitude , and month TM grazing. Global Biogeochem. Cycles **13**: 399–444.

Kieber, D. J., J. Jiao, P. Kiene, and T. S. Bates. 1996. Impact of dimethylsulfide photochemistry on methyl sulfur cycling in the Equatorial Pacific Ocean. J. Geophys. Res. **101**: 3715–3722.

Kiene, R. P., and L. J. Linn. 2000. The fate of dissolved dimethylsulfoniopropionate (DMSP) in seawater : Tracer studies using 35S-DMSP. Geochim. Cosmochim. Acta **64**: 2797–2810.

Kiene, R. P., L. J. Linn, and J. a. Bruton. 2000. New and important roles for DMSP in marine microbial communities. J. Sea Res. **43**: 209–224.

Kiene, R. P., L. J. Linn, J. González, M. a Moran, and J. a Bruton. 1999. Dimethylsulfoniopropionate and methanethiol are important precursors of methionine and protein-sulfur in marine bacterioplankton. Appl. Environ. Microbiol. **65**: 4549–58.

Kowalewsky, S., M. Dambach, B. Mauck, and G. Dehnhardt. 2006. High olfactory sensitivity for dimethylsulphide in harbour seals. Biol. Lett. **2**: 106–9.

Kwint, R. L. J., and K. J. M. Kramer. 1996. Annual cycle of the production and fate of DMS and DMSP in a marine coastal system. Mar. Ecol. Prog. Ser. **134**: 217–224.

Lana, a., T. G. Bell, R. Simó, S. M. Vallina, J. Ballabrera-Poy, a. J. Kettle, J. Dachs, L. Bopp, E. S. Saltzman, J. Stefels, J. E. Johnson, and P. S. Liss. 2011. An updated climatology of surface dimethlysulfide concentrations and emission fluxes in the global ocean. Global Biogeochem. Cycles **25**: 1–17.

Levasseur, M., M. G. Scarratt, S. Michaud, A. Merzouk, C. S. Wong, M. Arychuk, W. Richardson, R. B. Rivkin, M. S. Hale, E. Wong, A. Marchetti, and H. Kiyosawa. 2006. DMSP and DMS dynamics during a mesoscale iron fertilization experiment in the Northeast Pacific—Part I: Temporal and vertical distributions. Deep Sea Res. Part II Top. Stud. Oceanogr. **53**: 2353–2369.

Longhurst, A. 1998. Ecological geography of the sea Longhurst, Academy Pr.

Lovelock, J. E. 1972. Atmospheric Dimethyl Sulphide and the Natural Sulphur Cycle. Nature **237**: 452–453.

Luce, R. M., M. Levasseur, M. G. Scarratt, S. Michaud, S.-J. Royer, R. P. Kiene, C. Lovejoy, M. Gosselin, M. Poulin, Y. Gratton, and M. Lizotte. 2011. Distribution and microbial metabolism of dimethylsulfoniopropionate and dimethylsulfide during the 2007 Arctic ice minimum. J. Geophys. Res. **116**: 4–11.

MacIntyre, H. L., T. M. Kana, and R. J. Geider. 2000. The effect of water motion on short-term rates of photosynthesis by marine phytoplankton. Trends Plant Sci. **5**: 12–7.

Malin, G., and G. O. Kirst. 1997. Algal production of dimethyl sulfide and its atmospheric role. J. Phycol. **33**: 889–896.

Malin, G., S. Turner, S. L. Peter, P. M. Holligan, and D. S. Harbour. 1993. Dimethyisulphide and dimethyisulphoniopropionate in the Northeast Atlantic during the summer coccolithophore bloom. Deep Sea Res. Part I Oceanogr. Res. Pap. **40**: 1487–1508.

Martin, J. H., and S. E. Fitzwater. 1988. Iron deficiency limits phytoplankton growth in the north-east Pacific subarctic. Nature **331**: 341–343.

Martin, W., and M. J. Russell. 2003. On the origins of cells: a hypothesis for the evolutionary transitions from abiotic geochemistry to chemoautotrophic prokaryotes, and from prokaryotes to nucleated cells. Philos. Trans. R. Soc. Lond. B. Biol. Sci. **358**: 59–83; discussion 83–5.

McCreary, J. P., and K. E. Kohler. 2001. Influences of diurnal and intraseasonal forcing on mixed-layer and biological variability in the central Arabian Sea. J. Geophys. Res. **106**: 7139–7155.

Miles, C. J., T. G. Bell, and T. M. Lenton. 2009. Testing the relationship between the solar radiation dose and surface DMS concentrations using high resolution in situ data. Biogeosciences Discuss. **6**: 3063–3085.

Miles, C. J., T. G. Bell, and P. Suntharalingam. 2012. Investigating the inter-relationships between water attenuated irradiance, primary production and DMS(P). Biogeochemistry **110**: 201–213.

Moore, L. R., R. Goericke, and S. W. Chisholm. 1995. Comparative physiology of Synechococcus and Prochlorococcus: infleunce of light and temperature on growth, pigments, fluorescence and absorptive properties. Mar. Ecol. Prog. Ser. **116**: 259–275.

Moore, L. R., A. F. Post, G. Rocap, and S. W. Chisholm. 2002. Utilization of different nitrogen sources by the marine cyanobacteria Prochlorococcus and Synechococcus. Limnol. Oceanogr. **47**: 989–996.

Moran, M. A., C. R. Reisch, R. P. Kiene, and W. B. Whitman. 2012. Genomic Insights into Bacterial DMSP Transformations. Ann. Rev. Mar. Sci. **4**: 523–542.

Nemcek, N., D. Ianson, and P. D. Tortell. 2008. A high-resolution survey of DMS, CO2, and O2 /Ar distributions in productive coastal waters. Global Biogeochem. Cycles **22**: 1–13.

Nevitt, G. a. 2008. Sensory ecology on the high seas: the odor world of the procellariiform seabirds. J. Exp. Biol. **211**: 1706–13.

Nisbet, E. G., and N. H. Sleep. 2001. The habitat and nature of early life. Nature **409**: 1083–91.

Polimene, L., S. D. Archer, M. Butenschön, and J. I. Allen. 2011. A mechanistic explanation of the Sargasso Sea DMS "summer paradox." Biogeochemistry **110**: 243–255.

Quinn, P. K., and T. S. Bates. 2011. The case against climate regulation via oceanic phytoplankton sulphur emission. Nature **480**: 51–56.

Ruiz-González, C., M. Galí, E. Sintes, G. J. Herndl, J. M. Gasol, and R. Simó. 2012. Sunlight effects on the Osmotrophic uptake of DMSP-sulfur and leucine by polar phytoplankton. PLoS One **7**: 1–14.

Sarmiento, J. L., and N. Gruber. 2006. Ocean biogeochemical dynamics, Princetown.

Sarmiento, J. L., N. Gruber, M. A. Brzezinski, and J. P. Dunne. 2004. High-latitude controls of thermocline nutrients and low latitude biological productivity. Nature **427**, doi:10.1038/nature02204.1.

Sciare, J., N. Mihalopoulos, and F. J. Dentener. 2000. Interannual variability of atmospheric dimethylsulfide in the southern Indian Ocean. J. Geophys. Res. **105**: 369–377.

Seymour, J. R., R. Simó, T. Ahmed, and R. Stocker. 2010. Chemoattraction to dimethylsulfoniopropionate throughout the marine microbial food web. Science (80-.). **329**: 342–5.

Simó, R. 2001. Production of atmospheric sulfur by oceanic plankton: biogeochemical, ecological and evolutionary links. Trends Ecol. Evol. **16**: 287–294.

Simó, R. 2004. From cells to globe : approaching the dynamics of DMS (P) in the ocean at multiple scales. Can. J. Fish. Aquat. Sci. **684**: 673–684.

Simó, R., S. D. Archer, C. Pedrós-alió, L. C. Gilpin, and C. E. Stelfox-widdicombe. 2002. Coupled dynamics of dimethylsulfoniopropionate and dimethylsulfide cycling and the microbial food web in surface waters of the North Atlantic. Limnol. Oceanogr. **47**: 53–61.

Simó, R., and J. Dachs. 2002. Global ocean emission of dimethylsulfide predicted from biogeophysical data. Global Biogeochem. Cycles **16**: 1–10.

Simó, R., and C. Pedrós-alió. 1999. Short-term variability in the open cycle of dimethylsulfide. Global Biogeochem. Cycles **13**: 1173–1181.

Simó, R., and C. Pedrós-Alió. 1999. Role of vertical mixing in controlling the oceanic production of dimethyl sulphide. Nature **402**.

Sprintall, J., and M. Tomczak. 1992. Evidence of the Barrier Layer in the Surface Layer of the Tropics. J. Geophys. Res. **97**: 7305–7316.

Stefels, J. 2000. Physiological aspects of the production and conversion of DMSP in marine algae and higher plants. J. Sea Res. **43**: 183–197.

Stefels, J., and L. Dijkhuizen. 1996. Characteristics of DMSP-lyase in Phaeocystis sp. (Prymnesiophyceae). Mar. Ecol. Prog. Ser. **131**: 307–313.

Stefels, J., M. Steinke, S. Turner, G. Malin, and S. Belviso. 2007. Review: Environmental constraints on the production and removal of the climatically active gas dimethylsulphide (DMS) and implications for ecosystem modelling. Biogeochemistry **83**: 245–275.

Steinke, M., G. Malin, and P. S. Liss. 2002. Trophic interactions in the sea: an ecological role for climate relevant volatiles? J. Phycol. **38**: 630–638.

Sunda, W., D. J. Kieber, R. P. Kiene, and S. Huntsman. 2002. An antioxidant function for DMSP and DMS in marine algae. Nature **418**: 317–20.

Toole, D. a., and D. A. Siegel. 2004. Light-driven cycling of dimethylsulfide (DMS) in the Sargasso Sea: Closing the loop. Geophys. Res. Lett. **31**: 5–8.

Toole, D. a., D. Slezak, R. P. Kiene, D. J. Kieber, and D. a. Siegel. 2006. Effects of solar radiation on dimethylsulfide cycling in the western Atlantic Ocean. Deep Sea Res. Part I Oceanogr. Res. Pap. **53**: 136–153.

Tortell, P. D., C. Guéguen, M. C. Long, C. D. Payne, P. Lee, and G. R. DiTullio. 2011. Spatial variability and temporal dynamics of surface water pCO2, ΔO2/Ar and dimethylsulfide in the Ross Sea, Antarctica. Deep Sea Res. Part I Oceanogr. Res. Pap. **58**: 241–259.

Tortell, P. D., M. C. Long, C. D. Payne, A.-C. Alderkamp, P. Dutrieux, and K. R. Arrigo. 2012. Spatial distribution of pCO2, ΔO2/Ar and dimethylsulfide (DMS) in polynya waters and the sea ice zone of the Amundsen Sea, Antarctica. Deep Sea Res. Part II Top. Stud. Oceanogr. **71-76**: 77–93.

Tsuda, A., S. Takeda, H. Saito, J. Nishioka, Y. Nojiri, I. Kudo, H. Kiyosawa, A. Shiomoto, K. Imai, T. Ono, A. Shimamoto, D. Tsumune, T. Yoshimura, T. Aono, A. Hinuma, M. Kinugasa, K. Suzuki, Y. Sohrin, Y. Noiri, H. Tani, Y. Deguchi, N. Tsurushima, H. Ogawa, K. Fukami, K. Kuma, and T. Saino. 2003. A mesoscale iron enrichment in the western subarctic Pacific induces a large centric diatom bloom. Science (80-.). **300**: 958–61.

Turner, S. M., P. D. Nightingale, W. Broadgate, and P. S. Liss. 1995. The distribution of dimethyl sulphide and dimethylsulphoniopropionate in Antarctic waters and sea ice. Deep Sea Res. Part II Top. Stud. Oceanogr. **42**: 1059–1080.

Vallina, S. M., and R. Simó. 2007. Strong relationship between DMS and the solar radiation dose over the global surface ocean. Science (80-.). **315**: 506–8.

Vallina, S. M., R. Simó, and S. Gassó. 2006. What controls CCN seasonality in the Southern Ocean? A statistical analysis based on satellite-derived chlorophyll and CCN and model-estimated OH radical and rainfall. Global Biogeochem. Cycles **20**: GB1014.

Van Alstyne, K. L., P. Schupp, and M. Slattery. 2006. The distribution of dimethylsulfoniopropionate in tropical Pacific coral reef invertebrates. Coral Reefs **25**: 321–327.

Vézina, A. F. 2004. Ecosystem modelling of the cycling of marine dimethylsulfide : a review of current approaches. Can. J. Fish. Aquat. Sci. **61**: 845–856.

Vila-Costa, M., R. Simó, H. Harada, J. M. Gasol, D. Slezak, and R. P. Kiene. 2006. Dimethylsulfoniopropionate uptake by marine phytoplankton. Science **314**: 652–4.

Walter, M. 1993. Archaean stromatolites: evidence for the Earth's earliest benthos., p. 187–213. *In* J.W. Schopf [ed.], Earth's earliest biosphere: its origin and evolution.

White, R. H. 1982. Analysis of dimethyl sulfonium compounds in marine algae. J. Mar. Res. **40**: 529–536.

Wilde, S. a, J. W. Valley, W. H. Peck, and C. M. Graham. 2001. Evidence from detrital zircons for the existence of continental crust and oceans on the Earth 4.4 Gyr ago. Nature **409**: 175–8.

Wright, K. L. B., L. Pichegru, and P. G. Ryan. 2011. Penguins are attracted to dimethyl sulphide at sea. J. Exp. Biol. **214**: 2509–11.

Yoch, D. C. 2002. Dimethylsulfoniopropionate : Its Sources , Role in the Marine Food Web , and Biological Degradation to Dimethylsulfide. Appl. Environ. Microbiol. **68**: 5804–5815.

Annex

Submitted to Environmental Chemistry

Short-term effects of solar radiation on phytoplankton photophysiology and dimethylated sulfur production in two contrasting environments (Western Mediterranean Sea and the Arctic Ocean).

Sarah-Jeanne Royer[1], Martí Galí[1,2], Cristina Sobrino García[3], Antonio Fuentes-Lema[3], Marjolaine Blais[4], Michel Gosselin[4], Jonathan Gagnon[2], Jean-Éric Tremblay[2], Maurice Levasseur[2], Rafel Simó[1*]

1. *Institut de Ciències del Mar (CSIC), Barcelona, Catalonia, Spain.*
2. *Université Laval, Département de biologie (Takuvik and Québec–Océan), Québec, Québec, Canada.*
3. *Departamento de Ecoloxía e Bioloxía Animal, Facultade de Ciencias do Mar, Universidad de Vigo, Vigo (Pontevedra), Spain.*
4. *Institut des sciences de la mer (ISMER), Université du Québec à Rimouski, Rimouski, Québec, Canada.*

See Chapter 1

Biogeosciences, 10, 7983–7998, 2013
www.biogeosciences.net/10/7983/2013/
doi:10.5194/bg-10-7983-2013

Biogeosciences Open Access

Differential response of planktonic primary, bacterial, and dimethylsulfide production rates to static vs. dynamic light exposure in upper mixed-layer summer sea waters

M. Galí[1,*], R. Simó[1], G. L. Pérez[2], C. Ruiz-González[1,], H. Sarmento[1,***], S.-J. Royer[1], A. Fuentes-Lema[3], and J. M. Gasol[1]**

[1]Institut de Ciències del Mar (CSIC), Passeig Marítim de la Barceloneta, 37–49, 08003 Barcelona, Catalonia, Spain
[2]Laboratorio de Ecología y Fotobiología Acuática (IIB-INTECH), Chascomús, Argentina
[3]Departamento de Ecoloxía e Bioloxía Animal, Facultade de Ciencias do Mar, Vigo (Pontevedra), Spain
[*]now at: Takuvik Joint International Laboratory, Université Laval (Canada), CNRS (France), Département de Biologie and Québec-Océan, Université Laval, Pavillon Alexandre-Vachon 1045, avenue de la Médecine G1V 0A6 Québec, Canada
[**]now at: Département des Sciences Biologiques, Université du Québec à Montréal, Québec, Canada
[***]now at: Federal University of Rio Grande do Norte, Department of Oceanography and Limnology, "PPg Ecologia", Natal-RN, Brazil

Correspondence to: M. Galí (marti.gali.tapias@gmail.com)

Received: 6 May 2013 – Published in Biogeosciences Discuss.: 29 May 2013
Revised: 19 September 2013 – Accepted: 9 October 2013 – Published: 6 December 2013

Abstract. Microbial plankton experience short-term fluctuations in total solar irradiance and in its spectral composition as they are vertically moved by turbulence in the oceanic upper mixed layer (UML). The fact that the light exposure is not static but dynamic may have important consequences for biogeochemical processes and ocean–atmosphere fluxes. However, most biogeochemical processes other than primary production, like bacterial production or dimethylsulfide (DMS) production, are seldom measured in sunlight and even less often in dynamic light fields. We conducted four experiments in oligotrophic summer stratified Mediterranean waters, where a sample from the UML was incubated in ultraviolet (UV)-transparent bottles at three fixed depths within the UML and on a vertically moving basket across the same depth range. We assessed the response of the phyto- and bacterioplankton community with physiological indicators based on flow cytometry singe-cell measurements, fast repetition rate fluorometry (FRRf), phytoplankton pigment concentrations and particulate light absorption. Dynamic light exposure caused a subtle disruption of the photoinhibition and photoacclimation processes associated with ultraviolet radiation (UVR), which slightly alleviated bacterial photoinhibition but did not favor primary production. Gross DMS production (GP_{DMS}) decreased sharply with depth in parallel to shortwave UVR, and displayed a dose-dependent response that mixing did not significantly disrupt. To our knowledge, we provide the first measurements of GP_{DMS} under in situ UV-inclusive optical conditions.

1 Introduction

The characteristic response times of microbial plankton match the natural variability of light exposure, which changes at different temporal scales with solar elevation, the passage of clouds, vertical mixing and even wave focusing (Gallegos and Platt, 1985). In transparent oceanic waters, exposure to high irradiance (photosynthetically available radiation, PAR) is accompanied by exposure to detrimental ultraviolet radiation (UVR) in the upper portion of the water column (Vincent and Neale, 2000). Short-term irradiance fluctuations elicit fast and reversible responses (Roy, 2000), whereas continued exposure to high PAR and UVR may elicit photoacclimation (MacIntyre et al., 2002) or permanent physiological changes, i.e., irreversible damage (Buma et al., 2001).

Vertical mixing can have a positive, neutral or negative effect on water-column-integrated processes depending on the interplay between mixing rates, damage and repair kinetics, and underwater attenuation of PAR and UVR (Neale et al., 2003). In the absence of repair mechanisms, damage will be proportional to cumulative exposure (i.e., it will be dose-dependent). If moderate repair exists, mixing will allow the cells to recover in the UVR shaded portion of the upper mixed layer (UML) (Fig. 1a). In this situation the photodamage will no longer be dose-dependent and a steady state will be achieved provided that the cells spend sufficient time under constant exposure conditions. In the idealized situation where damage is completely counteracted by repair on a timescale much shorter than the mixing time, or in the absence of repair, vertical mixing will have neutral effects. These responses can change with exposure time.

The effects of dynamic light exposure have concerned the aquatic photosynthesis research community for almost 40 yr (see Gallegos and Platt, 1985, and references therein), and apparently contradictory findings have often been reached using either experimental or modeling approaches (Ross et al., 2011a, b). It appears that the ability to take advantage of dynamic light exposure may depend on the taxonomic composition and size structure of the phytoplankton community, their light history, and their nutritional status (Barbieri et al., 2002; Brunet and Lavaud, 2010; Helbling et al., 2013). Knowledge on the photoresponse of (bacterial) heterotrophic activity is much more limited, but a number of studies suggest that significant PAR-driven stimulation frequently occurs (Morán et al., 2001; Church et al., 2004), as does inhibition due to UVR (Aas et al., 1996; Kaiser and Herndl, 1997). There is mounting evidence that UVR resistance and photostimulation responses vary among bacterial phylogenetic groups (Agogué et al., 2005; Alonso-Sáez et al., 2006; Ruiz-González et al., 2012), which might be related to the occurrence of photoheterotrophic metabolisms in the ocean (Kolber et al., 2000; Béjà et al., 2000; Kirchman and Hanson, 2012) or to their interaction with other light-driven processes (see references in Ruiz-González et al., 2013).

Besides carbon and nutrient cycling, solar radiation modulates the biogeochemical cycles of other elements such as sulfur or halogens (Carpenter et al., 2012). The volatile dimethylsulfide (DMS) is produced mainly by the enzymatic cleavage of the phytoplankton osmolyte dimethylsulfoniopropionate (DMSP) as a result of microbial food web interactions (Simó, 2004). Marine DMS emission represents the main natural source of sulfur to the atmosphere (Lana et al., 2011) and has potential implications for climate regulation, which in turn depends on its response to solar radiation (Vallina and Simó, 2007). Yet, the climatic effects of DMS and the underlying atmospheric processes remain highly controversial (Quinn and Bates, 2011; Woodhouse et al., 2013).

The response of community DMS production to sunlight depends on a number of interdependent effects: phytoplankton DMSP production, its intracellular conversion to DMS followed by DMS permeation outside the algal cell, algal DMSP release (due to grazing, cell lysis or active exudation), and DMSP transformations by the microbial food web (Galí et al., 2013a). Phytoplankton culture studies have shown that acclimation to strong UV exposure (and also strong PAR) on a timescale of several days generally causes up-regulation of intracellular DMSP content (Sunda et al., 2002; Slezak and Herndl, 2003), although this view has been challenged (van Rijssel and Buma, 2002). Nutrient limitation (particularly nitrogen) also causes up-regulation of intracellular DMSP (Bucciarelli and Sunda, 2003; Yang et al., 2011), and may interact in complex ways with UVR (Harada et al., 2009). Evidence obtained from culture studies is supported by field observations of higher DMS and DMSP concentrations per unit phytoplankton biomass (and often in absolute terms) during summer stratification (Simó and Pedrós-Alió, 1999; Vila-Costa et al., 2008; Archer et al., 2009). Phytoplankton DMS production is also enhanced by UV exposure (Hefu and Kirst, 1997; Sunda et al., 2002; Archer et al., 2010) and nitrogen limitation (Sunda et al., 2007). Yet, most phytoplankton culture studies have failed to account for photochemical DMS loss, which has precluded a neat assessment of UV effects on phytoplankton DMS production. The ensemble of these observations tends to support the view that DMSP and its metabolites play an antioxidant role in phytoplankton cells (Sunda et al., 2002). In this regard, it is important to note that long- and short-term responses may differ. I.e., a long-term up-regulation response caused by acclimation to oxidative stress is compatible with a short-term decrease in the intracellular DMSP pool due to enhanced DMSP destruction, as observed by Hefu and Kirst (1997) and van Rijssel and Buma (2002). It has recently been shown that sunlight stimulates community gross DMS production (GP_{DMS}; Galí et al., 2011) in an irradiance- and spectrum-dependent manner (Galí et al., 2013a). Moreover, community gross DMS production rates followed the diurnal irradiance cycle in summer stratified waters (Galí et al., 2013b). Phytoplankton radiative stress was the primary explanation invoked by the authors, but food web interactions might also play a role, as thoroughly discussed in those articles.

We designed an experiment where a single surface seawater sample was incubated in UVR-transparent bottles at three fixed optical depths, approximately corresponding to the water subsurface, the optical middle, and the bottom of the UML. An additional set of bottles was regularly moved up and down across the same depth range and radiation gradient (Fig. 1; Table 1). Simulating turbulent mixing experimentally is extremely difficult, and the mixing rates applied to the dynamic incubations were probably not realistic due to being too fast, being constant and having a fixed oscillation period (see Sect. 3.1). Yet, dynamic light exposure might still be more realistic than fixed-depth incubations and provide relevant insights into the photoinhibition and photoacclimation processes occurring in upper mixing waters. The experimental design was aimed at answering two questions

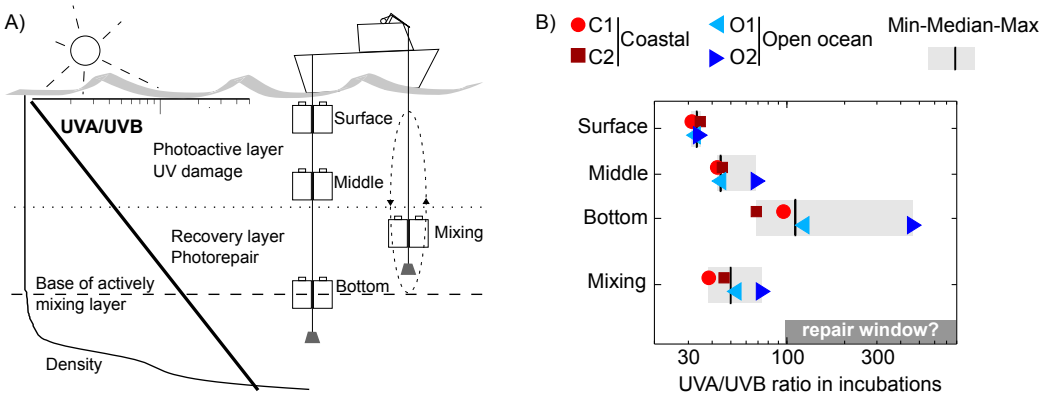

Fig. 1. (a) Illustration of the experimental design. Vertically moving and fixed-depth bottles were incubated in a spectral irradiance gradient, depicted by the UVA / UVB ratio. The dotted and the dashed lines represent the depth of the hypothetical photoactive layer and actively mixing layer, respectively; **(b)** UVA / UVB in the different treatments in each experiment. The horizontal bar indicates the UVA / UVB window where photolyase repair of bacterioplankton is more efficient, calculated from underwater UVR profiles according to Kaiser and Herndl (1997).

regarding the short-term response of planktonic activity to dynamic light exposure. (1) Photobiological: should the mixing bottles display the same response as the ones incubated at the middle optical depth considering that both treatments received a similar cumulative dose? If the response was the same this would imply that the measured processes were dose-dependent. (2) Biogeochemical and methodological: in UVR-transparent and shallow mixing layers, are the rates obtained from vertical integration of static bottle incubations equivalent to those obtained in vertically moving bottles?

2 Methods

2.1 Experimental setting and irradiance calculations

Surface (0.2 to 3 m deep) seawater samples were taken predawn in 20–30 L polycarbonate carboys dimmed with a black plastic bag. In the coastal experiments (C1 and C2) the samples were taken from a boat at the Blanes Bay Microbial Observatory coastal site (BBMO; 0.5 miles offshore over a water column depth of 20 m), brought to the lab, maintained within ±1 °C of the sea surface temperature, and incubated at the pier of the Barcelona Olympic Harbor during 4 h centered on the solar noon. The oceanic experiments (O1 and O2) were done in the open Mediterranean during a Lagrangian cruise over a water column depth of ca. 2000 m (R/V *García del Cid*). In these experiments the samples were maintained in a thermostated bath at the sea surface temperature until they were incubated in situ (Fig. 1a), beginning 4 h before solar noon and ending 2 h after solar noon (with an intermediate sample taken after the first 2 h). In C1 and C2 mixing was applied by moving the bottle basket (Fig. 1a) manually every 15 min, completing a mixing cycle every 60 min. In the ship-based experiments the mixing bottles were continuously moved using the winch of the ship at the smallest possible vertical speed (3–4 cm s^{-1}), completing a cycle in 10–18 min. Since the waters were less transparent in the harbor than at the BBMO, in C1 and C2 the bottles were incubated at shallower depths to approximate the equivalent in situ optical depths (Table 1). Mixing layer depths (MLD) were estimated from temperature profiles obtained with a conductivity-temperature-depth (CTD) probe, and defined by a >0.1 °C deviation with respect to 1 m depth. The buoyancy or Brunt–Väisälä frequency was calculated in 1 m bins (Fig. 2), and used as an additional criterion to distinguish the weakly stratified UML from the more stratified waters below.

The irradiance just below the water surface (subsurface irradiance) during the incubations was recorded with a PUV-2500 (Biospherical) multichannel filter radiometer, which was also used to measure underwater irradiance profiles in C1 and C2. In O1 and O2, the vertical profiles were measured with a PRR-800 (Biospherical). Diffuse attenuation coefficients of downward irradiance (K_d) were calculated as the linear regression between ln-transformed spectral irradiance and depth (z) in the optically homogeneous surface layer where the incubations were done. The time series of subsurface irradiance were converted to the irradiance seen by each water sample by applying the attenuation due to seawater ($e^{-K_d \cdot z}$) and the attenuation due to the incubation bottles. We used polytetrafluoroethylene (Teflon, Nalgene) bottles, which according to our measurements transmit 65 %, 77 % and 100 % of spectral irradiance in the UVB, UVA and PAR bands, respectively (Galí et al., 2013a). The bottles were placed in a metallic basket which caused a minimal alteration of the tridimensional light field. For the mixing bottles, the irradiance calculation was made using a time-varying depth that corresponded to the vertical displacement of the basket. In each incubation, the mean UVB (300–320 nm) and UVA (320–400 nm) irradiance was calculated by integrating over

Table 1. Summary of initial sample characteristics, ecosystem settings and experimental conditions. Phytoplankton group dominance is indicated in a qualitative manner, with biomass calculations made following Simó et al. (2009). All biogeochemical process rates refer to the experimental incubation except for LIR t0, which correspond to the initial sample. GP_{DMS} and $NP_{bio,DMS}$ stand for gross and net biological DMS production, respectively. Pro: *Prochlorococcus*; Syn: *Synechococcus*; PPeuk: photosynthetic picoeukaryotes; Diat: diatoms; Dino: dinoflagellates; Hapto: haptophytes; na: not available. See text for other abbreviations.

Experiment code	Coastal 1 (C1)	Coastal 2 (C2)	Oceanic 1 (O1)	Oceanic 2 (O2)
Date	27 Jul 2010	29 Jul 2010	16 Sep 2011	20 Sep 2011
Sampling position	41.67 N 2.81 E		40.9 N 2.67 E	40.9 N 2.44 E
Physicochemical characteristics of the upper mixed layer				
SST (°C)	23.0	22.7	25.2	23.6
Nitrate + nitrite (μmol L^{-1})	0.53	0.67	0.03	0.04
Phosphate (μmol L^{-1})	0.08	0.15	0.06	0.06
Silicate (μmol L^{-1})	0.77	1.05	0.53	0.59
MLD (m)	4	3	7	16
Z 10 % 320 nm (m)	7	7	12	11
Z 10 % 380 nm (m)	20	20	38	32
Buoyancy frequency (h^{-1})	6.2 ± 1.7	8.8 ± 2.7	8.1 ± 2.8	4.9 ± 0.9
Wind speed (m s^{-1})	2.4–6.7	1.4 –7.1	0.3–4.8	1.0–9.5
UVB range (W m^{-2})	0.4–1.4	0.4–1.1	0.3–1.1	0.04–1.1
UVA range (W m^{-2})	22–37	21–31	19–30	9–30
PAR range (μmol phontons m^2 s^{-1})	1100–1580	1010–1330	830–1360	410–1340
Experimental conditions				
Incubation depth (m)	0.3, 1, 3	0.5, 1.5, 3.5	0.5, 3, 11	0.5, 5.5, 18
Equivalent depth UVB (m)	1.3, 4, 10	1.3, 3.5, 6	2.5, 5, 13	2.5, 7, 20
Mixing time (min)	60	60	18	10
UVB range (W m^{-2})	0.04–0.9	0.13–0.7	0.09–0.7	0.01–0.65
UVA range (W m^{-2})	4–28	9–24	11–23	5–22
PAR range (μE)	460–1930	600–1210	610–1360	320–1290
Initial sample characteristics				
DMS (nmol L^{-1})	7.5	8.5	2.1	2.1
DMSPt (nmol L^{-1})	23.0	18.5	18.2	19.6
Chl a (μg L^{-1})	0.24	0.25	0.08	0.08
Dominant phytoplankton (biomass)	PPeuk > Diat > Pro		Syn > Dino > PPeuk (Hapto)	
Bacteria (10^5 cells mL^{-1})	9.0	7.3	9.4	7.3
Intact-membrane bacteria (%)	54	52	56	56
Biogeochemical process rates (min–max)				
PPp (nmol C L^{-1} h^{-1})	80–150	160–200	20–26	21–25
LIR t_0 (pmol leu L^{-1} h^{-1})	32	21	36	18
LIR (pmol leu L^{-1} h^{-1})	33–37	16–21	37–44	17–27
GP_{DMS} (nmol DMS L^{-1} h^{-1})	0.05–0.40	0.24–0.49	na	0.07–0.17
$NP_{bio,DMS}$ (nmol DMS L^{-1} h^{-1})	0.03–0.32	0.18–0.44	0.02–0.10	0.04–0.16

the spectrum the mean spectral irradiance in the 6 bands measured by the PUV-2500 (centered at 305, 313, 320, 340, 380 and 395 nm) as described by Galí et al. (2013a). PAR was measured in a single integrated band (400–700 nm) so that no spectral integration was required. The irradiance dose was calculated by multiplying the mean irradiance by the total incubation time.

2.2 Process measurements and analysis techniques

Primary production was measured as the ^{14}C incorporated into particles in duplicate 40 mL Teflon bottles inoculated with $NaH^{14}CO_3$ (Morán et al., 1999) and incubated in situ (including dark controls).

Bacterial heterotrophic production rates were measured as ^3H-leucine incorporation rates (LIRs; Kirchman et al., 1985;

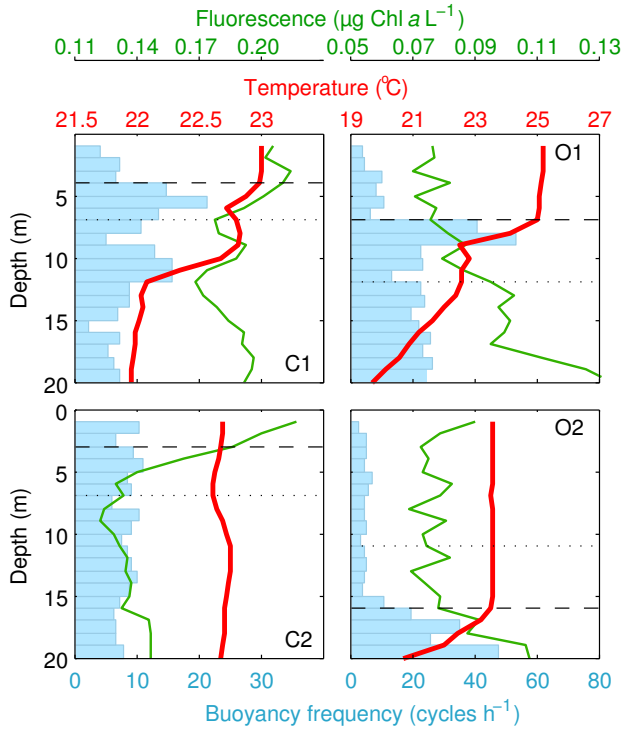

Fig. 2. Vertical profiles of temperature, Chl *a* fluorescence and buoyancy (Brunt–Väisälä) frequency at the time of sampling in the four experiments. The horizontal dashed line indicates the depth of the mixing layer and the dotted line the 10 % penetration of 320 nm radiation (see also Table 1).

Smith and Azam, 1992) in the initial samples and on subsamples taken from the larger (2.3 L) Teflon incubation bottles after in situ light exposure. Triplicate subsamples plus one killed control from each Teflon bottle were further incubated for 2 h in the dark at in situ temperature in 1.5 mL Eppendorf vials. In C1 and C2, LIRs were measured only in initial and final (4 h) samples. In O1 and O2, incubation-averaged LIRs were calculated as the time-weighted average of intermediate (2 h) and final time (6 h) incubations. We assumed the intermediate LIR measurement to represent the initial 2 h exposure, and the final LIR measurement the subsequent 4 h period. In C1 and C2 leucine incorporation was also measured during "in situ" sunlit incubations in 40 mL Teflon bottles to which ^{3}H-leucine had been added.

Samples for pigment analysis were obtained by filtering 1–2 L seawater onto GF/F filters at the beginning and the end of the incubations (O1 and O2 only) and the filters were immediately stored in liquid nitrogen. Pigments were extracted and analyzed by HPLC following Zapata et al. (2000) on a SpectraSYSTEM (Thermo) using a Waters Symmetry C8 column (150 × 4.6 mm, 3.5 μ particle size, 10 nm pore size). Calibration was made using commercial external pigment standards (DHI, Denmark), and the pigments were identified according to their elution time.

The absorption spectra of total particulate matter a_p were determined by the quantitative filter technique, using the simple transmittance method in a Lambda 800 (Perkin-Elmer) spectrophotometer. Water samples (2 L) were filtered onboard using 25 mm-diameter GF/F filters. Immediately after filtration absorbance scans were measured from 350 to 750 nm at 1 nm intervals. The quantitative filter technique was applied according to NASA's optics protocols for absorption coefficient measurements (Mitchell et al., 2000). In order to minimize light scattering, the wet filters were placed as close to the spectrophotometer detector as possible and measured against a blank clean filter wetted with filtered (0.2 μm) seawater. Absorption coefficients were estimated according to the relationship $a_p(\lambda) = \frac{2.303\, A_{filter}(\lambda)\, s}{V_{filt}\, \beta(\lambda)}$, where $A_{filter}(\lambda)$ is the measured absorbance, s is the clearance area of the filter, V_{filt} is the volume of filtered water, and $\beta(\lambda)$ is the amplification factor vector (Mitchell and Kiefer, 1984).

The maximum quantum yield of photosystem II photochemistry (F_v/F_m), an indicator of phytoplankton photosynthetic performance and photoinhibition, was measured by fast repetition rate fluorometry (FastTracka I, Chelsea), as detailed by Galí et al. (2013a).

A FACSCalibur (Becton & Dickinson) flow cytometer equipped with a 15 mW Argon-ion laser (488 nm emission) was used to enumerate picophyto- and bacterioplankton populations and to measure their performance at the single-cell level. The cell-specific fluorescence of each different picophytoplankton population (normalized to their side scatter – SSC, a proxy for cell size) was measured following Marie and Partensky (2006). At least 30 000 events were acquired for each subsample. Fluorescent beads (1 μm, Fluoresbrite carboxylate microspheres, Polysciences Inc., Warrington, PA, USA) were added at a known density as internal standards. Two subpopulations of heterotrophic bacterioplankton were distinguished based on the nucleic acid double-staining (NADS) viability protocol: intact-membrane (or "live") bacteria and membrane-compromised (or "dead") bacteria (Grégori et al., 2001). This protocol uses a combination of the cell-permeant nucleic acid stain SybrGreen I (SGI, Molecular Probes, Eugene, OR, USA) and the cell-impermeant propidium iodine (PI, Sigma Chemical Co.) fluorescent probe. We used a 1 : 10 SGI and 10 μg mL^{-1} PI concentrations that were added to live samples less than 2 h after sampling. After simultaneous addition of each stain, the samples were incubated for 20 min in the dark at room temperature and then analyzed.

DMS and total DMSP (DMSPt) were measured by purge and trap gas chromatography (Shimadzu GC14A) coupled to flame photometric detection. Net biological DMS production ($NP_{bio,DMS}$) was obtained by incubating whole water samples in 2.3 L Teflon bottles and correcting afterward for photochemical DMS loss, as described by Galí et al. (2013a). Gross DMS production was measured in the same way in additional bottles amended with 200 μmol L^{-1}

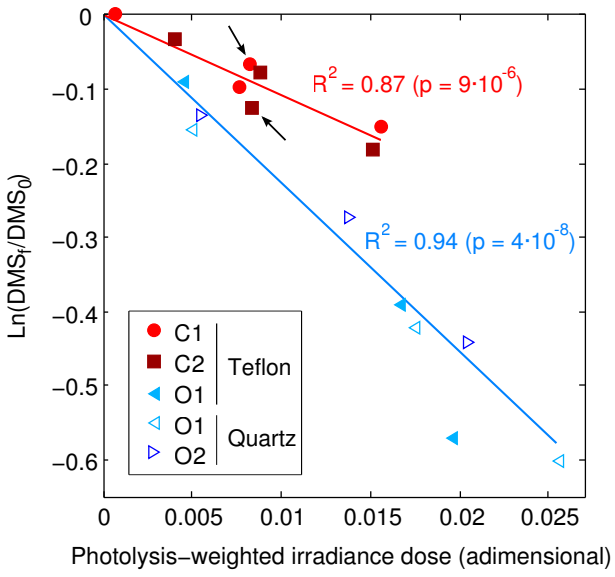

Fig. 3. DMS photolysis in fixed and vertically moving incubations. The two types of incubation showed consistent dose-response behavior. Filled symbols: Teflon bottles incubated in C1 and C2 at three fixed depths and in a vertically moving basket (marked by arrows). Empty symbols: Teflon or quartz flasks incubated on board and withdrawn at different times (samples taken on three different days during the SUMMER-I cruise). The slope of the regression lines is k^*_{photo}: the apparent quantum yield of DMS photolysis with respect to weighted spectral UV irradiance normalized to 300 nm (as defined by Galí et al., 2013a). k^*_{photo} was 10.8 and 23.9 at the coastal station and at the oceanic station, respectively.

dimethyldisulfide (Galí et al., 2011), an effective inhibitor of bacterial DMS consumption (Wolfe and Kiene, 1993; Simó et al., 2000).

DMS photolysis was measured in 0.2 μm filtered-water incubations in 40 mL Teflon bottles or 50 mL quartz flasks. As expected, DMS photolysis was linearly related to the photochemically weighted irradiance dose (Fig. 3). Since we observed distinct DMS photolysis yields in coastal (C1–C2) versus oceanic (O1–O2) experiments, a distinct photolysis rate constant (k^*_{photo}) for each type of experimental location (i.e., coastal or oceanic) was used to correct the biological rates for photochemical DMS loss.

The process rates and indicator variables were measured in duplicate with the exceptions of DMS production rates, pigment concentrations and particulate absorption coefficients due to water volume constraints. The measurement of DMS production rates requires large incubation volumes to properly account for food web processes like microzooplankton grazing (Saló et al., 2010).

2.3 Statistical analyses

Each variable was normalized within each experiment to the vertical integral of the fixed incubations. The integration was calculated as the area under the trapezoids formed by depth vs. rate data points. After pooling the four experiments together we checked for significant differences among treatments ($\mathrm{d}f = 3$). If the Bartlett's equal variance test was successfully passed ($p > 0.05$) a parametric one-way analysis of variance (ANOVA) was used. Otherwise, a non-parametric Kruskal–Wallis ANOVA was performed. After a significant ANOVA ($p < 0.05$) multiple comparisons were done with the Tukey–Kramer test.

3 Results and discussion

3.1 Oceanographic settings

The sampled UML was in all cases exposed to high proportions of UVR, i.e., > 10 % of the subsurface UVA and UVB levels. Only in C2 the deeper portion of the UML was exposed to < 10 % of subsurface UVB (Fig. 2; Table 1). The phytoplankton community was typical of oligotrophic conditions, with low biomass and large contributions of the pico-sized fraction (*Prochlorococcus, Synechococcus* and picoeukaryotes) though in different proportions (Table 1). The picoeukaryote fraction was likely dominated by haptophytes (prymnesiophytes) and pelagophytes in O1 and O2 according to HPLC pigment data (Pérez et al., unpublished). Diatoms in C1 and C2 and small dinoflagellates (< 10 μm) in O1 and O2 also made significant contributions to total phytoplankton biomass.

The mixing layer was very shallow at the coastal site (MLD of 3–4 m). In the oceanic setting, the UML deepened from 7 m (O1) to 16 m (O2) due to the passage of a storm (Fig. 2). The fact that all experiments took place in soft wind conditions, and the relatively high values of the buoyancy (Brunt–Väisälä) frequency within the UML suggest that it was not mixing actively at the time of the CTD casts (Table 1). If we assume that vertical diffusivity (K_z) in the UML interior was in the range 10^{-2}–10^{-4} m^2 s^{-1} (Denman and Gargett, 1983; Ross et al., 2011b), it would take ca. 0.25 to 100 h for a population of particles released at a single depth to diffuse across one optical depth in the UML depending on the wavelengths and MLD considered (Gallegos and Platt, 1985). A similar range is obtained by calculating the mixing timescale as MLD^2 / K_z as suggested by Ross et al. (2011a, b). The highest K_z might be representative of nighttime convective overturning, while the lowest K_z might be more representative of the daytime, when mixing was likely inhibited by solar heating (Brainerd and Gregg, 1995). From these calculations we conclude that the simulated mixing times were considerably faster than the actual mixing times. Although we tried to simulate the optical gradient experienced by the

organisms and solutes within the UML, in practice the incubations spanned a larger optical gradient once the attenuation due to seawater and the incubation bottles was taken into account (Table 1).

Indeed, some of the differences between experiments and particularly between O1 and O2 may arise from slight differences in experimental exposure and prior light history of the plankton. Yet, our discussion will focus on the general trends rather than the differences among individual experiments.

3.2 Phytoplankton photosynthetic performance and photoacclimation

Particulate primary production (PPp) was moderately inhibited at the surface, optimal at the middle depth, and slightly lower at the bottom, with the exception of C1 (Fig. 4a). PPp in mixing bottles resembled that in surface bottles and was 18 % lower than in middle bottles except in C1 ($p < 0.01$). As a result, vertically integrated PPp from fixed bottles generally exceeded that in mixing bottles by 10–17 % (except in C1). This result contrasts with that obtained by Bertoni et al. (2011), who observed a neutral to positive effect of dynamic light exposure in coastal Mediterranean waters in late spring. The response of primary production may be explained by different photoacclimation, photoprotection and damage and repair processes that will be explored in the paragraphs below.

At the end of the incubations, the average fluorescence of *Synechococcus* and picoeukaryote cell populations was generally lowest at the surface and increased with depth (Fig. 4b, c). Fluorescence was generally lower than average in mixing bottles (although different patterns were observed for picoeukaryotes in O2). Similar responses were observed for nanoeukaryotes in C2 and for *Prochlorococcus* in O1 (data not shown). In addition, we observed a ca. 30 % decrease in *Prochlorococcus* cell counts likely due to UV-caused mortality in surface bottles, as previously shown by Sommaruga et al. (2005). In concordance with the response of populations analyzed with single-cell techniques, bulk phytoplankton F_v / F_m tended to increase with incubation depth (Fig. 4d). F_v / F_m in mixing bottles was (again) lower than the vertical integral of fixed bottles in C1 and O1, but not in O2, potentially due to the high fluorescence yields of the picoeukaryote population (Fig. 4c). The decrease in fluorescence yields may simultaneously result from a decrease in chlorophyll *a* (Chl *a*) content per cell (MacIntyre et al., 2002), an increase in excess energy dissipation as heat by photoprotective carotenoids (non-photochemical quenching), photodamage of photosystem II, and pigment bleaching (Vincent and Neale, 2000).

Chl *a* concentrations generally increased (by 10–30 %) during the experiments except in O1, where a ca. 20 % decrease was found. In O1 and O2, the ratio of photosynthetic carotenoids to Chl *a* (PC / Chl *a*) increased with depth, from ca. 0.48 at the surface to ca. 0.56 in bottom bottles. PC / Chl *a* in mixing bottles was close to the vertical integral of fixed bottles (Fig. 4e). This suggests that phytoplankton photoacclimated during the time frame of the experiment (6 h) by adjusting PC / Chl *a* to the average spectral irradiance they were exposed to, likely seeking to optimize photosynthesis. Another physiological indicator that is worth analyzing is the ratio of photosynthetic carotenoids to non-photosynthetic carotenoids (PC / NPC; Fig. 4f), as defined by Bricaud et al. (1995). In the fixed bottles, this ratio increased from about 0.66 to 0.90 from surface to bottom. At the surface, the low PC / NPC values were due to the net synthesis of NPC (with a 20–40 % increase during the incubation). These results indicate an increasing investment in photoprotection through non-photochemical quenching at higher spectral irradiance. This is consistent with the decrease in photosystem II fluorescence yields (Fig. 4d), since NPC compete for excitation energy with the other energy dissipation pathways: photochemistry and fluorescence emission. Surprisingly, mixing bottles displayed the highest values of PC / NPC due to higher-than-average PC concentrations, a response that remains difficult to interpret.

The xanthophyll cycle pigments diadinoxanthin (Dd) and diatoxanthin (Dt) were up-regulated by about 35 % (up to 75 %) during the exposure relative to their initial concentration. Likewise, (Dd + Dt) concentrations relative to Chl *a* increased by 50 % in the ensemble of all treatments in O1 and O2. (Dd + Dt) / Chl *a* generally increased towards the surface, and showed intermediate values in mixing bottles (Fig. 4h). These xanthophylls constitute a photoprotective mechanism in haptophytes, dinoflagellates and diatoms (van de Poll and Buma, 2009) by which the epoxidated form (Dd) is enzymatically de-epoxidated to Dt, and vice versa, depending on the cells' need for photoprotection. No clear trends were observed in the de-epoxidation state index, defined as Dt/(Dd + Dt), perhaps because the Dt vs. Dd interconversion responds on a timescale of few minutes (van de Poll and Buma, 2009), which is shorter than the filtration time of the samples after the exposure.

UV-absorbing (sunscreen) compounds, possibly mycosporine-like amino acids (Shick and Dunlap, 2002), were observed in particulate absorption spectra in O1 and O2 (Fig. 4i). The ratio of particulate light absorption at 340 nm relative to that at the blue peak of Chl *a* at 440 nm, $a_{p,340} / a_{p,440}$, was highest (1–1.5) in surface bottles and lower (0.7–0.8) in middle and bottom bottles. Mixing bottles showed an ambiguous response, with low $a_{p,340} / a_{p,440}$ in O1 and slightly higher $a_{p,340} / a_{p,440}$ in O2.

The several photoresponse indicators we have explored indicate that, although phytoplankton deployed different photoprotection mechanisms, these were not enough to counteract high PAR- and UV-driven photoinhibition in surface bottles. Seen another way, the investment in photoprotection might have decreased the allocation of resources to carbon fixation. In middle bottles, conversely, the combination of high PAR and longwave UVA, which can also be used for photosynthesis, (Helbling et al., 2003) and a lower

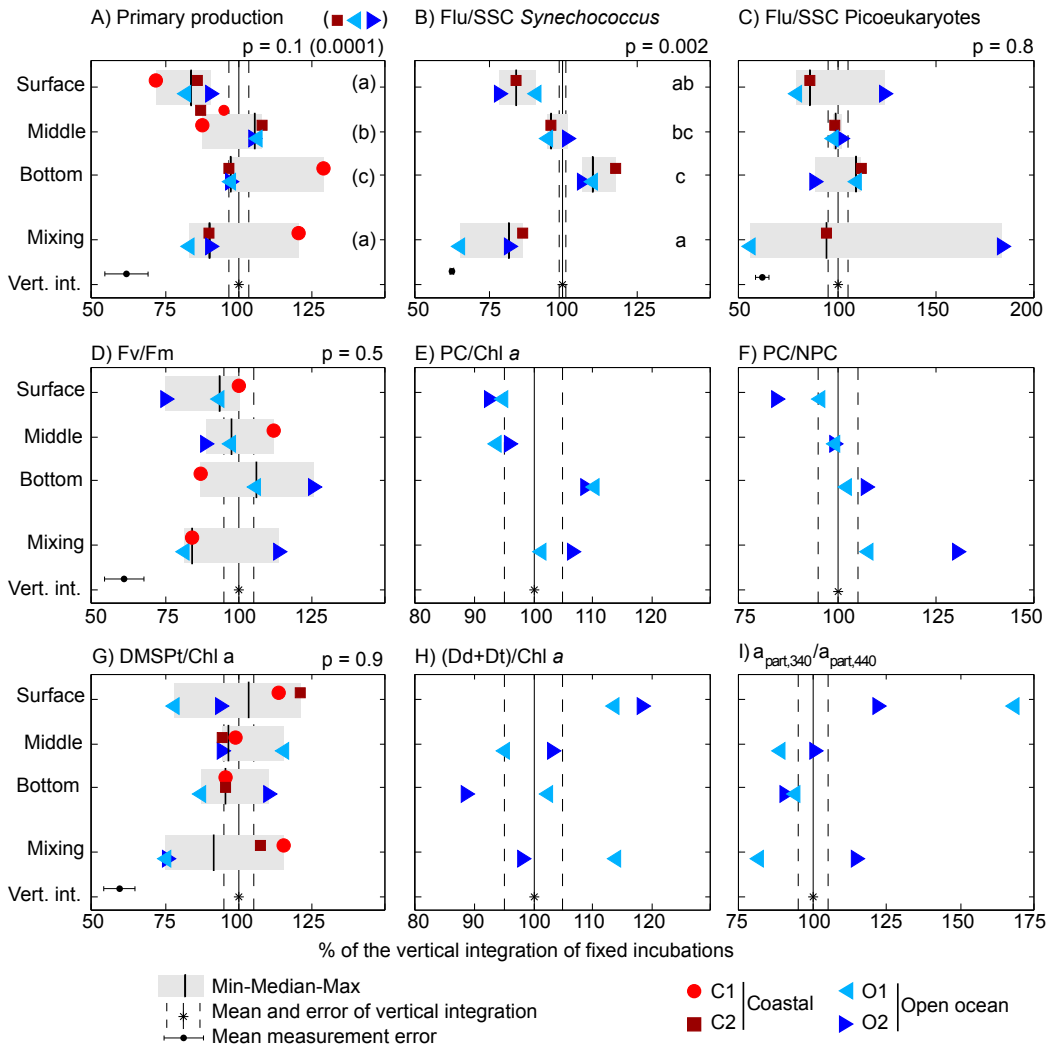

Fig. 4. Response of phytoplankton to irradiance gradients in static and vertically moving incubations. Primary production rates **(a)** and indicators of phytoplankton photoresponse **(b–i)** have been normalized, within each experiment, to the vertical integral of fixed incubations. Flu / SSC: side-scatter-normalized cell-specific fluorescence. F_v / F_m: maximum quantum yield of photosystem II photochemistry. PC: photosynthetic carotenoids. NPC: non-photosynthetic carotenoids. Dd: diadinoxanthin. Dt: diatoxanthin. $a_{p,340}$ / $a_{p,440}$: ratio of particulate light absorption coefficient at 340 nm and 440 nm. Differences between treatments are represented by p values of ANOVA tests followed by multiple comparisons (see text for details). In **(a)**, a test was performed on a subset of experiments (C2, O1 and O2) that exhibited a more coherent response, and the resulting p value and multiple comparisons are shown in parentheses.

investment in photoprotection due to lower proportions of UVR resulted in optimal PPp. It is also important to bear in mind that different phytoplankton groups likely preferred different photoprotection mechanisms within those cited.

The response of mixing bottles is more difficult to interpret. The reduced photosynthetic performance in C2, O1 and O2 might indicate that the short surface exposure received by mixing bottles was enough to cause some irreversible inhibition, and that phytoplankton repair capacity was limited. However, this is not clearly supported by the radiative stress indicators measured. In addition, repair is thought to be more efficient at elevated temperatures like those encountered in our study (Campbell et al., 1998; van de Poll and Buma, 2009). The fact that surface inhibition was only moderate and that highest PPp occurred in the middle bottle suggests that the photosynthetic machinery of phytoplankton was well adapted to a stratified system and thus not geared to take advantage of fast changes in spectral irradiance. This contrasts with what has been found for coastal tropical phytoplankton thriving in turbid waters (Helbling et al., 2003) or even for coastal Mediterranean assemblages in late spring (Bertoni et al., 2011).

3.3 Response of bacterial heterotrophic production

In fixed bottle incubations, LIRs were significantly inhibited at the surface by 14–28 % with respect to the vertical integral (except in C1), and increased with depth to find their optimum at the bottom of the mixed layer (Fig. 5a). LIRs in mixing bottles resembled those of bottom bottles in 3 out of 4 experiments, and were higher (though not significantly) than those in middle bottles and the vertical integral. This suggests that fast mixing favored recovery and photorepair over photodamage. It is well known that photolyase enzymes use UVA and blue light to repair damaged DNA. According to Kaiser and Herndl (1997), optimal photoreactivation occurs in a certain window of UVA / UVB that, in our experiments, would roughly correspond to the bottom half of the UML (Fig. 1b). This interpretation is supported by the higher proportions of intact-membrane bacteria found in mixing bottles at the end of the incubations with respect to the surface bottles (O1 and O2 only; Fig. 5c). Yet, the vertical trend shown by this cytometric indicator in fixed bottles contradicts this view, especially in O2, where the proportion of intact-membrane bacteria decreased with depth.

In addition to the post-exposure dark incubations, in C1 and C2 we measured LIRs during the sunlit incubations, i.e., with the ^{3}H-leucine added into exposed bottles (Fig. 5b). In these "in situ" incubations, surface and mixing bottles displayed more similar degrees of inhibition, and the trends of bacterial production with depth did not match those found in post-exposure dark incubations. We also measured LIRs in aluminum-foil-darkened bottles placed in the in situ incubation basket. Dark LIR was 22 % higher than the vertical integral of sunlit bottles in C1, but no differences were observed in C2 (Fig. 5b). The discrepancies between in situ and post-exposure leucine incorporation may be due to distinct photoinhibition and photorepair dynamics, and each approach has advantages and disadvantages. The tendency of in situ leucine incorporation to display less photoinhibition may be due to substrate incorporation at the beginning of the incubation, before the onset of severe photoinhibition. On the other hand, post-exposure LIRs reflect the photoinhibition state at the end of the exposure, resulting from the net balance between damage and repair in sunlight as well as from the net repair that might occur during the 2 h post-exposure dark incubation. These methodological issues might be overcome with the development of more sensitive methods that allow a faster determination of bacterial heterotrophic production, which is particularly challenging in oligotrophic waters with low activity.

Different explanations have been invoked to explain the responses of bacterial activity under sunlight, for instance, the occurrence of photoheterotrophic metabolisms in some bacterial groups, or the exudation of labile organic matter by phytoplankton at high irradiance (reviewed by Ruiz-González et al., 2013). Unfortunately, we did not investigate the phylogenetic composition of the bacterial communities in our experiments. No obvious patterns linking the response of LIR and PPp were found, perhaps because phytoplankton–bacteria interactions through the dissolved carbon pool are complex and group-specific (Sarmento and Gasol, 2012). Despite the numerous uncertainties, our study adds valuable information to the only previous study of bacterial production under dynamic light exposure (Bertoni et al., 2011), and agrees with that work in that the effect of mixing was neutral to positive compared to fixed incubations.

3.4 Response of community DMS production

Gross DMS production (GP_{DMS}) showed the strongest vertical gradient among the three processes, and increased significantly by about three-fold between the bottom and the surface of the UML in fixed incubations (Fig. 6a). Gross DMS production in mixing bottles was not significantly different from that in middle bottles, nor from the vertical integral, although a slight trend towards lower GP_{DMS} in mixing bottles occurred in C1 and C2.

Gross DMS production results from the addition and interaction of several processes, namely exudation of DMS by phytoplankton, bacterial degradation of DMSP released by phytoplankton as a result of grazing, viral infection, or cell death, and even the reduction of dimethylsulfoxide (Spiese et al., 2009; Asher et al., 2011). Galí et al. (2013a) showed that UVR stimulates GP_{DMS} in a spectral irradiance-dependent manner, a result that is confirmed by our present study. They also demonstrated that the stimulation is more effective at shorter and more energetic UVR wavelengths, with a spectral peak around 330 nm, and attributed the stimulation effect to phytoplankton DMS release caused by the additive effects of excess PAR (Stefels, 2000) and UVR stress (Sunda et al., 2002). Furthermore, it was suggested that lethal UVR exposure could promote DMS production as a result of phytoplankton cell lysis and subsequent DMSP release. This mechanism would make more DMSP available to bacteria and to algal DMSP cleavage enzymes ("lyases") released along with algal DMSP.

In the ensemble of all the experiments, experiment-normalized PPp and GP_{DMS} were negatively correlated (Pearson's $r = -0.58$; $p = 0.018$; Spearman's $\rho = -0.51$; $p = 0.044$). Moreover, the response of GP_{DMS} to radiative stress was generally consistent with the patterns of photoinhibition and photoprotection (Archer et al., 2010). Whether or not this response was the result of active physiological regulation of phytoplankton cells remains to be elucidated. Clearly, better methods are needed to study the relative weight of different DMS production processes and their modulation by spectral irradiance (Galí et al., 2013a). Sunda et al. (2002) suggested that intracellular DMSP cleavage to DMS plus acrylate and further oxidation products might help phytoplankton cells coping with oxidative stress. If we assume that the UV-driven increase in GP_{DMS} arose completely from up-regulated intracellular DMSP cleavage, which is

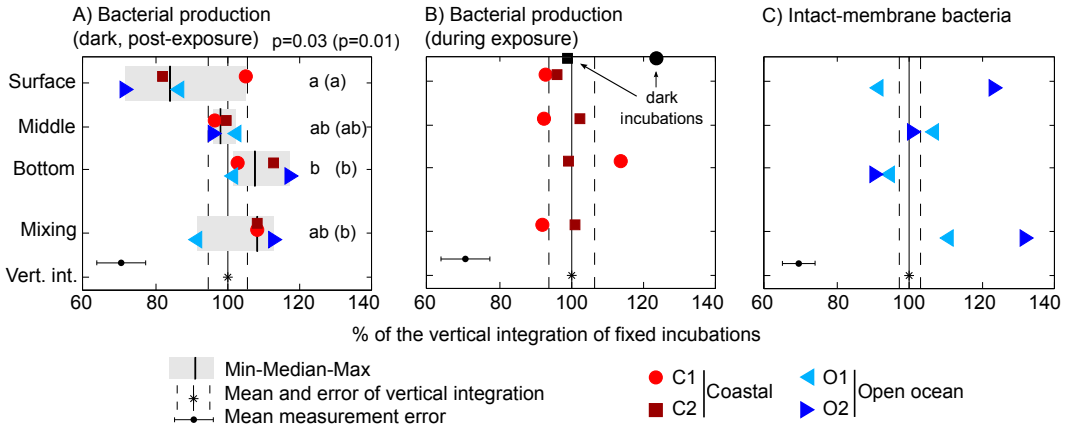

Fig. 5. Response of heterotrophic bacteria to irradiance gradients in static and vertically moving incubations. Leucine incorporation rates in **(a)** post-exposure dark incubations and **(b)** in situ light and dark incubations; **(c)** proportion of intact-membrane ("live") bacteria as deduced from the nucleic acid double-staining (NADS) protocol. Statistical comparisons as in Fig. 4. In **(a)**, a test was performed on a subset of experiments (C2, O1 and O2) that exhibited a more coherent response, and the resulting p value and multiple comparisons are shown in parentheses.

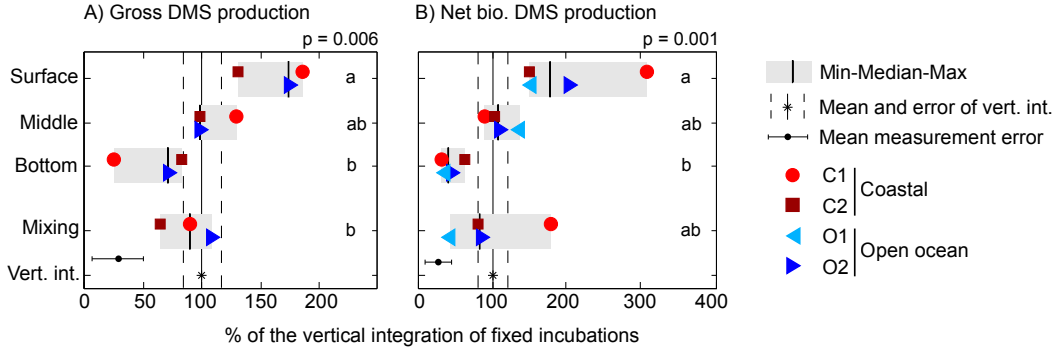

Fig. 6. Response of community DMS production to irradiance gradients in static and vertically moving incubations. **(a)** Gross DMS production (GP_{DMS}, DMDS-amended incubations); **(b)** net biological DMS production (non-amended incubations; equivalent to GP_{DMS} minus bacterial DMS consumption). Statistical comparisons as in Fig. 4. In **(b)**, a test was performed on a subset of experiments (C2, O1 and O2) that exhibited a more coherent response. Multiple comparisons did not show different patterns from those in the entire data set, although the p value decreased ($p = 0.0008$).

very unlikely, our data suggest that this antioxidant mechanism would still not be enough to counteract short-term photoinhibition and ameliorate photosynthetic performance, even if working in tandem with other photoprotection mechanisms.

DMSPt concentrations displayed only moderate changes (< 5 % variation in 13 out of 16 incubations) and no clear trends were found across treatments (data not shown). A strong DMSPt depletion in surface bottles was only found in O2 (21 %). The stability of the DMSPt concentration across spectral irradiance treatments is notable, given that (1) a lower amount of fixed carbon was available for DMSP synthesis in surface and mixing samples, and (2) higher amounts of DMSP were lost as DMS (and perhaps as dimethylsulfoxide) at higher irradiance. The quotient of GP_{DMS} to DMSPt was 0.42 d^{-1}, 0.29 d^{-1}, 0.18 d^{-1}, and 0.21 d^{-1} on average in surface, middle, bottom and mixing bottles, respectively. These data suggest that faster DMSP synthesis was required to sustain DMSPt concentrations at high irradiance. Gross DMSP synthesis rates were not measured in our experiments, but, interestingly, experiment-normalized net DMSP synthesis rates and PPp were correlated (Pearson's $r = 0.50$; $p = 0.048$; Spearman's $\rho = 0.65$; $p = 0.006$). Recent results suggest that DMS can be produced intracellularly in phytoplankton through DMSP cleavage by OH radicals, without the need for DMSP cleavage enzymes (D. J. Kieber, personal communication, 2012). In addition, some algal strains can reduce dimethylsulfoxide back to DMS, potentially enhancing their antioxidant protection (Spiese et al., 2009). Since DMS is membrane-permeable, it is reasonable to assume that a significant fraction will escape the cell without being oxidized, so that DMSP will play a more direct and important

role in antioxidant protection than in the original antioxidant hypothesis formulated by Sunda et al. (2002).

The similar short-term behavior of DMSPt in all the experiments contrasts with the differences in the ratios of total DMSP (DMSPt) to Chl *a* between the coastal (DMSPt / Chl *a* of 77–92 μmol g^{-1}) and the oceanic (196–315 μmol g^{-1}) settings. These differences may be explained by the presence of strong DMSP producers in O1 and O2, such as dinoflagellates and haptophytes. Besides taxonomy, also nutrient availability (particularly nitrogen) and the longer-term acclimation to elevated UVR and PAR contribute to regulate the DMSP content of phytoplankton (Bucciarelli and Sunda, 2003; Sunda et al., 2007; Archer et al., 2010). While the irradiance doses of the four upper mixed layers sampled were not significantly different (Table 1), lower nitrate concentrations in the open ocean waters might have contributed to set the higher DMSPt / Chl *a* ratios found in O1 and O2 by simultaneously decreasing Chl *a* and increasing DMSP cell quotas. Intriguingly, the DMSPt / Chl *a* ratios at the end of the experiments showed an opposite pattern in C1 and C2 compared to O1 and O2 (Fig. 4g). Overall, these results indicate that it is crucial to distinguish between short-term (hours) and long-term (days, weeks) responses if we are to understand the photophysiological mechanisms that drive DMS and DMSP cycling in phytoplankton cells and at the community level.

Net biological DMS production ($NP_{bio,DMS}$) showed a pattern similar to that of GP_{DMS} (Fig. 6b). $NP_{bio,DMS}$ is interesting in that it tells the net effect of sunlight on biological DMS cycling, that is, on the difference between GP_{DMS} and bacterial DMS consumption. Bacterial DMS consumption rates, calculated by subtracting $NP_{bio,DMS}$ from GP_{DMS}, consumed on average 11 %, 31 %, 43 % and 14 % of GP_{DMS} in surface, middle, bottom and mixing bottles, respectively. Thus, the imbalance between GP_{DMS} and bacterial DMS consumption increased with spectral irradiance due to UV and/or PAR inhibition of bacterial DMS consumption and stimulation of GP_{DMS}, making the vertical gradient of $NP_{bio,DMS}$ even larger than that of GP_{DMS} (Fig. 6b). The net stimulating effect of sunlight on biological DMS production was largely compensated by DMS photolysis, so that net overall DMS concentration changes were close to zero in all treatments, as already observed by Galí et al. (2013a) with other experimental settings.

Bacterial DMS consumption, expressed as the % of vertically integrated rates, was 49 %, 79 %, 125 % and 78 % in surface, middle, bottom and mixing bottles, respectively. Although these results suffer from a large uncertainty due to error propagation, they suggest that bacterial DMS consumption was more strongly inhibited than bulk LIR, and that it was photoinhibited in a dose-dependent manner. Severe photoinhibition was already observed by Toole et al. (2006), who reported a similar response of bacterial DMS consumption and LIR. Since only a portion of the bacterial community is able to consume DMS through oxidation, it is likely that the photoresponse of bacterial DMS consumers and that of bulk heterotrophic bacteria differ (as suggested by Galí and Simó, 2010) and also that the photoresponse of different metabolic activities differs in a given cell or strain. Clearly, these issues deserve further investigation.

3.5 Differential irradiance- and dose-response among biogeochemical processes

The experiment-normalized PPp, LIRs and community DMS production rates were plotted against the mean (UVB, UVA, PAR) incubation irradiance in the ensemble of all the experiments, and the points corresponding to fixed bottles were fitted with a linear regression (Fig. 7). We also calculated the Pearson correlation coefficient between the experiment-normalized process rates and (1) mean irradiance and (2) total irradiance dose for each radiation band (Fig. 8). The aim of this exercise was to identify whether a process was more dose-dependent or irradiance ("dosage-rate")-dependent, following the rationale exposed in the Introduction. Note that in our experimental setting it is hard to discriminate between the effects of each band of the spectrum, since the proportion of shortwave UV decreases along with total (or PAR) irradiance as we move deeper in the water column.

PPp showed a slight negative trend with respect to irradiance in fixed bottles in the three radiation bands, which was mainly driven by photoinhibition in surface bottles. In fact, the response was rather flat below an irradiance threshold of ca. 0.4 W m^{-2} UVB, 16 W^{-2} UVA and 1000 μmol photons m^{-2} s^{-1}. The correlation with irradiance was higher than that with dose (Fig. 8a), suggesting that some balance between inhibition and protection/repair could be attained in the different exposure regimes. The highest linear correlation was found with UVA irradiance, perhaps indicating that this band drives photoinhibition in UV-transparent waters. In concordance with this suggestion, some studies have shown that the spectral peak of UV photoinhibition occurs in the UVA, due to the combination of increasing irradiance and decreasing UV effectiveness as we move towards longer wavelengths (Neale and Kieber, 2000).

LIR decreased with increasing UVB, UVA and PAR with a slope very similar to that of PPp. Contrary to the other processes examined, the photoinhibition of LIR was more strongly correlated to the dose than to irradiance, particularly in the UVB band, suggesting that cumulative UVB-induced DNA damage occurred in bacterial cells in fixed incubations (Buma et al., 2001). This fits with the general idea that the radiation bands causing damage (UVB) elicit more dose-dependent responses than the radiation bands that are used by the cells to conduct physiological processes (PAR and longwave UVA).

Community DMS production rates showed a strong response to variations in spectral irradiance, with a steeper slope observed for $NP_{bio,DMS}$ than for GP_{DMS} (Fig. 7c, d). The strongest correlations were found between GP_{DMS} and irradiance in the three bands, particularly in the UVA. This

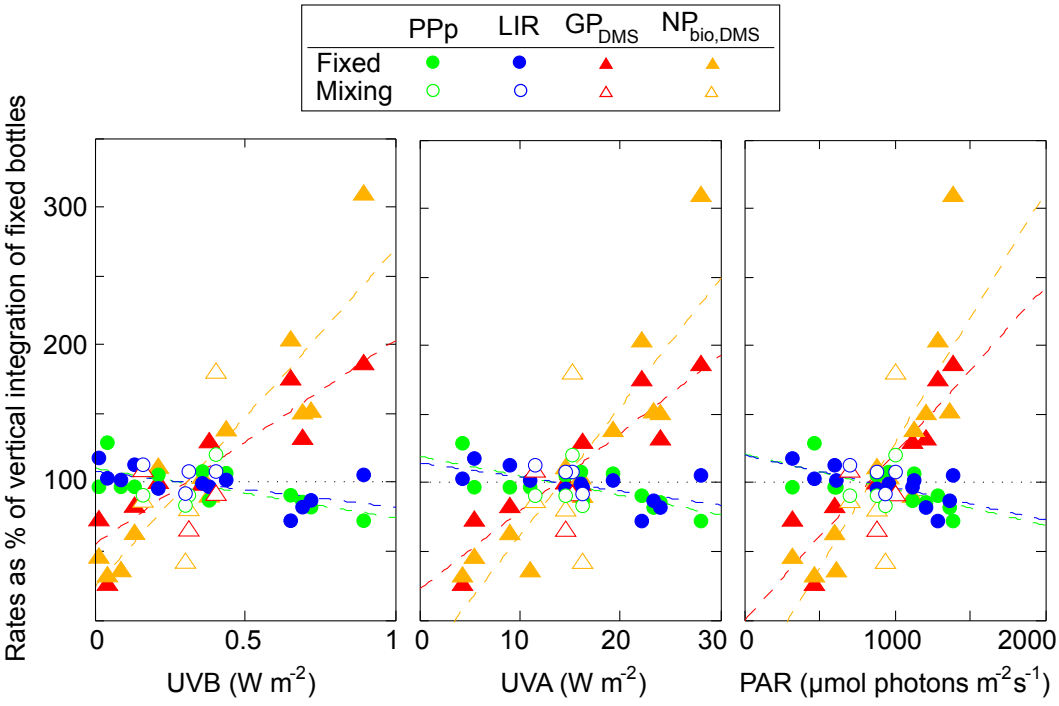

Fig. 7. Relationship between mean UVB, UVA and PAR irradiance during the incubations and particulate primary production (PPp), leucine incorporation rates (LIRs), gross DMS production (GP_{DMS}) and net biological DMS production ($NP_{bio,DMS}$). The rates have been normalized to the vertical integral of fixed-depth incubations (see text). The lines represent linear least squares fits to the fixed-depth incubations only (filled symbols). Vertically moving incubations ("mixing", open symbols) have not been included in the regressions.

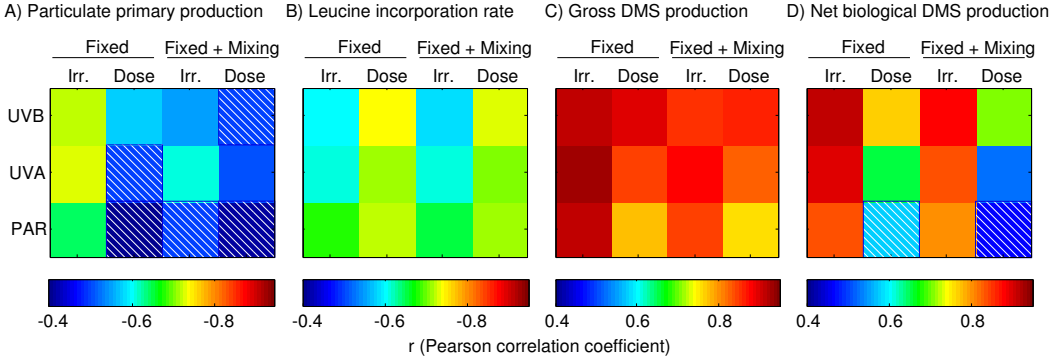

Fig. 8. Pearson's correlation coefficient (r) between biogeochemical process rates and mean incubation irradiance (Irr.) or cumulative dose in different radiation bands (UVB, UVA and PAR), in fixed bottles only and in the ensemble of fixed + mixing bottles. Note that r is negative in **(a)** and **(b)** and positive in **(c)** and **(d)**. The diagonal stripe pattern indicates non-significant r ($p > 0.05$).

agrees with previous studies that suggested, using distinct approaches, that the spectral peak of sunlight-induced DMS production occurs in the 330–340 nm region in surface UV-transparent waters (Toole et al., 2008; Levine et al., 2012; Galí et al., 2013a).

Finally, note that among all process and radiation combinations (Fig. 8) the correlation was stronger when mixing bottles were excluded. This illustrates in a loose way that mixing subtly disrupted the photoacclimation and photodamage processes, as thoroughly discussed in Sects. 3.2–3.4.

The results presented here on the enhancement of DMS production by increased irradiance and relative UVB exposure agree with those recently reported by our group using a variety of approaches, from light spectrum manipulation with optical filters (Galí et al., 2013a) to the study of diel cycles at sea (Galí et al., 2013b). They all provide mechanistic bases to the role of solar radiation as the main driver of DMS

production and concentration in the surface ocean (Vallina and Simó, 2007). In the short term (hours) sunlight directly affects the cellular machineries of DMS producers and DMS consumers, and favors DMSP-to-DMS conversion pathways; in the longer term (days to months) sunlight shapes the seasonality of the dynamics in upper-ocean physics and plankton succession, favoring DMSP producers. As a resulting emergent property, DMS tends to increase in summer even in regions where phytoplankton biomass is at its annual minimum. This phenomenon was termed the "DMS summer paradox" (Simó and Pedrós-Alió, 1999) and suggested to be at the base of a "seasonal CLAW" hypothesis by which plankton respond to higher summer irradiances by increasing the production of cloud-brightening DMS (Vallina and Simó, 2008). Whether this seasonal feedback will also operate efficiently at the longer timescale of anthropogenic global warming or Earth climate cycles cannot be easily predicted from short-term observations. Indeed, projections point to an enhancement, expansion and longer duration of stratification by global warming, with shallower mixed layers during longer periods (Sarmiento et al., 1998), which would result in increased exposures of plankton to UVR (Diaz et al., 2000). In view of our results, this might lead to increased DMS concentrations/emissions. However, the likely substitution of plankton species and communities by ones more adapted to the evolving conditions, and the development of protection strategies against environmental stress, hamper the straightforward applicability of our short-term observations to long-term trends.

4 Conclusions

The photoresponse of phytoplankton, bacterioplankton, and community DMS production displayed clear trends in bottles incubated at fixed depths in the UML (Fig. 7) despite the relatively small gradient in spectral irradiance. The irradiance dose response in mixing bottles was distinct (though subtle) in each of the processes measured, as well as for different physiological indicators. In the oligotrophic waters investigated, dynamic light exposure generally caused, compared to the middle bottles receiving the same cumulative exposure, (1) an adverse though non-significant effect on particulate primary production, concomitant with reduced cell-specific fluorescence in most experiments and phytoplankton groups; (2) a slightly alleviating effect on bacterial production photoinhibition, related to an increase in the proportion of intact-membrane, or live, heterotrophic bacteria in two of the experiments; and (3) a neutral effect or slight reduction in gross DMS production. These responses translated, in some experiments, into measurable deviations with respect to the vertically integrated rates in the water column; in others, the effects were close to neutral or too small to be reliably detected. Incubating the samples at a fixed intermediate optical depth appears as a reasonable and convenient solution for measuring GP_{DMS} and leucine incorporation, at least in UVR-transparent stratified UML waters. However, this solution might not be optimal for measuring UML-integrated primary production. Our results call for a more systematic assessment of the consequences of dynamic light exposure of microbial plankton in different oceanic regimes. This way, the photobiological processes governing, among other important processes, the ocean–atmosphere exchange of long-lived (CO_2) and short-lived (DMS) gases of climatic relevance will be better understood.

Acknowledgements. We thank the staff at Port Olímpic de Barcelona for their collaboration, and the crew and scientists aboard R/V *García del Cid* for their invaluable help in setting up the experiments during the SUMMER-I cruise. We also thank D. J. Kieber for his insightful comments on an earlier version of the manuscript, R. Bertoni for sharing his expertise, and two anonymous reviewers for their constructive suggestions. M. G. acknowledges the receipt of a CSIC JAE scholarship. This work was supported by the (former) Spanish Ministry of Science and Innovation through the project SUMMER (CTM2008-03309/MAR). This is a contribution of the Research Groups on Marine Biogeochemistry and Global Change and on Aquatic Microbial Food Webs, supported by the Generalitat de Catalunya.

Edited by: G. Herndl

References

Aas, P., Lyons, M., Pledger, R., Mitchell, D., and Jeffrey, W.: Inhibition of bacterial activities by solar radiation in nearshore waters and the Gulf of Mexico, Aquat. Microb. Ecol., 11, 229–238, doi:10.3354/ame011229, 1996.

Agogué, H., Joux, F., Obernosterer, I., and Lebaron, P.: Resistance of Marine Bacterioneuston to Solar Radiation, Appl. Environ. Microb., 71, 5282–5289, doi:10.1128/AEM.71.9.5282, 2005.

Alonso-Sáez, L., Gasol, J. M., Lefort, T., Hofer, J., and Sommaruga, R.: Effect of natural sunlight on bacterial activity and differential sensitivity of natural bacterioplankton groups in northwestern Mediterranean coastal waters, Appl. Environ. Microb., 72, 5806–5813, doi:10.1128/AEM.00597-06, 2006.

Archer, S. D., Cummings, D., Llewellyn, C., and Fishwick, J.: Phytoplankton taxa, irradiance and nutrient availability determine the seasonal cycle of DMSP in temperate shelf seas, Mar. Ecol. Prog. Ser., 394, 111–124, doi:10.3354/meps08284, 2009.

Archer, S. D., Ragni, M., Webster, R., Airs, R. L., and Geider, R. J.: Dimethyl sulfoniopropionate and dimethyl sulfide production in response to photoinhibition in *Emiliania huxleyi*, Limnol. Oceanogr., 55, 1579–1589, doi:10.4319/lo.2010.55.4.1579, 2010.

Asher, E. C., Dacey, J. W. H., Mills, M. M., Arrigo, K. R., and Tortell, P. D.: High concentrations and turnover rates of DMS, DMSP and DMSO in Antarctic sea ice, Geophys. Res. Lett., 38, 1–5, doi:10.1029/2011GL049712, 2011.

Barbieri, E. S., Villafañe, V. E., Helbling, E. W., and Nov, N.: Experimental assessment of UV effects on temperate marine phy-

toplankton when exposed to variable radiation regimes, Limnol. Oceanogr., 47, 1648–1655, 2002.

Béjà, O., Aravind, L., Koonin, E. V., Suzuki, M. T., Hadd, A., Nguyen, L. P., Jovanovich, S. B., Gates, C. M., Feldman, R. A., Spudich, J. L., Spudich, E. N., and DeLong, E. F.: Bacterial Rhodopsin: Evidence for a New Type of Phototrophy in the Sea, Science, 289, 1902–1906, doi:10.1126/science.289.5486.1902, 2000.

Bertoni, R., Jeffrey, W. H., Pujo-Pay, M., Oriol, L., Conan, P., and Joux, F.: Influence of water mixing on the inhibitory effect of UV radiation on primary and bacterial production in Mediterranean coastal water, Aquat. Sci., 73, 377–387, doi:10.1007/s00027-011-0185-8, 2011.

Brainerd, K. E. and Gregg, M. C.: Surface mixed and mixing layer depths, Deep Sea Res. Pt. I, 42, 1521–1543, 1995.

Bricaud, A., Babin, M., Morel, A., and Claustre, H.: Variability in the chlorophyll-specific absorption coefficients of natural phytoplankton, Analysis and parameterization, J. Geophys. Res., Oceans, 100, 13321–13332, doi:10.1029/95JC00463, 1995.

Brunet, C. and Lavaud, J.: Can the xanthophyll cycle help extract the essence of the microalgal functional response to a variable light environment?, J. Plankton Res., 32, 1609–1617, doi:10.1093/plankt/fbq104, 2010.

Bucciarelli, E. and Sunda, W. G.: Influence of CO_2, nitrate, phosphate, and silicate limitation on intracellular dimethylsulfoniopropionate in batch cultures of the coastal diatom *Thalassiosira pseudonana*, Limnol. Oceanogr., 48, 2256–2265, doi:10.4319/lo.2003.48.6.2256, 2003.

Buma, A. G., Helbling, E. W., de Boer, M. K., and Villafañe, V. E.: Patterns of DNA damage and photoinhibition in temperate South-Atlantic picophytoplankton exposed to solar ultraviolet radiation, J. Photoch. Photobio. B, 62, 9–18, 2001.

Campbell, D., Eriksson, M. J., Oquist, G., Gustafsson, P., and Clarke, A. K.: The cyanobacterium *Synechococcus* resists UV-B by exchanging photosystem II reaction-center D1 proteins, P. Natl. Aca. Sci. USA, 95, 364–9, 1998.

Carpenter, L. J., Archer, S. D., and Beale, R.: Ocean-atmosphere trace gas exchange, Chem. Soc. Rev., 41, 6473–6506, 2012.

Church, M. J., Ducklow, H. W., and Karl, D. M.: Light dependence of [3H]leucine incorporation in the oligotrophic North Pacific ocean, Appl. Environ. Microb., 70, 4079–87, doi:10.1128/AEM.70.7.4079-4087.2004, 2004.

Denman, K. L. and Gargett, A. E.: Time and space scales of vertical mixing in the upper ocean, Limnol. Oceanogr., 28, 801–815, 1983.

Dıaz, S. B., Morrow, J. H., and Booth, C. R.: UV physics and optics, The effects of UV radiation in the marine environment, 35–71, 2000.

Galí, M. and Simó, R.: Occurrence and cycling of dimethylated sulfur compounds in the Arctic during summer receding of the ice edge, Mar. Chem., 122, 105–117, doi:10.1016/j.marchem.2010.07.003, 2010.

Galí, M., Saló, V., Almeda, R., Calbet, A., and Simó, R.: Stimulation of gross dimethylsulfide (DMS) production by solar radiation, Geophys. Res. Lett., 38, 1–5, doi:10.1029/2011GL048051, 2011.

Galí, M., Ruiz-González, C., Lefort, T., Gasol, J. M., Cardelús, C., Romera-Castillo, C., and Simó, R.: Spectral irradiance dependence of sunlight effects on plankton dimethylsulfide production, Limnol. Oceanogr., 58, 489–504, 2013a.

Galí, M., Simó, R., Vila-Costa, M., Ruiz-González, C., Gasol, J. M., and Matrai, P.: Diel patterns of oceanic dimethylsulfide (DMS) cycling: Microbial and physical drivers, Glob. Biogeochem. Cy., 2013b.

Gallegos, C. L. and Platt, T.: Vertical advection of phytoplankton and productivity estimates: a dimensional analysis, Mar. Ecol. Prog. Ser., 26, 125–134, 1985.

Grégori, G., Citterio, S., Ghiani, A., Labra, M., Sgorbati, S., Brown, S., and Denis, M.: Resolution of viable and membrane-compromised bacteria in freshwater and marine waters based on analytical flow cytometry and nucleic acid double staining, Appl. Environ. Microb., 67, 4662–4670, 2001.

Harada, H., Vila-Costa, M., Cebrian, J., and Kiene, R. P.: Effects of UV radiation and nitrate limitation on the production of biogenic sulfur compounds by marine phytoplankton, Aquat. Bot., 90, 37–42, 2009.

Hefu, Y. and Kirst, G. O.: Effect of UV- radiation on DMSP content and DMS formation of *Phaeocystis* antarctica, Polar Biol., 18, 402–409, doi:10.1007/s003000050206, 1997.

Helbling, E. W., Carrillo, P., Medina-Sánchez, J. M., Durán, C., Herrera, G., Villar-Argaiz, M., and Villafañe, V. E.: Interactive effects of vertical mixing, nutrients and ultraviolet radiation: in situ photosynthetic responses of phytoplankton from high mountain lakes in Southern Europe, Biogeosciences, 10, 1037–1050, doi:10.5194/bg-10-1037-2013, 2013.

Helbling, E. W., Gao, K., Gonçalves, R., Wu, H., and Villafañe, V. E.: Utilization of solar UV radiation by coastal phytoplankton assemblages off SE China when exposed to fast mixing, Mar. Ecol. Prog. Ser., 259, 59–66, doi:10.3354/meps259059, 2003.

Kaiser, E. and Herndl, G. J.: Rapid Recovery of Marine Bacterioplankton Activity after Inhibition by UV Radiation in Coastal Waters, Appl. Environ. Microb., 63, 4026–4031, 1997.

Kirchman, D., K'nees, E., and Hodson, R.: Leucine incorporation and its potential as a measure of protein synthesis by bacteria in natural aquatic systems, Appl. Environ. Microbiol., 49, 599–607, 1985.

Kirchman, D. L. and Hanson, T. E.: Bioenergetics of photoheterotrophic bacteria in the oceans, Environ. Microbiol. Rep., 5, 188–199, doi:10.1111/j.1758-2229.2012.00367.x, 2012.

Kolber, Z., Van Dover, C., Niederman, R., and Falkowski, P.: Bacterial photosynthesis in surface waters of the open ocean, Nature, 407, 177–179, 2000.

Lana, A., Bell, T. G., Simó, R., Vallina, S. M., Ballabrera-Poy, J., Kettle, A. J., Dachs, J., Bopp, L., Saltzman, E. S., Stefels, J., Johnson, J. E., and Liss, P. S.: An updated climatology of surface dimethlysulfide concentrations and emission fluxes in the global ocean, Global Biogeochem. Cy., 25, 1–17, doi:10.1029/2010GB003850, 2011.

Levine, N. M., Varaljay, V. A., Toole, D. A., Dacey, J. W. H., Doney, S. C., and Moran, M. A.: Environmental, biochemical and genetic drivers of DMSP degradation and DMS production in the Sargasso Sea, Environ. Microbiol., 14, 1210–1223, doi:10.1111/j.1462-2920.2012.02700.x, 2012.

MacIntyre, H. L., Kana, T. M., Anning, T., and Geider, R. J.: Photoacclimation of photosynthesis irradiance response curves and photosynthetic pigmentspigments in microalgae and cyanobacteria, J. Phycol., 38, 17–38, 2002.

Marie, D. and Partensky, F.: Analyse de micro-organismes marins, in: La cytométrie en flux, edited by: Ronot, X., Grunwald, D., Mayol, J. F., and Boutonnat, J., Lavoisier, 211–233, 2006.

Mitchell, B., Bricaud, A., Carder, K., Cleveland, J. S., F., G. M., and Gould, R.: Determination of spectral absorption coefficients of particles, dissolved material and phytoplankton for discrete water samples, in: Ocean Optics Protocols for Satellite Ocean Color Sensor Validation, Revision 2, edited by: Fargion, G., Mueller, J., and McClain, C., NASA, 125–153, 2000.

Mitchell, B. G. and Kiefer, D. A.: Determination of absorption and fluorescence excitation spectra for phytoplankton, in: Marine Phytoplankton and Productivity, edited by: Holm-Hansen, O., Bolis, L., and Giles, R., 157–169, Springer, 1984.

Morán, X. A. G., Gasol, J. M., Arin, L., and Estrada, M.: A comparison between glass fiber and membrane filters for the estimation of phytoplankton POC and DOC production, Mar. Ecol. Prog. Ser., 187, 31–41, 1999.

Morán, X. A. G., Massana, R., and Gasol, J. M.: Light Conditions Affect the Measurement of Oceanic Bacterial Production via Leucine Uptake, Appl. Environ. Microb., 67, 3795–3801, doi:10.1128/AEM.67.9.3795-3801.2001, 2001.

Neale, P. J. and Kieber, D. J.: Assessing Biological and Chemical Effects of UV in the Marine Environment: Spectral Weighting Functions, Issues in Environmental Science and Technology, 2000.

Neale, P. J., Helbling, E. W., and Zagarese, H. E.: Modulation of UVR exposure and effects by vertical mixing and advection, in: UV effects in aquatic organisms and ecosystems, The Royal Society of Chemistry Cambridge, 107–134, 2003.

Quinn, P. K. and Bates, T. S.: The case against climate regulation via oceanic phytoplankton sulphur emissions, Nature, 480, 51–6, doi:10.1038/nature10580, 2011.

Ross, O. N., Geider, R. J., Berdalet, E., Artigas, M. L., and Piera, J.: Modelling the effect of vertical mixing on bottle incubations for determining in situ phytoplankton dynamics. I. Growth rates, Mar. Ecol. Prog. Ser., 435, 13–31, doi:10.3354/meps09193, 2011a.

Ross, O. N., Geider, R. J., and Piera, J.: Modelling the effect of vertical mixing on bottle incubations for determining in situ phytoplankton dynamics Pt.II., Primary production, Mar. Ecol. Prog. Ser., 435, 33–45, doi:10.3354/meps09194, 2011b.

Roy, S.: The strategies for minimization of UV damage, in: The Effects of UV Radiation in the Marine Environment, edited by: de Mora, S. J., Demers, S., and Vernet, M., chap. 3, 177–205, Cambridge University Press, Cambridge, 2000.

Ruiz-González, C., Galí, M., Lefort, T., Cardelús, C., Simó, R., and Gasol, J. M.: Annual variability in light modulation of bacterial heterotrophic activity in surface northwestern Mediterranean waters, Limnol. Oceanogr., 57, 1376–1388, doi:10.4319/lo.2012.57.5.1376, 2012.

Ruiz-González, C., Simó, R., Sommaruga, R., and Gasol, J. M.: Away from darkness: A review on the effects of solar radiation on heterotrophic bacterioplankton activity, Front. Microbiol., 4, 131, doi:10.3389/fmicb.2013.00131, 2013.

Saló, V., Simó, R., and Calbet, A.: Revisiting the dilution technique to quantify the role of microzooplankton in DMS(P) cycling: laboratory and field tests, J. Plankton Res., 32, 1255–1267, doi:10.1093/plankt/fbq041, 2010.

Sarmento, H. and Gasol, J. M.: Use of phytoplankton-derived dissolved organic carbon by different types of bacterioplankton., Environ. Microb., 14, 2348–60, doi:10.1111/j.1462-2920.2012.02787.x, 2012.

Sarmiento, J. L., Hughes, T. M., Stouffer, R. J., and Manabe, S.: Simulated response of the ocean carbon cycle to anthropogenic climate warming, Nature, 393, 245–249, 1998.

Shick, J. M. and Dunlap, W. C.: Mycosporine-like amino acids and related Gadusols: biosynthesis, acumulation, and UV-protective functions in aquatic organisms, Ann. Rev. Physiol., 64, 223–62, doi:10.1146/annurev.physiol.64.081501.155802, 2002.

Simó, R.: From cells to globe : Approaching the dynamics of DMS(P) in the ocean at multiple scales, Can. J. Fish. Aquat. Sci., 61, 673–684, doi:10.1139/F04-030, 2004.

Simó, R. and Pedrós-Alió, C.: Role of vertical mixing in controlling the oceanic production of dimethyl sulphide, Nature, 402, 396–399, 1999.

Simó, R., Pedrós-Alió, C., Malin, G., and Grimalt, J. O.: Biological turnover of DMS, DMSP and DMSO in contrasting open-sea waters, Mar. Ecol. Prog. Ser., 203, 1–11, doi:10.3354/meps203001, 2000.

Simó, R., Vila-Costa, M., Alonso-Sáez, L., Cardelús, C., Guadayol, O., Vázquez-Domínguez, E., and Gasol, J.: Annual DMSP contribution to S and C fluxes through phytoplankton and bacterioplankton in a NW Mediterranean coastal site, Aquat. Microb. Ecol., 57, 43–55, doi:10.3354/ame01325, 2009.

Slezak, D. and Herndl, G.: Effects of ultraviolet and visible radiation on the cellular concentrations of dimethylsulfoniopropionate (DMSP) in Emiliania huxleyi (strain L), Mar. Ecol. Prog. Ser., 246, 61–71, doi:10.3354/meps246061, 2003.

Smith, D. C. and Azam, F.: A simple, economical method for measuring bacterial protein synthesis rates in seawater using 3H-leucine, Marine Microbial Food Webs, 6, 107–114, 1992.

Sommaruga, R., Hofer, J. S., Alonso-Saez, L., and Gasol, J. M.: Differential sunlight sensitivity of picophytoplankton from surface Mediterranean coastal waters, Appl. Environ. Microb., 71, 2154–2157, doi:10.1128/AEM.71.4.2154, 2005.

Spiese, C., Kieber, D. J., Nomura, C., and Kiene, R. P.: Reduction of dimethylsulfoxide to dimethylsulfide by marine phytoplankton, Limnol. Oceanogr., 54, 560–570, 2009.

Stefels, J.: Physiological aspects of the production and conversion of DMSP in marine algae and higher plants, J. Sea Res., 43, 183–197, doi:10.1016/S1385-1101(00)00030-7, 2000.

Sunda, W., Kieber, D. J., Kiene, R. P., and Huntsman, S.: An antioxidant function for DMSP and DMS in marine algae., Nature, 418, 317–20, doi:10.1038/nature00851, 2002.

Sunda, W. G., Hardison, R., Kiene, R. P., Bucciarelli, E., and Harada, H.: The effect of nitrogen limitation on cellular DMSP and DMS release in marine phytoplankton: climate feedback implications, Aquat. Sci., 69, 341–351, doi:10.1007/s00027-007-0887-0, 2007.

Toole, D. A., Slezak, D., Kiene, R. P., Kieber, D. J., and Siegel, D. A.: Effects of solar radiation on dimethylsulfide cycling in the western Atlantic Ocean, Deep Sea Res. Pt. I, 53, 136–153, 2006.

Toole, D. A., Siegel, D. A., and Doney, S. C.: A light-driven, one-dimensional dimethylsulfide biogeochemical cycling model for the Sargasso Sea, J. Geophys. Res., 113, 1–20, doi:10.1029/2007JG000426, 2008.

Vallina, S. M. and Simó, R.: Strong relationship between DMS and the solar radiation dose over the global surface ocean., Science, 315, 506–508, doi:10.1126/science.1133680, 2007.

Vallina, S. M. and Simó, R.: Re-visiting the CLAW hypothesis, Environ. Chem., 4, 384–387, 2008.

van de Poll, W. H. and Buma, A. G. J.: Does ultraviolet radiation affect the xanthophyll cycle in marine phytoplankton?, Photochem. Photobiol. Sci., 8, 1295–1301, doi:10.1039/B904501E, 2009.

van Rijssel, M. and Buma, A.: UV radiation induced stress does not affect DMSP synthesis in the marine prymnesiophyte Emiliania huxleyi, Aquat. Microb. Ecol., 28, 167–174, doi:10.3354/ame028167, 2002.

Vila-Costa, M., Kiene, R. P., and Simó, R.: Seasonal variability of the dynamics of dimethylated sulfur compounds in a coastal northwest Mediterranean site, Limnol. Oceanogr., 53, 198–211, 2008.

Vincent, W. F. and Neale, P. J.: Mechanisms of UV damage to aquatic organisms, in: The Effects of UV Radiation in the Marine Environment, edited by de Mora, S. J., Demers, S., and Vernet, M., chap. 6, 149–176, Cambridge University Press, Cambridge, 2000.

Wolfe, G. and Kiene, R. P.: Radioisotope and chemical inhibitor measurements of dimethyl sulfide consumption rates and kinetics in estuarine waters, Mar. Ecol. Prog. Ser., 99, 261–269, 1993.

Woodhouse, M. T., Mann, G. W., Carslaw, K. S., and Boucher, O.: Sensitivity of cloud condensation nuclei to regional changes in dimethyl-sulphide emissions, Atmos. Chem. Phys., 13, 2723–2733, doi:10.5194/acp-13-2723-2013, 2013.

Yang, G., Li, C., and Sun, J.: Influence of salinity and nitrogen content on production of dimethylsulfoniopropionate (DMSP) and dimethylsulfide (DMS) by *Skeletonema costatum*, Chin. J. Oceanol. Limn., 29, 378–386, 2011.

Zapata, M., Rodríguez, F., and Garrido, J. L.: Separation of chlorophylls and carotenoids from marine phytoplankton: a new HPLC method using a reversed phase C8 column and pyridine-containing mobile phases, Mar. Ecol. Prog. Ser., 195, 29–45, doi:10.3354/meps195029, 2000.

CSIRO PUBLISHING

Environ. Chem.
http://dx.doi.org/10.1071/EN13203

Research Paper

Development and validation of a shipboard system for measuring high-resolution vertical profiles of aqueous dimethylsulfide concentrations using chemical ionisation mass spectrometry

Sarah-Jeanne Royer,[A] *Martí Galí,*[A] *Eric S. Saltzman,*[B] *Cyril A. McCormick,*[B] *Thomas G. Bell*[B,C] *and Rafel Simó*[A,D]

[A]Institut de Ciències del Mar (CSIC), Passeig Marítim de la Barceloneta 37-49, E-08003 Barcelona, Catalonia, Spain.
[B]University of California, Irvine, CA 92697-3100, USA.
[C]Present address: Plymouth Marine Laboratory, Plymouth, PL1 3DH, UK.
[D]Corresponding author. Email: rsimo@icm.csic.es

Environmental context. Dimethylsulfide, a trace gas produced by oceanic plankton, is a key chemical species in the global cycles of sulfur and aerosols, with implications that span marine ecology to climate regulation. Knowledge of what governs dimethylsulfide production in the surface ocean depends on our ability to measure concentration changes over time and depth. We describe a sampling and analytical system that provides continuous shipboard measurements of dimethylsulfide concentrations in high-resolution vertical profiles.

Abstract. A sampling and analytical system has been developed for shipboard measurements of high-resolution vertical profiles of the marine trace gas dimethylsulfide (DMS). The system consists of a tube attached to a conductivity–temperature–depth (CTD) probe with a peristaltic pump on deck that delivers seawater to a membrane equilibrator and atmospheric pressure chemical ionisation mass spectrometer (Eq-APCIMS). This allows profiling of DMS concentrations to a depth of 50 m, with a depth resolution of 1.3–2 m and a detection limit of nearly 0.1 nmol L^{-1}. The seawater is also plumbed to allow parallel operation of additional continuous instruments, and simultaneous collection of discrete samples for complementary analyses. A valve alternates delivery of seawater from the vertical profiler and the ship's underway intake, thereby providing high-resolution measurements in both the vertical and horizontal dimensions. Tests conducted on various cruises in the Mediterranean Sea, Atlantic, Indian, and Pacific Oceans show good agreement between the Eq-APCIMS measurements and purge and trap gas chromatography with flame photometric detection (GC-FPD) and demonstrate that the delivery of seawater from the underway pump did not significantly affect endogenous DMS concentrations. Combining the continuous flow DMS analysis with high-frequency hydrographic, optical, biological and meteorological measurements will greatly improve the spatial–temporal resolution of seagoing measurements and improve our understanding of DMS cycling.

Received 13 November 2013, accepted 14 February 2014, published online 5 June 2014

Introduction

Dimethylsulfide (DMS) is ubiquitous in the pelagic ocean and plays a key role in the global sulfur cycle.[1–3] The knowledge gained in recent decades about this volatile sulfur compound and its precursor dimethylsulfoniopropionate (DMSP) is of such extent that they are some of the best-studied organic substances in the world's ocean. The global surface seawater DMS concentration database[4,5] is the third largest oceanic trace gas database behind those of CO_2 and N_2O. DMS plays a significant role in the formation, growth and chemistry of marine aerosols,[6] the long-term return of sulfur from the oceans to the continents via the atmosphere,[7] and the chemical ecology of many marine living beings.[8–11] It has been argued that DMS plays a central role in a plankton–climate regulatory feedback loop, but this remains controversial.[12–14]

The analytical methods most used to determine aqueous DMS concentrations over the last 40 years consist of gas chromatography (GC) with flame photometric or chemiluminescence detectors (e.g. Andreae and Barnard,[15] Turner and Liss,[16] Bates et al.,[17] Dacey et al.[18] and Simó[19]) on samples collected with Niskin bottles or shipboard pumping systems. Most of the reported oceanic DMS observations are from near-surface samples (1 to 10-m depth) or from unequally spaced and sparse samples collected from vertical profiles. The limited vertical resolution of the sampling technique (usually Niskin bottles attached to a conductivity–temperature–depth (CTD) rosette), together with the time needed for the analysis of discrete samples, result in a poor resolution of the obtained vertical concentration profiles.

Today, mass spectrometric techniques with high sensitivity and fast response allow the determination of DMS without pre-concentration. These techniques, supplied with seawater pumped continuously from the ocean and coupled to either bubbling or membrane equilibration to remove the volatiles

from their aqueous matrix, provide high-frequency measurements of seawater DMS concentrations. Recently, several systems that involve coupling of water–gas equilibrators to electron impact, chemical ionisation and proton transfer mass spectrometers have been developed.[20–22] These systems have the potential to dramatically increase the collection of surface ocean DMS data. The 30+ year global DMS database contains nearly 50 000 data points.[5] Today, a single cruise of 20 days with one of these systems working continuously provides ~10 000 measurements for 5 min averaged data. These systems are suited to resolve sub-mesoscale and short-term variability features.[23–25] However, before thousands of new data are archived into the global database, it is important to intercompare the new techniques with each other and with the traditional GC methods.[26] To our knowledge, only one study[27] has reported a comparison exercise of a high-frequency mass spectrometric technique (MIMS) with purge and trap GC. The results showed good consistency in capturing DMS variability but exhibited a variable offset.

The increasing resolution on the horizontal and temporal scales has not yet been matched in the vertical scale, because the aforementioned instruments have been coupled to shipboard underway intake systems that pump water from a single depth. To date, vertical profiles of DMS concentration are obtained from discrete samples and measured manually using non-automated instruments (e.g. GC), with a depth resolution of several meters and a time resolution of hours between casts. This lack of high-resolution concentration profiles limits description of DMS dynamics on short temporal scales and understanding of the complex biogeochemical interactions that drive oceanic DMS cycling across the water column.

Here we present the development of a technique for sampling and analysing DMS concentrations at high frequency through the upper water column along with parallel measurements of physical and biological variables. The technique consists of a profiling sampler, connected to a membrane equilibrator and atmospheric pressure chemical ionisation mass spectrometer (Eq-APCIMS). We describe the system components and its operation, and compare the results with those from the purge and trap gas chromatograph with flame photometric detection (GC-FPD) technique. To our knowledge, this is the first time that a continuous sampling technique has enabled vertical DMS concentration profiles at high resolution over depth and time.

Experimental

The analytical system

This study used a tubular counter-flow membrane equilibrator. Details of equilibrator design, construction and operating conditions are given in Saltzman et al.[22] and Table 1. The equilibrator consists of a porous hydrophobic Teflon-membrane tube mounted inside a coiled larger internal diameter tube. Seawater flows through the annular space between the porous membrane and outer tubes and high purity (zero) air counter-flows through the porous inner tube. Dissolved gases, including DMS, diffuse across the pores in the inner tube wall into the air stream, such that the exiting air reaches equilibrium with the seawater DMS. The air exiting the equilibrator is mixed with a larger dilution flow of zero air and directed to the source of the APCIMS. The residence time of seawater and zero air in the equilibrator are respectively ~10 and 20 s.

DMS was detected using an APCIMS. The instrument used in this study is the 'mini-CIMS', developed and described in detail by Saltzman et al.[22] The mini-CIMS is a single quadrupole mass spectrometer based on the Stanford Research Systems residual gas analyser, with a heated ^{63}Ni radioactive source. DMS is ionised by proton transfer from protonated water ($H_2O{\cdot}H^+$), declustered, mass filtered and detected by an electron multiplier. Table 1 reports the lens potentials, ion source temperature and gas flow rates used to obtain optimal sensitivity for DMS. Fig. 1a shows a mass scan of the equilibrator outflow using the shipboard system on board the *R/V* Garcia del Cid in May 2012.

Table 1. Equilibrator and atmospheric pressure chemical ionisation mass spectrometer (APCIMS) operating parameters used in this study

Equilibrator	Flow rates (mL min^{-1})
Seawater flow	1800–2100
Air flow	60
Non-equilibrator gas lines	**Flow rates (mL min^{-1})**
Dilution (bypass) air	600
CH_3SCD_3 standard in air	70
APCIMS	
Region	Lens potential (V, direct current)
Lens	
Ion source (760 Torr)	
pinhole	65
Collision region (1 Torr)	
cone 1	34
cone 2	8
Analyser region (10^{-5} Torr)	
mesh 1	−110
aperture 2	12
aperture 3	−4
aperture 4	−90
focus plate	50
	Temperature (°C)
Ion source	350

DMS is quantified by monitoring the ratio of signals from ambient DMS ($CH_3SH_3\ H^+$, *m/z* 63) and an isotopically labelled internal standard (triple-deuterated DMS, $CH_3SCD_3\ H^+$, *m/z* 66). During regular operation in the field, data were recorded continuously by single ion monitoring (SIM) of DMS (*m/z* 63), CH_3SCD_3 (*m/z* 66), isoprene (*m/z* 69), $(H_2O)H^+$ (*m/z* 19), and $(H_2O)_2H^+$ (*m/z* 37) (Fig. 1b). The internal standard was provided by a CH_3SCD_3 permeation tube (0.78 ng min^{-1}; Dynacal, VICI Metronics, Valco Instruments, Houston, TX, USA) maintained at 30 °C in a permeation chamber diluted in a flow of 70 mL min^{-1} of zero air. The permeation rate was monitored in the laboratory before the cruises using high precision weight measurements, and validated by GC-FPD by cross calibration with a higher permeation rate DMS standard (183 ng min^{-1}) that in turn had been calibrated by high precision weighing and displayed a constant weight loss rate over a period of 4 years ($R^2 = 0.9999$). The output from the CH_3SCD_3 permeation tube was added to the air stream exiting the equilibrator. The level of DMS (*m/z* 63) impurity in the CH_3SCD_3 standard (*m/z* 66) corresponded to ~1.9 % of the signal at *m/z* 66 and was corrected from the raw *m/z* 63 data. Blank measurements in the dilution air were also run, but were typically negligible. Fig. 1b shows the raw signals typically acquired in SIM mode.

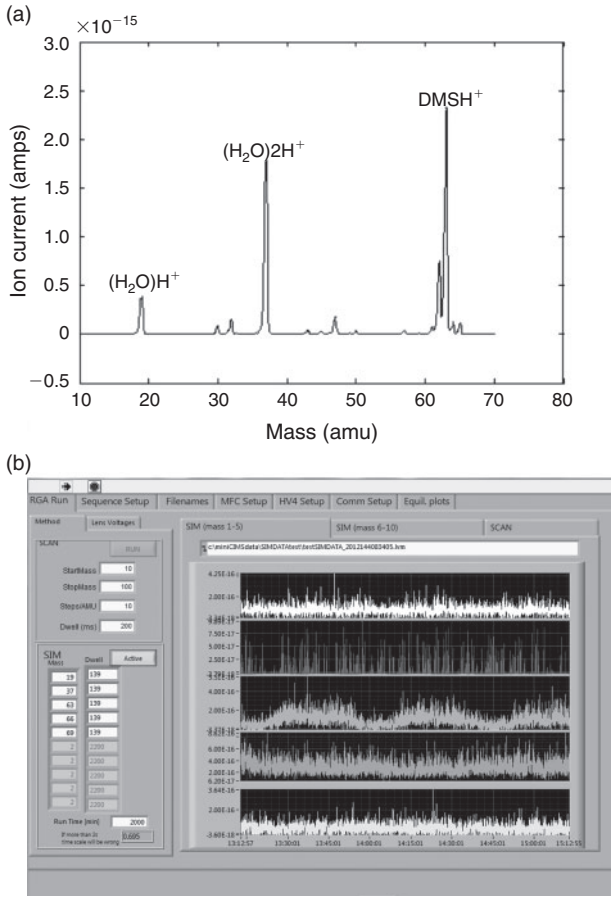

Fig. 1. (a) Ion scan from the equilibrator and atmospheric pressure chemical ionisation mass spectrometer (Eq-APCIMS) instrument running a seawater sample with no standard on-line. Sample collected with the underway-pumping system aboard the *R*/*V* Garcia del Cid in the Mediterranean Sea, May 2012. (b) A screen capture of the signal acquisition on the Eq-APCIMS; from top to bottom, raw signal for water molecules (*m*/*z* 19, $H_2O(H^+)$), clustered water molecules (*m*/*z* 37, $(H_2O)_2(H^+)$), dimethylsulfide (DMS) (*m*/*z* 63, $(CH_3)_2S(H^+)$), trideuterated DMS standard (*m*/*z* 66, $CH_3SCD_3(H^+)$), and isoprene (*m*/*z* 69, $C_5H_8(H^+)$).

The molar mixing ratio of ambient DMS (X_{DMS}) in the gas stream exiting the equilibrator is calculated as follows:

$$X_{DMS} = (C_{63}/C_{66}) \times (p/F_{eq})$$

where C_{63} and C_{66} are the blank corrected-signals (in amps) for *m*/*z* 63 and 66, p is the permeation rate (mol s^{-1}) and F_{eq} is air flow rate in the equilibrator (mol s^{-1}) determined from the measured mass flow and ideal gas law. The gas phase DMS mixing ratio (X_{DMS}) was converted into a seawater concentration (DMS_{sw}), using the temperature- and salinity-dependent Henry's law constant for DMS (H_{DMS}, M atm^{-1}; Dacey et al.[28]):

$$DMS_{sw} = X_{DMS} \times p_{atm} \times H_{DMS}$$

where p_{atm} is the atmospheric pressure.

The instrument was operated in an automated operational cycle consisting typically of a 12-h seawater data collection period (in SIM mode), followed by equilibrator blanks (no internal standard; 5 min SIM, 10 full scans) and standard-only blanks (equilibrator bypassed; 5 min SIM, 10 full scans). The blanks were used to account for the contribution of non-isotope DMS in the internal standard and to detect DMS contamination in the system tubing and electronic noise. These were very small corrections (1.9 %), and are minor contributors to the overall uncertainty of the measurement. It is important to note that these blanks do not account for any contamination of the equilibrator itself. The regular ambient data acquisition accounted for 95 % of the operation time.

The zero air for both the equilibrator and the internal standard was supplied either from a pressurised cylinder or by an ultra-zero air generator (model GT6000, LNI Schmidlin, Neuheim, Switzerland) fed by the compressed air supply of the ship.

The overall shipboard system layout

A schematic of the whole system on board is presented in Fig. 2. The setup allowed alternation between the underway intake while steaming, and vertical profiling when the ship was on station. The Eq-APCIMS was located in one of the ship laboratories, next to the outlet of the clean underway intake system. A valve allowed switching between the underway and profiler seawater supplies. A multitap set divided the incoming water flow into three parallel flows directed to: (1) the equilibrator and Eq-APCIMS, (2) a fast repetition rate fluorometer (FRRF; FASTracka, Chelsea Technologies, Surrey, UK) recording in continuous mode and (3) a tube for filling bottles for discrete measurements.

The underway seawater intake system

The underway seawater intake system used the ship's clean water intake pump, which provides an uncontaminated (non-toxic), continuous source of near-surface seawater. The water was brought to the laboratories through epoxide-free silicone pipes. A branch of the flow was directed through continuously logged thermo-salinograph, fluorometer and temperature sensors. The data reported in the present study were collected on three cruises: one conducted aboard the *R*/*V* Hesperides across the Atlantic, Indian and Pacific oceans (Malaspina cruise, January–June 2011), and the other two aboard the *R*/*V* Garcia del Cid in the north-western Mediterranean Sea (SUMMER cruises, September 2011 and May 2012). On the *R*/*V* Hesperides, the water intake is located 5 m below sea level, and the parts of the centrifugal pump (BKMKC-10.11, Tecnium, Manresa, Spain) in contact with the fluid are made of polypropylene and glass. On the *R*/*V* Garcia del Cid, the intake is located 4 m below sea level and the interior of the pump (BKMKC-8.10, Tecnium) is also made of polypropylene.

The vertical profiling system

The system developed for measuring high-resolution vertical profiles consisted of a CTD operated manually in up and down motion, with a tied hose through which water was pumped to the ship's laboratory. The device used for drawing seawater was an in-laboratory peristaltic pump (model 620UN, Watson-Marlow, Wilmington, MA, USA), which is free of valves, seals or glands to avoid clogging or corrosion. The pumped seawater flow contacts only the bore of the tube (Marprene, inert thermoplastic elastomer, Watson-Marlow), eliminating the risk of sample contamination. The pump flow rate was 3.5 L min^{-1}. The pump intake tubing was a 50–70-m non-toxic latex hose reinforced with polyester thread mesh (model Mallalatex, Espiroflex, Barcelona, Spain), with inner and outer diameters of 15 and 21 mm. A 10-cm diameter plastic funnel was mounted at the hose inlet and covered with 5-mm nylon mesh to avoid drawing

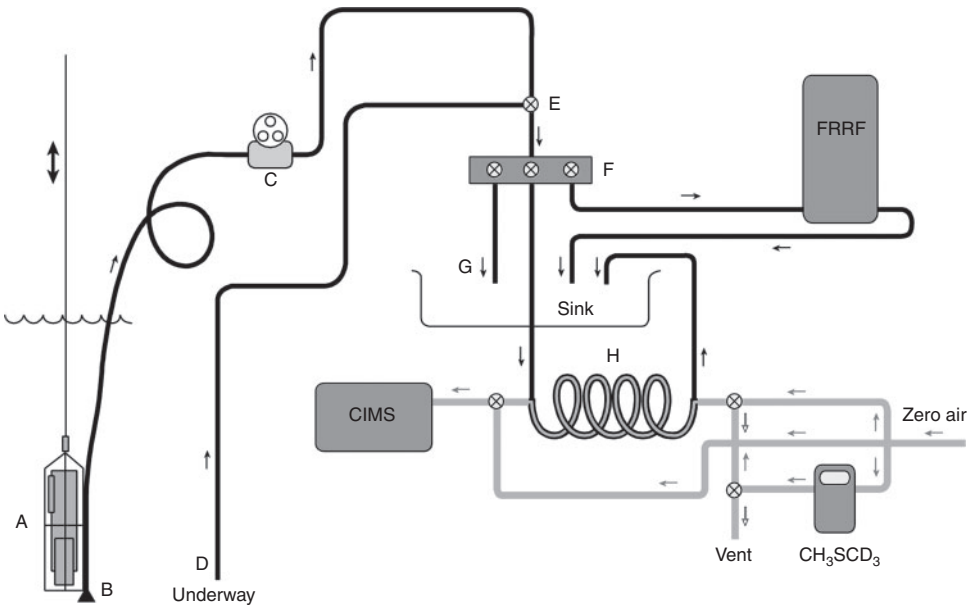

Fig. 2. Diagram of the system designed for either underway or vertically profiled high-resolution measurements of dimethylsulfide (DMS) aboard an oceanographic vessel. Black circuit represents the water flow; grey circuit corresponds to the air flow. (a) conductivity–temperature–depth (CTD) sensors in a protected cage (the double arrow indicates operation from the winch in yo-yo mode); (b) hose inlet; (c) peristaltic pump on board; (d) silicone pipe from the ship's underway pump; (e) switch tap; (f) multitap; (g) flow outlet into the sink; (h) equilibrator loop; CH_3SCD_3: standard permeation device. CIMS, atmospheric pressure chemical ionisation mass spectrometer; FRRF, fast repetition rate fluorometer. Small arrows signal the direction of the flow. In the circuit for the zero air supply to the equilibrator, filled arrows indicate the flow in normal conditions. The open arrows indicate operation through a bypass of the equilibrator and venting of the standard to check for blanks.

large jellyfish that might clog the system. The first meter of the hose was tied to the cage of the CTD probe with the aid of a segment of semi-rigid plastic tubing that prevented bending of the hose. The CTD (SBE-19, Seabird, Bellevue, WA, USA) was manually controlled to cycle from 1- to 35- or 50-m depth at a speed of ~2.5–4 m min^{-1}. A complete cycle from the surface to 35 m and back took ~20–25 min. Profiling to 50 m and back took 30 min. Vertical profiles of conductivity and temperature were measured with the CTD sensors as seawater was drawn through the hose for DMS measurements.

Parallel DMS analysis by GC-FPD

A traditional purge and trap GC-FPD was used to analyse discrete DMS samples on the cruises in parallel with the Eq-APCIMS.[29–30] Samples were collected in glass vials either from Niskin bottles (Seabird, Bellevue, WA, USA) attached to a CTD rosette or from the underway-pumped flow using the open tap. In all cases, some overflow was allowed to avoid headspace and bubbles while sampling and filling the vials. Subsamples of 3–10 mL were gently filtered through a glass fibre filter (GF/F, Whatman, GE Healthcare, Freiburg, Germany), purged for 3–5 min with ultra-high purity helium and the stripped DMS was cryogenically trapped in liquid nitrogen. The trapped volatiles were desorbed by dipping the trap in water at room temperature. Gases were separated on a Carbopack 60/80 mesh column (Supelco, Sigma–Aldrich, St Louis, MO, USA) at 170 °C. A Shimadzu GC14A gas chromatograph (Kyoto, Japan) and flame photometric detector were used. All samples were processed shortly after collection. DMS concentrations were determined by comparison with a standard curve constructed by injecting different volumes of gas standards from a DMS permeation device (183 ng min^{-1}, Dynacal, VICI Metronics) maintained at a constant temperature and diluted in zero air.[29] The detection limit was 3 pmol of DMS (0.3 nmol L^{-1} aqueous DMS in a 10-mL seawater sample). All samples were analysed in duplicate and the coefficient of variation between the duplicates was generally ≤5 %.

Results

Eq-APCIMS data averaging, measurement precision and sensitivity

The Eq-APCIMS instrument acquired data for each ion for 139 ms with a frequency of 0.5 Hz but, as depicted by Fig. 1b, time averaging (binning) of the data was required to improve the signal-to-noise ratio. In order to determine the optimal averaging time we used 6.2 h of continuous, near-surface underway measurements conducted in the Mediterranean Sea on the *R*/*V* Garcia del Cid, with the ship closely following a pair of surface Lagrangian drifters. Because we stayed in a coherent water patch, the DMS concentration underwent only a small and smooth drift during the sampling period. Raw data (*m*/*z* 63 : 66 ratios) were binned into increasing intervals between 4 and 400 s, bin averages were computed and the standard deviation of the mean of all bins over the 6.2-h period was calculated. Fig. 3 illustrates the effect of averaging (binning) time on the variance of the signal. Increasing the averaging time rapidly reduces the standard deviation essentially because it increases the signal-to-noise ratio, until a point where further lengthening the bins does not significantly reduce the variance, as shown by the flattening of the curve in the figure. Based on these results, an averaging time of 60 s was used to process underway data. With the ship steaming at 10 knots (~18.5 km h^{-1}), a 60 s averaging time yields a datum every 300 m. When profiling at an ascent–descent speed of 2.5–4 m min^{-1}, averaging every 60 s

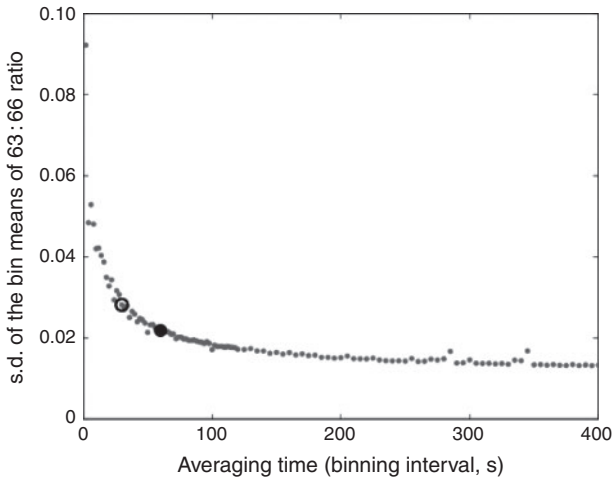

Fig. 3. Standard deviation of averaged bin means of equilibrator and atmospheric pressure chemical ionisation mass spectrometer (Eq-APCIMS) data *v.* binning time. Data are the values of the ratio of ion 63 (dimethylsulfide (DMS)(H^+)) to ion 66 ($CH_3SCD_3(H^+)$), which is the ratio used to calculate the aqueous DMS concentration, over a period of 6.2 h. Binning times increase by 2 s until 120 s and then by 5 s up to 400 s. The filled circle shows the optimal averaging (binning) time chosen for surface underway data (60 s); the open circle shows the optimal averaging (binning) time selected for vertical profiles (30 s). See text for details.

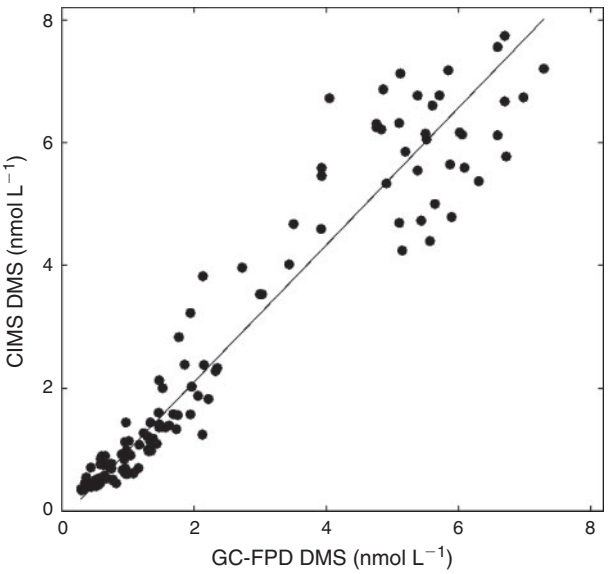

Fig. 4. Model II regression for equilibrator and atmospheric pressure chemical ionisation mass spectrometer (Eq-APCIMS) against gas chromatography with flame photometric detection (GC-FPD) dimethylsulfide (DMS) concentrations in 125 samples; $y = 1.12\ (\pm 0.03)x - 0.13\ (\pm 0.09)$; $R^2 = 0.92$; $P < 0.0001$.

would yield a vertical resolution of 2.5–4 m, which was deemed too coarse to observe DMS gradients. Therefore, an averaging time of 30 s (equivalent to 1.3–2 m) was used for vertical profiles.

An estimate of the overall uncertainty in the DMS analysis was obtained using the same Lagrangian data series. This included the error associated with the mean of the *m*/*z* 63 : 66 ratio within each bin, and the uncertainty in solubility associated with the variance in equilibrator seawater temperatures. Assuming these uncertainties are uncorrelated, the resulting coefficient of variation of DMS concentration in 60-s bins was 8 %. This can be regarded as the experimental error or precision of the underway DMS concentration measurements. For vertical profile DMS measurements, which used a binning time of 30 s, the experimental error was 11 %.

As for the instrument's sensitivity, the detection limit of the Eq-APCIMS is estimated as 220 ppt in the equilibrated air stream.[22] Based on the solubility of DMS in seawater, this is equivalent to respective aqueous concentrations of 0.12, 0.10 and 0.08 nmol L^{-1} at temperatures of 15, 20 and 25 °C.

Eq-APCIMS v. *GC-FPD measurements*

On the *R*/*V* Hesperides 2011 cruise across oligo- and mesotrophic regions of the world's oceans, discrete DMS samples were collected from the underway pumped flow, using the open outlet of the multitap system throughout the day. These samples were analysed by purge and trap GC-FPD as described above. The exact time of discrete sampling was noted and matched to the corresponding 1-min averaged Eq-APCIMS datum. On Lagrangian cruises aboard the *R*/*V* Garcia del Cid, discrete GC samples were collected from several depths using the open outlet of the multitap system while measuring vertical profiles with the profiler. The corresponding time and depth were matched to the 30-s averaged Eq-APCIMS data. All of these GC-FPD and Eq-APCIMS data are compared in Fig. 4. Each of the two techniques was calibrated with its own permeation standard.

A Model II linear regression of the Eq-APCIMS *v.* GC data yields a significant relationship, with $R^2 = 0.92$ ($P < 0.0001$), slope of 1.12 ± 0.03 and intercept of -0.13 ± 0.09. This average discrepancy between the Eq-APCIMS and GC-FPD measurements is within the experimental error of the Eq-APCIMS (~±10 %) and within the estimated inherent variability of other DMS measurement methods.[26] The agreement is reasonably good given the independent calibrations, the differences in sample handling (e.g. the GC-FPD requires filtration, the Eq-APCIMS does not; the Eq-APCIMS method equilibrates the sample with air and measures the equilibrated fraction only, whereas the GC-FPD method sparges the sample), and the fact that GC-FPD is run on discrete 3–10-mL samples whereas the Eq-APCIMS datum is the average of 30–60 s of acquisition and therefore averages DMS concentration over 1.5–2 m of water column or 300 m of horizontal track.

Test for potential pumping artefacts

Possible concerns associated with measuring DMS using the underway intake pumping system include: (1) damage to phytoplankton cells and associated DMS release or production through enzymatic cleavage of DMSP, (2) loss of DMS as a result of bacterial metabolism associated with biofilms in the system or (3) loss of analytes through volatilisation or wall losses. To validate the use of underway pumping systems for DMS, we compared discrete samples collected from the underway intake system with samples collected simultaneously at a similar depth (3 m) using Go-Flo bottles launched overboard. Both sets of samples were analysed by GC-FPD using identical methods (Fig. 5). There is good agreement between the two series. Model II linear regression gives a strong and significant relationship ($R^2 = 0.91$, $P < 0.0001$), with an underway/bottle slope of 0.94 ± 0.024 and an intercept of 0.15 ± 0.036, i.e. the agreement is almost within the measurement uncertainty of the GC-FPD method (±5 %).

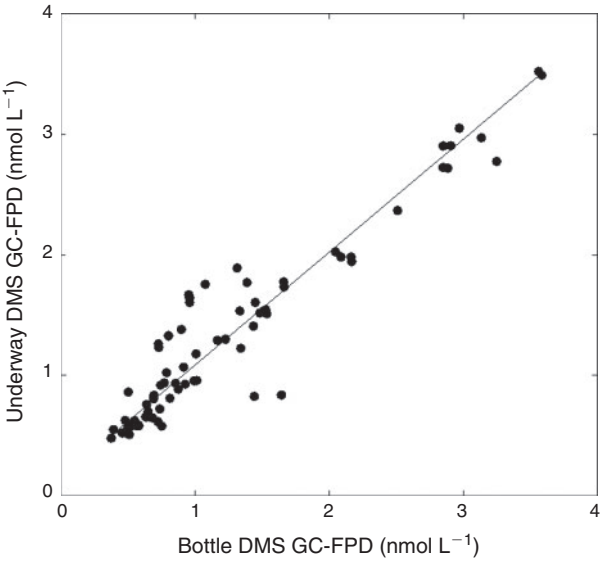

Fig. 5. Model II regression for underway dimethylsulfide (DMS) sampling against co-located overboard bottle sampling using gas chromatography with flame photometric detection (GC-FPD) for the analysis of all 75 samples; $y = 0.94\ (\pm 0.024)x + 0.15\ (\pm 0.036)$; $R^2 = 0.91$; $P < 0.0001$.

Vertical profiles at sea

The profiler–Eq-APCIMS system was field tested for high-resolution vertical profiles of DMS concentrations during the two cruises in the Mediterranean Sea on board the *R/V* Garcia del Cid in September 2011 and May 2012. As a token example, data collected during a 2.5-h run in the evening of 14 September 2011 are shown in Fig. 6 to illustrate the performance of the profiling technique. The depth *v.* time plot shown here corresponds to six complete up–down cycles from the surface water to ~35-m depth. In a later cruise, the technique was proven to work well up to a depth of 50 m.

Fig. 6 also shows profiles of seawater temperature and potential density derived from the CTD probe of the profiler, and chlorophyll *a* fluorescence measured with the FRRF installed in parallel to the Eq-APCIMS. It clearly illustrates that steep gradients with depth occur for all variables, with DMS showing maximum concentrations near the warmer surface, completely decoupled from the deeper fluorescence maximum that occurs in the colder waters at the bottom of the pycnocline. It also reveals a rapid change in stratification, with the upper mixed layer turning shallower as the sun approached sunset (~1800 hours GMT). This rapid change in water physics was not matched at the same pace by significant changes in the DMS concentration profile. The full dataset from the cruises will be presented and discussed elsewhere.

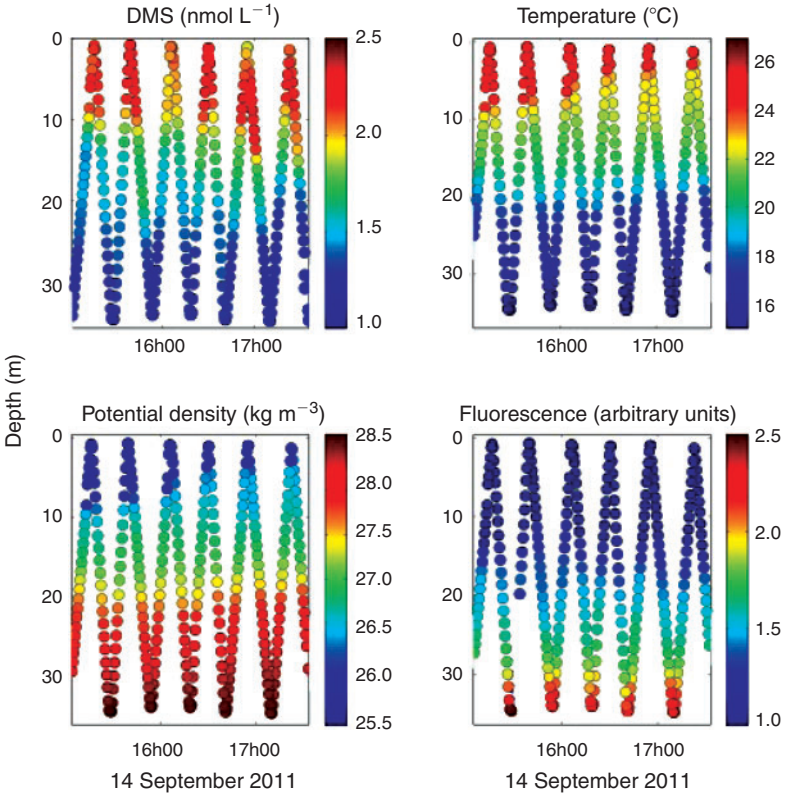

Fig. 6. Repeated depth profiles of dimethylsulfide (DMS), seawater temperature and potential density, and chlorophyll *a* fluorescence measured for 2.5 h during a Mediterranean cruise aboard the *R/V* Garcia del Cid on 14 September 2011. The profiler was cycled from the near surface to 35 m and DMS and fluorescence were measured using the equilibrator and atmospheric pressure chemical ionisation mass spectrometer (Eq-APCIMS) and the fast repetition rate fluorometer (FRRF) (see text for details). Temperature and potential density were respectively measured and calculated from the conductivity–temperature–depth (CTD) sensors of the profiler. The *x*-axis is GMT time. Half minute average data are shown.

The pressure sensor of the CTD probe provided the sampling depth at any time. However, attributing each Eq-APCIMS measurement to its corresponding depth was not trivial because the sampled water took 3.5 min to flow from the hose inlet to the Eq-APCIMS. There were some slight variations in time lag because of changes in flow rate associated with transitory bending of the hose under water. Because the Eq-APCIMS equilibrator was equipped with a temperature data-logging sensor, we matched the temperature profiles of the equilibrator and CTD sensors to determine the depth at which the equilibrator seawater was sampled.

One concern of any profiler working from a floating platform is the effect that platform motion (primarily ship roll) may have on the depth accuracy of the measured profile. In this sense, having a depth (pressure) probe continuously recording at the mobile sampling point (hose inlet) allows accounting for variations in the sampling depth attributable to ship roll. Another concern relates to the potential smearing or homogenisation of the target analyte(s) in the sampled water owing to mixing in the profiler pipe. Calculations for our hose dimensions and pumping rate following Taylor[31] give an e-folding mixing length along the hose of ~1 m or a mixing time scale of ~3 s (i.e. 13–20-cm depth resolution at speeds of 2.5–4 m min^{-1}). Laboratory experiments indicate that the response time constant for the Eq-APCIMS to a step change in seawater concentration is ~10 s due to mixing within the equilibrator and equilibration time. When these two sources of uncertainty are added together in a non-linear way, the resulting response time of the system is $SQRT(3^2 + 10^2) = 10.4$ s. Therefore, the effects of the tubing and equilibrator response times limit the best depth resolution achievable with the profiling system to ~0.4–0.7 m for profiling speeds of 2.5–4 m min^{-1}. Nonetheless, the aforementioned need for averaging the signal in 30-s bins sets the actual depth resolution of the profiler to 1.3–2 m.

Discussion

The profiling system described here achieved DMS depth profiles with a time resolution of 30 s, a depth resolution of 1.3–2 m, a measurement precision of 11 % and a detection limit of nearly 0.1 nmol L^{-1}. The resolution of the profiling system can be improved by varying the pumping and profiling rates, and improving the time response of the Eq-APCIMS and its sensitivity. The mini-CIMS used in this study is a relatively low cost, low sensitivity instrument, and a more sensitive Eq-APCIMS such as that used by Bell et al.[32] would increase signal to noise by approximately one order of magnitude. However, theoretical time resolution limits of 3 and 10 s are imposed by the mixing in the pumping pipeline and the mixing and equilibration response in the equilibrator. Even at the resolution presented here, the profiling approach represents a significant advance in data coverage from the use of Niskin bottles on CTD casts followed by purge and trap analysis.

Hale and Takahashi[33] developed a vertical profiler by which water was pumped from a SeaSoar CTD through a 750-m tube, while undulating from near the surface to depths near 200 m. Even though the Lamont Pumping SeaSoar (LPS) allows deeper profiles, it has to be operated while steaming and its launch and recovery is far from quick and easy. This prevents its use on station, either at a fixed location or in Lagrangian drift. Our profiler, conversely, is used with the ship stopped on site, and it is very easy to recover from water, which makes it particularly suited for on-station or Lagrangian studies. As for depth resolution, the LPS is less affected by ship's vertical motion and more affected by mixing in the longer pipe. The authors[33] estimated a mixing time constant of 7.5–10 s, which corresponded to a vertical resolution of 1.9–2.5 m when used at dive and climb rates of 15 m min^{-1}. These figures are similar to and even coarser than our aforementioned resolution of 1.3–2 m.

This study provides validation for the continuous flow measurement of DMS by Eq-APCIMS. The method used here involves use of an internal gas standard added after the equilibrated gas stream. This approach assumes complete equilibration in the membrane equilibrator. It does not correct for possible clogging of membrane pores in the equilibrator as a result of fouling. Extensive use of this equilibrator in prior studies suggests that the porous Teflon tube membrane does not experience biofouling in oligo- and mesotrophic conditions.[22,32,34–36] However, during the Malaspina cruise aboard the *R/V* Hesperides, abundant jellyfish in the Benguela current region caused some clogging of the equilibrator, which had to be dismounted and cleaned with 10 % hydrochloric acid. Bell et al.[32] recently modified the technique to introduce an isotopically labelled internal standard as an aqueous solution at the inlet of the equilibrator. This method corrects for any loss of signal in the event of fouling or incomplete equilibration. Neither standardisation technique accounts for possible artefact production of DMS in the equilibrator resulting from growth on the tube interior or mechanical stress to organisms in the pump and tubing. However, the observed agreement between the Eq-APCIMS and the GC-FPD methods (Fig. 5) across a broad DMS concentration range (0.3 to 8 nmol L^{-1}) suggests that under most typical oceanic conditions[5] the equilibrator provides accurate and repeatable measurements.

The agreement of GC-FPD measurements in seawater from Go-Flo bottles and underway intake indicates that the underway systems did not have a significant effect on endogenous DMS concentrations during this study. Bell et al.[32] carried out a similar comparison using the Eq-APCIMS with similar results. However, the results of these studies do not necessarily apply to all ships because of variations in shipboard underway pump types, pipe materials and maintenance procedures. The fact that some respiratory activity (oxygen consumption) has been measured in underway seawater lines of several ships[37] calls for caution regarding microbial activity that might consume DMS. Likewise, the tests in the present study were conducted with picophytoplankton-dominated waters; phytoplankton assemblages more susceptible to mechanical stress or damage by pumping and filtration (e.g. those with colonial *Phaeocystis*) may yield larger differences between underway and bottle-derived measurements.

One of the strengths of the continuous flow DMS measurement is that it can be coupled with other instruments that also provide continuous measurements. For instance, our system was coupled by a multitap split of the seawater flow to a FRRF, which provides fluorescence of organisms and data on the performance of photosystem II.[38] This is an interesting complement to DMS measurements, because DMS has been linked to algal physiological stress.[39] Like the Eq-APCIMS, the FRRF was used to either record fluorescence response in surface waters while steaming or in vertical profiles when coupled to the profiling sampler. In addition, the CTD probe of the profiler provided physical data such as salinity, temperature and the derived density profiles. Fig. 6 shows the importance of obtaining high-resolution measurements over depth and time to study

the dynamics of DMS within its biophysical context. The setup can easily be complemented by adding further sensors to the probe, thereby obtaining high-resolution vertical profiles of variables such as oxygen, underwater light, beam transmission, organic matter fluorescence, turbidity or nitrate, which will provide a more comprehensive context for the DMS profiles.

In summary, high-resolution vertical profiles and near surface underway measurements of DMS demonstrate that membrane equilibrator–APCIMS is a valuable new tool to describe short-term DMS variability and its relationship to other physical and biogeochemical parameters. This approach facilitates the study of DMS distribution, cycling and environmental forcing at unprecedented resolution, also along the vertical dimension.

Acknowledgements

The authors thank the marine technicians (UTM) and the crews aboard the *R/V* Hesperides and Garcia del Cid for their assistance and cooperation. They also thank Anoop S. Mahajan for invaluable assistance with data processing codes. The insightful comments of three anonymous reviewers helped improve the manuscript. This work was supported by the former Spanish Ministry of Science and Innovation through projects Consolider-Ingenio Malaspina (CSD2008-00077), SUMMER (CTM2008-03309/MAR) PRISMA (CTM2009-10193) and PEGASO (CTM2012-37615), and through a Ph.D. scholarship to S.-J. Royer. Support was also provided by the USA National Science Foundation (grants 0851472 and 1143709).

References

[1] M. O. Andreae, Ocean-atmosphere interactions in the global biogeochemical sulfur cycle. *Mar. Chem.* **1990**, *30*, 1. doi:10.1016/0304-4203(90)90059-L

[2] T. S. Bates, B. K. Lamb, A. Guenther, J. Dignon, R. E. Stoiber, Sulfur emissions to the atmosphere from natural sources. *J. Atmos. Chem.* **1992**, *14*, 315. doi:10.1007/BF00115242

[3] R. Simó, Production of atmospheric sulfur by oceanic plankton: biogeochemical, ecological and evolutionary links. *Trends Ecol. Evol.* **2001**, *16*, 287. doi:10.1016/S0169-5347(01)02152-8

[4] A. J. Kettle, M. O. Andreae, D. Amouroux, T. W. Andreae, T. S. Bates, H. Berresheim, H. Bingemer, R. Boniforti, M. A. J. Curran, G. R. DiTullio, G. Helas, G. B. Jones, M. D. Keller, R. P. Kiene, C. Leck, M. Levasseur, G. Malin, M. Maspero, P. Matrai, A. R. McTaggart, N. Mihalopoulos, B. C. Nguyen, A. Novo, J. P. Putaud, S. Rapsomanikis, G. Roberts, G. Schebeske, S. Sharma, R. Simó, R. Staubes, S. Turner, G. Uher, A global database of sea surface dimethylsulfide (DMS) measurements and a procedure to predict sea surface DMS as a function of latitude, longitude, and month. *Global Biogeochem. Cycles* **1999**, *13*, 399. doi:10.1029/1999GB900004

[5] A. Lana, T. G. Bell, R. Simó, S. M. Vallina, J. Ballabrera-Poy, A. J. Kettle, J. Dacha, L. Bopp, E. S. Saltzman, J. Stefels, J. E. Johnson, P. S. Liss, An updated climatology of surface dimethlysulfide concentrations and emission fluxes in the global ocean. *Global Biogeochem. Cycles* **2011**, *25*, GB1004. doi:10.1029/2010GB003850

[6] A. D. Clarke, D. Davis, V. N. Kapustin, F. Eisele, G. Chen, I. Paluch, D. Lenschow, A. R. Bandy, D. Thornton, K. Moore, L. Mauldin, D. Tanner, M. Litchy, M. A. Carroll, J. Collins, G. Albercook, Particle nucleation in the tropical boundary layer and its coupling to marine sulfur sources. *Science* **1998**, *282*, 89. doi:10.1126/SCIENCE.282.5386.89

[7] J. E. Lovelock, R. J. Maggs, R. A. Rasmussen, Atmospheric dimethyl sulphide and the natural sulphur cycle. *Nature* **1972**, *237*, 452. doi:10.1038/237452A0

[8] R. P. Kiene, L. J. Linn, J. A. Bruton, New and important roles for DMSP in marine microbial communities. *J. Sea Res.* **2000**, *43*, 209. doi:10.1016/S1385-1101(00)00023-X

[9] J. Stefels, Physiological aspects of the production and conversion of DMSP in marine algae and higher plants. *J. Sea Res.* **2000**, *43*, 183. doi:10.1016/S1385-1101(00)00030-7

[10] J. R. Seymour, R. Simó, T. Ahmed, R. Stocker, Chemoattraction to dimethylsulfoniopropionate throughout the marine microbial food web. *Science* **2010**, *329*, 342. doi:10.1126/SCIENCE.1188418

[11] J.-B. Raina, D. M. Tapiolas, S. Forêt, A. Lutz, D. Abrego, J. Ceh, F. O. Seneca, P. L. Clode, D. G. Bourne, B. L. Willis, C. A. Motti, DMSP biosynthesis by an animal and its role in coral thermal stress response. *Nature* **2013**, *502*, 677. doi:10.1038/NATURE12677

[12] J. R. Charlson, J. E. Lovelock, M. O. Andreae, S. G. Warren, Oceanic phytoplankton, atmospheric sulphur, cloud albedo and climate. *Nature* **1987**, *326*, 655. doi:10.1038/326655A0

[13] P. K. Quinn, T. S. Bates, The case against climate regulation via oceanic phytoplankton sulphur emission. *Nature* **2011**, *480*, 51. doi:10.1038/NATURE10580

[14] Y. Iizuka, R. Uemura, H. Motoyama, T. Suzuki, T. Miyake, M. Hirabayashi, T. Hondoh, Sulphate-climate coupling over the past 300 000 years in inland Antarctica. *Nature* **2012**, *490*, 81. doi:10.1038/NATURE11359

[15] M. O. Andreae, W. R. Barnard, Determination of trace quantities of dimethyl sulfide in aqueous solutions. *Anal. Chem.* **1983**, *55*, 608. doi:10.1021/AC00255A006

[16] S. M. Turner, P. S. Liss, Measurements of various sulphur gases in a coastal marine environment. *J. Atmos. Chem.* **1985**, *2*, 223. doi:10.1007/BF00051074

[17] T. S. Bates, J. D. Cline, R. H. Gammon, S. R. Kelly-Hansen, Regional and seasonal variations in the flux of oceanic dimethylsulfide to the atmosphere. *J. Geophys. Res.* **1987**, *92*, 2930. doi:10.1029/JC092IC03P02930

[18] J. W. H. Dacey, F. A. Howse, A. F. Michaels, S. G. Wakeham, Temporal variability of dimethylsulfide and dimethylsulfoniopropionate in the Sargasso Sea. *Deep Sea Res. Part I Oceanogr. Res. Pap.* **1998**, *45*, 2085. doi:10.1016/S0967-0637(98)00048-X

[19] R. Simó, Trace chromatographic analysis of dimethyl sulfoxide and related methylated sulfur compounds in natural waters. *J. Chromatogr. A* **1998**, *807*, 151. doi:10.1016/S0021-9673(98)00086-7

[20] P. D. Tortell, Dissolved gas measurements in oceanic waters made by membrane inlet mass spectrometry. *Limnol. Oceanogr. Methods* **2005**, *3*, 24. doi:10.4319/LOM.2005.3.24

[21] S. Kameyama, H. Tanimoto, S. Inomata, U. Tsunogai, A. Ooki, Y. Yokouchi, S. Takeda, H. Obata, M. Uematsu, Equilibrator inlet-proton transfer reaction-mass spectrometry (EI-PTR-MS) for sensitive, high-resolution measurement of dimethyl sulfide dissolved in seawater. *Anal. Chem.* **2009**, *81*, 9021. doi:10.1021/AC901630H

[22] E. S. Saltzman, W. J. De Bruyn, M. J. Lawler, C. Marandino, C. McCormick, A chemical ionization mass spectrometer for continuous underway shipboard analysis of dimethylsulfide in near-surface seawater. *Ocean Sci.* **2009**, *6*, 1569.

[23] P. D. Tortell, M. C. Long, Spatial and temporal variability of biogenic gases during the Southern Ocean spring bloom. *Geophys. Res. Lett.* **2009**, *36*, L01603. doi:10.1029/2008GL035819

[24] E. C. Asher, A. Merzouk, P. D. Tortell, Fine-scale spatial and temporal variability of surface water dimethylsufide (DMS) concentrations and sea–air fluxes in the NE Subarctic Pacific. *Mar. Chem.* **2011**, *126*, 63. doi:10.1016/J.MARCHEM.2011.03.009

[25] S. Kameyama, H. Tanimoto, S. Inomata, H. Yoshikawa-Inoue, U. Tsunogai, A. Tsuda, M. Uematsu, M. Ishii, D. Sasano, K. Suzuki, Y. Nosaka, Strong relationship between dimethyl sulfide and net community production in the western subarctic Pacific. *Geophys. Res. Lett.* **2013**, *40*, 3986. doi:10.1002/GRL.50654

[26] T. G. Bell, G. Malin, G. A. Lee, J. Stefels, S. Archer, M. Steinke, P. Matrai, Global oceanic DMS data inter-comparability. *Biogeochem.* **2012**, *110*, 147. doi:10.1007/S10533-011-9662-3

[27] P. D. Tortell, C. Guéguen, M. C. Long, C. D. Payne, P. Lee, G. R. DiTullio, Spatial variability and temporal dynamics of surface water pCO_2, ΔO_2/Ar and dimethylsulfide in the Ross Sea, Antarctica. *Deep Sea Res. Part I Oceanogr. Res. Pap.* **2011**, *58*, 241. doi:10.1016/J.DSR.2010.12.006

[28] J. W. H. Dacey, G. Wakeham, B. L. Howes, Henry's law constants for dimethylsulfide in freshwater and seawater. *Geophys. Res. Lett.* **1984**, *11*, 991. doi:10.1029/GL011I010P00991

[29] R. Simó, J. O. Grimalt, J. Albaigés, Sequential method for the field determination of nanomolar concentrations of dimethyl sulfoxide in natural waters. *Anal. Chem.* **1996**, *68*, 1493. doi:10.1021/AC9510907

[30] M. Galí, C. Ruiz-González, T. Lefort, J. M. Gasol, C. Cardelús, C. Romera-Castillo, R. Simó, Spectral irradiance dependence of sunlight effects on plankton dimethylsulfide production. *Limnol. Oceanogr.* **2013**, *58*, 489.

[31] G. I. Taylor, Dispersion of soluble matter in solvent flowing slowly through a tube. *Proc. Roy. Soc. A.* **1953**, *219*, 186. doi:10.1098/RSPA.1953.0139

[32] T. G. Bell, W. De Bruyn, S. D. Miller, B. Ward, K. Christensen, E. S. Saltzman, Air/sea DMS gas transfer in the North Atlantic: evidence for limited interfacial gas exchange at high wind speed. *Atmos. Chem. Phys.* **2013**, *13*, 11073. doi:10.5194/ACP-13-11073-2013

[33] B. Hales, T. Takahashi, The pumping SeaSoar: a high-resolution seawater sampling platform. *J. Atmos. Ocean. Technol.* **2002**, *19*, 1096. doi:10.1175/1520-0426(2002)019<1096:TPSAHR>2.0.CO;2

[34] C. A. Marandino, W. J. De Bruyn, S. D. Miller, E. S. Saltzman, Eddy correlation measurements of the air/sea flux of dimethylsulfide over the North Pacific Ocean. *J. Geophys. Res.* **2007**, *112*, D03301. doi:10.1029/2006JD007293

[35] C. A. Marandino, W. J. De Bruyn, S. D. Miller, E. S. Saltzman, DMS air/sea flux and gas transfer coefficients from the North Atlantic summertime coccolithophore bloom. *Geophys. Res. Lett.* **2008**, *35*, L23812. doi:10.1029/2008GL036370

[36] C. A. Marandino, W. J. De Bruyn, S. D. Miller, E. S. Saltzman, Open ocean DMS air/sea fluxes over the eastern South Pacific Ocean. *Atmos. Chem. Phys.* **2009**, *9*, 345. doi:10.5194/ACP-9-345-2009

[37] L. W. Juranek, R. C. Hamme, J. Kaiser, R. Wanninkhof, P. D. Quay, Evidence of O_2 consumption in underway seawater lines: Implications for air-sea O_2 and CO_2 fluxes. *Geophys. Res. Lett.* **2010**, *37*, L01601. doi:10.1029/2009GL040423

[38] Z. Kolber, O. Prasil, P. P. G. Falkowski, Measurements of variable chlorophyll fluorescence using fast repetition rate techniques: defining methodology and experimental protocols. *Biochim. Biophys. Acta* **1998**, *1367*, 88. doi:10.1016/S0005-2728(98)00135-2

[39] W. Sunda, D. J. Kieber, R. P. Kiene, S. Huntsman, An antioxidant function for DMSP and DMS in marine algae. *Nature* **2002**, *418*, 317. doi:10.1038/NATURE00851

To be submitted

A high-resolution time-depth view of dimethylsulfide cycling in the surface sea

S-J. Royer[1], M. Galí[1,2], A.S. Mahajan[3], O.N. Ross[1,4], G. Pérez[5], E. Saltzman[6], R. Simó[1*]

1. *Institut de Ciències del Mar, CSIC, Passeig Marítim de la Barceloneta 37-49, 08003 Barcelona, Catalonia, Spain.*
2. *Takuvik Joint International Laboratory and Québec-Océan, Université Laval, G1V OA6, Québec, QC, Canada.*
3. *Indian Institute of Tropical Meteorology (IITM), Pashan Road, 411 008, Pune, India.*
4. *Aix-Marseille University, CNRS, University of Toulon, IRD, MIO UM 110, 13288, Marseille, France.*
5. *Instituto INIBIOMA (CRUB Comahue, CONICET), Quintral 1250, 8400 S.C. de Bariloche, Rio Negro, Argentina.*
6. *University of California, Earth System Science Department, 3200 Croul Hall St, Irvine, California, 92697, United States.*

See Chapter 4

AGU PUBLICATIONS

Geophysical Research Letters

RESEARCH LETTER
10.1002/2014GL062543

Key Points:
- The variability in open ocean DMS concentrations occurs at the submesoscale
- DMS and phytoplankton patchiness increase with productivity
- No single pattern of diel variation in DMS is valid for the global ocean

Supporting Information:
- Readme
- Tables S1 and S2 and Figure S1

Correspondence to:
R. Simó,
rsimo@icm.csic.es

Citation:
Royer, S.-J., A. S. Mahajan, M. Galí, E. Saltzman, and R. Simó (2015), Small-scale variability patterns of DMS and phytoplankton in surface waters of the tropical and subtropical Atlantic, Indian, and Pacific Oceans, *Geophys. Res. Lett.*, *42*, doi:10.1002/2014GL062543.

Received 19 NOV 2014
Accepted 29 DEC 2014
Accepted article online 5 JAN 2015

Small-scale variability patterns of DMS and phytoplankton in surface waters of the tropical and subtropical Atlantic, Indian, and Pacific Oceans

S.-J. Royer[1], A. S. Mahajan[2], M. Galí[1,3], E. Saltzman[4], and R. Simó[1]

[1]Institut de Ciències del Mar, CSIC, Barcelona, Catalonia, Spain, [2]Indian Institute of Tropical Meteorology, Pune, India, [3]Now at Takuvik Joint International Laboratory and Québec-Océan, Université Laval, Québec City, Québec, Canada, [4]Department of Earth System Science, University of California, Irvine, California, USA

Abstract High-resolution surface measurements of dimethylsulfide (DMS), chlorophyll *a* fluorescence, and the efficiency of photosystem II were conducted together with temperature and salinity along five eastward sections in the tropical and subtropical Atlantic, Indian, and Pacific Oceans. Analysis of variability length scales revealed that much of the variability in DMS concentrations occurs at scales between 15 and 50 km, that is, at the lower edge of mesoscale dynamics, decreasing with latitude and productivity. DMS variability was found to be more commonly related to that of phytoplankton-related variables than to that of physical variables. Unlike phytoplankton physiological data, DMS did not show any universal diel pattern when using the normalized solar zenith angle as a proxy for solar time across latitudes and seasons. The study should help better design sampling and computing schemes aimed at mapping surface DMS and phytoplankton distributions, taking into account latitude and productivity.

1. Introduction

Dimethylsulfide (DMS) is a biogenic gas produced by the microbial food web within the photic layer of the ocean. Oceanic emission of DMS is important because it plays a crucial role for the recycling of sulfur to continents through the atmosphere [*Lovelock et al.*, 1972] and because DMS serves as a precursor for the formation and growth of atmospheric sulfate aerosols [*Andreae and Barnard*, 1984; *Hegg et al.*, 1991]. This has important implications for cloud microphysics in marine regions remote from continental emissions [*Vallina et al.*, 2007; *Andreae and Rosenfeld*, 2008; *Lana et al.*, 2012]. Sea surface DMS concentration and emission result from a complex web of ecological, chemical, and biogeochemical processes interacting with the physics of the environment [*Malin and Kirst*, 1997; *Kiene et al.*, 2000; *Simó*, 2001].

Resolving the spatial/temporal pattern of DMS variability and its relationships to other biogeochemical and biophysical variables is important in order to understand the factors controlling DMS cycling. Analyses of remotely sensed global ocean color have demonstrated that mesoscale (10–200 km) variability occurs similarly for biological and physical variables, dominates over most of the oligotrophic regimes, and contributes up to a third of the total variability of high-productivity regions [*Doney et al.*, 2003]. The database of DMS measurements used for the DMS climatology [*Lana et al.*, 2011] shows that large-scale spatial and temporal variabilities occur in the surface oceans, but coverage is insufficient to resolve the fine-scale dynamics [*Belviso et al.*, 2004; *Tortell et al.*, 2011].

Most of seawater DMS measurements to date have been obtained using standard purge and trap and gas chromatography (GC) methods, with a measurement frequency typically of a few measurements per hour at the best [*Bell et al.*, 2012]. As a result, the distribution of DMS is still coarse considering the number of field campaigns targeted at this compound. The development of high-frequency DMS analysis mass spectrometers over the last decade has the potential to greatly expand the coverage and resolution of surface ocean DMS observations and their relationship to other oceanographic variables [*Tortell*, 2005a; *Kameyama et al.*, 2009, 2013; *Saltzman et al.*, 2009; *Royer et al.*, 2014].

Tortell [2005b] reported significant small-scale heterogeneity in the distribution of DMS across oceanic regimes and suggested that previous field studies might have underestimated the true spatial variability of

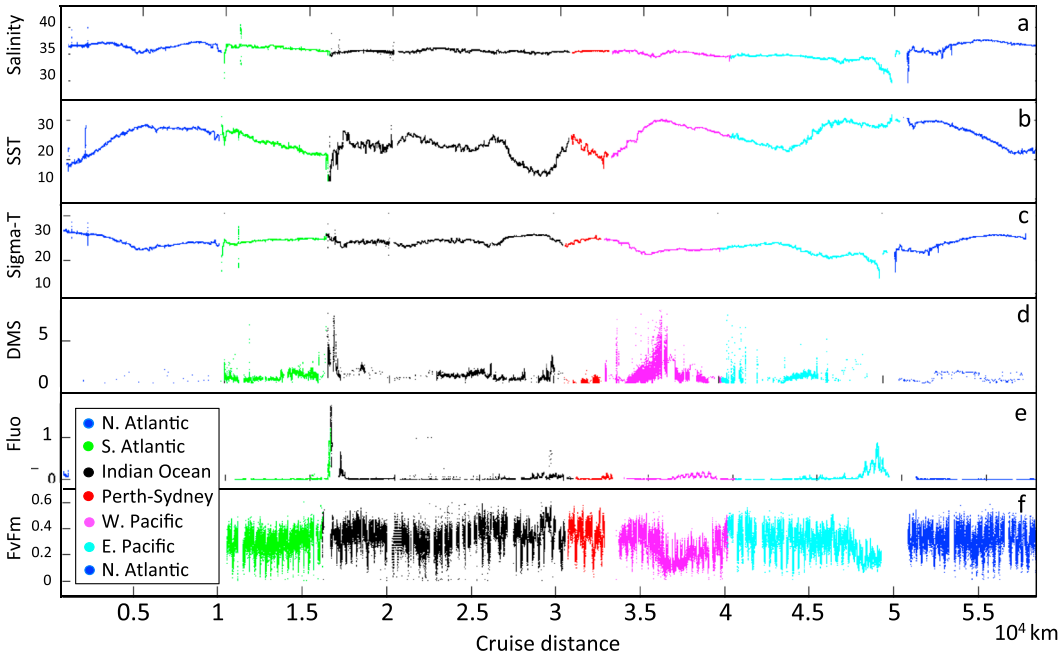

Figure 1. Variables measured at high frequency during the Malaspina 2010 Expedition. (a) Salinity (kg m^{-3}); (b) SST (°C); (c) Sigma T (potential density, kg m^{-3}); (d) DMS concentration (nmol L^{-1}); (e) Chlorophyll *a* fluorescence (Fluo, arbitrary units); and (f) efficiency of photosystem II (FvFm). Colors indicate broad oceanic regions. The instrument measuring Fluo and FvFm was not operative during the first leg in the North Atlantic. Note that there are sections where no continuous but discrete DMS measurements exist. These are shown to provide the circumnavigation results context but have not been used for the variability analysis.

DMS in dynamic marine systems. Subsequent work by the same group in the northeast subarctic Pacific [*Nemcek et al.*, 2008; *Asher et al.*, 2011] used decorrelation and variability length scales to show that DMS concentration varied over shorter distances (approximately 7 km) compared to sea surface temperature (SST) and salinity (11–14 km), and shorter or longer than that of chlorophyll *a* (chl*a*; 3.5–12.5 km). On the western side of the subarctic North Pacific, *Kameyama et al.* [2009] observed elevated DMS peaks associated with patches of high biological activity. In the eastern Atlantic, *Zindler et al.* [2014] observed variability in DMS and isoprene concentrations across mesoscale hydrographic eddies that was related to nitrogen-phosphorous limitation. Studies of this kind are scattered and mostly regional, hence not necessarily representative of most of the world's oceans.

Here we use atmospheric pressure chemical ionization mass spectrometry (APCIMS) to explore DMS concentration and some of the hydrographic and biophysical variables that may influence it at very fine scale within the low-latitude oceans. We collected continuous underway data across the tropical and subtropical Atlantic, Indian, and Pacific Oceans over spring, summer, and fall during the 7 month Malaspina 2010 Circumnavigation Expedition. Analysis of variability length scales (VLS) for DMS, along with potential hydrographic and biological drivers in surface waters, provides insight into how DMS distributes on the map of the physics and biology of the surface oceans.

2. Methods

2.1. Sampling Scheme

This study was conducted on board the R/V *Hespérides* from January to July 2011 during the Malaspina 2010 Circumnavigation Expedition. The expedition covered 22 biogeochemical provinces [*Longhurst*, 1998] and a total distance of 58,890 km across the Atlantic, Indian, and Pacific Oceans, mostly within latitudes ranging between 30°N and 30°S (Figure S1 in the supporting information). DMS was measured continuously in near-surface seawater along a total distance of approximately 21,300 km, when the analytical system was operative (Figure 1). Seawater was sampled using the underway pump of the ship (4 m inlet) and supplied

continuously for DMS and Fast Repetition Rate fluorometer (FRRf) measurements. A third tap allowed discrete sampling for manual analyses. Details of the underway sampling setup can be found elsewhere [*Royer et al.*, 2014]. Go-Flo sampling bottles (General Oceanics, Miami, FL, USA) were also used to collect seawater samples overboard from a depth of 3 m, with the purpose of intercomparison with the underway pump.

2.2. Analytical Instruments and Methods

Continuous DMS measurements were performed with a gas equilibrator APCIMS (Eq-APCIMS) as described by *Saltzman et al.* [2009] and *Royer et al.* [2014]. In brief, aqueous DMS is equilibrated with air across using a hydrophobic Teflon membrane with seawater and clean air flowing in opposite directions. The resulting air stream is diluted with air containing an isotope-labeled CD_3SCH_3 internal standard from a permeation tube and directed toward the mass spectrometer inlet. DMS molecules are ionized via proton transfer from H_3O^+, and subsequently declustered, quadrupole mass filtered, and detected by an ion multiplier. Seawater DMS (*m/z* 63) is quantified from the ratio to the isotope-labeled internal standard (*m/z* 66). Details of the calculation required to convert the raw data into ambient concentrations are given elsewhere [*Royer et al.*, 2014]. For data collected every 2 s and averaged every minute, the sensitivity of the instrument was equivalent to 0.1 nmol L^{-1}, and the precision was 8%. The Eq-APCIMS measurements were matched with the ship georeferenced position system, meteorological data, and salinity and SST measurements.

Purge and trap and GC coupled to flame photometric detection (FPD) were also used through the entire cruise for DMS measurements in discrete samples. This instrument had a detection limit equivalent to 0.3 nmol L^{-1} and a precision better than 5% [*Galí et al.*, 2013a]. Intercomparison exercises between the Eq-APCIMS and the GC-FPD gave satisfactory results (slope = 1.12; $R^2 = 0.92$; $p < 0.0001$). Further tests demonstrated that the delivery of seawater from the underway pump did not significantly affect endogenous DMS concentrations [*Royer et al.*, 2014].

The FRRf (FASTracka, Chelsea Technologies, Surrey, UK) was used in parallel for underway measurements of phytoplankton photophysiology, including the maximum quantum efficiency of photosystem II photochemistry (FvFm). Seawater flowed continuously through dark tubes for approximately 3 min before reaching the dark chamber of the FRRf. The fluorescence induction protocol consisted of 100 saturation flashlets (1.3 μs duration, 2.8 μs interflash delay) followed by 20 relaxation flashlets (separated by 50 μs). Different physiological parameters such as initial fluorescence (F_0), maximum fluorescence (Fm), variable fluorescence ($Fv = Fm - F_0$), and the ratio of variable to maximum fluorescence ($FvFm = Fv/Fm = (Fm - F_0)/Fm$) were derived from the curve of fluorescence induction in the photosystem II (PSII) according to *Kolber et al.* [1998]. Blank calibrations with 0.2 μm filtered seawater were performed before and after instrument deployment. No significant biofouling was observed during the cruise. The data were processed using the Chelsea FRS Software (v.1.8), with reference and baseline corrections.

2.3. Data Processing and VLS

All high-frequency data (DMS, FRRf-derived parameters, SST, salinity, and derived potential density—sigma T) were processed using MATLAB. First, the data were quality controlled and calculations were made to find the optimum averaging time for improving the signal-to-noise ratio. Based on these results for DMS, an averaging time of 60 s was used to process underway data, which yields a datum every 300 m for a ship steaming speed of 10 knots (18.5 km h^{-1}) [*Royer et al.*, 2014]. Data acquired during oceanographic sampling stations were discarded, and only measurements obtained during steaming were used. These yielded analyzable transects ranging between 115 km and 1132 km.

To assess the spatial scale at which underway variables undergo critical variations, we chose the VLS over several other similar analyses for its flexibility in using unequally spaced data and transects of different lengths. The VLS can be regarded as the minimum spatial resolution necessary to fully describe the distribution of a variable along a data series. We followed an analytical approach similar to that described by *Asher et al.* [2011]. Each transect's high-resolution data series over distance was first binned with increasing distance bin sizes. Binning consisted of grouping consecutive data within the binning distance and computing their average. The data were then interpolated linearly between bin averages to the resolution of the original measurements. A mean squared error (MSE) between the interpolated data and observations was calculated for each binning scheme. The MSE obviously increases proportionally with increasing binning

distance. The VLS is identified as the binning or interpolation distance at which there is a change in slope in the relationship between MSE and interpolation distance (inset in Figure 2), that is, the distance beyond which the fitness of the interpolation to the observations degrades faster. We defined a continuous transect as one with a maximum gap distance of 1 km between two consecutive data points. Only transects with lengths of continuous data >100 km were analyzed. We computed the VLS for each variable in each transect and then calculated regional averages in the 11 biogeochemical provinces in which the study was conducted [*Longhurst*, 1998].

2.4. Solar Zenith Angle Computation

The solar zenith angle (SZA) is the angle of the Sun away from vertical. It is 0 at noon at the equinox in the equator and at the solstice in the tropics; on the same dates and latitudes, it is 180° at midnight. The time at which the Sun reaches a given SZA varies according to the latitude and the seasons, except for the fact that, by definition, the Sun always rises at SZA −90° and sets at 90°, no matter where and what season the data are collected. The SZA corresponding to each 60 s average of high-resolution data was computed according to date, local time, and latitude. A normalization of the SZA was applied to make it vary between −180° or +180° (midnight) and 0° (noon) through the diel cycle regardless of date and latitude. The normalized SZA (SZAn) was computed using the following equations:

$$\mathrm{SZAn} = ((\mathrm{SZA} + \mathrm{SZAmin})/(90 - \mathrm{SZAmin}))\times 90 \quad \text{for } -90 < \mathrm{SZA} < 0;$$

$$\mathrm{SZAn} = ((\mathrm{SZA} - \mathrm{SZAmin})/(90 - \mathrm{SZAmin}))\times 90 \quad \text{for } 0 < \mathrm{SZA} < 90;$$

$$\mathrm{SZAn} = (((\mathrm{SZA} + 90)/(\mathrm{SZAmax} - 90)) - 1)\times 90 \quad \text{for } -180 < \mathrm{SZA} < -90;$$

$$\mathrm{SZAn} = (((\mathrm{SZA} - 90)/(\mathrm{SZAmax} - 90)) + 1)\times 90 \quad \text{for } 90 < \mathrm{SZA} < 180,$$

where SZAmin and SZAmax are the daily minimum and maximum SZA at a particular date and location. Every 60 s average of every measured variable was matched to its SZAn, thus allowing exploring their variability over a universal diel cycle irrespective of season and latitude.

3. Results and Discussion

3.1. DMS Distribution Patterns

Most of the circumnavigation took place across oligotrophic waters of the central oceanic gyres, where chl*a* concentrations were very low. Cruise mean chl*a* was 0.14 $\mu g\,L^{-1}$, range 0.015–0.693 $\mu g\,L^{-1}$ (data not shown). Cruise mean DMS concentration, including the regions with discrete sampling, was 1.1 $nmol\,L^{-1}$, with a minimum value below 0.1 $nmol\,L^{-1}$ observed in the ultraoligotrophic waters of the South Atlantic and Pacific Oceans (South Atlantic Gyre (SATL) and South Pacific Subtropical Gyre (SPSG)), and a maximum value of 9.6 $nmol\,L^{-1}$ near the South African coast (Figure 1).

Over the total length of the expedition, DMS appeared to change sharply at salinity and SST gradients in localized areas (for example, in the Equatorial Pacific, around km 35,000), suggesting a direct or indirect physical influence on DMS concentrations. Such harmonious changes also occurred occasionally with chl*a* fluorescence: peaks were coincident in the Agulhas-Benguela region (around km 17,000) and in the Western Australian current (around km 29,000), which suggested DMS production associated with biological drivers. However, for the full data set, neither salinity nor SST nor fluorescence was good predictors of DMS concentration. *Simó and Dachs* [2002] successfully combined biological and physical variables to predict broad regional and seasonal DMS distributions using low-resolution measurements of the mixed-layer depth (MLD) and the chl*a*/MLD ratio. Unfortunately, our high-frequency DMS data set was not paralleled with same resolution MLD and chl*a* measurements as to be able to explore the behavior of the *Simó and Dachs* [2002] relationship at the high resolution. The lack of covariance between DMS and biophysical variables over most of the cruise (Figure 1) resulted in no significant statistical relationship of global applicability.

3.2. VLS Across Biogeographical Provinces

In order to better understand DMS distribution and its drivers, the data set was divided into biogeographical domains (Trades, Westerlies, and Coastal) and subdivided further into 11 biogeographical provinces [*Longhurst*, 1998]. Province averages of the VLS of DMS, salinity, SST, sigma T, in situ fluorescence (F_0 from the FRRf, hereafter Fluo), and FvFm are shown in Figure 2 and Table S1 in the supporting information. In general,

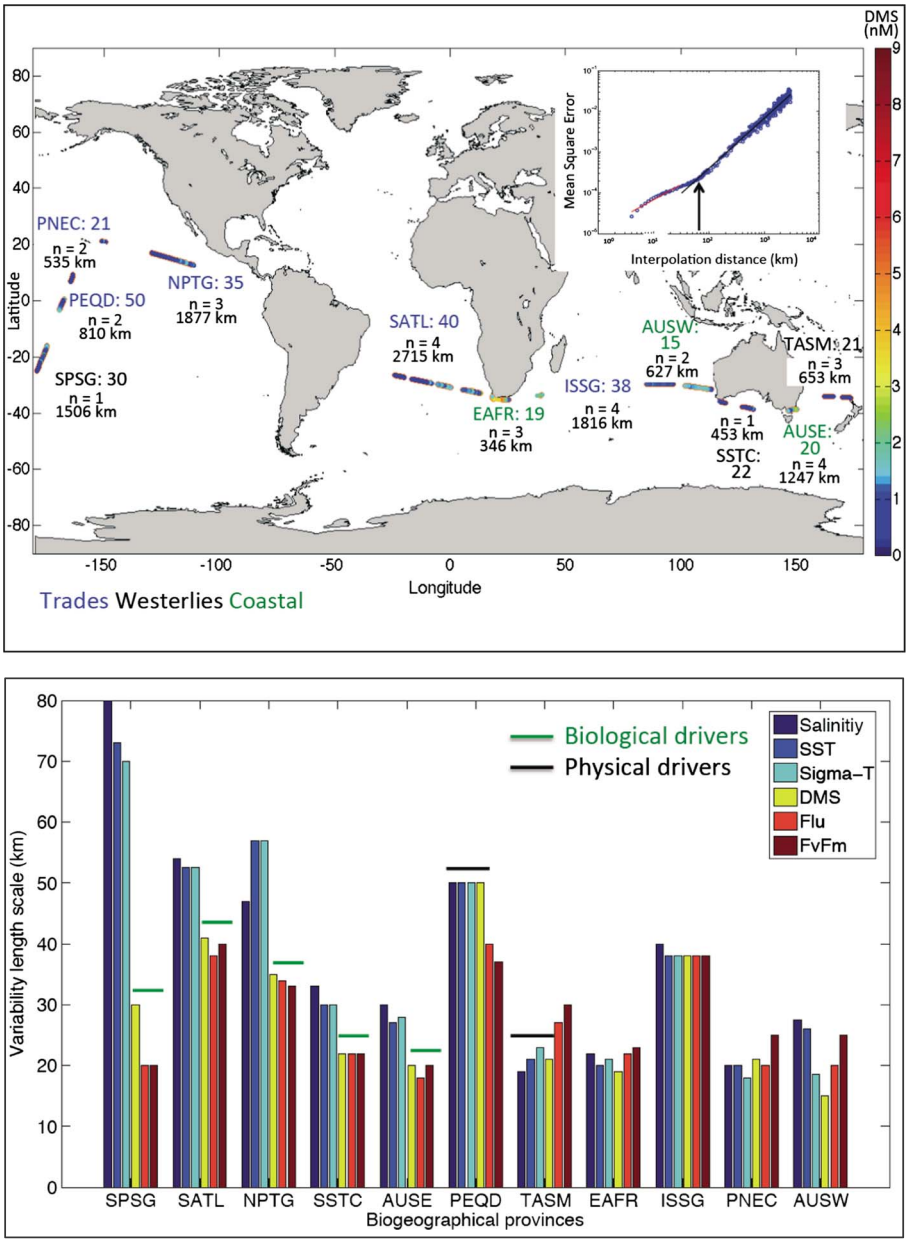

Figure 2. Distribution of high-resolution DMS concentrations and DMS VLS across provinces along the track of the Malaspina 2010 Expedition. (top) Dots on the map are surface DMS concentrations (nmol L^{-1}) as measured with the Eq-APCIMS. Concentration is depicted by the color bar on the right. The acronyms refer to Longhurst's biogeographical provinces: SPSG is South Pacific Subtropical Gyre; PEQD is Pacific Equatorial Divergence; PNEC is North Pacific Equatorial Countercurrent; NPTG is North Pacific Tropical Gyre; SATL is South Atlantic Gyre; EAFR is East Africa Coastal; ISSG is Indian South Subtropical Gyre; AUSW is Australia-Indonesia Coastal; SSTC is South Subtropical Convergence; AUSE is East Australian Coastal; TASM is Tasman Sea. The colors of province acronyms refer to the following biogeographical domains: blue = trades, black = westerlies, and green = coastal. The number next to the province acronym is the mean VLS (km) of DMS. The number of transects analyzed per province is termed *n*, and the number of km comprised by all transects in an individual province is indicated below. The inset graph shows an example of how the VLS is calculated: it represents the measurement interpolation errors as a function of interpolated distance (km) within the SPSG province; the VLS is marked by the arrow. (bottom) Province-averaged VLS (km) for salinity, SST, sigma T, DMS, Fluo, and FvFm. The green or black line above bars identifies the provinces where DMS VLS is similar to that of biological or physical variables, respectively.

the VLS of salinity, SST, and sigma T were similar to each other, an expected feature that depicts the physical structure of the surface ocean. The VLS of these physical properties ranged 18–80 km across provinces (Table S1), with a circumnavigation average of 38 km. Biological variables related to phytoplankton biomass and physiology generally showed shorter VLS: across province range of 18–40 km (mean of 27 km) for Fluo and 20–40 km (mean of 28 km) for FvFm (Table S1). These scales of variability of physical and biological properties are in agreement with the typical ranges for cross-stream widths of ocean's swift currents (10–100 km) and about one fourth of the typical radii of low-latitude surface eddies as revealed by satellite altimetry (60–200 km) [*Fu et al.*, 2010]. This is a reasonable result, as open ocean chl*a* patches are typically formed by horizontal advection within rotating eddies [*Chelton et al.*, 2011]. Examining the VLS by provinces, the VLS of Fluo and FvFm are generally equal or smaller than those of salinity, SST, and sigma T. This was already observed by *Strutton et al.* [1997] as an indication that the chl*a* spatial variability is not always associated with the physical heterogeneity of the environment. It is also consistent with the notion that faster responding tracers develop smaller scales of variability, or more patchiness, than slower or more conservative tracers [*Mahadevan*, 2004]. Actually, both Fluo and FvFm are even shorter lived tracers than chl*a* since they are photophysiological variables that do not only depend on phytoplankton biomass but also on pigment packaging in the cell, nutrient status, and photoacclimation to incident irradiance, among other things.

The VLS of DMS was similar to those of physical and biological variables, ranging from 15 to 50 km (mean of 28 km; Table S1). These values are consistently larger than those reported with similar methodologies in the North Pacific [*Nemcek et al.*, 2008; *Asher et al.*, 2011]. Interestingly, DMS VLS exhibited a significant inverse correlation with latitude (Pearson's $r = -0.71$, $P < 0.05$; Table S2 in the supporting information). This correlation remains significant after including the VLS reported by the aforementioned studies at 50°N and the VLS reported by *Tortell et al.* [2011] in the Ross Sea ($r = -0.74$, $P < 0.005$). This decrease in the VLS with increasing latitude parallels the decrease of the Rossby deformation radius and eddy size with latitude [*Chelton et al.*, 1998]. In other words, ocean hydrographic mesoscale structures tend to get smaller with increasing latitude, and DMS variability distribution follows a similar general pattern.

By comparing the VLS of DMS to those of physical and biological variables in all individual transects across different provinces, we aim to obtain insight into the relative roles of the two types of variables in driving spatial DMS variability. The DMS VLS was more similar to that of the biological parameters (Fluo and FvFm) than to that of the physical parameters in 65% of the transects (Figure 2). This occurred mainly in the oligotrophic gyres of the Atlantic and Pacific Oceans (SATL, SPSG, and North Pacific Tropical Gyre (NPTG)) as well as the waters south of Australia (South Subtropical Convergence (SSTC) and East Australian Coastal (AUSE)). DMS VLS more closely matched that of the physical variables in only 15% of the analyzed transects. This occurred in the Pacific Equatorial Divergence (PEQD) and Tasman Sea (TASM). In most of the remaining 20% of the transects (within East Africa Coastal (EAFR), Indian South Subtropical Gyre (ISSG), and North Pacific Equatorial Countercurrent (PNEC)), all of the VLS were similar. In those waters, the relative influences of physics and biology on DMS could not be discerned. Only in Australia-Indonesia Coastal (AUSW), was the DMS VLS smaller than any of the other variables' VLS.

In general, the coastal domain presented the smallest VLS for biological variables and DMS (Figure 2; Table S1), while oligotrophic waters showed the largest. In support of this emerging pattern, a significant anticorrelation was observed between DMS VLS and Fluo across the regions where DMS variability is driven by biology ($r = -0.86$, $P < 0.05$; Table S2). In other words, more productive waters, usually associated with the coastal domain, tend to be patchier for both biological and biogenic tracers. Again, this pattern is consistent with the previous studies by *Nemcek et al.* [2008] and *Asher et al.* [2011], where much smaller DMS VLS (approximately 7 km) was associated with highly productive waters (chl*a* up to 33 $\mu g\, L^{-1}$) in coastal domain waters off British Columbia.

3.3. DMS and Phytoplankton Physiology Over the Normalized Diel Cycle

Diel oscillations in solar irradiance are an additional potential source of DMS variability encountered during this study. The day-night alternation and the hourly underwater light regime exert an obvious rhythmic forcing on biological circadian rhythms, photochemical and photobiological processes, and potentially on biogeochemical fluxes [*Doney et al.*, 1995; *Poretsky et al.*, 2009; *Ottesen et al.*, 2014]. Our data set is not particularly well suited for assessing diel oscillations because spatial variability occurred simultaneously to temporal variability, and the cruise covered a number of latitudes and seasons. To overcome this

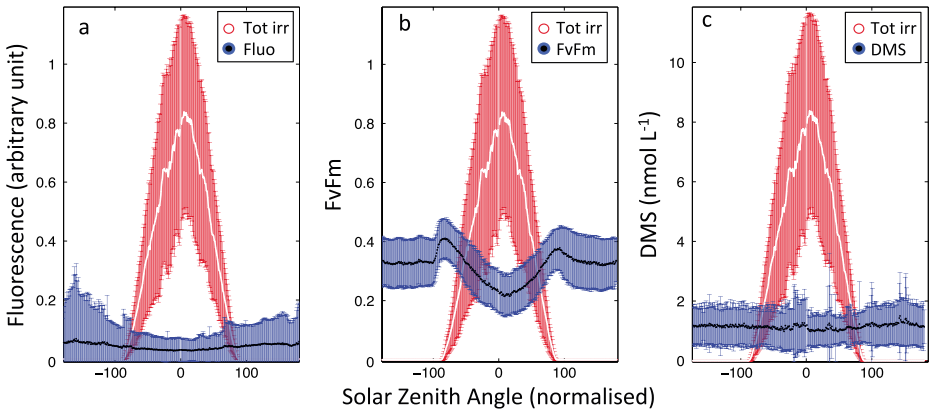

Figure 3. Normalized solar zenith angle (SZAn) dependence across the entire circumnavigation for (a) Fluorescence (Fluo), (b) FvFm, and (c) DMS. Total surface irradiance ($W\,m^{-2} \times 1000$ in Figures 3a and 3b; $W\,m^{-2} \times 100$ in Figure 3c) is given in red. Means and standard deviations are shown for each SZAn.

limitation, we examined our data as a function of SZAn (Figure 3), which allows collapsing all data into a single solar diel cycle.

Average chl*a* fluorescence (Fluo) showed hardly any day-night oscillation, yet a subtle photoacclimation pattern was apparent for the upper envelope of the statistical variability (Figure 3a), pointing out to photoacclimation processes where Fluo decreases at daytime and increases at nighttime according to the need for less or more efficient photosynthetic antenna. A much more remarkable diel pattern was found for the maximum photosystem II quantum yield or photochemical efficiency, FvFm (Figure 3b). As in *Behrenfeld et al.* [2006], photoacclimation and photoinhibition of phytoplankton (translated into low-FvFm values) appeared at low SZAn while higher FvFm occurred at dawn and dusk. The sudden increase in FvFm at dawn results from the oxidation of the plastoquinone pool by the photosystem I electron turnover, and higher FvFm at dusk results from complete recovery after the depressing effect of high light during daytime, due to nonphotochemical quenching and photodamage to PSII. This common pattern across latitudes and seasons indicates that time of the day, and not only the instantaneous or daily integrated irradiance, is more important for phytoplankton physiology.

Interestingly, DMS concentration did not show a significant relationship to SZAn (Figure 3c). Strong diel cycles have been reported for gross community DMS production in Lagrangian studies conducted in highly irradiated and stratified waters at sea [*Galí et al.*, 2013b]. Suggested causes are the diel oscillations of UV radiation exposure and grazing [*Galí et al.*, 2013a, 2013b]. As for DMS losses, photolysis follows an obvious oscillation that parallels irradiance. Weaker yet significant cycles have also been observed for microbial DMS consumption. Although these processes tend to cancel each other and buffer DMS concentration changes, clear diel variability is often encountered. Using the Eq-APCIMS in two Lagrangian studies, we recently observed repeated day-night DMS oscillations in the Mediterranean Sea (results not shown); however, the diel pace in September was in antiphase of that in May. Therefore, the absence of a pattern in Figure 3c is not to be interpreted as the lack of diel patterns in DMS concentration and cycling processes, but the absence of a *universal* diel cycle of global applicability similar to those of Fluo and FvFm.

3.4. Implications

Broad spatial coverage with high-frequency measurements is essential to decipher the scales of variability and patchiness of DMS. In some instances, high-resolution measurements showed strong gradients, e.g., an abrupt change from 1 to 8 nmol L^{-1} was observed within 1.5 km in the Benguela province. *Tortell* [2005b] observed an increase of 30 nmol L^{-1} over 750 m along the Queen Charlotte Islands. In contrast, traditional field sampling and measurement protocols, with sampling and analysis times in the order of 10–20 min at the shortest, would clearly fail to resolve this level of spatial heterogeneity. These results emphasize the need for high-frequency DMS measurements that match the resolution of sensor-based physical and biological data, in order to better understand the mechanisms driving DMS distribution.

The VLS analysis revealed that most spatial DMS variability occurs at the low mesoscale (15–50 km). *Nemcek et al.* [2008] and *Asher et al.* [2011] had already reported even shorter scales of variability with similar methods. However, these works were conducted in highly productive temperate waters across two biogeographical provinces, one coastal. Our study covers 11 biogeographical provinces in 3 domains, mostly low latitude oligotrophic waters. Thus, we largely expand the variability analysis to the tropical and subtropical regions that make up the most of the world's oceans in terms of area.

Our study shows that, similar to what occurs with phytoplankton, the DMS variability scale is smaller in productive waters and larger in oligotrophic waters. This, along with its dependence on latitude, should be considered when designing sampling schemes in future field studies aimed at describing DMS distribution and its drivers. The spatial coverage and gridding of sampling (when analysis is to be done on discrete samples) should be designed to, at the least, cover the low mesoscale, taking into account that this contracts as we move poleward. Satellite imagery can assist with sampling design: both ch*la* patchiness from ocean color as well as physical structure information based on satellite altimetry and infrared radiation can be helpful; we strongly recommend to increase the sampling grid density at high latitudes and in highly productive waters. Similar criteria should apply when we aim to construct regional to global maps of surface ocean DMS concentration using objective analysis schemes [*Lana et al.*, 2011]. Our results indicate that distance-weighted interpolations steps [e.g., *Barnes*, 1964] should scale to latitude-dependent sizes of mesoscale variability.

The lack of correlation of DMS with SZAn revealed that there is no such a thing as a universal diel pattern of global applicability for DMS. Only Lagrangian studies in representative oceanic regions provide the proper strategy to investigate the mechanisms of short-term DMS dynamics. However, the absence of a unique diel cycle, along with the observation that DMS tracks spatial variability in patchy or abruptly varying environments, increases the difficulty in extrapolating from local studies when developing prognostic numerical modeling for this trace gas at the global scale. Global models are close to resolve mesoscale DMS variability [*Chu et al.*, 2004], but will still have a hard time to reproduce the lower edge mesoscale and submesoscale variability presented here.

Acknowledgments

Data can be requested to Sarah-Jeanne Royer (royer@icm.csic.es). Data supporting Figure 2 are available in Table S1 in the supporting information. We wish to acknowledge the assistance and cooperation of the marine technicians (UTM) and crew aboard the R/V *Hesperides*, as well as the leadership of C.M. Duarte. This research has been funded by the Spanish Ministry of Economy and Competitiveness through projects Malaspina Expedition 2010 (INGENIO 2010 CONSOLIDER program, CSD2008-00077) and PEGASO (CTM2012-37615) and through a PhD scholarship to S.J.R. Support was also provided by the U.S. National Science Foundation (grants 0851472 and 1143709). The Indian Institute of Tropical Meteorology is funded by the Ministry of Earth Sciences, Government of India.

The Editor thanks two anonymous reviewers for their assistance in evaluating this paper.

References

Andreae, M. O., and W. R. Barnard (1984), The marine chemistry of dimethylsulfide, *Mar. Chem.*, *14*, 267–279.

Andreae, M. O., and D. Rosenfeld (2008), Aerosol-cloud-precipitation interactions. Part 1. The nature and sources of cloud-active aerosols, *Earth Sci. Rev.*, *89*(1–2), 13–41, doi:10.1016/j.earscirev.2008.03.001.

Asher, E. C., A. Merzouk, and P. D. Tortell (2011), Fine-scale spatial and temporal variability of surface water dimethylsufide (DMS) concentrations and sea-air fluxes in the NE Subarctic Pacific, *Mar. Chem.*, *126*(1–4), 63–75.

Barnes, S. L. (1964), A technique for maximizing details in numerical weather map analysis, *J. Appl. Meteorol.*, *3*, 396–409.

Behrenfeld, M. J., K. Worthington, R. M. Sherrell, F. P. Chavez, P. Strutton, M. McPhaden, and D. M. Shea (2006), Controls on tropical Pacific Ocean productivity revealed through nutrient stress diagnostics, *Nature*, *442*(7106), 1025–1028, doi:10.1038/nature05083.

Bell, T. G., G. Malin, G. A. Lee, J. Stefels, S. Archer, M. Steinke, and P. Matrai (2012), Global oceanic DMS data inter-comparability, *Biogeochemistry*, *110*(1–3), 147–161.

Belviso, S., C. Moulin, L. Bopp, and J. Stefels (2004), Assessment of a global climatology of oceanic dimethylsulfide (DMS) concentrations based on SeaWiFS imagery (1998–2001), *Can. J. Fish. Aquat. Sci.*, *61*, 804–816, doi:10.1139/F04-001.

Chelton, D. B., A. DeSzoeke, and M. G. Schlax (1998), Geographical variability of the first baroclinic Rossby radius of deformation, *J. Phys. Oceanogr.*, *28*, 433–460.

Chelton, D. B., P. Gaube, M. G. Schlax, J. J. Early, and R. M. Samelson (2011), The influence of nonlinear mesoscale eddies on near-surface oceanic chlorophyll, *Science*, *334*, 328–332, doi:10.1126/science.1208897.

Chu, S., S. Elliott, and M. Maltrud (2004), Ecodynamic and eddy-admitting dimethyl sulfide simulations in a global ocean biogeochemistry/circulation model, *Earth Interact.*, *8*, 11, doi:10.1175/1087-3562(2004)008<0001:EAEDSS>2.0.CO;2.

Doney, S. C., R. G. Najjar, and S. Stewart (1995), Photochemistry, mixing and diurnal cycles in the upper ocean, *J. Mar. Res.*, *53*, 341–369.

Doney, S. C., D. M. Glover, and S. J. Mccue (2003), Mesoscale variability of Sea-viewing Wide Field-of-view Sensor (SeaWiFS) satellite ocean color: Global patterns and spatial scales, *J. Geophys. Res.*, *108*(C2), 3024, doi:10.1029/2001JC000843.

Fu, L.-L., D. B. Chelton, P.-Y. Le Traon, and R. Morrow (2010), Eddy dynamics from satellite altimetry, *Oceanography*, *23*(4), 14–25.

Galí, M., R. Simó, M. Vila-Costa, C. Ruiz-González, J. M. Gasol, and P. Matrai (2013a), Diel patterns of oceanic dimethylsulfide (DMS) cycling: Microbial and physical drivers, *Global Biogeochem. Cycles*, *27*, 1–17, doi:10.1002/gbc.20047.

Galí, M., C. Ruiz-González, T. Lefort, J. M. Gasol, C. Cardelús, C. Romera-Castillo, and R. Simó (2013b), Spectral irradiance dependence of sunlight effects on plankton dimethylsulfide production, *Limnol. Oceanogr.*, *58*(2), 489–504, doi:10.4319/lo.2013.58.2.0489.

Hegg, A., F. Radke, and V. Hobbs (1991), Measurements of Aitken nuclei and cloud condensation nuclei in the marine atmosphere and their relation to the DMS-Cloud-climate hypothesis, *J. Geophys. Res.*, *96*(D10), 18,727–18,733, doi:10.1029/91JD01870.

Kameyama, S., H. Tanimoto, S. Inomata, U. Tsunogai, A. Ooki, Y. Yokouchi, S. Takeda, H. Obata, and M. Uematsu (2009), Equilibrator inlet-proton transfer reaction-mass spectrometry (EI-PTR-MS) for sensitive, high-resolution measurement of dimethyl sulfide dissolved in seawater, *Anal. Chem.*, *81*(21), 9021–9026, doi:10.1021/ac901630h.

Kameyama, S., H. Tanimoto, S. Inomata, H. Yoshikawa-Inoue, U. Tsunogai, A. Tsuda, M. Uematsu, M. Ishii, D. Sasano, and Y. Nosaka (2013), Strong relationship between dimethylsulfide and net community production in the western subarctic Pacific, *Geophys. Res. Lett.*, *40*, 3986–3990, doi:10.1002/grl.50654.

Kiene, R. P., L. J. Linn, and J. A. Bruton (2000), New and important roles for DMSP in marine microbial communities, *J. Sea Res.*, *43*(3–4), 209–224.

Kolber, Z., O. Prasil, and P. P. G. Falkowski (1998), Measurements of variable chlorophyll fluorescence using fast repetition rate techniques: Defining methodology and experimental protocols, *Biochim. Biophys. Acta*, *1367*(1–3), 88–106, doi:10.1016/S0005-2728(98)00135-2.

Lana, A., et al. (2011), An updated climatology of surface dimethlysulfide concentrations and emission fluxes in the global ocean, *Global Biogeochem. Cycles*, *25*, 1–17, doi:10.1029/2010GB003850.

Lana, A., R. Simó, S. M. Vallina, and J. Dachs (2012), Potential for a biogenic influence on cloud microphysics over the ocean: A correlation study with satellite-derived data, *Atmos. Chem. Phys.*, *12*(17), 7977–7993, doi:10.5194/acp-12-7977-2012.

Longhurst, A. (1998), *Ecological Geography of the Sea*, Academy Pr, London.

Lovelock, J. E., R. J. Maggs, and R. A. Rasmussen (1972), Atmospheric dimethyl sulphide and the natural sulphur cycle, *Nature*, *237*, 452–453.

Mahadevan, A. (2004), Spatial heterogeneity and its relation to processes in the upper ocean, in *Ecosystem Function in Heterogeneous Landscape*, edited by G. M. Lovett et al., pp. 165–182, Springer, New York.

Malin, G., and G. O. Kirst (1997), Algal production of dimethyl sulfide and its atmospheric role, *J. Phycol.*, *33*, 889–896.

Nemcek, N., D. Ianson, and P. D. Tortell (2008), A high-resolution survey of DMS, CO_2, and O_2/Ar distributions in productive coastal waters, *Global Biogeochem. Cycles*, *22*, 1–13, doi:10.1029/2006GB002879.

Ottesen, E. A., C. R. Young, S. M. Gifford, J. M. Eppley, R. Marin, S. C. Schuster, C. A. Scholin, and E. F. DeLong (2014), Ocean microbes. Multispecies diel transcriptional oscillations in open ocean heterotrophic bacterial assemblages, *Science*, *345*(6193), 207–212, doi:10.1126/science.1252476.

Poretsky, R. S., I. Hewson, S. Sun, A. E. Allen, J. P. Zehr, and M. A. Moran (2009), Comparative day/night metatranscriptomic analysis of microbial communities in the North Pacific subtropical gyre, *Environ. Microbiol.*, *11*(6), 1358–1375, doi:10.1111/j.1462-2920.2008.01863.x.

Royer, S.-J., M. Galí, E. S. Saltzman, C. A. McCormick, T. G. Bell, and R. Simó (2014), Development and validation of a shipboard system for measuring high-resolution vertical profiles of aqueous dimethylsulfide concentrations using chemical ionisation mass spectrometry, *Environ. Chem.*, *11*(3), 309–317, doi:10.1071/EN13203.

Saltzman, E. S., W. J. De Bruyn, M. J. Lawler, C. Marandino, and C. McCormick (2009), A chemical ionization mass spectrometer for continuous underway shipboard analysis of dimethylsulfide in near-surface seawater, *Ocean Sci.*, *6*(2), 1569–1594.

Simó, R. (2001), Production of atmospheric sulfur by oceanic plankton: Biogeochemical, ecological and evolutionary links, *Trends Ecol. Evol.*, *16*(6), 287–294.

Simó, R., and J. Dachs (2002), Global ocean emission of dimethylsulfide predicted from biogeophysical data, *Global Biogeochem. Cycles*, *16*(4), 1078, doi:10.1029/2001GB001829.

Strutton, P. G., J. G. Mitchell, J. S. Parslow, and R. M. Greene (1997), Phytoplankton patchiness: quantifying the biological contribution using Fast Repetition Rate Fluorometry, *J. Plankton Res.*, *19*(9), 1265–1274, doi:10.1093/plankt/19.9.1265.

Tortell, P. D. (2005a), Dissolved gas measurements in oceanic waters made by membrane inlet mass spectrometry, *Limnol. Oceanogr. Meth.*, *2*, 24–37.

Tortell, P. D. (2005b), Small-scale heterogeneity of dissolved gas concentrations in marine continental shelf waters, *Geochem. Geophys. Geosyst.*, *6*, Q11M04, doi:10.1029/2005GC000953.

Tortell, P. D., C. Guéguen, M. C. Long, C. D. Payne, P. Lee, and G. R. DiTullio (2011), Spatial variability and temporal dynamics of surface water pCO_2, ΔO_2/Ar and dimethylsulfide in the Ross Sea, Antarctica, *Deep Sea Res., Part I*, *58*(3), 241–259, doi:10.1016/j.dsr.2010.12.006.

Vallina, S. M., R. Simó, S. Gassó, C. de Boyer-Montégut, E. del Río, E. Jurado, and J. Dachs (2007), Analysis of a potential "solar radiation dose—dimethylsulfide—cloud condensation nuclei" link from globally mapped seasonal correlations, *Global Biogeochem. Cycles*, *21*, GB2004, doi:10.1029/2006GB002787.

Zindler, C., C. A. Marandino, H. W. Bange, F. Schütte, and E. S. Saltzman (2014), Nutrient availability determines dimethyl sulfide and isoprene distribution in the eastern Atlantic Ocean, *Geophys. Res. Lett.*, *41*, 3181–3188, doi:10.1002/2014GL059547.

To be submitted

Sea surface DMS distribution patterns and environmental and biological drivers across the tropical and subtropical oceans

S-J.Royer[1], M.Galí[1,2], A. S. Mahajan[3], A. Delgado-Huertas[4], Dolors Blasco[1], Marta Estrada[1], Susana Agustí[5], Antonio Bode[6], R. Sánchez-Leal[7], Mikel Latasa[8], E. Marañón[9], R. Simó[1*]

1. *Institut de Ciències del Mar (CSIC), Barcelona, Spain.*
2. *Takuvik Joint International Laboratory and Québec-Océan, Université Laval, Québec, Canada.*
3. *Indian Institute of Tropical Meteorology (IITM), Pune, India.*
4. *Instituto Andaluz de Ciencias de la Tierra (IACT), CSIC-UGR, Granada, Spain.*
5. *Instituto Mediterráneo de Estudios Avanzados (IMEDEA), CSIC-UIB, Mallorca, Spain.*
6. *Instituto Español de Oceanografía, A Coruña, Spain.*
7. *Instituto Español de Oceanografía, Cádiz, Spain.*
8. *Instituto Español de Oceanografía, Gijón, Spain.*
9. *Universidad de Vigo, Vigo, Spain.*

See Chapter 6